Encapsulation of Metallic Oxide Nano-particles and Synthetic Antibiotics to Combat Mastitis Causing Multidrug Resistant Pathogens

A dissertation submitted in the partial fulfillment of the requirements for the degree of Doctor of Philosophy

In

Biotecnology

By

Naheed Zafar

(22-FBAS/PHDBT/F14)

Department of Biological Sciences,

Faculty of Basic and Applied Sciences,

International Islamic University,

Islamabad

(2021)

PhD
615.19
NAE

Mastitis in animals - Treatment

Nanoparticles - Therapeutic use

Metal oxides - "

Antibiotics - "

Drug resistance in microorganisms

Veterinary microbiology

Encapsulation (Pharmacy)

Encapsulation of Metallic Oxide Nano-particles and Synthetic Antibiotics to Combat Mastitis Causing Multidrug Resistant Pathogens

By

Naheed Zafar

(22-FBAS/PHDBT/F-14)

Supervisor

Dr. Bushra Uzair (IIUI)

Co-Supervisor

Dr. Bilal Khan Niazi

Department of Biological Sciences

Faculty of Basic and Applied Sciences,

International Islamic University,

Islamabad

(2021)

Encapsulation of Metallic Oxide Nano-particles and Synthetic Antibiotics to Combat Mastitis Causing Multidrug Resistant Pathogens

By

Naheed Zafar

(Registration No. 22-FBAS/PHDBT/F14)

A thesis submitted to

Department of Biological Sciences

For the award of the degree of

PhD Biotechnology

Signature: _____

(Chairman, Department of Biological Sciences)

Signature: _____

(Dean FBAS, IIU, Islamabad)

Department of Biological Sciences

Faculty of Basic and Applied Sciences,

International Islamic University,

Islamabad

(2021)

FINAL APPROVAL

Dated: 27-12-21

It is certified that work presented in this thesis entitled **"Encapsulation of Metallic Oxide Nano-particles and Synthetic Antibiotics to Combat Mastitis Causing Multidrug Resistant Pathogens"** by **Ms. Naheed Zafar** bearing **Registration No. 22-FBAS/PHDBT/F14** is of sufficient standard in scope and quality for the award of degree of PhD in Biotechnology from International Islamic University, Islamabad.

COMMITTEE

Supervisor

Dr. Bushra Uzair

Assistant Professor

Department of Biological Sciences, IIUI

Co-supervisor

Dr. Bilal Khan Niazi

Associate Professor

SCME, NUST Islamabad

External Examiner

Dr. Rani Faryal

Professor

Department of Microbiology, QAU, Islamabad

External Examiner

Dr. Iftikhar Ahmed

Principal

~~Senior~~ Scientific Officer, NARC, Islamabad

Internal Examiner

Dr. Shaheen Shahzad

Assistant Professor

Department of Biological Sciences, IIUI

A thesis submitted to

Department of Biological Sciences

International Islamic University, Islamabad

As a partial fulfilment for the award of the degree of

Doctor of Philosophy

Declaration

I hereby declare that this thesis, neither as a whole nor a part of it has been copied out from any source except the following publications and research efforts:-

1. **Zafar, N.,** Uzair, B., Niazi, M. B. K., Sajjad, S., Samin, G., Arshed, M. J., &Rafiq, S. (2020). Fabrication & characterization of chitosan coated biologically synthesized TiO2 nanoparticles against PDR E. coli of veterinary origin. *Advances in Polymer Technology, 2020.*
2. **Zafar, N.,** Uzair, B., Niazi, M. B. K., Samin, G., Bano, A., Jamil, N., &Menaa, F. (2021). Erratum: Zafar et al. Synthesis and Characterization of Potent and Safe Ciprofloxacin-Loaded Ag/TiO2/CS Nanohybrid against Mastitis-Causing E. coli. Crystals 2021, 11, 319. *Crystals*, *11*(6), 573.
3. **Zafar, N.,** Uzair, B., Niazi, M. B. K., Menaa, F., Samin, G., Khan, B. A., &Menaa, B. (2021). Green Synthesis of Ciprofloxacin-Loaded Cerium Oxide/Chitosan Nanocarrier and Its Activity Against MRSA-Induced Mastitis. *Journal of Pharmaceutical Sciences.*
4. **Zafar, N.,** Uzair, B., Niazi, M. B. K., Sajjad, S., Samin, G., Arshed, M. J., &Rafiq, S. (2021). Isolation, molecular characterization of antibiotics resistant MDR pathogens causing mastitis and application of green synthesis nanomaterials by using plant extracts. (Submitted).
5. **Zafar, N.,** Uzair, B., Niazi, M. B. K., Sajjad, S., Samin, G., Arshed, M. J., &Rafiq, S. (2021). Biologically engineered CIP-Ag/TiO_2/ Fe_2O_3/ CS ternary composite broad-spectrum heterostructure to combat mastitis causing MDR pathogens of cattle (Submitted).

Further work presented in this dissertation has not been submitted in support of any application for any other degree or qualification to any other university or institute and is considerable under the plagiarism rules of Higher Education Commission (HEC), Pakistan.

Naheed Zafar

(22-FBAS/PHDBT/F14)

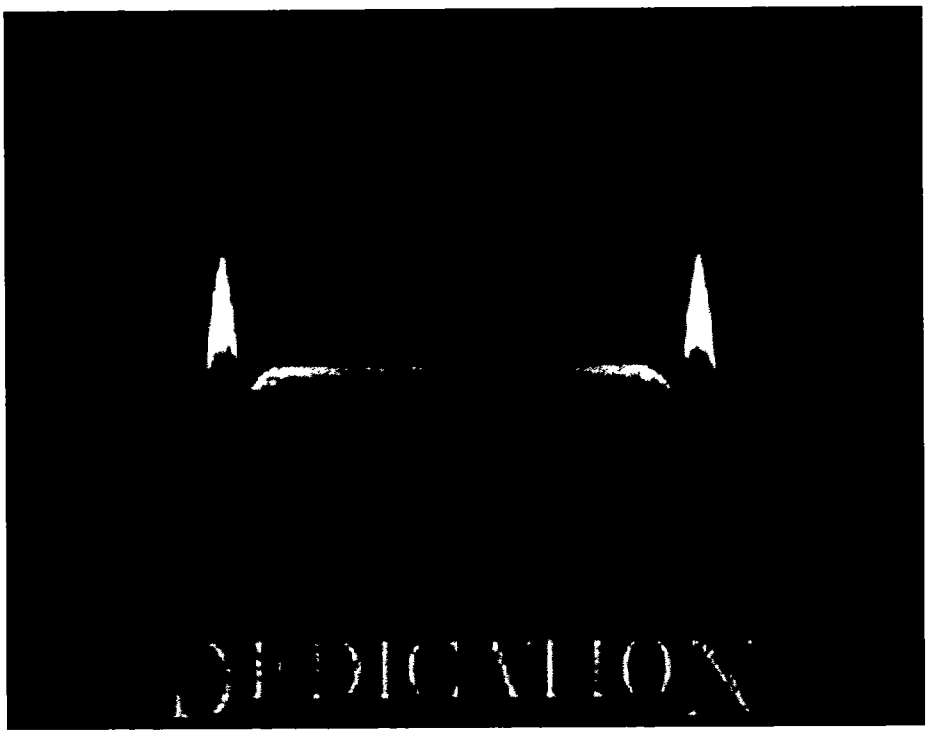

Goes

To

My Teachers and My Family

ACKNOWLEDGEMENT

I would like to take this opportunity First and foremost, to **thanks ALLAH** Almighty for giving me the strength, knowledge, ability and opportunity to undertake this research study and to persevere and complete it satisfactorily. Without His blessings, this achievement would not have been possible

I feel great honour to place on the record my sincere thanks to my respected supervisor **Dr. Bushra Uzair**, supervised my research light-heartedly and proficiently made the dispatch of intimidating workload possible by persistent guidance and scholarly criticism communicated to me during the course of this study and execution of this manuscript. I would like to express my sincere gratitude to my Co-Supervisor **Dr. Bilal Khan Niazi** for the continuous support during of my Ph.D. research work. I am really obliged for his patience, motivation and immense knowledge that enlighten the journey of my Ph.D.

I owe my gratitude to my mentors Dr. Javed Arshad, Dr. Naeem Haider, Mr. Eid Nawaz, Dr. Shumaila Sajjad, Dr. Saima Noor, and Dr. Barkat who were extremely supportive in the research activities. I would like to show gratitude to all for their unceasing encouragement and guidance in the years and for keeping me motivated throughout the writing and editing of the thesis.

A special thanks to my Mother who looked after me and my kids with highest degree of tolerance. I did my Ph.D due to humble prayers of my father, Zafar Iqbal Toor after every prayer, Sehri, and Aftari, without these strong hands that hold me whenever I disappointed. I further extend my regards and acknowledged my sister Tasleem Zafar for everything she did for me, searching resources, concerned about Lab activities and special prayers for my success. Here I would like to acknowledged specially my sister Sadaf Batool Zafar and my brother, Mudassar Zafar Toor for their entire support, encouragements during hard times. I would like to thanks my friend, Sadaf Sherazi for sincere prayers, emotional attachment and appreciation at every stage that have sustained me this far.

Finally, but by no means least, thanks to my husband and my innocent kids, who are the pride and joy of my life and I truly appreciate their patience and support during Ph.D Studies. I would compensate the gap of my absence created during PhD research by giving extra attention.

Naheed Zafar

Table of Contents

LIST OF FIGURES

LIST OF TABLE

LIST OF APPENDICES

LIST OF ABREVATIONS

Ag	Silver
$AgNO_3$	Silver Nitrate
AMR:	Antimicrobial Resistance
AST:	Antibiotic Sensitivity Testing
ARG:	Antimicrobial Resistance Gene
BHI:	Brain Heart Infusion
dH_20:	Distilled water
CIP-CeO_2/CS	Ciprofloxacin-loaded Cerium Oxide/Chitosan
CeO_2:	Cerium Oxide
CeO_2/CS:	Cerium oxide/Chitosan
CFU:	Colony Forming Unit
CIP:	Ciprofloxacin
CMT:	California Mastitis Test
CS:	Chitosan
DMEM:	Dulbecco's Modified Eagle Medium
DMSO:	Dimethylsulfoxide
E. coli	*Escherichia coli*
EDTA:	Ethylenediaminetetraacetic Acid
EDX/A:	Energy dispersive X-ray/analyser -Also called EDS = EDX spectroscopy
ELISA:	Enzyme-Linked Immunosorbent Assay
ESBL	Extended-spectrum Beta-lactamases
FACS:	Fluorescence-Activated Cell Sorting
FOX:	Cefoxitin
FTIR:	Fourier Transform Infrared Spectroscopy
GA:	Glutaraldehyde

Fe_2O_3	Ironoxide
MHA:	Muller-Hinton Agar
MIC:	Minimum Inhibitory Concentration
MRSA:	Methicillin Resistant *S. aureus*
MTT:	3-(4, 5-dimethylthiazol-2-yl)-2, 5-diphenyl tetrazolium bromide
NA:	Nutrient Agar
NB:	Nutrient Broth
NC:	Negative Control
NPs:	Nanoparticles
OD:	Optical Density
OX:	Oxacillin
PBP:	Penicillin Binding Protein
PBS:	Phosphate-Buffered Saline
PC:	Positive Control
PCR:	Polymerase Chain Reaction
PI:	Propidium Iodide
RBCs:	Red Blood Cells
ROS:	Reactive Oxygen Species
RT:	Room Temperature
SEM:	Scanning Electron Microscopy
TEM:	Transmission Electron Microscopy
TiO_2	Titanium dioxide
TTP:	Titanium tetra isoproxide
TPP:	Tripolyphosphate
XRD:	X-ray Diffractometer

ZI:	Zone of Inhibition
ZP:	Zeta Potential

ABSTRACT

Encapsulation of Metallic Oxide Nano-particles and Synthetic Antibiotics to Combat Mastitis Causing Multidrug Resistant Pathogens

Pakistan is the world's fourth-largest producer of milk and dairy products. Mastitis is the most prevalent and expensive disease affecting dairy cattle worldwide. Reduced milk output, antibiotic residues in milk, medical costs, culling of chronically diseased cows, and occasional deaths are all examples of economic losses caused by mastitis. The presence of resistant pathogenic strains in the food matrix creates a direct risk to public health. Treatment of highly prevalent mastitis-causing multidrug resistant strains has become a challenging task for the present reservoir of antibiotics. New target-oriented antimicrobials are expressly required for fighting infections caused by multidrug resistant (MDR) strains. Mastitis is becoming a monster threat to the dairy industry due to treatment failure by available expensive antibiotics. Nanobiotechnology is an emerging field to apply the new trends of nanotechnology find more reliable and eco-friendly methods for developing alternative nano-antibiotics with improved antimicrobial potentials. The major aim of the current study is to improve the efficacy of existing antibiotics by conjugating them with green synthesized metallic oxide nanoparticles to lower their MICs. Chitosan biopolymer played a major role to make enclosed nanomaterials biocompatible and biodegradable for targeted delivery. In the 1st phase of the study, 35 dairy farms in Pakistan's two largest cities, Rawalpindi and Islamabad, were selected for milk samples of suspected cows and buffaloes. The California mastitis test (CMT) was performed to screen milk samples, and 875 cows out of 1289 were CMT positive, while 173 buffaloes out of 191 were CMT positive. Microbial analysis revealed *E.coli* (n=155), *S. aureus* (n=118) and *C .albicans* (n=35) *as* major causative agents of mastitis. Disc diffusion method was employed to study antibiotic sensitivity testing of fifteen commonly used antibiotics and the highest resistance pattern of Augmentin (100%), Ciprofloxacin (96%), Ampicillin (91.6%), Oxacillin (61%) and Cefoxitin (30%) were displaying challenge to livestock industry to treat infectious diseases. Nanoparticles of the following metallic oxides were synthesized i.e. Ag NPs, CeO_2 NPs, TiO_2 NPs, and Fe_2O_3 NPs, which are considered as generally recognized as safe chemicals (GRAS), to tackle MDR pathogens. Nanoparticles of metallic oxides were synthesized using medicinally important plants i.e. aqueous extractof *Moringa concanensis* leavesand *Amomum subulatum* (black cardamoms seeds). GC-MS analysis profile revealed the presence of 2-Ethylacridine, alpha.-Amyrin, δ-Tocopherol, Pyridine-3-carboxamide reducing agents in *M .concanensis,* and black cardamom seeds extract displayed the following compounds i.e.α-terpinyl acetate Pyridine-3-carboxamide and 1,8-cineole. All the green synthesized Ag, CeO_2, TiO_2, Fe_2O_3 NPs were encapsulated in chitosan NPs by ionic gelation method (CS NPs). The synthesized

nanomaterials Ag NPs CeO_2 NPs, TiO_2 NPs, and Fe_2O_3 NPs were conjugated with ciprofloxacin (CIP) as it was found highly resistant broad spectrum antibiotic. Gold standard techniques were used to characterize all the synthesized nanomaterials including Field Emission Scanning Electron Microscopy (FESEM) with Energy Dispersive X-ray spectrometry (EDX), Transmission Electron Microscopy (TEM), X-ray Diffraction (XRD) transform-infrared (FTIR) spectroscopy, Optical properties, and Zeta potential analysis. All the nanomaterials were synthesized as alternative Nano antibiotics for mastitis-causing MDR strains. The antimicrobial potential of Nano antibiotics was screened using various antimicrobial assays including minimum inhibitory concentration (MIC) determination, disc diffusion assay to define the zones of inhibition (ZI), killing kinetics,LIVE/DEAD assay by flow cytometry, and antibiofilm activity. A rabbit model was selected for *Invivo* antimicrobial activity of the most effective nanomaterial against the most prevalent MDR *E.coli* strains. The morphological alterations were examined after treatment with nanomaterials by FESEM and TEM at various time intervals against selected MDR strains of *E.coli*, *S .aureus,* and *C.albicans*. The biocompatibility analysis of all synthesized nanomaterials was done by using two different methods i.e MTT (3-(4,5-Dimethylthiazol-2-yl)-2,5-diphenyltetrazolium bromide) assay (bovine mammary gland epithelial cells)and haemolytic study (red blood cells of cows).

Following four nanomaterials were prepared in the current study i.e. nanomaterial A, is chitosan coated Titanium dioxide nanoparticles (CS-NPs encapsulated TiO_2), nanomaterial B: is Ciprofloxacin loaded Cerium oxide nanoparticles encapsulated with chitosan NPs (CIP- CeO_2/ CS NPs), nanomaterial C: is Ciprofloxacin loaded Silver and Titanium dioxide composite encapsulated with chitosan (CIP-Ag/TiO_2/CS nanohybrid) and nanomaterial D is Ciprofloxacin loaded Silver, Titanium dioxide and Iron oxide ternary composite encapsulated with chitosan NPs (CIP-Ag/TiO_2/Fe_2O_3/CS ternary composite). Nanomaterial A, CS-NPs encapsulated TiO_2 was spherical and size range of 65-75nm by FESEM analysis. The UV-Vis Spectra and band gap values illustrated the redshift in CS-NPs encapsulated TiO_2 NPs, Fourier transform infrared (FTIR) spectroscopy confirmed the linkages between TiO_2 NPs and chitosan biopolymer, Zeta potential confirmed the stability of CS-NPs encapsulated TiO_2 NPs by showing 95mV peak value. The promising antibacterial activity of CS-NPs encapsulated TiO_2 NPs was noted against MDR *E.coli* strain with the prominent zone of inhibition of 23mm. The growth killing curve against MDR *E.coli* displayed a significant (0.01) drop in OD values which showed its proficiency. Morphological changes on *E.coli* cells after the treatment with MIC concentration (0.78µg/ml) of CS-NPs encapsulated TiO_2 NPs were studied by TEM analysis which clearly showed that morphology and structure of *E.coli* cells were smashed up. The encapsulation efficiency was determined 85% ± 1.59. Cytotoxicity (BMGE cell line) and hemolytic studies confirmed the nontoxic nature of CS-NPs encapsulated TiO_2 NPs. Nanomaterial B, CIP-CeO_2/CS composite which was found most efficient against MRSA as compared to MDR *E.coli*

and *C.albicans*. XRD determined the crystalline nature of CIP-CeO_2/CS composite and SEM showed spherical morphology with the size of 40± 0.91 nm. The surface linkage of CS and CIP in CeO_2 NPs was confirmed by FTIR analysis. ZP demonstrated the colloidal stability of CIP-CeO2/CS composite, which was +110 ± 0.65mV. The minimum inhibitory concentration (MIC) of CIP-CeO_2/CS composite was determined 8 µg/mL and ZIs was 12±0.45 was observed against MRSA. The toxicity to MRSA was deep-rooted by flow cytometry 87.04% ± 3.92 and morphological alteration by FESEM and TEM on 6th hrs of treatment. Encapsulation efficiency was 75% ± 1.58 and the highest cumulative drug release was found (88± 1.09) at the 8hrs of incubation study (37 °C). Eventually, the nanocomposite was found nontoxic and nonhemolytic when tested in BMGE cell line and RBCs of cow, respectively. Nanomaterial C, CIP-Ag/TiO_2/CS nanohybrid was spherical with the particle size of 20-80nm revealed by FESEM and TEM analysis. XRD patterns of the hetero system transmitted diffraction peaks of the anatase phase of TiO_2 and centered cubic metallic Ag crystals with excellent crystalline features. FTIR confirmed the Ti-O-Ag linkage in the nanohybrid. The zeta potential of CIP-Ag/TiO_2/CS nanohybrid was found 67.45 ± 1.8 mV suggesting stable nano-dispersion in the media. While MIC of CIP-Ag/TiO_2/CS was 0.0512µg/ml, which is much lower than the reference value recorded by the global CLSI system (Clinical Laboratory Standards Institute). CIP-Ag/TiO_2/CS nanohybrid was found effective against mastitis-causing MDR *E.coli.* Killing kinetics showed an excellent reduction of *E.coli* cells at 6 hrs of treatment. Flow cytometry further confirmed antibacterial potential by computing 67.87% late apoptosis at 6hrs of treatment. The encapsulation efficiency of CIP-Ag/TiO_2/CS nanohybrid was 90% ± 2.07 and drug release kinetic revealed sustained release of CIP-Ag/TiO_2/CS nanohybrid 89± 2.43. FESEM and TEM confirmed structural damages in MDR *E.coli.* CIP-Ag/TiO_2/CS nanohybrid was found biocompatible as more than 93.08% of bovine mammary gland epithelial cells remained viable.
Nanomaterial D was CIP-Ag/TiO_2/Fe_2O_3/CS ternary composite, XRD analysis confirmed the crystalline nature of ternary composite, and nanorods were observed by TEM and FESEM with 3-6nm of diameter. FTIR further confirmed the Fe-O-Ti- linkages which confirmed the successful encapsulation of CS. The most efficient antimicrobial agent was CIP-Ag/TiO_2/Fe_2O_3/CS ternary composite by exhibiting prominent ZIs against MRSA (22 ± 0.06), MDR *E. coli* (33±1.40), and MDR *C.albicans* (28± 1.45) at MICs of 0.112 µg/ml, 0.022 µg/ml and 0.004 µg/ml respectively. ZP of CIP-Ag/TiO2/Fe_2O_3/CS ternary composite was determined 85.26± 0.12. Morphological alterations of MDR pathogensafter treatment (at 0,6,12 hrs of incubation) with MIC values of CIP-Ag/TiO2/Fe_2O_3/CS ternary composite were studied by FESEM and TEM analysis which clearly showed the deformed shape and structural damage to MDRpathogens ultimately lysed cells were quite evident. The FACS analysis further confirmed late apoptotic of selected MDR pathogens i.e. MDR *E.coli* (80.85%), MRSA (75.34%), *C.albicans* (89.01%) after treatment with CIP-Ag/TiO_2/Fe_2O_3/CS ternary composite which

further confirmed structural damages. The highest drug release was observed 89% ± 0.57 at the 8th hrs of interval and encapsulation efficiency was calculated 94% ± 1.26. Cytotoxicity and hemolysis study revealed safety at all the tested concentrations of CIP-Ag/TiO_2/Fe_2O_3/CS ternary composite and viability of mammalian cells remains more than 90%. At the last stage of the experiment, CS encapsulated CIP-Ag/TiO_2/Fe_2O_3/CS was found to be the best candidate of antimicrobial potential with a broad spectrum display of activity at the lowest MICs values. In a rabbit model, the antibacterial activity of the most promising nanomaterial was investigated. In this investigation, MDR *E.coli* was determined to be the most common strain causing mastitis. In the rabbit model, infection was caused by injecting MDR *E.coli* intraperitoneally. In vivo antibacterial activity was monitored by Colony Forming Unit (CFU) on blood agar which showed no visible colony after 72hrs of treatment by CS encapsulated CIP-Ag/TiO_2/Fe_2O_3/CS ternary composite. Furthermore, synthesized antimicrobial formulation CS encapsulated CIP-Ag/TiO_2/Fe_2O_3/CS was observed safe for Invivo application as indicated by histopathological and biochemical analysis. Rabbit vital organs i.e heart, liver, and kidney didn't show any hemorrhage and necrosis in the fixed slides. The CS encapsulated CIP-Ag/TiO_2/Fe_2O_3/CS ternary composite was found the most suitable alternative therapeutic agent when all of the findings of In vitro and In vivo antibacterial potential were taken into account.

CHAPTER 1

INTRODUCTION

1.1. Background of Study

Mastitis remains a major challenge to the worldwide dairy industries and still there is no established treatment for such a commonly occurring infection. Currently, the use of antibiotics is the most common method of treatment of bovine mastitis. Antibiotic use has some demerits due to low cure rate, increasing occurrence of resistance and the presence of antibiotics residues in the milk. Therefore, an alternative to antibiotics need to be investigated in order to find an effective approach for rapid treatment of bovine mastitis. Mastitis is a global disease that has yet to be solved in the livestock industry. Similarly, Pakistan has a considerable number of cattle and buffaloes in its agriculture sector, with 46.1 million and 38.8 million cattle and buffaloes, respectively, which contributing about 56 percent of animal husbandry and contribution in GDP is 11% (Rehman et al., 2017). Pakistan's livestock industry is facing health issues of animals, one of them is mastitis which limits the progress of this industry (Akhtar et al., 2012) and make huge loss by reduced milk yield, milk conviction, animal reproduction and slaughtering. Furthermore, in under developed countries infectious disease may cause milk to deteriorate by about 15%, are resulting in a loss of 169 billion rupees per year (Burton et al., 2012). Although the private sector is rapidly growing dairy farming, it can only supply 5% of the demand for milk and dairy products. To establish relevant strategies for Pakistan's dairy business, a study strategy is required that focuses on specific qualities such as cold storages, value-added, and packaging.

Nowadays antibiotic treatment is commonly used against mastitis (Seegers et al., 2003). However, it contains some disadvantages because of less cure ratio, increased drug resistance and residual antibiotic in milk (Seegers et al., 2003). So, many scientists had studied significant techniques to cope with mastitis among them nanoparticles, vaccines, bacteriophages and probiotics had found successful substitutes of antimicrobials agents(Sharma et al., 2018). Animal productivity is reduced, economic losses and long and short term efficiency decline

occur due to disease (Sansoucy, 1995). These are significant losses of economy than death rates (Hazlett et al., 1984). Other cattle based activities like agriculture, transportation and tourism also became a cause of declined income source most effectively to small farmers totally dependent on livestock profit. In addition, farmers don't consider positively to subclinical issues with no mortality rate. Antimicrobials used to treat animal diseases and improvement in health are stimulation to evolve AMR in livestock due to pathogenic immunity against antimicrobials (Diaz, 2013). Antibiotic resistance in animals evolved due to excessive use of antimicrobial against mastitis. This bacterial resistance emerged because of four reasons (1) antimicrobial modifications (2) change in target site (3) changes in pathways of metabolisms (4) increasing active efflux of antibacterial agents (Martinez & Baquero, 2000). Microbial resistance can be enhanced against antibiotics by adopting mutation in already present genes (Martinez & Baquero, 2000) or by getting new genes from ambiance or other strains (horizontal gene transfer) that becomes possible due to presence of phages, plasmids, and transposons (Jeters et al., 2009; Palmer et al., 2010).Situation is becoming worse because of no serious developments for modern antimicrobials. Since 2000, to defeat MDR strains only 22 modern medicines were launched since but still resistance sustained (Butler et al., 2013). Development of new antimicrobial agents is challenging tasks due to many reasons including antimicrobial isolation difficulty, extended production time, huge cost of clinical trials and resistance evolving mechanisms to newly introduced antimicrobial agent. Modern studies of chemistry, genomics and proteomics are now focusing to evolve medicine through computer designs (Medema et al., 2011). Although technological advancements been occur but no significant results are found regarding advanced antibiotics (Butler et al., 2013).

Nanotechnology is evolving field intending suitable solution to grab resistance issues and has presented significant results against targeted MDR strains that are growing immensely. Therefore comprehensive knowledge for its mode of action, safety issues and impact on the environment and society is necessary. Physical and chemical features of metal NPs synthesised using green innovations, such as plant extracts, have been found to be appealing and increasingly used in biotechnology due to their low toxicity and significant environmental and human

benefits. Green NPs are more stable and high yielding, and they also have antibacterial action. Plant extracts which are enriched with phenols and alcoholic compounds were effective as antibacterial agents. These extracts are helpful to reduce and stabilize NPs by reducing of metal salt without harming environment by toxic chemical residues (Raveendran et al., 2003). Moringa plants are combined with antibiotic and chitosan to encapsulate but not pervious much explored for the synthesis of NPs (Balamurugan et al., 2015; Nouman et al., 2014).

Antimicrobial agents delivered to the site action by incorporating in nanocarrier system therefore nanomedicines are developed using biopolymers such as chitosan polymer, which has found prominent results in drug delivery and NPs formation. According to reports, cationic property and ability to dissolve in aqueous media are the distinctive factors of its success. Moreover, it can bind to mucosal surface to stay longer and help to enhance epithelial permeability. Additionally, biopolymers are biocompatible and less toxic, fundamental requirements in antibiotic translocation. It is worthy that, compared with solutions, chitosan is more effective in improving drug absorption when synthesize in the form of nanoparticles (Gao et al., 2011; Yadav et al., 2020). Chitosan comprised of metal NP as antibiotic vector in nano-carrier structure (Yusof et al., 2019) and binding to drugs make it biodegradable, environment friendly, cost efficient, easy to synthesize with least hazards. Through the, the size and shape of NPs in chitosan NPs is stabilized in an electrostatic interaction between the amine group of chitosan and the hydroxyl group of antibiotics. Encapsulated antibiotic agents of chitosan NPs expressed great enhancement in antibiotic activity (Yadav et al., 2020). Nano-carriers have ability to provide controlled antibiotic release until certain level at targeted site. Nanoparticles have successfully been used as vector using liposomes, polymeric nanoparticles, dendrimers and inorganic NPs to deliver antibiotic (Huh & Kwon, 2011). Encapsulation, adsorption or chemical bonding with antibiotics has expressed reputed therapeutic index. Consistent research studies and positive outcomes have led to many NPs-based drug translocation structures being approved for clinical treatment of infectious diseases, while many other drugs are currently in various stages of preclinical and clinical trials (Briones et al., 2008). Although there are various preventive and

management measures, there is an urgent need for efficient treatment of mastitis (Dilshad et al., 2010).

Therefore, the aim of the present research work is to synthesize new and unique nanomaterialsbased on metallic oxide NPs that were green synthesized then these metallic oxides NPs were conjugated with Ciprofloxacin and encapsulated in chitosan NPs by using ionic gelation method. The synthesized various combinations of nanomaterialswerecharacterized by gold standard techniques and evaluation for antimicrobial studies against mastitis causing microbial pathogens during this study. Invivo antimicrobial activity of the most effective and broad-spectrum nanomaterial was also evaluated using rabbit as animal model.This new strategy is expected to extend the life of antibiotics while decreasing and reversing the concept of multidrug resistance. There is passionate hope for battling against MDR pathogenscausing mastitis in the livestock animals of Pakistan.

1.2. Mastitis

Mastitis, is define as inflammation of udder tissues due to pathogenicity of bacteria, algae and fungi, which injures mammary glands and causes pain and swelling. (Radostits et al., 2006).The inflammatory response occurs to destroy or counterpoise noxious substances and allow the glands to function normally to heal. Invasion of leukocytes develops inflammation causing an increased somatic cell count (SCC) of milk which in indication of unhealthy udder and poor quality of milk (Harmon, 1995). Mastitis is the common diseases that dairy industry is suffering from with massive losses in reduced production capacity of dairy cows, decreased animal value and expensive to treat (**Figure 1.1**).

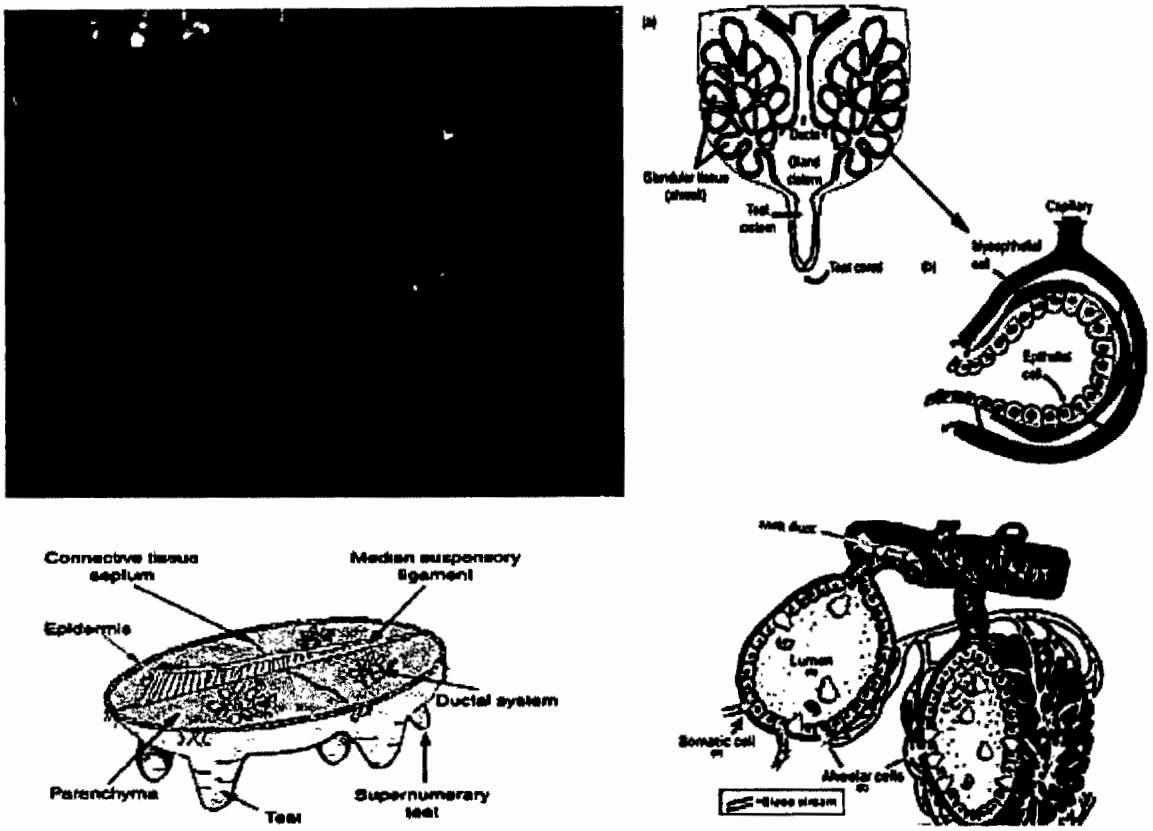

Figure 1.1: Cattle suffered from mastitis , mammary gland, internal structure of teats and udder (Maqbool, 2015; Sharif & Muhammad, 2008).

1.2.1. Types of Mastitis

Subclinical and clinical are two major types of mastitis causing decline in milk production, the discarded milk after medication, the cost of treatment and the significant economic loss caused by premature slaughtering (Abebe et al., 2016; Bradley, 2002). Strong inflammation develops clinical mastitis with drastic changes in milk (blood clots, flakes), swelling of mammary glands, appetite loss and high fever otherwise mostly mild clinical mastitis is not detectable until fore-milking. *Streptococcus agalactiae*and *Staphylococcus aureus* mastitis bacteria been restrained effectively by post-milking treatment, dry milk therapy, well-maintained milking equipment and slaughtering of cows suffering from acute mastitis (Makovec & Ruegg, 2003).

1.2.2. Symptoms and Causes

Some general mastitis symptoms been observed in cows, such as blood, flakes, sanies in milk, fever, swelling of mammary glands, appetite, blocked teats, decreased production, salty milk taste and teats ulcers. Bacteria (*E.coli, Proteus spp, Pseudomonas spp, Klebsiella spp, Seratia spp)* are major causative agents of mastitis (Ghafar et al., 2020) while yeasts (*Candida albicans*), algae and mycoplasmas barely cause mastitis (Harmon, 1995). *Staphylococcus aureus, Streptococcus agalactiae*, *Mycoplasma spp.* and *Corynebacteriumbovis* are known as contagious pathogens to cause acute sub-clinical infection by residing at teats and spreading through milking (Radostits et al., 2006). The main cache for these pathogens (*E. coli, Klebsiella spp, Strept. dysgalactiae* and *Strept. uberis*) is the living environment of cattle where they cause sub-clinical and short duration infections (Smith et al., 1985). The epidemiological characteristics of exposure to mastitis involves transmissible factors, unsanitary conditions and inappropriate milking habits (Ghafar et al., 2020).

1.3. Commercial Impact of Livestock Industry

Livestock accounts for 40% of estimated global agricultural production. This has provided employment opportunities for approximately 1.3 billion people around the world and directly helped the lives of 600,000 farmers of under developed countries by contributing milk production, fiber, fertilizers and fuels and meat production directly from domestic animals (Salmon et al., 2020; Sansoucy, 1995).

1.4. Financial Status and Milk Production in Pakistan

Pakistan holds 3rd position among the world's highest milk producing countries, almost 36 million tons milk from approximately 130 million animals, 47.8 M cows while 40 M buffalo (Finance, 2017; Hemme, 2007). Livestock raises milk in four ways: (1) subsistence level dairy farming in rural areas (2) countryside centered small farming (3) countryside business farming (4) sub-metropolitan business farming (Thomson et al., 2000). Small dairy farming (rural life and rural market-oriented) in Pakistan < 10 cattle per flock account for more than 90% of the total

number of cattle (Zia et al., 2011). These small farms on average produce about 1,200 liters per lactation from buffalo, and that of dairy cows is about 1,000 liters, which accounts about half of the national average of these two breeds (Ghafar et al., 2020; Iqbal et al., 1999; Zia et al., 2011).

Livestock is an important food source for nearly one billion people around the globe (McLeod, 2011; Raney, 2009). Milk as a major product comes from approximately 123 million dairy farms around the world. It occupies a major position among agroindustry and cattle farming within Asia and Africa (Hemme, 2007). It is estimated as 68% dairy farmers are located in Indian subcontinent and more than 80% are modest-scaled. Pakistan and India in South Asia shares two-third dairy farms and quarter of the world's milk production (Ghafar et al., 2020; Hemme, 2007). Livestock health issues are the main limiting factor in milk production, especially in small-scaled farming, caused by substandard disease identification, examining and less knowledge of disease epidemiology (Devendra, 2001).

1.5. Interlacingthe Economy of Pakistan with Agriculture, Livestock and Dairy Industry

Pakistan has fertile land and proper irrigation structure, so around 27% of the country's 79.6 million hectares of land is availed for agriculture which provides 47% employment with 24% GDP share in economy (Burton et al., 2012). This is a very vital research aspect that Pakistan has been waiting for to fully utilize its potential with largest economy sector (Iqbal et al., 2005). In the agricultural industry, animal husbandry is extremely significant and accounts for 51.1% share of agricultural economy in Pakistan's with 167.5 million animal heads (Nouman et al., 2014). In Pakistan agriculture and livestock sectors are significantly correlated with each other because animal husbandry perform significant role to promote social and economic progress in countryside (Akhtar et al., 2012; ul Hassan et al., 2014). About 53 million rural populations of 8 million families directly or indirectly depend on livestock for living (Finance, 2017; Ghafar et al., 2020; Rehman et al., 2017). Nowadays, due to substandard quality of fodder, high disease ratios such as mastitis, obnoxious protection and costly modern veterinary medicines, production rate of meat and milk in Pakistan has decreased rapidly (Mathias, 2004). Most farmers have 4-5

animals so costly modern drugs are unreachable by them and more interestingly these drugs produce adverse effects to consumers and animals, such as high antibiotic residues in milk and other animal by-products.

1.6. The Influence of Cattle Breeds On Milk Production In The Dairy Industry of Pakistan

Buffaloes are the major milk producing animals in Pakistan, signifying about 48 percent of the total dairy herd and providing 62 percent of total milk production. The three principal breeds famous for milk production are Nili, found mostly in Punjab province, and Ravi and Kundi, found mostly in Sindh (Gao et al., 2013). The cattle population is slightly larger than that of buffaloes, but cows produce on average only about 55 percent of the yield of buffaloes. All Pakistan's indigenous cattle are Zebu (humped type, Bosindicus). There are 15 recognized breeds in the country which are Red Sindhi and Sahiwal found well known internationally dairy cattle breeds**(Figure 1.2)**(Iqbal et al., 2019; Stafuzza et al., 2017).

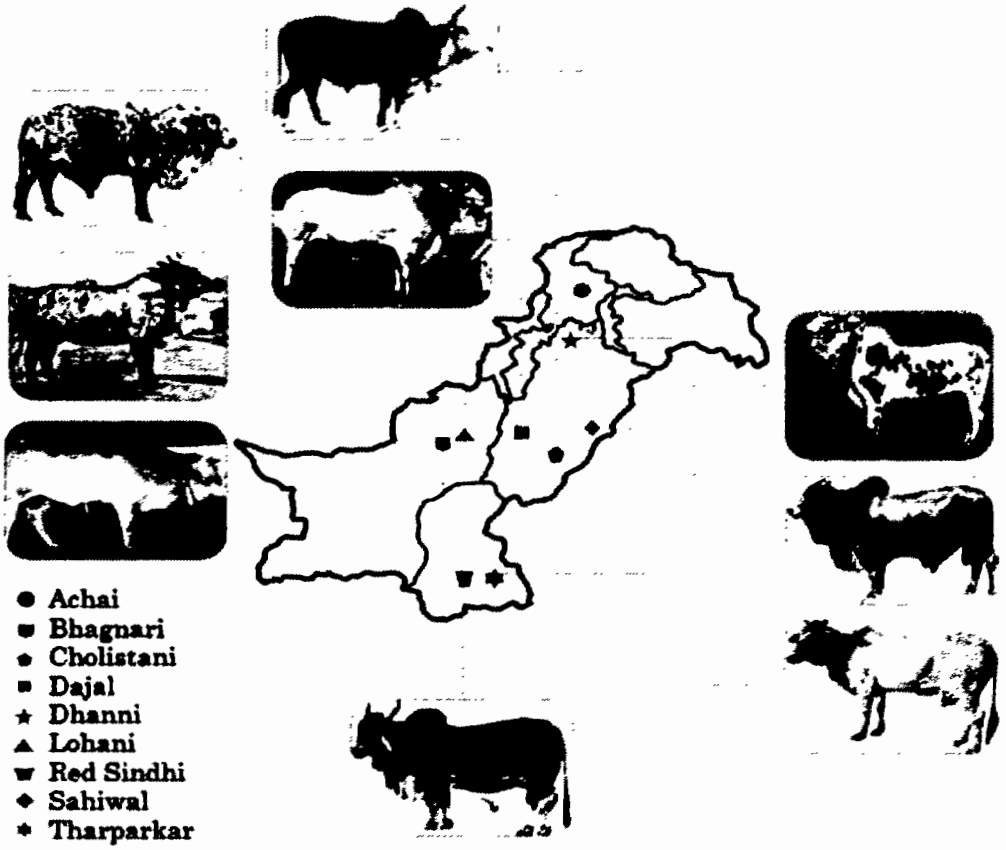

Figure 1.2: The dairy farms of Pakistan have various breeds (Iqbal et al., 2019).

1.7. The Adaptation of Pakistani Breeds of Cattle Against Infectious Diseases

Some of Pakistani breeds have specific adaptations against infectious diseases in which presence of receptors which are important and that have certain pattern recognition with peculiar behavior to detect microbial pathogens and generate instinctive immune responses against infectious microorganisms. These mammalian receptors are membrane-bounded, coupled to macrophages and dendritic cells, and respond to the microbial components of antigens. Receptors induces cytokine production after binding to bacterial lipopolysaccharide in mammary gland and endometrium epithelial cells, thereby playing a key role in arousing intrinsic immunity against pathogen attack (Cronin et al., 2012; Ibeagha-Awemu et al., 2008). The expression of Toll-like receptor signal transduction pathways in Red Sindhi, Tharparkar, Achai, Bhagnari, and Lohani in

39 medium-impact variants with genes, was found unnecessarily excessive, which indicated that most Pakistani marker varieties has developed its immunity-related genes against high or medium impact to changes in infectious environment in tropical regions (Iqbal et al., 2019).

1.8. Human Health Concern and Mastitis

Mastitis is considered as highly pervasive and expensive disease in dairy cows worldwide, especially concerned with dairy industry of under developed countries (Abebe et al., 2016). Economic loss caused by mastitis involves decreased lactations, veterinary costs, slaughtering of acute infected cattle and seldom deaths also (Seegers et al., 2003). Resistant pathogenic strains (*S. aureus, E. coli, Listeria monocytogenes, Salmonella spp*, etc) in dairy products are source of food-borne diseases and direct risk to public health. Most frequently effecting pathogen strain *S. aureus* abundantly found in livestock products and 68.8 percent of its strains are resistant to antibiotics. *S. aureus* is frequently found in mucosae and skin of cattle linked with subclinical mastitis from where it enters in milk chain (Normanno, Corrente, et al., 2007).In addition, mastitis has the potential for serious zoonotic diseases, which is related to the shedding of bacteria and their toxins in milk (Cervinkova et al., 2013).

1.9. Conventional Treatment of Mastitis

Treatments for mastitis are generally recommended based on the inflammation of mammary gland (without bacteria's information). Several researches on mastitis have been published in New York, documenting the effects of antibiotics on both untreated and antibiotic-treated cattle. (Lago et al., 2011; Pyorala; Pyörälä et al., 1994; Suojala et al., 2013). Another study reported that variety of Gram-negative pathogens treated with Fostiofur can better cure clinical mastitis through bacteriology, but this treatment did not change SCC or milk production during the rest of the lactation period (Schukken et al., 2011). Although, treatment with gram-negative (coliform) bacteria is not very effective yet, *Streptococci* and *Staphylococci* in United States are treated with intra-mammary antibiotics but *Klebsiella* and many clinical mastitis causing pathogens has no approved antibiotics. Only these two β-lactams (amoxicillin, ceftiofur(Schukken et al., 2011), cephapirin, cloxicillin, hetacillin, and penicillin) and a lincosamide (pirlimycin) classes have

sanctioned antibiotics by U.S. food and drug administration (FDA) but no intra-mammary product for milking animals since 2006 (Schukken et al., 2011).

Therapy is an alternative but cure against pathogenic mastitis (*Pseudomonas*) does not responds effectively. Therapy does not responds positively unless complete information about bacteria type. *E coli* mastitis has its intra-mammary antibiotics but mostly they are moderate cases and don't find any use of products for cure (Suojala et al., 2013). To cure infections, breast antibiotic tubes are the most common treatment for mild and moderate mastitis are commonly cured by using intra-mammary antibiotic tubes but generally antibiotics are applied while bacteria type is not known (Ruegg, 2014; Schukken et al., 2011). Mastitis in which the immune system is bacteria negative usually does not benefit of using antibiotics (Smith et al., 1985). Despite of that, bacteria-negative samples may appear in case if number of bacteria is less than the laboratory's limit of detection but cow still has infection, in such cases, antibiotic treatment is recommended.

In 1960s, semi-synthetic penicillins (ampicillin and carbenicillin) were introduced, and then were combined with β-lactamase inhibitors (amoxicillin plus clavulanic acid) to successfully treat infections induced by Enterobacteriaceae. For next 10 years, plasmid-encoded β-lactamases (especially TEM) greatly challenged this therapeutic advantage, lead to aminoglycosides (gentamicin and amikacin), the third-generation cephalosporin (cefotaxime and ceftazidime) and quinolone (ciprofloxacin) increased usage (Wellington et al., 2013) but bacteria became resistant eventually. Plasmid-mediated aminoglycoside resistance led to the massive use of third-generation cephalosporins and quinolones in late 1970s. In the early 2000s, the massive rise in extended-spectrum β-lactamases (ESBLs) in Europe had been most striking phenomena in antimicrobial resistance.

ESBLs are usually obtained through horizontal gene transfer and pose resistance to oxyimino-cephalosporins. Some are mutants of β-lactamase (TEM or SHV) carried by established plasmids stimulated from environmental bacteria (Wellington et al., 2013).

1.10. Discovery Timelines and Mode of Action of Antimicrobial Agents

Penicillin, the 1st antibiotic, prevented spread of contagious infections and cured diseases which ultimatly save many lives, especially at the period of Second World War (**Figure 1.3**). Despite that, in 1945 speech of Nobel Prize ceremony Sir Alexander Fleming pointed out the development of resistance may occur by bacteria to antibacterial treatments and shortly after, cases of inefficiency of penicillin were stated (Organization, 2014). This started to report the collapse of other micro-biotic agents against contiguous diseases, which were after that named as drug resistance or antibiotic resistance, a challenge to the efficiency of modern treatment options.

According to the mechanism of antibacterial activities, antimicrobial agents can be categorized in several groups. The main categories are: drugs to restrict cell wall formation, depolarization of cell membranes, inhibitory protein synthesis, inhibitory nucleic acid formation, and inhibition of bacterial metabolic pathways. In Table 1.1 summary of mode of action of agents from each groups of antimicrobials are described. Such a wide range of mechanisms seems to provide efficient control of organisms. Unfortunately, mismanagement of antimicrobials has led to the huge drug resistance problems by the time. Factors that evolved problem of drug resistance include: increased exhaustion of antibiotic drugs and inappropriate antimicrobial treatment prescriptions (Venter et al., 2017). Moreover, previous antibiotics utilizing patients are more susceptible of being infected by resistant bacteria and highly exposed to resistant organisms (Reygaert, 2018).

Table 1.1: Mode of action of different class of antimicrobials (Reygaert, 2018)

Mechanism of action	Antimicrobial Groups
Inhibit cell wall synthesis	β-Lactams Carbapenems Cephalosporins Monobactams Penicillins Glycopeptides
Depolarize cell membrane	Lipopeptides
Inhibit protein synthesis	Bind to 30S Ribosomal Subunit Aminoglycosides Tetracyclines Bind to 50S Ribosomal Subunit Chloramphenicol Lincosamides Macrolides Oxazolidinones Streptogramins
Inhibit DNA synthesis	Quinolones Fluoroquinolones
Inhibit metabolic pathways	Sulfonamides Trimethoprim

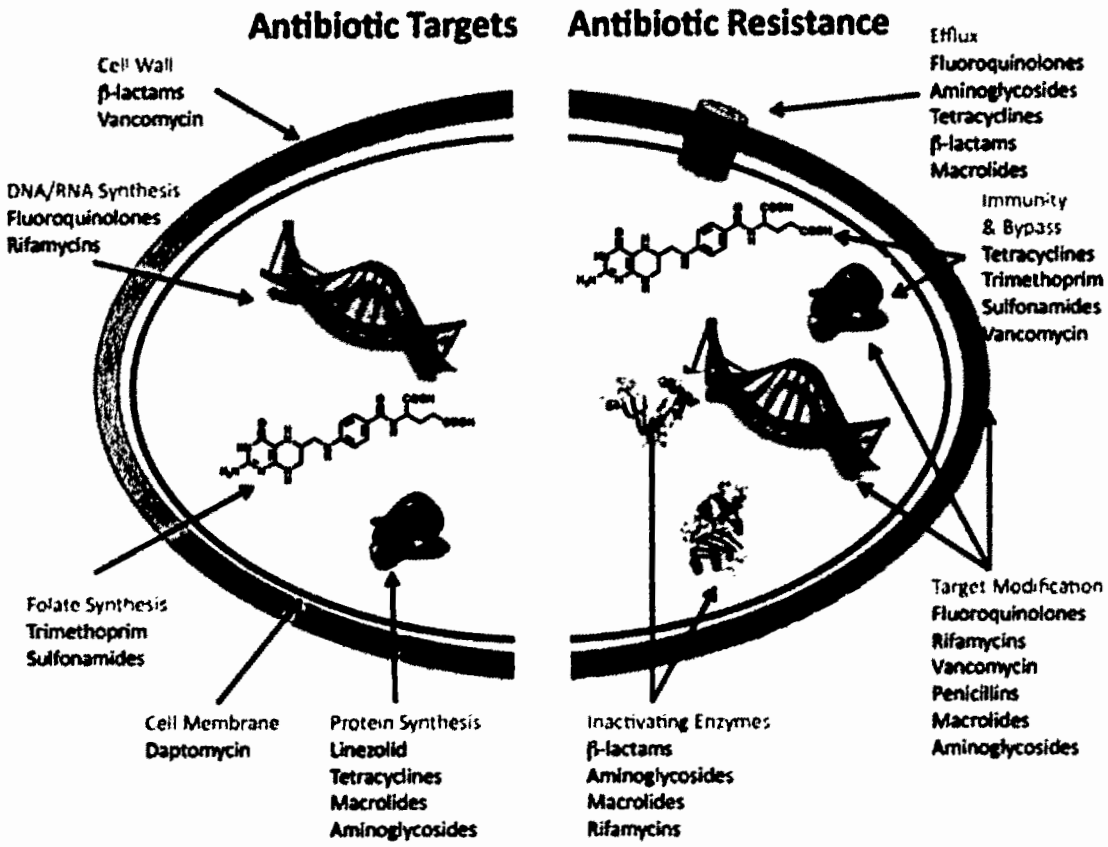

Figure 1.3: Targets of antibiotics and resistance mechanisms(Gualerzi et al., 2013).

1.11. Antimicrobial Resistance

Antimicrobial resistance (AMR) in microorganisms is specified as no response against standard dosage of clinical antibiotics (Group, 2011). It is the characteristics of microorganisms that overcome the antagonism of antibiotics and antibiotics seem to be less sensitive to them. Even if exposed to standard dosage of antibiotics, their survival rate is very high. By this mean, AMR phenomena enhanced rapidly due to misuse of antibiotics has lead huge risk to expanding scope of rational therapies of microbial diseases, decreasing efficiency, expensive and jeopardized treatments. Every newly discovered microbial drugs becomes ineffective by emerging resistance against it (Organization, 2014).

Moreover, AMR frequency may increase exponentially by transmitting resistant strains between humans and animals if it would not monitored and controlled (Littmann&Viens, 2015). In this globalization era, the prescribed treatment methods cannot detect resistant strains and diseases evolved into contagious. Uses of antibiotics during major surgeries is very common therefore eventually drug-resistant forms can developed freely (Hawkey& Jones, 2009). Several countries and research institutions have responded to the AMR problem and spent millions of dollars on monitoring and research to reduce AMR in animals. As extensive use of antibiotic agents as treatment, prophylactic or growth promoters in food animals has caused widespread public health issues (Woolhouse et al., 2015), the gradual ban of all antimicrobial growth promoter (AGP) in livestock being forced by European Union (EU) to control the AMR issue (Brown et al., 2017).

The development and expansion of drug-resistant bacteria originate from natural or man-propelled evolutionary interacting reasons. The prevalence dependence among animals by the use of antimicrobial usage (AMU) leads to selective pressure, under which mutations that mediate resistance or resistance genes are acquired by bacteria. AMU seems to occur major cause of AMR and its propagation (Moudgil et al., 2018). Rapidly developing resistance against antimicrobial agents is causing to move one step forward towards unique and progressive techniques of effective strategies for public health (Fridkin et al., 2015; Raghunath, 2008). Therefore, it is critical to investigate and study animal symbiosis and pathogenic bacteria, particularly the prevalence of AMR with economic value (such as milking animals), to know about possible AMR technique and develop innate cure systems having new targets. Therefore, a brief study of multidrug resistant (MDR) eukaryotes (quantitative knowledge of kinetics) and numerous determination of resistance in different hosts (humans and animals) and various ecological aspects are needed to address for effective estimations and design regulatory methods nationally and internationally.AMR in Gram negative bacteria has always caused severe infections worldwide, with increasing mortality rate (Vasoo et al., 2015). Antibiotic group of beta-lactam is increasingly facing resistant problem reportedly due to mobile beta-lactamases vulnerable to spread rapidly. There are many types of β-lactamases. Although AMR is reported

to be on the rise globally, ESBLs and carbapenemase are still spreading rapidly, and drug resistance in different regions very differently (Vasoo et al., 2015). Monitoring of AMR in clinically important pathogens in different parts of the word has been studied to cope with resistant microbes which has found to be severe in Asia where carbapenem resisted against colistin drug severely (Veeraraghavan et al., 2018). Colistin is still very effective against CR-organism but FDA has already introduced better substitutes like ceftazidime/avibactam and ceftolozane/tazobactam according to varied resistant microbes (Vasoo et al., 2015; Veeraraghavan et al., 2018).

1.12. Emergence of Resistant Pathogens

Mastitis is usually caused by *S. aureus* the gram positive bacteria but antimicrobial agents are becoming ineffective against *S. aureus Methicillin – resistant* (Edmond et al., 1999). The evolution of gram-negative bacteria resistance has attained a certain level, and clinical microbiologists have reached a consensus: multidrug-resistant gram-negative bacteria are new risk to public health. Animal mastitis is spread by *Enterobacteriaceae* and coliform. Modern medicines and policies needed to fight against gram negative MDR bacteria but no new antimicrobial product is at developmental stage (Wellington *et al.*, 2013). Gram negative MDR bacteria majorly reside in the intestines of humans and animals, especially getting antibiotic treatments. Contaminated water, food and environment are key pathways of its transmission, whether it is transmitted from humans or cattle, so it is a key area of control (Wellington et al., 2013). Bacteria become resistant due to specific structure. All G-ve bacteria contain a complex outer envelope comprised of two membranes separated by periplasmic space (Bolla et al., 2011). Bacterial lipopolysaccharides (LPS) pledge the cells with negative charge which makes specific molecules impermeable, especially hydrophilic molecules and negatively charged molecules, while promoting the attachment of positively charged molecules. Variety of protein channels in the outer membrane allow substances, nutrients, drugs and chemicals transportation inside and outside the cell (**Table 1.2**) (Bolla et al., 2011).

1.12.1. Modifications of Porins

In bacteria, the concentration of intracellular and extracellular drugs is mainly controlled by porin and efflux transporters. Hydrophobic elements can move across membrane through concentration gradient, while hydrophilic elements use porin for actively transportation because LPS resist permeability hence, this modified resistance is embraced by Gram negative bacteria (Bolla et al., 2011).

1.12.2. Over Expression of Efflux Pumps

Efflux resistant mechanism occur due to plasmid-encoded tetracycline efflux pumps in *E. coli* and *1st* discovered in 1980 (McMurry et al., 1980). Antimicrobial resistance was thought to be similar as antibiotic resistance genes due to acquisition from horizontal gene transfer (HGT) from the tetracycline producer (Benveniste & Davies, 1973) but later antibiotic efflux compounds were not found plasmid encoded or antibiotic specific (George & Levy, 1983). Prokaryotic chromosomes, as well as the chromosomes of archaea and eukaryotes are rich with genes coding of these compounds (Stavrovskaya & Stromskaya, 2008). Many scientists have elaborated AMR by certain bacteria due to antibiotic efflux compounds (Poole, 2007). In Gram negative microorganisms, the down-regulation of porins and the over-expression of efflux pumps have been identified as the main factor of resistance to all bacterial elements. Genes to regulate the efflux pump can be present on plasmids and chromosomes so, resistance can be inherent or acquired (Bolla et al., 2011).

1.12.3. Antibiotic Target Sites Modifications

Modifying the target site also develop resistance in Gram negative microorganisms. Penicillin binding proteins (PBPs) develop cross-links among peptidoglycan units, β-lactam antibiotics capture the PBPs, and further cell wall formation stops because it does not support cell wall synthesis mechanism any further. Because the target site of antimicrobial is modified, the enzyme active site does not allow binding of antibiotic.

1.12.4. Beta Lactamase Production

An important resistance method among Gram negative bacteria is the evolution of particular catalytic enzymes to cleave and after that rendering antibiotic ineffective. Most important

enzyme degrade β-lactamase (Bolla et al., 2011). β-lactamases is present in several forms, such as penicillin enzyme, cephalosporinase, ESBL, carbenicillinase, oxalamidase and carbapenemase divided into two classes, namely Bush-Jacoby-Medeiros classification system and Ambler classification (Bush & Jacoby, 2010).

Table1.1: Resistance mechanism developed by microbes against antimicrobial agents.

Resistance Mechanism	Antimicrobial Agents
Limiting Drug Uptake	Glycopeptides
Modification of Drug Target	*β*-lactams
	Glycopeptides
	Lipopeptides
	Aminoglycosides
	Tetracyclines
	Macrolides
	Lincosamides
	Oxazolidinones
	Streptogramins
	Fluoroquinolones
	Metabolic Pathway Inhibitors
Inactivation of Drug	*β*-lactams
	Chloramphenicol
Active Drug Efflux	Tetracyclines
	Fluoroquinolones

1.13. Antimicrobial Resistance (AMR) and One Health

One Health is the collaborative effort of multiple health science professions to attain optimal health for people, domestic animals, wildlife, plants, and our environment. The drivers of antimicrobial resistance include antimicrobial use and abuse in human, animal, and environmental sectors and the spread of resistant bacteria and resistance determinants within and

between these sectors and around the globe. Most of the classes of antimicrobials used to treat bacterial infections in humans are also used in animals. Given the important and interdependent human, animal, and environmental dimensions of antimicrobial resistance, it is logical to take a One Health approach when addressing this problem. This includes taking steps to preserve the continued effectiveness of existing antimicrobials by eliminating their inappropriate use and by limiting the spread of infection(Udaondo & Huertas, 2020). Major concerns in the animal health and agriculture sectors are mass medication of animals with antimicrobials that are critically important for humans, such as third-generation cephalosporins and fluoroquinolones, and the long-term, in-feed use of medically important antimicrobials, such as colistin, tetracyclines, and macrolides, for growth promotion. In the human sector it is essential to prevent infections, reduce over-prescribing of antimicrobials, improve sanitation, and improve hygiene and infection control(McEwen & Collignon, 2018).

1.14. Emergence of Resistance in Dairy Animals

Milk is the very famous natural healthy commodity among people of all ages around the world, which staged a big dairy industry for dairy products and byproducts. The cattle raised on small-scale and organic farms, dairy animals rose on large-scale and commercial farms found more exposed to antimicrobial agents. Moreover animals as food product is consumed abundantly (Krehbiel, 2013). Increased demand as food product, veterinary drugs value has also increased up to US$20 billion in 2010 from US$8.65 billion in 1992 and was expected to reach US$42.9 billion by 2018 internationally (Hao et al., 2014). Bacterial strains are found resistant is due to resistant genes among them blaTEM gene resist against penicillin/amoxicillin/ampicillin (Bailey et al., 2011). Several other resistance genes against antibiotics are mentioned in given **Table 1.3**.

Table 1.2: Bacterial resistance genes against antimicrobial agents

Bacterial Genes	**Antimicrobial agents**	**References**
Van	Glycopeptides (avoparcin/vancomycin)	(Leavis et al., 2003)
Erm	Macrolides (erythromycin/tylosin/tilmicosin/kitasamycin/oleandomycin)	(Ramos et al., 2012)
vatD, vatE, erm, satA	streptogramins (virginiamycin/quinupristin-dalfopristin)	(Ramos et al., 2012)
Sul	Sulfonamides (sulfisoxazole/sulfadimethoxine/sulfamethazine)	(Cain et al., 2010)
Tet	Tetracyclines (chlortetracycline/oxytetracycline/doxycycline)	(Ramos et al., 2012)
rgpA–F, mbrA–D	Polypeptides (bacitracin)	(Cain & Hall, 2012)
cmaA, floR, fexA, fexB, cfr, cat	Amphenicols (chloramphenicol)	(Cain & Hall, 2012)

S. aureus bacterial strains has found consistently resistant against methicillin and vancomycin in several research studies in cattle (Sasidharan et al., 2011). Out of 2,650 samples, only methicillin resistant were found 16.2% (Jamali et al., 2015) and about 3.75% resistance showed by *S. aureus* in experiment conducted by previous study(Normanno, La Salandra, et al., 2007). Several other researches held in western laboratories had extracted resistant pathogens from dairy products for example *L.monocytogenes* for oxacillin and penicillin resistance in Lebanon (Harakeh et al., 2009), MDR *Listeria spp.* from Iranian 7% dairy items (Rahimi et al., 2010), *Salmonella spp.* in Ethiopia of almost 10.7% livestock samples (Addis et al., 2011). *E. coli* and ESBLs isolated from healthy milk and food cattle having infections (Sawant et al., 2007). Some

of the research conducted in Asia also reported antibiotic resistant pathogens in milk and milk products (Carattoli, 2008; Ewers et al., 2012).

1.15. Animal–Human Interface

As reported in humans' medicine, even at reasonable dosage, Antimicrobial usage (AMU) in veterinary practice may choose genes that encode drug resistance. These antibiotic resistant strains can easily transmit to humans by any means of food chain, environment or direct animal interaction (Lhermie et al., 2017). AMU and antibiotic resistant traits transmission among animals and humans have been reported directly correlated in many studies. Famers, food workers and vets are more likely to affect directly to AMR compared to consumer of contaminated dairy products (Chang et al., 2015; Marshall & Levy, 2011).

Recent studies have reported the existence of abundant resistant bacteria and related genes in various dairy items (Coetzee et al., 2016; Liu et al., 2016). This problem is particularly severe in under developed countries, because these countries do not have reputable strategies or instructive measures, overloaded contagious diseases and poor health care facilities are also prevailed (Jamali et al., 2015). MDR bacteria have been reported from food cattle in under developed countries where AMU is not regulated (Maron et al., 2013).

1.16. Surveillance and Monitoring

In view of the increasing pressure of antimicrobial resistance (AMR) in the veterinary system, World Organization for Animal Health (OIE) launched monitoring protocols in some countries and surveillance programs in 1997. These protocols were acknowledged in 2003 and at the same time the WHO's Global Strategy against AMR contamination was introduced. Collaborative consultations between WHO/OIE/FAO experts established the Codex Alimentarius Ad Hoc Commission's Intergovernmental committee for AMR and suggested "Guidelines for Risk Analysis of Food-borne Antimicrobial Resistance" endorsed in 2011 (Commission, 2011). The Terrestrial Animal Health Code discussed the harmonization of national level monitoring plans,

discussed the monitoring of AMU models in food cattle, and the wise use of antibiotics in veterinary drugs; and animal AMU causing AMR risk evaluation (OIE, 2013; OIE, 2010).

1.17. Alternate Management Strategies to overcome resistance

AMR escalation with slow emerging new antibiotics has led to a lack of reasonable treatments for microbial diseases. At present, from the discovery, clinical efficacy and safety evaluation to the approval stage, the transportation of new medicine costs more than twice (DiMasi et al., 2016; DiMasi et al., 1991). Therefore, research and introduction of new drug is becoming more difficult, and antibiotic studies are no more a striking opportunity to invest for fast and generous outcome. Now is the time to seek novel and modern ideas to reduce resistance against antibiotics and accelerate the evolution and launch of new, safe and non-resistant medicine.

1.17.1. Vaccines

Vaccination is described as a potent method to prevent or even eliminate livestock diseases. Since no resistance to vaccines been reported, vaccines are considered an effective substitute to antibiotics have attracted widespread attention due to their characteristics and mode of action (Mishra et al., 2012). Generally, vaccines can be divided into three categories, namely, inactive (antigens with adjuvants), attenuated (live vaccines) and recombinant vaccines (subunit antigens or genetically engineered organisms) (Wang et al., 2016). Vaccinations in cattle help to prevent infections and are beneficial to animal health and food production. Reduced consumption of antibiotic elements, increased food production, decreased antibiotic resistance and most importantly decreased zoonotic and food transmitting pathogens targets has been achieved through vaccination (Founou et al., 2016; McVey & Shi, 2010).

1.17.2. Phytocompounds

Humans and animals are taking medicinal benefits from plants since ages. Underdeveloped countries has common practice of traditional medication of animal diseases especially in villages (Kalayou et al., 2012). The agricultural community easily goes toward traditional, natural, non-toxic, cost efficient and easily available therapies that are mainly composed of plant ingredients/extracts. Ethnic veterinary science denotes the interdisciplinary research of old-school knowledge, practices and techniques related to livestock health (Kalayou et al., 2012).

Plants are comprised of various biologically active secondary metabolites or phytocompounds i.e. glycosides and alkaloids, anthocyanins, coumarins, flavonoids, phenols, saponins and terpenoids(Atanasov et al., 2015; Dhama et al., 2014), many of them are part of animal diet for growth promoters and health protection agents (Cheng et al., 2014; Hashemi & Davoodi, 2011). Phytocompounds with broad-spectrum antibacterial performance can become a substitute against conventional vet antibiotics (Atanasov et al., 2015; Savoia, 2012). Phytobiotics serve meditative performance in animal diet i.e. anti-microbial, anti-inflammatory and antioxidant activity. Tea tree oil and its active component (terpinen-4-ol) resulted as significant role in mastitis cure (Taga et al., 2012).

1.17.3. Plant Essential Oils (EOs)

In addition to other plant ingredients, EOs are now being used commonly in dairy farming. Phenolics can be retrieved from rich antioxidant, anti-inflammatory and antimicrobial properties of pomegranate extract (Reddy et al., 2007). Phytocompounds from 18 herbal plants showed effective results to cope with MDR *Acinetobacter baumanni* growth (Kipre et al., 2017). Moreover, MRSA (Kipre et al., 2017) and bacteria forming ESBLs (Singh et al., 2012) were restricted by phytocompounds possessing antimicrobial property under in-vitro condition. In-vivo studies are extensively needed to validate the results phytocompounds in animals (Huyghebaert et al., 2011).

Several research studies peen performed on phytocompounds antimicrobial characteristic and their influence on pathogen virulence and other host factors (Dhama et al., 2014). Antimicrobial characteristic may amplify resistance, regulate cytokinins or reduce inflammation, remove toxin from cell but ultimately decrease cell signaling, damage cell membrane and electrolytes and promote phagocytosis (Dhama et al., 2014) .

1.17.4. Mastitis and Ethno Medicine

Mastitis is 2nd most commonly found infectious disease of cattle in Pakistan (Akhtar et al., 2012). Many traditional plants have been found medicinally beneficial against mastitis like *Zingiberofficinale* resist against *S. aureus* and *Streptococcus agalactiae* development

(Poeloengan, 2011). *Allium sativum* showed remarkable performance against gram positive and gram negative bacteria resistant to antibiotics (Fujisawa et al., 2009). Moreover *Allium* crops pose strong antibiotic activity for variety of pathogens as 150 g of *Allium cepa* mixed with *Trachyspermumammi* can cure mastitis in just 5 days (Dilshad et al., 2010).

1.17.5. Probiotics, Prebiotics, and Synbiotics

The ban of dietary antimicrobial agents attracted a great deal of attention toward the application of probiotics, prebiotics, and synbiotics for production of safe food along with improved gut health. With the advent of new antibiotic resistance strains, probiotic strains are gaining popularity in both medical and livestock sector. Restricting the antibacterial drugs use in diet has made alternatives choice to apply probiotics, prebiotics and synbiotics to produce safe food and better intestinal health. Prebiotics strains are progressing rapidly in medical science against antibiotic resistant traits (D'Orazio et al., 2015; Imperial & Ibana, 2016). Probiotic strains are suggested to directly feeding as growth promoter and best substitute of AMR (Muñoz-Atienza et al., 2013). Consistent use of antibiotics damages intestinal systems while giving selective probiotics and prebiotic ingredients can supplement antibiotics.

1.17.6. Phage Therapy

Bacteriophages have attracted the scientists as antibacterial agents with medical benefits because they have intrinsic potential for bacterial infection and lysis. Phage therapy specifies a small bacterial group and can avoid malnutrition usually linked with antibiotic treatments(Calap & Martínez, 2018).

1.17.7. CRISPR-Cas

Genetic techniques for temperate phages to deliver DNA have been suggested to eliminate AMR by increasing the sensitivity of bacteria against antibiotics and kill resistant strains selectively. Sensitivity traits are associated with tellurite resistance genes, which allow tellurite and antibiotics sensitive gene selection leaving resistant gene apart. Anyhow, it has some disadvantages like unable to stop horizontal gene transfer, contracted host range and strains only sensitive to selective antibiotics (Sharma et al., 2018).

1.17.8. Quorum Quenchers (QQ)

Quorum sensing helps bacteria to communicate and coordinate among themselves and the ambient environment, and also been suggested as one of the bacterial pathogenicity method to colonize and express virulent genes in host. Hence, any method for QS event in microbes, in addition to expressing drug resistance, may also combat bacterial infections in veterinary medicine as reported against fish pathogens earlier. Widespread impact of QQ against MDR strains with possible effects is needed to be addressed precisely (Sharma et al., 2018).

1.17.9. Beta-lactamases Inhibitors

β-lactamase comprised of fundamental Enterobacteriaceae resistance method. Two techniques can be adopted to overcome it either find its inhibitors or discover new non-β-lactamase targeted antibiotic (Babic et al., 2006). Three β-lactamase inhibitors: clavulanic acid, sulbactam and tazobactam are already present. They become target of β-lactamase due to their similar structure to β-lactam, so they can save actual drug site (Babic et al., 2006).

1.17.10. Enhancing Antibiotic Influx

Due to restricted access in Gram negative bacteria against resistance, the antibiotics penetration is needed to be enhanced. Certain bioactive molecules and chemosensitizers like detergents, surfactants, chaotropic agents, polymyxins and antimicrobial peptides may prove as efficient elements (Babic et al., 2006).

1.17.10. Destabilization of LPS Barrier

Destabilizing LPS layer can make outer membrane possible to invade by usage of chaotropic agents to promote diffusion of hydrophilic compounds through lipid bilayer membrane (Bolla et al., 2011; May & Grabowicz, 2018).

1.17.11. Blocking the Efflux

Several antibiotics pass through the outer membrane barrier ejected by the efflux pump. Currently, efflux pump activity blockers are specific drugs to test Gram negative bacteria from natural and synthetic origins (Kourtesi et al., 2013; Martins et al., 2008). Although future for substitutes against MDR strains in cattle is bright but strain-specific action of probiotic strains

limits its applications. More problems needed to be addressed include variations among host species, age, food plan and pathogenic stress extent and dosage control.

1.18. Nanoparticles Development, Alternative Strategies To Combat MDR Pathogens

Nanomaterials having inherent antibacterial property or can enhance the overall efficiency and safety of antibiotics are called "nano antibiotics" (Huh & Kwon, 2011). Encapsulation of nanomaterials may come under its definition, which works as vector to transfer drugs to the target. They enablepermeation of antimicrobials , drug absorption, augment route of antibiotics without humiliation of antibiotics (Thorley & Tetley, 2013). Recently alternative strategies that are in line for the development as potential alternatives to conventional antibiotics. Apart from efforts were being made to develop new antibiotics, several other approaches are being explored, which can help to tackle infections caused by MDR pathogens. This includes the development of plant-based drugs, antimicrobial peptides, bacteriophage therapy, CRISPR-Cas9, and antibiotic conjugates with nanoparticles. Among all the alternative therapeutic approaches, nanotechnology is more popular and fascinating field of science, which can inhibit the growth of microbes efficiently at nano-scale where materials displayed excellent properties. Nanotechnology has high efficacy and therapeutic index against pathogens, making it an attractive therapeutic strategy. Nanoparticles are an exciting new treatment option for infections, especially those triggered by multidrug-resistant bacteria. Nanoparticles could be applied alone or in combination with antibiotics that can provide excellent synergistic outcomes to combat MDR pathogens(Patra et al., 2018).

1.19. Nano-antimicrobial agents (NAMs) with Intrinsic Antimicrobial Properties

NAMs divided in two classes, first class possess pure nanoparticlesand their metallic oxides with direct killing effect on microbial pathogens including silver, gold, iron, copper, zinc, titanium, and cerium. Whereas second class comprised of nanomaterials containing metallic oxides and synthetic antibiotics encapsulated with polymers and act as vector by enhancing antimicrobial

potential of coated nanomaterials and antibiotics(Jamil & Syed, 2017).Antimicrobial mechanism of metallic oxides nanomaterials mainly preceded after the attachment and penetration in the bacterial cells may occurs which was facilitated by electrostatic attraction. In the next step, generation of ROS occurred after the interaction of microbes with NAMs. The generation of cations by the oxidation of metallic oxides NPs and reactive oxygen radicals (ROS) followed by the dispersion of nanomaterials into the growth medium under incubation during the antibacterial activity against microorganism. The generation of ROS (•O2 –, •OH and H_2O_2) take place which ultimately initiate lysis of bacterial cell by damaging cellular content like cell wall, cell membrane, DNA and inhibits protein synthesis as shown in the **Figure 1.4**.

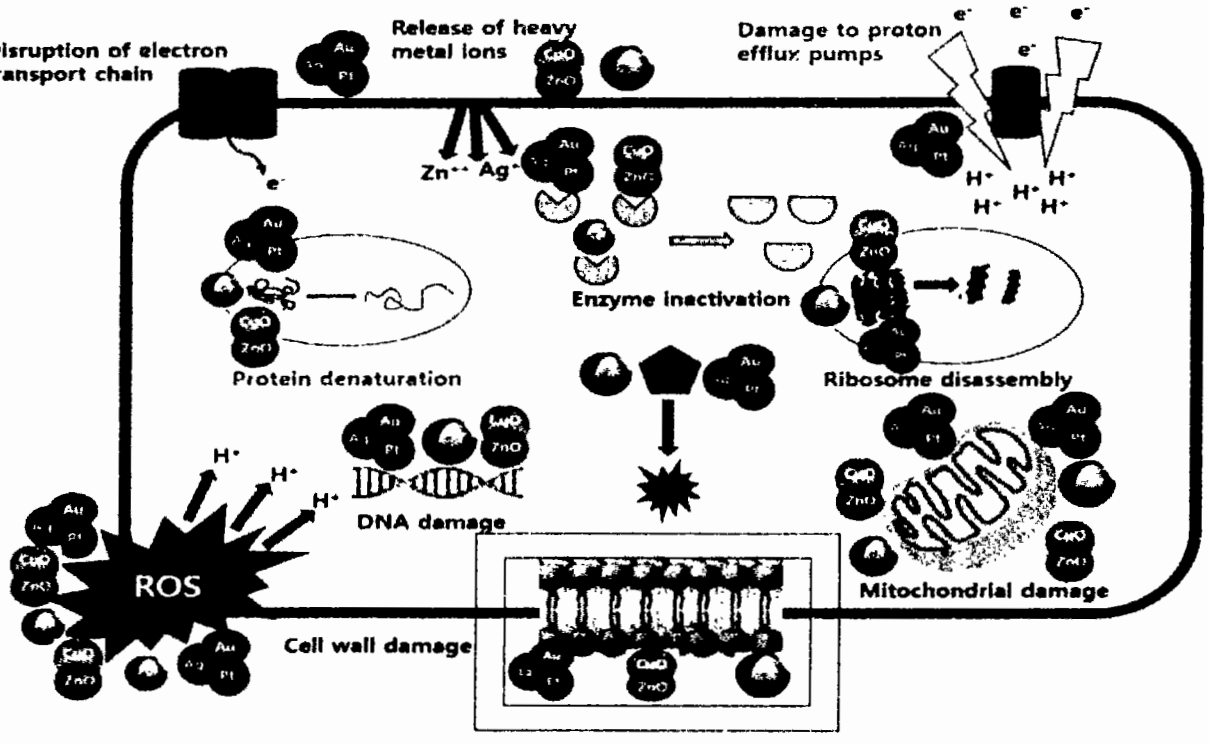

Figure1.4: Antimicrobial mechanism of metals and metallic oxides nanoparticles (Basavegowda& Baek, 2021).

1.19.1. Titanium dioxide (TiO_2) nanoparticles

TiO_2 NPs has been considered as generally recognized as safe (GRAS) additive in medical devices and biomaterials, hence it has been found attractive material for efficient adhesiveness and bactericidal activities (Kim et al., 2021). TiO_2 NPs synthesized using the proactive strategy, and nanoparticles of TiO_2 coated with chitosan nanoparticles to battle *E.coli* bacterial infections that cause mastitis in food animals. Despite considerable progress, pharmacists are limited in their antibiotic options due to fast evolving mechanisms of antibacterial resistance to traditional antibiotics (Zafar et al., 2020). TiO_2 work as antibiotic element (Hossain et al., 2014) and

bacteria resist very ineffectively against it because they produce reactive oxygen species to kill microorganism in photocatalytic process (Bald & Koul, 2013). Co-enzyme A (CoA) is also reduced by TiO_2 NPs (Hossain et al., 2014). Even so, some researchers denied the photocatalytic activity and reported the antibiotic performance of TiO_2 NPs actively (Hossain et al., 2014; Pelgrift & Friedman, 2013). TiO_2 NPs are reported with magical antibiotic effects to resist Gram neagtive bacteria and to disinfect water (Hossain et al., 2014). TiO_2 was found significant against *Staphylococcus aureus* resistant to methicillin and also possessed eradication ability of biofilm against *S. aureus*(Jesline et al., 2015).

1.19.2. ZnO nanoparticles

Zinc consider as an crucial trace element broadly occurs in all body tissues, including the brain, muscle, bone, skin, and so on. Zinc is coreconstituent of severalenzyme, due to this reason play important role in the synthesis of proteins, RNA and DNA. The US Food and Drug Administration (FDA) grade zinc oxides as a "GRAS" (generally recognized as safe) substance. With these possessions, ZnO NPs have gained more consideration in biomedical applications. Zinc oxide NPs have antibiotic featuresand extensively used as excellent antimicrobial agent (Jiang et al., 2018). The antibiotic activity of ZnO occurs through various methods, one of which is the production of intracellular ROS. ZnO NPs can cause cell death or excessive release of Zn^{+2} ions can cause changes in cell metabolism. *S aureus*, *S. epidermidis*, *Streptococcus pyogenes*, *Enterococcus faecalis Bacillus subtilis*, *Escherichia coli* and *Klebsiella pneumonia* are found vulnerable to ZnO exposure, due to their existence in food and water causing acute diseases ZnO can create a difference (Yusof et al., 2019).

1.19.3. Iron oxide (III) (Fe_2O_3) nanoparticles

Fe_2O_3 as a stable oxide occurs in nature as hematite mineral α-Fe_2O_3 (Irshad et al., 2017; Rufus et al., 2016). Its formation in crystalized hexagonal form has well explored but its possible antibiotic study has rarely reported. In the previous study, Fe_2O_3 had a potential antibacterial activity on *E. coli* and *S. aureus* with the increase in Fe_2O_3 NPs concentration (Rufus et al., 2016). Moreover, *Pseudomonas aeruginosa* also had a bactericidal effect, with a minimum inhibitory concentration of 0.06 mg/L (Irshad et al., 2017).

1.19.4. Magnesium oxide (MgO) nanoparticles

MgO is a mineral peroxidase with antibiotic properties against Gram positive and Gram-negative bacteria. MgO NPs has ability to destroy cell membranes, loss of intracellular contents and can lead bacterial cells to death(Stanić & Tanasković, 2020). Alkaline surface of MgO can produce ROS. MgO NPs were used to evaluate antibiotic properties against different bacteria i.e. *E. coli*, *P. aeruginosa*and *S. aureus*(Krishnamoorthy et al., 2012). Antibacterial property of MgO was reported because of attachment of surface oxygen on bacteria which increased surface area of NPs and degraded bacterial cell membrane effectively (Jin & He, 2011).

1.19.5. CuO nanoparticles

CuO NPs synthesized by using plant extracts is environmentally friendly, non-toxic, and biocompatible due to the existence of various metabolites. The metabolites such as flavonoids, amino acids, proteins, and saponins present in the green extract are responsible for the formation of Cu ions to CuO NPs (Akintelu et al., 2020).

The recent reports have demonstrated the synthesis of CuO NPs using various plant extracts such as *Ruelliatuberosa*, *Sidaacuta*, *Solanumlycopersicum*,*VerbascuThapsus*, *Acalyphaindica* and *Citr us aurantifolia* (Zaman et al., 2020). CuO NPs has antibiotic properties against universal bacterial strains like *E. coli* and *S. aureus* (Heinlaan et al., 2008; Lee et al., 2011). They have bioactive decontamination characteristics for many contiguous microbes and may be used as antibacterial agent (Akhavan & Ghaderi, 2010).

1.19.6. CeO_2 nanoparticles

Cerium was very scarce earth element commercially used asantimicrobial agent, polishing agents, ultraviolet absorbing compounds in sunscreens and solid electrolytes in solid oxide fuels. CeO_2 NPs have gained attraction due to its antibacterial activity and expressed effectively good results against Gram positive and Gram negative bacteria (Arumugam et al., 2015). Therefore, phytogenic development of CeO_2NPs is a user-friendly, inexpensive, safe and environment friendly technique to avoid multiple purification steps using toxic solvents (Uzair et al., 2020). *Oleaeuropea* leaf extract has already been used to synthesize NPs and to assess their antibiotic activity against Gram positive and Gram negative ATCC strains (Maqbool et al., 2016).

1.19.7. Polymeric Nano Carrier Systems (NCS)

NCS involves either inside or on surface addition of drugs.Nano-carriers comes under its definition, which works as vector to transfer drugs to the target. They facilitate in cell penetration, drug absorption, enhance pharmacokinetic and pharmacodynamics and avoid drug degradation (Yadav et al., 2020). NCS has ability to remove metabolites and can be degraded, no matter from any origin synthetic or natural. They act like liposomes against intracellular pathogens in the body and quickly captured by phagocytes. NCS encapsulation contribute more stable structure, whichmakes it preferable and compared to free antimicrobials to cope with MDR microorganisms. In addition, controlled and targeted release of drug operation can be performed by NCS (Briones et al., 2008).

1.20. Drug Loaded Nano Carrier Systems

Polymeric nanocarriers have recently emerged as suitable drug carriers mainly due to biocompatibility. In addition, their ability to transport therapeutic agents directly to the active site or target ensures drug safety and efficacy. Natural, synthetic, and semisynthetic polymers used to make nanoscale drug conveyors. These materials not only transfer potentially hazardous medications to the body's most vulnerable places (Mann et al., 2021). Drug release can be extended and sustained, so pharmaceuticals protected from chemical and proteolytic degradation thanks to biomimetic properties.Generally, encapsulated medicines have higher performance due to nano carrier system. Liposomes, solid lipid nanoparticles, polymer chitosan and dendrimers serve as complex and modern nano carriers to supply drugs largely (Bertrand & Leroux, 2012).

1.21. Significance of Chitosan Encapsulation

Chitosan has potential use in encapsulation of several therapeutic drugs, such as antimicrobial drugs, anti-inflammatory drugs, proteins and amino acids, by making sure its effectiveness at target site and other benefits of controlled releasing. This makes chitosan attractive not only in medical field, but also widely used in all scientific fields. Chitosan serve as antibiotic agent and antioxidant, because amino groups can scavenge free hydroxyl radicals, and its high degree of deacetylation improves its antioxidant performance, which can encapsulate many food materials

to make protection against harsh outer environment (low pH). Chitosan encapsulation also reduces the odor and unpleasant taste of bioactive materials and extends durability of food ingredients. Rather than antimicrobials and NPs encapsulated with chitosan they have many other benefits like wound healing , shelf life enhancement and nanocarrier of various compounds (Raza et al., 2020).

1.22. Release Profile of Active Ingredient from Chitosan

Encapsulation is usually categorized into three main steps. First step involves incorporation of active ingredients within the core of the microcapsules in emulsion condition. Second step involves formation of dispersion and solid material from liquid solution by spraying contents during stirring process. During final step, the droplets are sustained using various physical and chemical methods. Microencapsulation can ensure the stability and fixation of active ingredients, while the coating can achieve different degrees of release and protection as shown in the **Figure 1.5** (Raza et al., 2020).

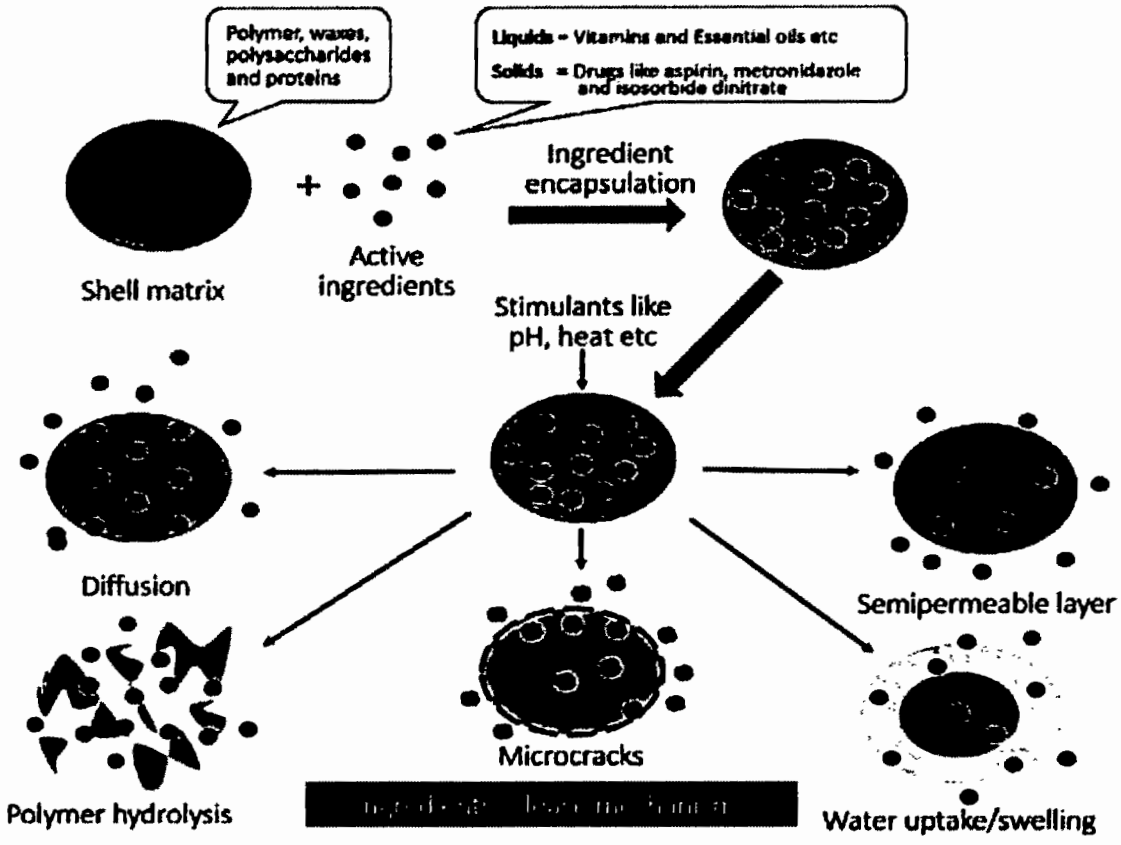

Figure 1.5: Release of active ingredient from chitosan encapsulation (Raza et al., 2020).

1.23. Advantages of Nano-antibiotics Over Conventional Antibiotics

Nano-antibiotics are preferred compared to traditional ones due to improved bioavailability by increased solubility, protection against premature degradation of drugs, both in vivo and storage duration. Bioavailability at low dosage will make able to get therapeutic results by reducing toxic effects of medicine and targeted release only. Infectious site will receive highest degree of medicine, and the antibiotic activity will be the best. Targeted and sustained availability of nano-antibiotics can minimize therapeutic dosage and frequency. The most critical problem of traditional antimicrobial treatment is development of antibiotic resistance (Shahverdi et al., 2007; Shrivastava et al., 2018) that can also be outclassed by nano-antibiotics (Pelgrift & Friedman,

2013). Most importantly nano-antibiotics are cost efficient and stable during manufacturing and transportation (Huh & Kwon, 2011; Sosnik et al., 2010).

The method of designing hybrid nanomaterials coupled with several antimicrobial action mechanisms is providing a new field to research on drug-resistant bacteria. Chitosan NPs have become an effective drug carrier due to their environment friendly and biodegradability behavior and are easy to modify. As a new antibiotic delivery mechanism, their broad spectrum use in loading antibiotic medicines or metal oxide NPs has opened up a slew of new possibilities for dealing with MDR strains and mastitis disease in the livestock industry.

Problem statement

Mastitis is becoming a major risk to the dairy industry because economy of Pakistan is mainly dependent on dariy products. The prevalence of pathogenic strains that are resistant to available antibiotics, in the food matrix poses a direct threat to public health. Treatment of widespread multidrug resistant mastitis-causing bacteria has become a difficult challenge for the current antibiotic reservoir. In order to combat infections caused by multidrug-resistant (MDR) bacteria, new target-oriented antimicrobials are urgently needed.

Aim and Objectives

The present study was carried out to synthesize metallic oxide nanoparticles using green route and conjugate with synthetic antibiotics simultaneous encapsulation in chitosan NPs to combat MDR pathogens that induce mastitis, as well as to test the efficiency of novel nanomedicines in an animal model.

1. To develop bio-based nano-carrier systems by encapsulating metallic oxides and synthetic antibiotic to combat MDR pathogens.

2. Invitro and *Invivo* evaluation of antimicrobial activity of developed bio-based nano-carrier systems.

CHAPTER 2

MATERIALS AND METHODS

2.1. Materials

The study was conducted using following materials and the details of the manufacturers are given respectively.

2.1.1. Materials

Chemicals: Ethanol (C2H5OH Sigma-Aldrich ,USA), Acetic acid (CH3COOH Sigma-Aldrich ,USA) , Titanium tetra isoproxide (TTP), Silver nitrate (AgNO3), Cerium chloride (CeCl3) , Iron chloride (FeCl3) and chitosan (Product number 448877 Sigma-Aldrich ,USA), glacial acetic acid and tripolypentasodium phosphate (TPP Sigma-Aldrich (St Louis, MO, USA)). DNA Taq polymerase (Perkin-ElmerTM, USA). Autoclaved dH_2

Reagents: Fetal bovine serum (FBS, Capricorn Scientific, America) ,California Mastitis Test (CMT, Pakistan), MTT (3-(4, 5-dimethylthiazol-2-yl)-2, 5-diphenyl tetrazolium bromide)

Culture Media: Muller-Hinton Agar (MHA), Brain Heart Infusion (BHI) broth, Nutrient agar (NA), Nutrient broth (NB), MacConkey agar, Citramide Agar, ESBL Media, Chrome Agar, Sabouraud Dextrose agar and Manitol Salt agar were also obtained from Sigma-Aldrich.

Cell Proliferation media: Dulbecco's modified Eagle medium (DMEM, GIBCO ,USA)

Cells stains: Annexin V, Propidium iodide (PI) The Gram staining chemicals (i.e. crystal violet, safranin, and iodine (Pakistan)

Kits: API 20E, API Staph, API 10S and API *C.albicans* (Biomerieux ,France), DNA Extraction Kit (Thermo Fisher, England, UK)

2.1.2. Apparatus and Equipment

Bacteriology

Following equipments were used for microbiological analysis i.e. Biosafety Cabinet of Level 2 (Model AC2-4S8-NS, UK), Compound and Light Microscope (ACCU, USA), Flow Cytometry, Fluorescence-Activated Cell Sorting (BD FACScan ,USA)). ELISA Micro plate

reader (BioTek China), PCR (Thermocycler, System 9700, Singapore), pH Meter (S/N07877, USA), Incubator (BK 4266, Japan), Colony Counter (CU, China) Hematology Analyzer (ACT, USA).

Synthesis of Nanomaterials

Following equipment were used for the synthesis of Nanomaterials, Magnetic Stirrer (ARE , Europe) , Hot Plate (IKA-RCT-B, China, Sonicator (LC30H Elma, Germany), Centrifuge (Sigma K8-14,Germany).

Characterizations Tools

Following equipment were used for characterization of synthesized Nanomaterials, FESEM (MIRA3 TESCAN), EXD (MIRA3 TESCAN), TEM (JEOL JEM-1010), XRD (Bruker D8 Advance), Zetasizer (Malvern), FTIR (Perkin Elmer ,Spectrum 100). The Perkin-Elmer UV-Vis spectrophotometer (Lambda 950 , UK).

2.2. Isolation of Mastitis Causing Microbes

2.2.1. Sampling Procedure and Diagnosis of Mastitis

A total of 1480 milk samples were collected from various dairy farms of Rawalpindi and Islamabad, two major cities of Pakistan including suspected milk samples which were submitted in National Veterinary Laboratory Islamabad for diagnosis of infection from nearby area of Rawalpindi and Islamabad. Milk samples were collected from May 2018 and August 2019 and screened for the diagnosis of mastitis by using California mastitis test. The microbial strains were isolated from mastitis positive samples including both Gram positive, Gram negative and yeast strains at the National Veterinary Laboratory Islamabad.

2.2.2. California Mastitis Test

California Mastitis Test was performed for the diagnosis of mastitis from the collected milk sample of suspected cattle by using Gonzalez et al method (Gonzalez et al., 1980). In the udder inflammation rise in leukocytes and a high level of alkalinity in milk would be expected, which was detected by California Mastitis Test (CMT). To perform CMT, standard peddle cup were used, 0.5 ml of suspected milk sample from each quarter was taken in the cup and equal quantity of CMT solution was mixed uniformly by circular movement of peddle cup. CMT

positive milk samples were identified by the formation of flakes which ultimately indicated animals were suffered from mastitis. In suspected milk samples pH was also noted by using pH meter as alkaline pH is also indication of infection.

2.2.3. Microbial Isolation and Identification

For the isolation of Gram negative bacterial strains different culture media were used i.e. MacConkey agar, ESBL, Citramide, Nutrient agar were used, and to isolate Gram-positive bacteria blood agar was preferred.Whereas yeast was isolated on the Chrom agar (CAC, Becton Dickinson, Heidelberg, Germany) and Sabouraud dextrose agar.

For the isolation of bacterial strains from the mastitis positive milk samples by direct inoculation of 500 µl of milk sample on the culture media including Blood agar, Citramide agar, Nutrient agar, MacConkey agar for bacterial strains however for yeast strains (C.albicans) Chrom agar (CAC) and Sabouraud dextrose agar were used. Milk samples were spread on the respective culture media with the help of spreader and subjected to incubation for 24 hours at 37°C. There were many different colonies observed on the culture plate, single colony was selected and picked carefully with the help of loop for streaking on the respective media for the isolation of microbes. Pure colonies of Gram positive, Gram negative and yeast was done using standard techniques of culturing and sub-culturing. Primary identification of MDR isolates was performed by colonial morphology on the respective culture media. To differentiate Gram positive and Gram negative bacteria Gram staining was performed. The identification of microbes was performed according to Bergey's Manual of Systematic bacteriology (Holt et al., 1994). The precise identification of microbes was done by using various biochemical tests, including Catalase , Coagulase ,Oxidase, Urease, Triple sugar iron, Motility, Citrate and Indol tests .Isolated bacterial strains were further identified by using Analytical profile index strip system including API strip tests 20E, 20NE for Gram negative bacteria ,API staph for Gram positive cocci whereas yeast strains were identified by using API Candida strips that were comprised of API ID32C tests (Hoog et al., 2000).

2.2.4. Antibiotic Susceptibility Testing

Antibiotic sensitivity testing patterns of Gram negative bacteria and Gram positive bacteria were carried out using the discs diffusion method (Unnerstad et al., 2009). Commonly prescribed fifteen broad spectrum antibiotics for mastitis treatment were selected for AST i.e. Ceftazidime (CAZ) 30µg, Cefazolin (KZ) 30µg, Cefoxitin (FOX) 30µg, Imipenem (IPM) 10 µg, Ceftriaxone (CRO) 30µg, Ampicillin (AMP) 10µg, Ciprofloxacin (CIP) 5µg, Meropenem (MEM) 10 µg, Augmentin (AMC) 20µg, Gentamicin (CN) 10 µg, Doxycycline (DO) 30µg ,Norfloxacin (NOR) 30µg, Fosfomycin (FOS) 10 µg, Tetracycline (TE) 30µg, Trimethoprim/Sulfamethoxazole (SXT) 30 µg and oxacillin (OX 1 µg). Antibiotics Cefoxitin (FOX) and oxacillin (OX) were employed to assess Gram positive bacteria resistance patterns specifically. In the present study following antifungal antibiotics were studied to evaluate sensitivity pattern of C.albicans i.e. Amphotericin B, Fluconazole, Ketoconazole, Itraconazole, Voriconazole, Nystatin, Ciclopirox, Caspofungin, Flucytosine, Posaconazole, Anidulafungin and Clotrimazole(Hoog et al., 2000) .

Discs and E-strip impregnated with drugs were placed with the help of sterile forcep on MHA plate which were inoculated with pathogenic isolates (10^8 log) and incubated for 24 hrs at 37oC. The respective zone of inhibition (ZI) was measured (mm) and data was interpreted following guideline (CLSI, 2016).

2.3. Fabrication of Nanomaterials Using Ecofriendly Green Synthesis Approach

2.3.1. Synthesis of Moringa concanensis Aqueous Leaves Extract

Plant leaves (Moringa concanensis) were collected from National Agriculture Research Council Islamabad Pakistan and collected plant was authenticated by Professor Mushtaq Ahmed, Department of Botany, QAU Islamabad. A total of 50 g dried leaves Moringa concanensis was added into ddH2O in 500 mL beaker and kept at a hot plate at 40°C over night and then subjected to constant shaking at 250rpm at 37°C for 72hrs, prior to further usage the extract was filtered using Whatman No 1 filter paper and prepared aqueous extract of leaves was stored at 4°C for further use (Raveendran et al., 2003).

2.3.2. Synthesis of A. subulatum (Black Cardamom) Seeds Extract

Black cardamom seeds were obtained from Herbal expert in Rawalpindi, Professor Mushtaq Ahmed, Department of Botany, QAU Islamabad, validated the plant seeds. Seeds of A. subulatum (BC) were thoroughly washed with dH_20 and air dried following similar previously published method of Raveendran(Raveendran et al., 2003). Initially BC powder (50 g) was mixed in 300 mL of ddH_2O, and kept in shaking incubator for 72 hrs at constant speed of 150 rpm at 37 °C. The extract of BC seeds was sieved using Whatman No 1 filter paper and stored at 4 °C in 500 mL Erlenmeyer flask.

2.3.3. GC-MS Analysis of Moringa Concanensis Leaves and Black Cardamom Seeds Extract

GC-MS equipment GC-MS (Agilent, 6890 series and Hewlett Packard, 5973 mass selective detector) was used to screen phytocompounds for the synthesis of nanoparticles as reducing/capping agents. Separations of phytochemicals were achieved using HP-5MS column (30 m in length × 250 μm in diameter × 0.25 μm in thickness of film). Spectroscopic detection by GC–MS involved an electron ionization system which utilized high energy electrons (70 eV). Injector temperature 220 °C; transfer line 240 °C; oven temperature programmed 60 °C-246 °C at 3 oC /min; carrier gas pure helium gas (99.995%) at 1.02 ml/min at 210 oC). 1.0 μL prepared extracts diluted with respective solvents was injected in a split less mode at 250 °C. Pure helium gas (99.995%) was used as the carrier gas with flow rate of 1.02 mL/min. The initial temperature was set at 50 –150 °C with increasing rate of 3 °C/min and holding time of about 10 min. Finally, the temperature was increased to 300 °C at 10 °C/min. Detection was done using full scan mode between 35 to 600m/z and with gain factor 5 and the phytochemicals identification was performed using NIST 2011 MS Library.

2.3.4. Synthesis of Nanomaterials A: Chitosan Coated Titanium Dioxide Nanoparticles (CS-Coated TiO_2 NPs)

Step 1: Green Synthesis of TiO_2 Nanoparticles

Moringa concanensis leaves extract was used for the synthesis of TiO_2 nanoparticles ascribing to its medical effectiveness (Arumugam et al., 2015). Titanium tetraisoproxide solution

was prepared in 100ml of 0.4M under magnetic stirring at room temperature. Under mild magnetic stirring, about 5ml of leaf extract was added to the titanium tetraisoproxide solution. The prepared mixture was centrifuged 3-5 times at 10000 rpm for 15 minute for the removal of unreacted ions. Final product was dried at 60°C, grounded and calcined at 500°C in muffle furnace for about 3 hours to obtain pure TiO2 NPs as explained in Scheme 1 and kept for storage at room temperature for further study.

Step 2: Synthesis of Chitosan Nanoparticles

CS-NPs were prepared using ionic gelation process with few modifications (Fan et al., 2012). For this purpose, two solutions were prepared. Chitosan (CS solution A) and tripolyphosphate (TPP solution B) solution. CS solution A was prepared by adding 0.3 g CS in 1% acetic acid solution (100 mL). It was subjected to continuous stirring until a clear solution was obtained. Whereas TPP solution B was prepared by adding 0.1 g TPP in water (10 mL), TPP solution B (4 mL) was added drop wise to the CS solution A (100 mL) with continuous stirring. Chitosan nano-particles (NPs) formed spontaneously upon addition of TPP aqueous solution B. The mixture was stirred at room temperature for 2 more hrs. The NPs were then subjected to extensive ultra-sonication at 35 Hz for at least 30 min on the ice bath to avoid temperature rise. It was subjected to centrifugation at 10000 rpm for 15 min at 4°C , supernatant was discarded and CS-NPs were obtained in the pallet and suspension of CS NPs were stored at 4°C for further use as shown in the **Scheme 1**.

Step 3: Synthesis of Chitosan coated TiO_2 NPs

For the coating of CS-NPs, CS Solution A, was kept on constant stirring at room temperature for 30min, TPP Solution B containing TiO_2NPs was mixed slowly drop wise in the CS solution A and continued stirring was done for 2hrs. The NPs were sonicated by ultra-sonication at 35 Hz for at least 30 min on the ice bath to maintain the temperature. Mixture was centrifuged at 10000 rpm for 15 min at 4°C, supernatant was discarded and pallet was air dried to attain CS coated TiO_2 NPs suspension that were stored at 4°C (Fan et al., 2012).

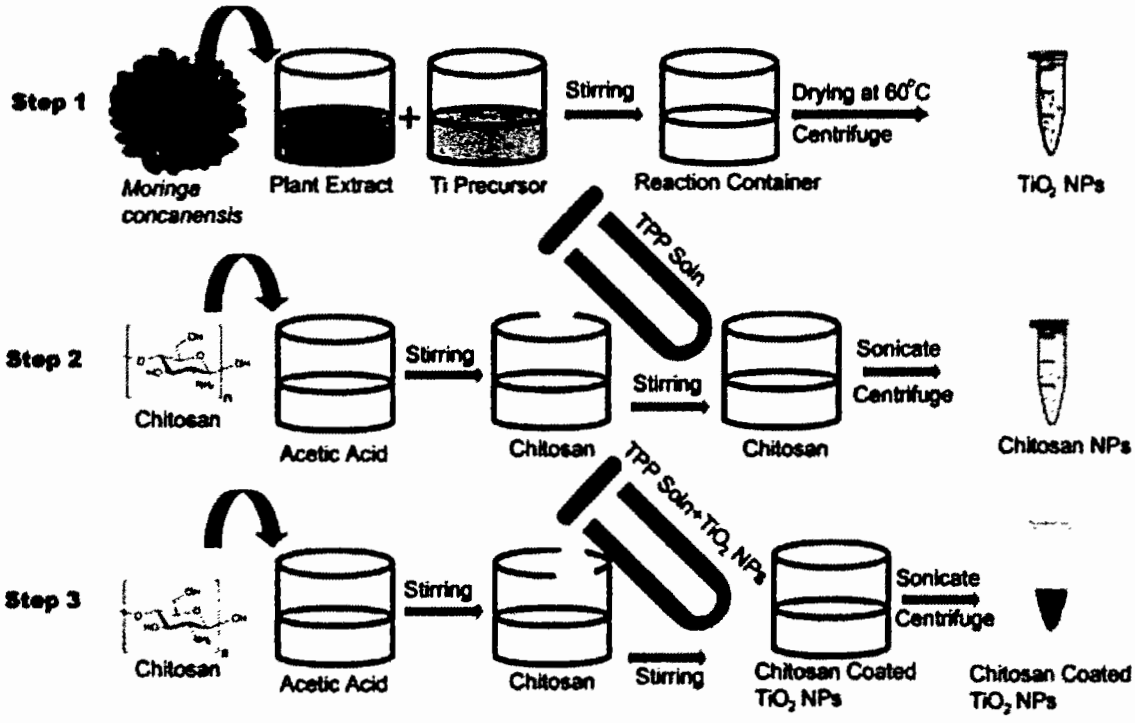

Scheme 1: Nanomaterial A: Synthesis of CS-NPs coated TiO_2 NPs,

Key: Step 1: Green synthesis of TiO_2NPs, Step 2: Synthesis of chitosan NPs, Step3: Synthesis of final product CS coated TiO_2 NPs.

2.3.5. Synthesis of Nanomaterial B: Ciprofloxacin Conjugated Chitosan Encapsulated Cerium Oxide NPs (CIP-CeO_2/CS NPs)

Step 1: Green synthesis of CeO_2 NPs

The prepared black cardamom seeds (BC) aqueous extract was used for the synthesis of CeO_2 NPs , 300ml of BC seeds extract was allowed to react with 11.16 g of $CeCl_3$ salt and kept for constant stirring at 60-70°C for 4 hrs, until the color change (from white to a creamy yellow precipitate) was observed. Subsequently, the final reaction product was centrifuged at 6000 rpm for 20 min at 25°C to obtain the pelleted CeO_2 NPs. The supernatant was discarded. Following previously published method explained by Arumugam et al (Arumugam et al., 2015), calcination was done at 400°C for 2 hrs in the hot furnace to attain pure crystalline CeO_2 NPs and stored at room temperature for further use as shown in the **Scheme 2.**

Step 2: Synthesis of Chitosan Encapsulated CeO_2 NPs (CeO_2/CS Nanohybrid)

The synthesis CeO_2 NPs were encapsulated with CS NPs by using the ionic gelation method, as previously described (Ciro et al., 2019). Ionic gelation technique is based on the ionic interactions between the positively charged primary amino groups of chitosan and the negatively charged groups of polyanion, such as sodium tripolyphosphate (TPP), which is the most extensively used ion cross-linking agent due to its non-toxic and multivalent properties (Fan et al., 2012). In 100 mL of acetic acid solution (1% V/V dH20), 0.3 g of CS was solubilized precisely. The resultant solution was stirred for 30 minutes at 1400 rpm until it became transparent. Then, TPP solution was prepared by mixing 0.1 g of TPP powder in 10 mL dH_2O. Greenly synthesized CeO_2 NPs were dissolved in 4 mL TPP solution and poured drop wise into the CS solution. The mixture was homogenized by stirring by magnetic stirrer for 3 hrs at 500 rpm at 25°C. The CeO_2/CS composite were then centrifuged at 12000 rpm for 30 min at 4°C. Chitosan encapsulated CeO_2/CS NPs were sonicated at 35Hz for 30 min to obtain dispersed solution and stored in refrigerator at 4°C for further uses as shown in the **Scheme 2.**

Step 3: Ciprofloxacin Conjugated Chitosan Encapsulated CeO_2 NPs (CIP-CeO_2/CS Nanohybrid)

Similarly, 0.01g CIP and 0.01g CeO2 was dissolved in 4 mL of TPP solution and poured drop wise into the CS solution. The mixture was subjected to dynamic stirring by magnetic stirrer for 3 hrs at 500 rpm at 25°C. Then synthesized CIP-CeO2/CS composite was centrifuged at 12000 rpm for 30 min at 4°C. Finally, CIP-CeO2/CS NPs were sonicated at 35Hz for 30 min to avoid agglomeration (Jamil et al., 2016) as described in the Scheme 2.

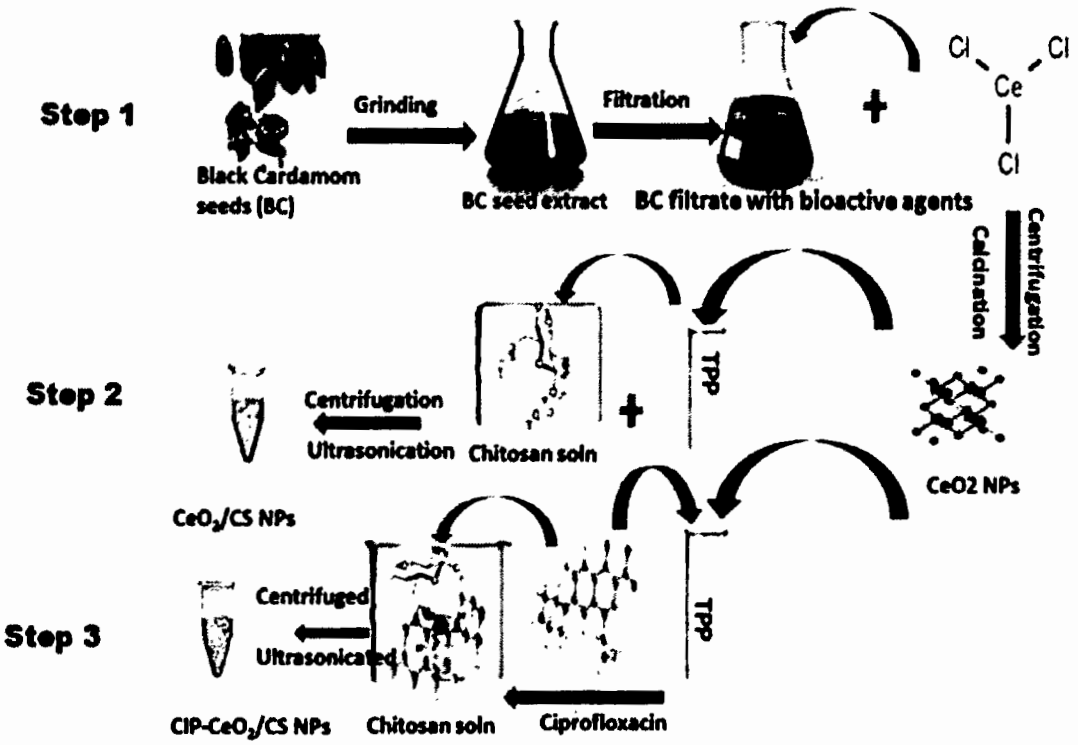

Scheme 2: Nanomaterial B: Ciprofloxacin Conjugated Chitosan Encapsulated CeO_2 NPs (CIP-CeO_2/CS Nanohybrid)

Key: Step 1: Green synthesis of CeO_2NPs using black cardamom (BC) seeds extract, Step 2: Synthesis of CeO_2/CS, Step 3: Synthesis of final product CIP- CeO_2/CS NPs

2.3.6. Synthesis of Nanomaterial C: Ciprofloxacin Conjugated Chitosan Encapsulated Silver and Titanium Dioxide Composite (CIP-Ag/TiO_2/CS nanohybrid)

Step 1: Green Synthesis of TiO_2 and Ag Nanoparticles

For the Synthesis of TiO_2NPs and AgNPs as shown in **Scheme 3**, just 500 ml of the aqueous extract of *M. concanesis* leaves was added to 100 mL titanium tetraisoproxide (TTP) solution (0.4M) and to 1 mM solution of silver nitrate ($AgNO_3$) under mild magnetic stirring at 28°C. A change in color of the resultant solution from colorless to brown confirmed the reduction of Ag+ to Ag° moreover in case of TiO_2 color turned to creamy white. Each mixture

was centrifuged three times at 12000 rpm to extract unreacted ions for 10 minutes. The respective final products were dried at 60°C, grounded and calcined at 500°C for 3 hours in a muffle furnace to get pure NPs TiO_2NPs and AgNPs (Arumugam et al., 2015) which were kept at room temperature.

Step 2: Formation of TiO_2/Ag Nanocomposite

Ag/TiO_2nanocomposite was prepared by wet chemical impregnation method (Shameli et al., 2010). For that purpose, synthesized AgNPs and TiO_2NPswere mixed in equal amount (0.01g) into 10ml of ethanol and the mixture was homogenized by sonication for 3 hrs. The precipitate was obtained after 3-5 times washing with dH_2O and centrifugation was done at 6000rpm at 25 ^{0}C. The final mixture was dried at 60°C temperature to obtain the final product Ag/TiO_2 as shown in **Scheme 3** and stored at room temperature for further experiments.

Step 3: Synthesis of Chitosan Encapsulated Ag/TiO_2 Nanocomposite (Ag/TiO_2/CS Nanohybrid)

Ag/TiO_2/CS nanocomposite was added in the 4mL of TPP solution and kept for continuous magnetic stirring at 28°C for 2 hours. Following complete homogenization of the combination, a 0.3g CS solution produced in 1% acetic acid was held for continuous stirring, and TPP solution comprising 0.01g Ag/TiO_2/CS nanocomposite was poured drop wise into the CS solution. After 2 hrs of continuous stirring resultant solution was subjected to ultrasonication at 35 Hz for 30 min to scatter the solution particles. Afterward, solution was centrifuged at 14000 rpm for 30 min at 4°C, the supernatant was discarded and the pellet was resuspended in ddH2O and kept at 4°C for further use (Fan et al., 2012).

Step 4: Synthesis of Ciprofloxacin conjugated Chitosan Encapsulated Ag/TiO_2 Nanocomposite (CIP-Ag/TiO_2/CS Nanohybrid)

CIP-Ag/TiO_2/CS nanohybrid was synthesized by using the ionic gelation method, as previously described (Ciro et al., 2019). In a 100 mL acetic acid solution (1 % V/V dH_2O) 0.3 g of CS was solubilized. The resultant solution was stirred at 1400 rpm for 30 minutes until it became transparent. TPP solution was then made by combining 0.1 g of TPP powder with 10 mL dH_2O. Then, 0.01g Ag/TiO_2 and 0.01g CIP antibiotic were dissolved in 4 mL TPP solution and

put drop by drop into the CS solution. The flask was exposed to ultrasonication at 35 Hz for 30 minutes after complete homogenization of the mixture to scatter the solution particles and agglomeration. The mixture was then centrifuged for 30 minutes at 4°C at 14000 rpm, the supernatant was discarded, and the pellet was resuspended in dH_2O. Finally CIP-Ag/TiO_2/CS nanohybrid was obtained kept for storage at 4°C in refrigerator until further use (**Scheme 3**).

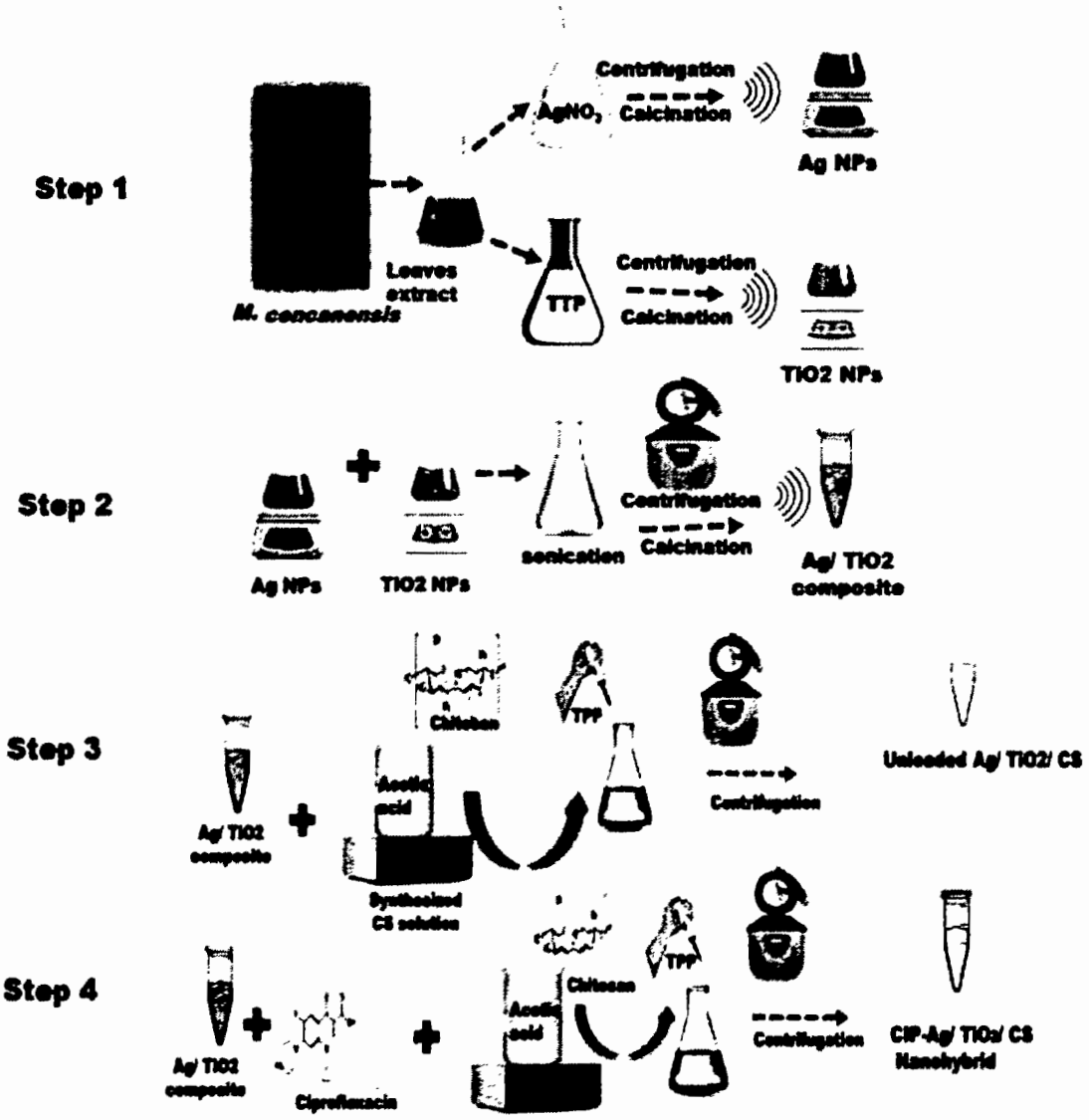

Scheme 3: Nanomaterial C, Synthesis of Ciprofloxacin conjugated Chitosan EncapsulatedAg/TiO_2 Nanocomposite (CIP-Ag/TiO_2/CS Nanohybrid)

Key: Step 1: Green Synthesis of TiO_2 and Ag nanoparticles, Step 2: Synthesis of TiO_2/Ag nanocomposite Step 3: Synthesis of Chitosan Encapsulated Ag/TiO_2 Nanocomposite, Step 4: Synthesis of Ciprofloxacin conjugated Chitosan Encapsulated Ag/TiO_2 nanohybrid.

2.3.7. Synthesis of Nanomaterial D: Ciprofloxacin conjugated Chitosan Encapsulated Silver, Titanium Dioxide and Iron Oxide Ternary Composite (CIP-Ag/TiO_2/Fe_2O_3 /CS ternary composite)

Step 1: Green Synthesis of TiO_2, Fe_2O_3 and Ag Nanoparticles

For the Synthesis of TiO_2NPs, Fe_2O_3 NPs and AgNPs, first of all 500 ml of *Moringa concanensis* aqueous leaves extract supplemented to 100 mL Titanium tetra isoproxide (TTP) solution (0.4M), $FeCl_3$ solution and 1 mM solution of silver nitrate ($AgNO_3$) respectively in the separate containers (flasks) under mild magnetic stirring at 28°C. The resulting solution changed color from colorless to brown indicating Ag+ reduction to Ag°, in case of TiO2 color turned to creamy white while Fe_2O_3 turned red. Resultant solutions were centrifuged three times at 12000 rpm separately to extract unreacted ions for 10 minutes (Ahmed et al., 2016). The respective final products were subjected to moisture removal at 60°C, then grounded and calcined at 500°C for 3 hours using muffle furnace to get pure TiO_2 NPs, Fe_2O_3 NPs and AgNPs as shown in **Scheme 4** whereas these NPs were stores at room temperature for further studies.

Step 2: Formation of Ag/TiO_2/Fe_2O_3 Ternary Composite

To synthesized Ag/TiO_2/Fe_2O_3 ternary composite was prepared by wet chemical impregnation method and hydrothermal treatment (Shameli et al., 2010). For that purpose, Ag NPs, Fe_2O_3 NPs and TiO_2NPs were mixed in equal amount (0.01g) into 5ml of ethanol and 5ml of NaOH (pH less than 12).Then mixture was homogenized by continuous stirring for 3 hrs at 1600 rpm. The composite of tri metals was subjected to hydrothermal treatment for 24hrs at 180 0C (Wang & Li, 2003). Resulting mixture was obtained in the form of precipitate, the pH was adjusted to 7 after 3-5 times washing with ethanol by centrifugation at 6000rpm at 40C.The pallet was then dried at 60°C to get the desired Ag/TiO_2/Fe_2O_3ternary composite powder retained for storage at room temperature as shown in **Scheme 4**.

Step 3: Synthesis of Chitosan Encapsulated Ag/TiO_2/Fe_2O_3 nanocomposite (Ag/TiO_2/Fe_2O_3 /CS)

To synthesized Chitosan encapsulated Ag/TiO_2/Fe_2O_3/CS, 0.01g Ag/TiO_2/Fe_2O_3ternary composite dissolved in the 4 mL of TPP solution and kept for continuous magnetic stirring at

28°C for 2 hours. After complete homogenization of mixture, flask subjected to ultrasonication at 35 Hz for 30 min to scatter the solution particles and agglomeration. Subsequently, the centrifugation was performed for 30 minutes at 14000 rpm and 4°C (Jamil et al., 2016), the pellet was resuspended in ddH_2O after discarding the supernatant to obtain Chitosan encapsulated Ag/TiO_2/Fe_2O_3/CS ternary composite as shown in the **Scheme 4.**

Step 4: Synthesis of Ciprofloxacin Conjugated Chitosan Encapsulated Ag/TiO_2/Fe_2O_3 Ternary Composite (CIP-Ag/TiO_2/Fe_2O_3 /CS Ternary Composite).

Ionic gelation method was used for the synthesis of Ciprofloxacin conjugated CIP-Ag/TiO_2/Fe_2O_3/CS Ternary Composite. More specifically, chitosan of 0.3% w/v was allowed to be dissolved in 1% acetic acid. Chitosan solution was given 30 minutes of stirring at room temperature prior to filtration for removal of impurities. TPP solution was then made by mixing 0.1 g of TPP powder with 10 mL dH_2O. Then Ag/TiO_2/Fe_2O_3 (0.01g) and CIP (0.01g) was added in the TPP solution and kept for stirring for 15min at room temperature. After complete homogenization of TPP solution containing Ciprofloxacin and Ag/TiO_2/Fe_2O_3ternary composite was added with help of micropipette in 25 ml of chitosan solution (0.3% w/v) that was constantly stirred for 30 minutes. The nanomaterials in the CS mixture were sonicated for 30 minutes at 25 kHz. This intense agitation allows the large agglomerations of nanomaterials to breakdown and that are then centrifuged for 30minutes at 12000 rpm (Jamil et al., 2016) with resuspension of pellet and supernatant is discarded to obtain CIP-Ag/TiO_2/Fe_2O_3/CS Ternary Composite and stored at 4 °C in the refrigerator for further use as shown in the **Scheme 4** .

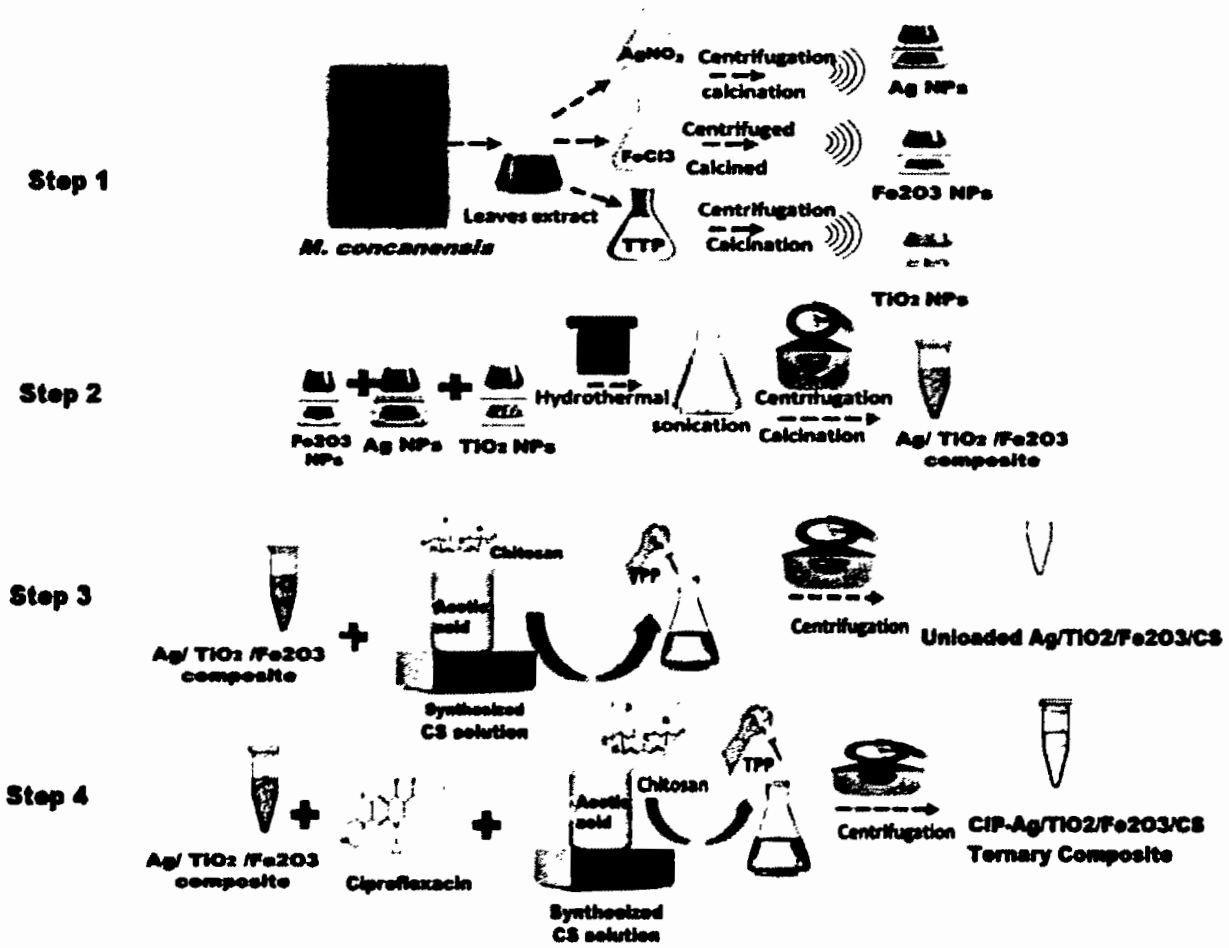

Scheme 4: Nanomaterial D, Synthesis of Ciprofloxacin Conjugated Chitosan Encapsulated Ag/TiO_2/Fe_2O_3Ternary Composite (CIP-Ag/TiO_2/Fe_2O_3 /CS Ternary Composite).

Key: Step 1: Green Synthesis of TiO_2, Fe_2O_3 and Ag Nanoparticles, Step 2: Formation of Ag/TiO_2/Fe_2O_3 ternary composite Step 3: Synthesis of chitosan encapsulated Ag/TiO_2/Fe_2O_3 /CS by Encapsulation of chitosan, Step 4: Synthesis of Ciprofloxacin conjugatedAg/TiO_2/Fe_2O_3 /CS Ternary composite

2.4. Characterization of Synthesized Nanomaterials

Due to the size extremity of Nano-particles i.e., 10^{-9} their properties and surface analysis cannot be conducted by naked eye. So, the particles detection and characterization that have

trivial dimensions requires the utilization of specific techniques and instrumentation. X-ray diffractometer (Rigaku D/MAX 2550) was used to determine the crystalline nature and the crystal phase composition of the prepared nanomaterials (Yang et al., 2014). The diffraction was obtained by using XRD and was observed at around 10–80° (2θ) (Cu Kα1 radiation, λ = 1.5406 Å) at 100 mA and 80 kV. The Scherrer equation has been used to estimate the crystalline dimension. Field Emission Scanning Electron Microscopy (MIRA3 TESCAN) photographs at 500nm scale and EDX spectra of nanomaterials were used to analyze the size and shape of the nanomaterials. The unknown functional groups were analyzed using FTIR spectrometer at 400-5000 cm-1 (Zafar et al., 2020). The optical properties of synthesized nanomaterials were observed in the range of 200-800nm using UV-Vis spectrophotometer. TEM (JEOL JEM 1010) was used to analyze the size and shape of the nanohybrid at 200 keV, while the selected area electron diffraction (SAED) was used for phase analysis. Malvem Zeta seizer was utilized to calculate the Zeta potential of the nanomaterial. All the particle analysis including Zeta potential and particle size were carried out at room temperature (Zhao, 2018).

2.5. Determination of Encapsulation Efficiency of Chitosan

An indirect method was used to calculate the encapsulation efficiency (EE) of all the synthesized nanomaterials in accordance with Abreu protocol (Abreu et al., 2012). Centrifugation was used to separate the drug-loaded CSNPs from the free drug at 10000 rpm for 15 min. The amount of free drug in the supernatant was measured using a spectrophotometer at λmax (295), which was obtained from a wave scan. The equation derived from the standard curve was used to determine the drug concentration in the supernatant. Experiments were carried out in triplicate, and the encapsulation efficiency was determined using the following formula:

EE = [Loaded CIP into nanohybrid/Total amount of nanohybrid (free + loaded)] X 100

2.6. MIC Determination of Synthesized Nanomaterials

The synthesized nanomaterials were subjected to MICs analysis by using broth microdilution method using MH broth (Luber et al., 2003). MDR *E. coli*, MRSA, and MDR C.albicans strains suspensions were prepared by comparing the turbidity of the overnight

inoculated culture with the 0.5 McFarland standard. While test tubes containing various concentrations (0-500 mg/mL) of synthesized nanomaterials were inoculated with microbial suspensions and incubated for 24 hrs at 37°C. Then, the dilution containing at lowest concentration capable of inhibiting the microbial growth called MIC. Results were recorded and analyzed by comparing with positive control MH broth inoculated only negative control base on MH broth only.

2.7. Genomic DNA isolation From MRSA and ESBL *E.coli* Isolates

Genomic DNA isolation followed the method used in a previously report (Ernst et al., 2019). Thereby, single colonies of MRSA and ESBL *E.coli* isolates were cultured in BHI broth at 37°C for 16 hrs. Thereafter, palletization of 0.1 mL overnight culture (10^8 log CFU) was performed using centrifugation at 5000 rpm on 5 °C and resuspension was done in 300 µL of lysis buffer [150 mMNaCl, 1% (vol/vol, 100 mM EDTA, 50 mM Tris-HCl pH 8.0) sodium dodecyl sulfate] comprising lysostaphin 100 µg and 100 µg of RNase before incubation for 30 minutes at 37°C.After adding proteinase K 200 µg at 37°C for 30 min, the one volume of phenol–chloroform–isoamyl alcohol (25:24:1) followed by 1 volume of chloroform–isoamyl alcohol (24:1) was added before precipitation with 2 volumes of 95% ethanol-0.2 M NaCl at -20 °C for 1 hour. Palletization of all the genomic DNA samples was done by centrifugation (5000rpm/5 °C) and washing with 80% ethanol followed by air drying and resuspension in 200 µL dH20. The DNA concentration was determined by spectrophotometry at MAX=260 nm. Stock solutions of purified bacterial genomic DNA were made to concentration of 5 ng/µL and storage was done at -20 °C.

2.8. Antibiotic Resistant Genes Amplified By PCR from Genomic DNA of MRSA and ESBL *E. coli*

The following DNA sequences of primers, routinely used to amplify mecA gene (310 bp) by PCR (Turutoglu et al., 2009), were used to amplified mecA in MRSA genomic DNA samples. Moreover, resistance to beta-lactams (blaTEM, blaSHV, blaCTX) was used as measure of

presence of ESBL genes by PCR (Awad, 2017) and the primer (Germany) being used were listed in **Table 2.1**.

Concisely, 90 µL of a PCR mixture contained 10 µL DNA samples with10 mM Tris-HCl (pH 8.8), 50 mMKCl, 1.5 mM MgCl2, 100 pmol of each above-mentioned primer, 0.1% Triton X-100, 0.25 mM (each) dNTPs, , and 1.25 U DNA Taq polymerase. DNA amplification with 34 cycles was that consisted of denaturation at 92 °C /1 min, annealing 56°C/1 min, extension 72 °C /2 min and final extension at 72 °C /3 min. Each reaction series included a positive control (MRSA strain ATCC 43,300, ESBL *E.coli* NSCU,10455), a negative control (S. aureus strain ATCC 25923), and two blanks (i.e. the lysis solution and the ddH_2O). Analysis of products from PCR reaction was performed using 2% agarose gel after electrophoresis at 80-150 V for 1 hr. Discrete ethidium bromide (EtBr)-stained DNA fragments (310 bp), corresponding to the amplified genes (mecA blaTEM, blaSHV and blaCTX) were eventually visualized on a UV trans-illuminator at 300 nm, while the size was determined with a standard XIV Marker (Turutoglu et al., 2009).

Table 2.1: The specificities of the primers used for PCR

Primer	Sequence	Length	Reference
bla_{SHV}	AGGATTGACTGCCTTTTTG ATTTGCTGATTTCGCTCG	392 bp	(Colom et al., 2003)
bla_{TEM}	ATCAGCAATAAACCAGC CCCCGAAGAACGTTTTC	516 bp	(Colom et al., 2003)
mecA	(885-5'TGGCTATCGTGTCACAATCG3'-904) (1194-5'CTGGAACTTGTTGAGCAGAG3'-1175)	310 bp	(Turutoglu et al., 2009)
bla_{CTX}	ATG TGC AGY ACC AGT AAR GTK ATG GC TGG GTR AAR TAR GTS ACC AGA AYC AGC GG	593 bp	(Archambault et al., 2006)

Antimicrobial Activity of Synthesized Nanomaterials

The green synthesized nanomaterials were evaluated by disc diffusion method against most prevalent mastitis causing bacterial strains and Yeast i.e. MDR *E. coli* , MRSA, MDR *C.albicans* respectively (Birla et al., 2009). On the separate petri plates contained MHA standard media were inoculated with over night inoculated culture of MDR *E. coli,* MRSA, MDR *C.albicans* suspensions turbidity was adjusted (McFarland 0.5) swabbed equally to obtain uniform lawn. Sterile filter paper disc were loaded with nanomaterials (at MIC) and placed aseptically on the MH agar plate gently, DMSO was used as negative control and Chitosan encapsulated nanoformulation (as internal control). The zone of Inhibitions (ZIs) were measured

with the help of scale (mm) after incubation of 24 hrs at 37°C, experiment were performed in triplicate and SD was calculated.

2.9. Kinetics of Antimicrobial Effects of Synthesized Nanomaterials

Time-course study of antibacterial activity of synthesized nanomaterials were determined through standard microdilution broth assays in a 96-wells plate(Jamil et al., 2016). Briefly, 50 µL of all nanomaterials at respective MICs were added in the 96 wells plated followed by 10 µL of MDR *E. coli* , MRSA, MDR *C.albicans* ($1x10^4$) at log phase added into 100 µL of sterilized MH broth and turbidity of strains was already compared to the McFarland standard (0.5 turbidity). Measurement of OD values was done at 600 nm using a Multi-plate ELISA reader at various time points (24hrs) of incubation at 37°C after treatment (i.e.0, 2, 4,6,8,12,16 and 24 hrs). Positive and negative controls included the inoculated broth only and autoclaved MH broth only, respectively. The experiment was run in triplicate.

2.10. Live/Dead Assessment of MDR Pathogens after Treatment with Synthesized Nanomaterials by Flow Cytometry Analysis

To study Live/Dead MDR *E. coli* , MRSA, MDR *C.albicans* suspensions treated and untreated with synthesized nanomaterials was determined by Flow cytometer (BD FACScan, USA)(O'Brien-Simpson et al., 2016), according to the manufacturer's protocol (CUS Ever bright Inc., Suzhou, China) using Propidium Iodide (PI) and Annexin V double staining technique was used. Briefly, Log-Phase MDR *E. coli*, MRSA, MDR *C.albicans* suspension ($1x10^8$ CFU/ml) were centrifuged for 20 mins at 3000 rpm with pellet resuspension in 50 µL PBS 1X (pH 7.4). MDR *E. coli*, MRSA, MDR *C.albicans* suspensions were treated with synthesized nanofromulations at respective MICs and kept for 6hrs of incubation. After treatment MDR *E. coli*, MRSA, MDR *C.albicans* suspensions were centrifuged at 1000 rpm for 15 min, the supernatant was discarded, and the pellet was resuspended in 500 µl of PBS 1X (pH 7.4). The cells were carefully labeled with 10 µl of Annexin V binding buffer and 5 µL of Annexin V-FITC (Fluorescein isothiocyanate) followed by 5 µl of PI stain and incubated in the dark for 20 min at RT, and the resulting stained cells were diluted with 200 µl PBS 1X (pH 7.4) and 400 µl

of Annexin binding buffer. After staining, cells were analyzed for rapid detection of ciprofloxacin conjugated nanoparticles internalize in live cells and increased damage to cell membrane by FACS (fluorescence-activated single cell sorting flow cytometer).

2.11. FE-SEM Analysis of PDR *E.coli*, MDR *E. coli*, MRSA, MDR *C.albicans* after Treatment with Synthesized Nanomaterials

FE-SEM analysis was done to observe morphological changes in the microbes treated with synthesized nanomaterials using respective MICs. The morphological effect after treatment with synthesized nanomaterials was investigated at various time intervals on MDR *E. coli*, MRSA, MDR *C.albicans* using exponentially growing cells (Huang et al., 2017). Briefly, a tiny drop (10 µl) of treated and untreated (control) cells ($1x10^4$) were put on a glass slide, and slides were placed in 2% glutaraldehyde (GA) and paraformaldehyde HEPES buffer (30 mM) for one hr at 37°C. Increasing concentration of alcohol in water was then used for dehydration of the cells and the slides were kept on water-alcohol solutions for 10 minutes each in each container having alcohol/water gradient solution. Eventually, one minute slide washing was performed by tertiary butyl alcohol and dried slides were subjected to Gold sputter coating for 1min from three directions before their observation under the FE-SEM microscope.

2.12. TEM Analysis of MDR *E.coli* after Treatment with Synthesized Nanomaterials

The bacterial cells were treated with synthesized nanomaterials at respective MICs for various intervals of time and observed under TEM to visualize morphological changes, untreated cells served as negative control. Hartmann et al modified model was applied to reveal morphological changes in the MDR *E.coli* by transmission electron microscopy (TEM) (Hartmann et al., 2010). After the treatment with nanomaterials (MICs) at various intervals of time (0.6, 12 hrs), 10µl of Log phase ($1x10^4$) of MDR *E.coli* were shifted to clean slide. Paraformaldehyde in buffer HEPES (30mM) with glutaraldehyde (2%) was used for cellular fixation and untreated cells were taken as negative control. Then cells were washed by ethanol

subsequent dilutions (30, 50,70,90,95 and 99.5%) for 10 min per grade. Soaking of the slides was done in terl.butyl alcohol for 1min three times and drying was done prior to TEM analysis for morphological changes.

2.13. Biocompatibility Analysis of Synthesized Nanomaterials

Biocompatibility assay was conducted using two standard techniques including hemolysis assay using blood of cows and cells viability assay using Bovine mammary gland epithelial cells.

A: Cell Viability Using MTT Assay

To evaluate biocompatibility of all the synthesized Nanomaterials, Cell viability assay was conducted on Bovine Mammary Gland Epithelial Cells (BMGE Cells). To observe Viability of cells MTT assay was performed following modified protocol (Mohammadi et al., 2019), Celecoxib treated cells were taken as positive control and PBS treated cells were considered negative control. Then the Dulbecco's modified Eagle medium (DMEM) was used for cell growth in 96 well plate, then (1×10^5 cells) distributed into wells before incubation for 24 hrs in the CO_2 incubator at 37°C. Synthesized Nanomaterials at various concentrations were treated with viable Bovine mammary gland epithelial cells (BMGE) ($1x10^5$) incubated at 37°C for 24hrs, keeping Celecoxib as PC and PBS as NC. After incubation, 100 µL of fresh DMEM was thoroughly mixed with MTT (10 µL) solution crafted in PBS 1X, DMEM (Caputo et al., 2017). The 96-well plates incubation was again performed for 4 hours. Eventually, the formazan crystal dissolution was achieved by 0.1 mL DMSO solution, then the optical density of the MTT formazan (internal control) and the test samples was analyzed at 570 nm and 620 nm respectively. The percentage of viable cells was recorded using the following standard equation:

$$\text{Viability of Cells (\%)} = \frac{(Test\ 570nm - 620nm)}{(Control\ 570nm - 620nm)} \times 100$$

B: Hemolysis study of Synthesized Nanomaterials

To evaluate biocompatibility of all the synthesized Nanomaterials, hemolysis assay was conducted. For hemolysis testing standard method of ASMT was used on healthy blood of cows, Triton 100X treated blood as positive control and PBS treated blood as negative control .From

the healthy cow, blood (3 cc) was taken with the help of a sterile syringe in the vacutainer carefully. And 1.5 ml of Blood was incubated at 37 °C after treatment with respective MICs of all the synthesized nanomaterials (50 µL) for 2-4 hrs of time interval, and then spinning was done at 1500 rpm to separate the RBCs from blood (ASTM, 2000). After that, 100 µL of the supernatant of all samples was transferred to a 96-well plate. The absorbance values of the supernatant were taken at 570 nm by using a micro plate reader. The percentage of hemolysis of RBCs was determined by the following equation:

$$\text{Viability of Cells (\%)} = \frac{(\text{Absorbance of Sample} - \text{Negative control})}{(\text{Absorbance of Positive Control} - \text{Negative control})} \times 100.$$

2.14. Ex-Vivo Ciprofloxacin Release Study of Synthesized Nanomaterials

Ex-vivo Ciprofloxacin release study of greenly synthesize nanomaterials B,C and D was performed by using New Zeeland rabbit (n=5) weighing 1.5-2kg were obtained from National Institute of Health Islamabad (Mamatha et al., 2010). The anesthetic ether was used for sacrificing animals and hair trimming was carefully done using scissors and surgical razor/blade was employed to detach skin from the belly of rabbit. The Synthesis of epidermis was achieved by technique of heat separation (Zhao & Singh, 1999), that used the soaking of skin taken from belly region for 45 seconds in water at 60°C followed by epidermis removal. Ex-vivo drug release study was performed using Franz diffusion cell .The skin was loaded between the compartments of Franz diffusion cells with face of stratum corneum to donor side whereas donor compartment was exposed to atmosphere loaded with respective MICs of nanomaterials. The side facing stratum corneum was kept in direct contact with nanomaterials and the control of ciprofloxacin. At a constant temperature of 37±0.5°C with uniform stirring of 200 rpm, the receiver compartment was settled with 13 ml of PBS at pH of 7.4. The ex-vivo drug released estimation was evaluated by taking 3 mL of sample continually at 0, 1, 2, 4, 8,16,24 hrs replenishing the equal volume of fresh medium (Mamatha et al., 2010). The syringe filter (Sartorius 0.45µ) was used to filter estimation of drug contents, UV/visible spectrophotometer at 276 nm was used to observe OD. The released drug cumulative percentage was evaluated by using following formula:

$$\text{Percent of drug release (\%)} = \frac{\text{Absorbance of sample (nm)}}{\text{Absorbance of control (nm)}} \times 100$$

2.15. Anti-biofilm Activity of Synthesized Nanomaterials

The assessment of anti-biofilm activity for nanomaterials was evaluated MDR *E. coli* which was found most prevalent causative agent of mastitis. Micro titer plate (MTP) assay was used to grow biofilms of MDR *E.coli* and anti-biofilm activity was observed after interacting with synthesized nanomaterials using respective MICs with micro titer plates having 96-well with flat bottom. The George method was employed for ELISA plate reading to confirm the biofilm formation and antibiofilm activity of nanomaterials by measuring the OD of samples in 96-well plate (O'Toole, 2011).

$$\text{Viability of Cells (\%)} = \frac{\text{(Absorbance of Sample - Negative control)}}{\text{(Absorbance of Positive Control - Negative control)}} \times 100$$

2.16. *Invivo* Antibacterial Potential of the Most Efficient Synthesized Nanoformulation

To reveal the Invivo antibacterial potential of the most efficient nanoformulation against the induced infection caused by MDR *E.coli* in rabbit model , experimental design was according to previous literature (Tian et al., 2007).

2.16.1. Experimental Design and Rabbit Model of Induced Bacteremia and Efficacy of Nanomaterial.

Setup for the experiment

Four groups of female rabbits weighing approximately 1.5kg was arranged and housed in the cages (3 rabbits per cage) in a well-ventilated space at room temperature. Groups were classified i.e. 1- Ciprofloxacin treated, 2-positive control group had infection while no treatment was given, 3- negative control contained animals without infection and treatment healthy rabbits and 4- last group contained nanoformulation treated rabbits. All the study groups were acclimated first before beginning the experiment, and they were reared with free access to feed

and water. Rabbit immune suppressed for three weeks by intraperitoneal injection of 30 mg cyclophosphamide (Mapara et al., 2012). All rabbits fasted overnight on the last day of immune suppression, followed by administration of 0.1 mL of sodium bicarbonate to counteract stomach pH immediately before infection. Rabbit groups were subjected to induced infection by injecting saline solution containing approximately $1.5x10^8$ CFU/mL of selected model MDR *E. coli* strains via intraperitoneal injection; the non-infected groups received normal saline only. The bacterial load in the blood of rabbits was estimated to confirm the presence of infection; the initiation of infection was indicated a steady increase in bacterial load over the course of two days. The corresponding treated groups were received 0.004 µg/kg body weight daily of synthesized nanoformulations and Ciprofloxacin for one week. Both guidelines for using rabbit models in this study was adhere to the Institutional Animal Care and Use Committee's and International Islamic University's ethics regulations.

2.17. Bacteriologic Analysis

At the end of the acclimatization phase, blood samples from all groups were collected and bacteriologic research was performed on a regular basis to investigate the killing kinetics of MDR *E. coli* in the rabbits. Every day after the treatment regimen was started and MDR *E. coli* counted in all infected classes after enrichment ,incubation and culturing of blood on the growth media i.e. blood agar and nutrient agar. The sampling was done on each day of treatment with synthesized nanoformulation. The blood samples were injected into bottles with 0.193 liter of a lysing solution (pH 10) containing 0.08% Na_2CO_3 and 0.005% Triton X-100 .Then equal volume of nutrient broth and blood sample was incubated for 3 days at 37°C. The negative culture plates were kept for long compared with positive ones to confirm the absence of growth (Zierdt et al., 1982).

2.18. Hematologic and Biochemical Parameters Analysis

Following the completion of the treatment regimen, rabbits were anesthetized with chloroform vapor prior to dissection. Prior to sampling, the skin of the rabbit ear was cleaned with 70% ethanol. With the help of sterile syringe containing heparin solution 1ml of Blood

samples was drawn and transferred into tubes containing sodium polyanaetholsulfonate (0.5ml, Becton Dickinson & Co., Rutherford, N.) and ethylene diaminetetraacetic acid (EDTA)-containing tubes (Gatsing et al., 2005). An automated veterinary hematology analyzer can use the blood in the EDTA tube to estimate hematology parameters. The serum was separated by centrifuging a plain vacutainer at 3000 rpm for 10 minutes and stored at 20°C until serum albumin, alanine aminotransferase (ALT), urea, and creatinine levels were determined by using specialized test kits in accordance with the manufacturer's instruction

2.19. Examination of Histopathology

Following the completion of treatment and blood collection, rabbits were euthanized and dissected. The liver, heart and kidney was carefully removed and fixed in a 10% formalin saline solution. Parts of liver, heart and kidney with a depth of 5mm was organized and stained with hematoxylin and eosin dye before being microscopically examined and photographed (Bancroft & Gamble, 2008; Fodouop et al., 2017).

2.20. Ethics Approval and Informed Consent

The ethical approval of the study was taken in accordance with Pakistan Research Council that employs the guide for usage and care of laboratory animals as per National Institute of Health (NIH), Islamabad rules. The local Institutional Bioethical Committee of International Islamic University, Islamabad approved experimental protocols (Reg #22-FBAS/PHDBT/F-14) were used wherever necessary. At the end of experiments, animals were sacrificed by using an excess of sodium pentobarbital anesthesia (40 mg/kg bw). Efforts were made to lessen the misery.

2.21. Statistics

As every experiment was performed in triplicates so the average values along with average SD were reported in each case. All statistical analyses were performed using GraphPad Prism 8.1 (GraphPad Software, USA) and SPSS. The value of $P \leq 0.05$ was taken as significance threshold throughout the experiments.

CHAPTER 3

ISOLATION AND IDENTIFICATION OF MDR PATHOGENS CAUSING MASTITIS

3.1. Introduction

Mastitis, inflammation of udder tissues due to pathogenicity of bacteria, algae and fungi, which cause infection in the mammary glands with noticeable redness and swelling (Ashraf & Imran, 2020; Radostits et al., 2006). The inflammatory response occurs to destroy and counterpoise noxious substances that allow the glands to function normally to heal. Invasion of leukocytes develops inflammation causing an increased somatic cell count (SCC) of milk, a general indication of healthy udders and better milk quality (Harmon, 1995). Detection of subclinical mastitis is best done by testing milk for somatic cell counts (SCCs) (predominantly leukocytes) using California Mastitis Test (Gonzalez et al., 1980) .Milk yield decreases in cows with subclinical mastitis while clinical cases that include only local signs are referred to as mild or moderate. If the inflammatory response includes systemic involvement (fever, anorexia, shock), the case is termed severe (Ashraf & Imran, 2020; Lago et al., 2011).

Mastitis is the common diseases due to which dairy industry is suffering with massive losses in milk reduced production capacity of dairy cows, decreased animal value and also expensive treatment. The consequence of mastitis is restricted not only to the dairy farmers but is also a concern to the consumers because of increasing antimicrobial resistance due to the extensive and indiscriminate use of antimicrobials for the management of mastitis (Hogeveen et al., 2011) .

Mastitis, mainly caused by bacterial pathogens and occasionally fungus (*C. albicans*) (Halasa et al., 2007; Kaszak et al., 2012). It has been reported that more than 150 bacterial species implicated with the mastitis and they have been categorized into three main categories viz., environmental, contagious and opportunistic (Kuang et al., 2009). Coliforms, i.e. *E. coli* and

Klebsiella spp., are found likely with intestinal flora of the bovine (Pyörälä et al., 1994). So they can spread and contaminates the environment and ultimately udder which results in clinical and subclinical mastitis.*S. aureus,* Gram-positive bacterium is actually the most leading pathogenic bacterium present in the intramammary bovine mastitis worldwide (Condas et al., 2017).Moreover, *S. aureus* strains have been associated with persistent infections and high resistance to antibiotic therapy (Moon et al., 2007). These associations can be explained by the fact that *S. aureus* strains elicit a very high mutation rate and permeability to the horizontal transference of virulence factors compared to that of other mastitis-associated pathogens (Taponen & Pyörälä, 2009).

Multiple drug resistance of mastitis causing pathogens has been stated worldwide (Waller et al., 2011). The emergence of MDR especially those exhibiting resistance to cephalosporins due to production beta- lactamases has attracted attention worldwide. Antimicrobial resistance mechanism can be spread by genetic mutation which occur at low rate and acquistation to a lot of genes that mediate the resistance to their host microorganism.This acquistation of resistant gene is the main contributor for spreading of antimicrobial resistance and this occur either by horizontal transfer or vertical transfer, the horizontal transfer include: mobile genetic parts such as plasmid and transponsintegronalso have been documented to play major role in spreading of the resistant genes (Palmer et al., 2010; Xu et al., 2011). The conventional antimicrobials and their impact on the development of antimicrobial resistance remain a public health concern(Oliver et al., 2011). A subsequent research investigated the impact of consumption of raw milk containing antimicrobial, and reported an increased occurrence of antimicrobial resistance in MDR strains of dairy origin (Pereira et al., 2014). MDR bacterial strains, such as *E.Coli* and *S. aureus* strains, cause an increasing grave hazard to global public health concern as some antibiotics lessen their functions against infectious diseases (Blecher et al., 2011; Laxminarayan et al., 2013). Moreover, classical antibiotics are less and less effective to overcome the infectious diseases (Birla et al., 2009).

The rise of the resistant pathogens is considered as big challenge worldwide while global reduction in the veterinary antibiotics due to overuse of essential antibiotics by the food

industry. because of scientific evidence that AMR strains were found in live stocks is also increasing risk for post antibiotic era (Agga et al., 2015).There is an urgent need for the development of biocompatible antibacterial formulations, which could control bacterial growth with their upgraded and efficient mechanisms (Lima et al., 2019; Moo et al., 2019).

Keeping in view the above facts the present study was designed with an objective to isolate and identify mastitis causing pathogens from the mastitis suspected milk and then antibiotic sensitivity tests was employed to evaluate resistance patternsin the mastitis casing pathogens.

3.2. Results

A total of 35 dairy farms and herds of Islamabad and Rawalpindi, twin cities of Pakistan was selected randomly for the collection of milk samples for the isolation of mastitis causing microbial strains. During milk sampling important information were also gathered about environmental condition of dairy farms and associated mastitis cases in the cattle as shown in the **Figure 3.1**. Meanwhile milk samples of suspected cattle were also screened for mastitis which were collected for diagnosis at National Veterinary Laboratories of Pakistan .Out of 1480 milk samples of selected animals ,1048 were found positive for CMT screening which confirmed mastitis suffering as shown in the **Figure 3.2**. The prevalence of Sub-clinical mastitis was 90% in the buffaloes and 67% in cows of various breeds of Punjab, Pakistan as shown in **Table 3. 1**. Prevalence of mastitis based on various mastitis prompting factors in the cattle described in **Table 3.1**.Mastitis is infectious disease and controlled by various factors such as breed, age, lactation period, hygiene of udder,environment and bedding of animal.

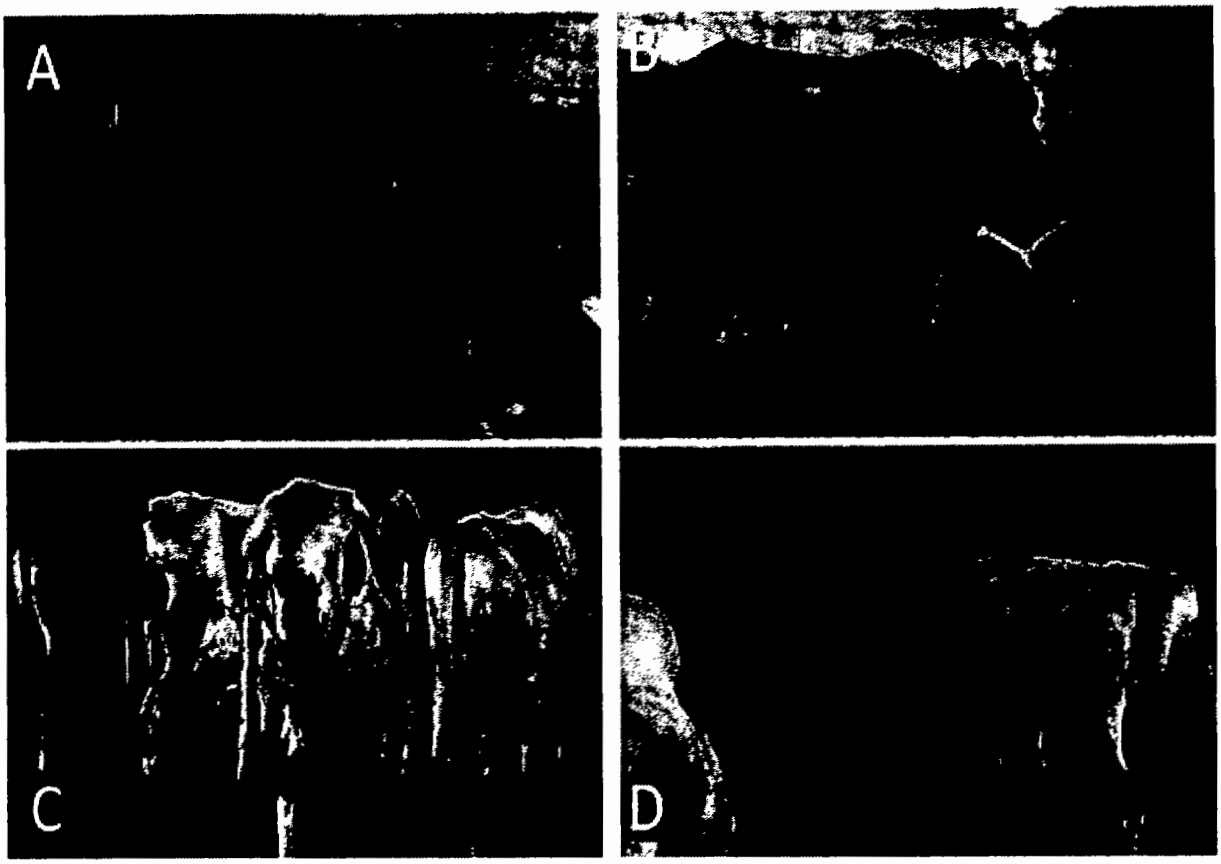

Figure 3.1: The Cattle has diagnosed mastitis in the different farms of Islamabad and Rawalpindi.

Key:-

A-Immun's Dairy Farm Islamabad

B- Koko Islamabad Banni Gala

C-Gondal Dairy Farm Rawat

D-Fareed Dairy Farm Rawat.

Table 3.1: Prevalence of mastitis based on various mastitis prompting factors in the cattle

Risk factors	**Types**	**Number of animals**	**CMT 1048 positive**	**Prevalence (%)**
Breed (1480)	Cows	1289	875	67
	Buffaloes	191	173	90
Age	5 years	550	213	38
	≥ 6years	930	835	89
Milk yield	7 -11liters	1202	989	82
	≥ 12 liters	78	59	75
Lactation period	80 days	66	49	74
	150 days	696	603	86
	≥ 160 days	445	398	89
hygienic condition of udder	Good	140	57	40
	Satisfactory	634	315	49
	Poor	706	676	**95**
Environment /bedding	Grassy/muddy	912	756	82
	Good concrete	568	292	51

Diagnosis of mastitis by California Mastitis Test (CMT)

Mastitis suspected cows and buffaloes were subjected to CMT test and appearance of flakes in the milk samples confirmed the subclinical mastitis as shown in the **Figure 3.2 D.** Some common apparent symptoms of udder was noticed inflammation and swelling **Figure 3.2 A** and **B** , redness of udder and teats was shown in clinical mastitis as described in the **Figure 3.2 B**

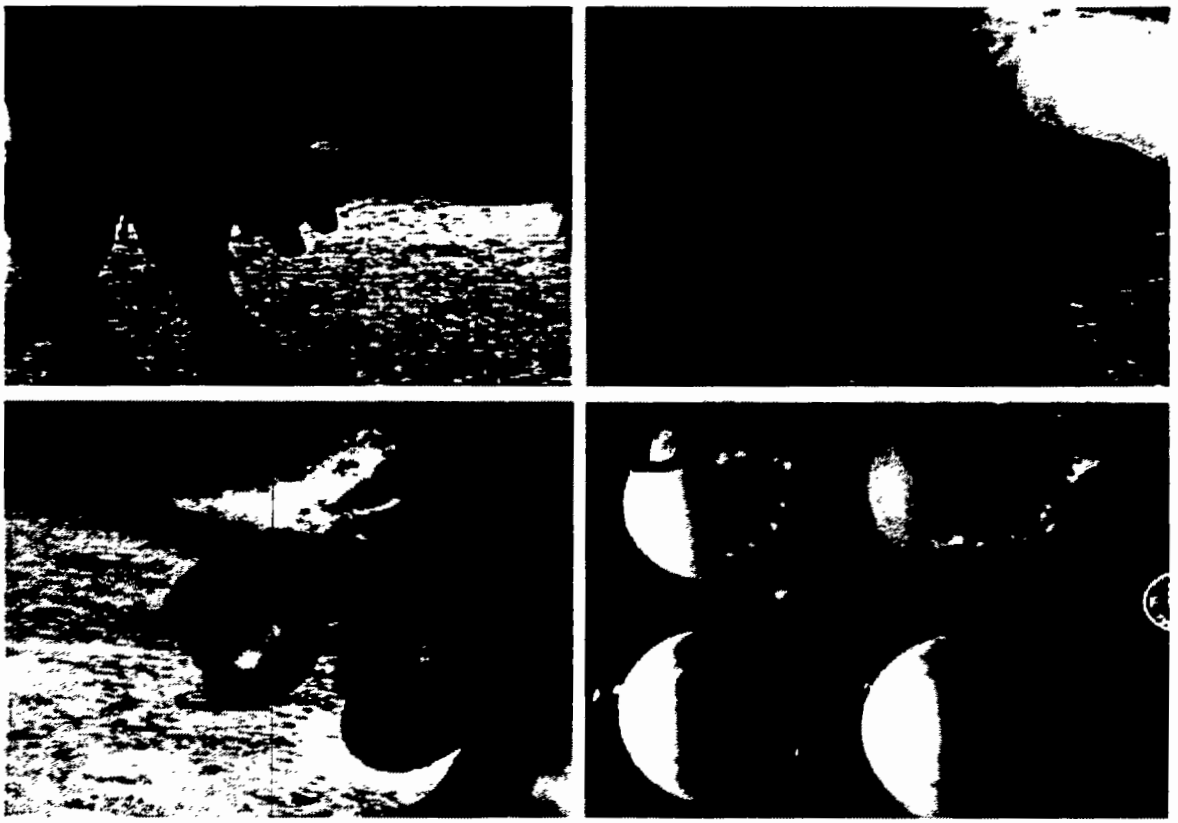

Figure 3.2 Simple method for the diagnosis of mastitis by CMT in the suspected animal for each teat of udder.

Key: A- Subclinical mastitis normal udder, B- clinical mastitis, C- abnormal appearance of udder positive for mastitis, D- flakes present the milk sample positive for mastitis test

Prevalence of mastitis causing factors

The prevalence of pathogenic strains of mastitis positive samples of cattle as shown in the **Table 3.2.**It was observed *E.coli* strains (40.2 %) were most prevalent among the Gram negative genera of bacteria cause mammary gland infection in the cattle as shown in the **Table 3. 2** and **Figure 3.3** while *S. aureus* (30.6%) was highly prevalent Gram positive pathogen causing mastitis while mastitis triggered by *C.albicans* was (9%) observed in the suffered cattle.

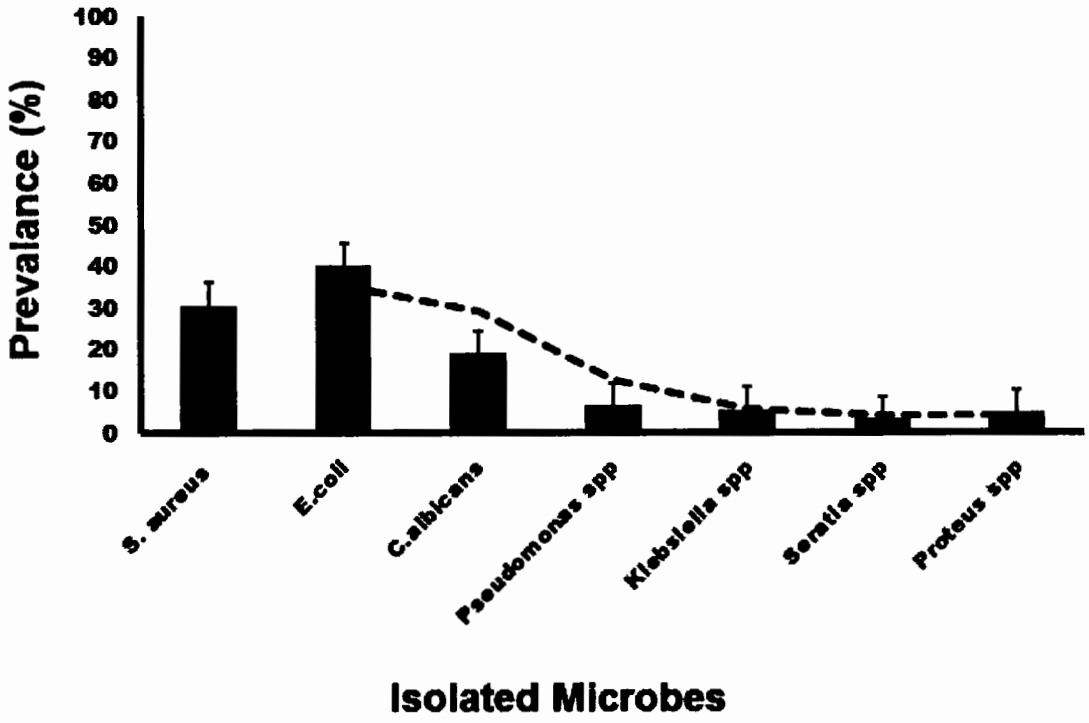

Figure 3.3: Occurrence of pathogenic microbes isolated from the milk sample of mastitis positive cows and buffaloes.

Table 3.2: Causative agents isolated from mastitis positive milk samples (n=385)

Isolated Microorganisms	**Number of isolates**	**Prevalence (%)**
S. aureus	118	30.6
MDR *S. aureus*	73	62
PDR S. aureus	2	1.6
MRSA	43	36
E.coli	155	40.2
ESBL *E.coli*	56	36
MDR *E.coli*	87	56
PDR *E.coli*	12	8
C. albicans	35	9
MDR *C. albicans*	27	77
PDR *C. albicans*	8	23
Pseudomonas spp	25	6.4
Klebsiella spp	21	5.4
Seratia spp	12	3.1
Proteus spp	19	4.9

Differential agar media for the culturing of MDR pathogens

MDR strains of *E.coli* were isolated from milk samples of cattle which were positive by CMT, on the MacConkey agar *E. coli* produced pink colored, smooth and round colonies **Figure 3.4A**. While ESBL differential media used to isolate ESBL *E.coli* strains from the isolated *E. coli* strains which produced purple to pink colonies **Figure 3. 4B**. The pink color indicated that *E.coli* is a Lactose fermenter .The culture of milk on blood agar allowed to observe small round, and yellow-orange colonies of *S. aureus* **Figure 3. 4C**. Candida showed green color of colonies on chrome agar media**Figure 3.4D** which is differential media for candida spp isolation.Morphology of isolated microbes was summarized in the **Table 3.3.**

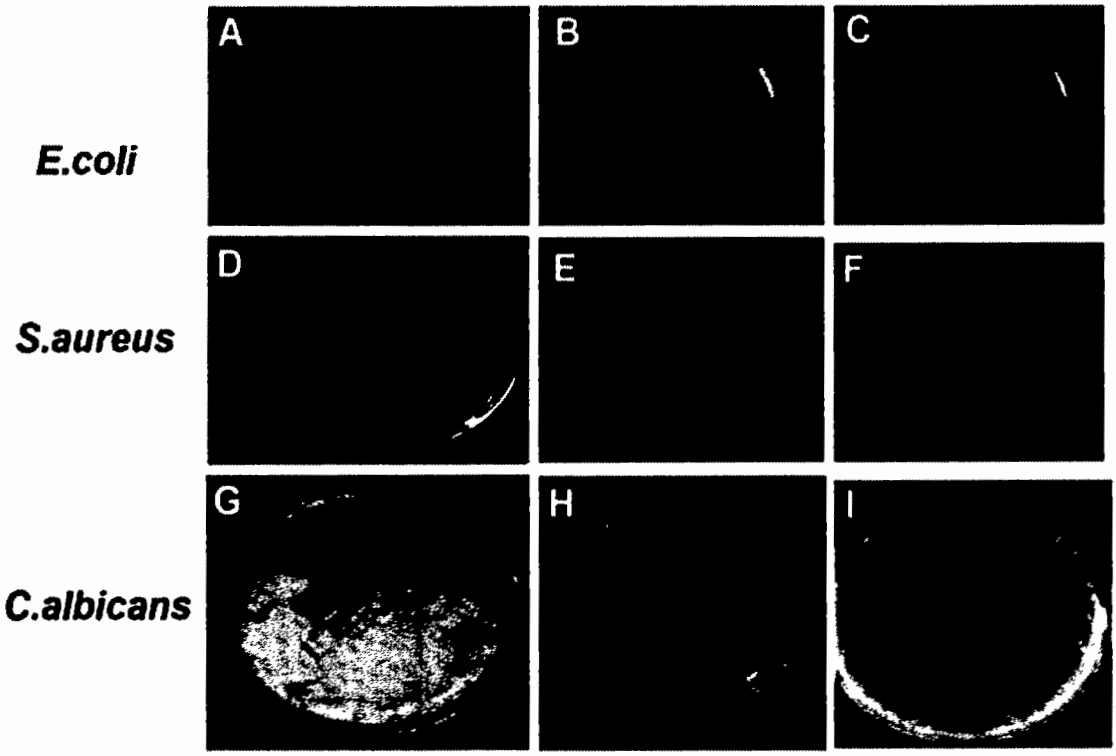

Figure 3.4: Mastitis causing pathogens isolated from the milk samples displayed colonial morphology on the selected media.

Key: A- *E.coli* on MacConkey agar, B-ESBL *E.coli* on ESBL media, C-*E .coli* on MacConkey agar - D,E &F- *S. aureus* on blood agar, E-, F-, G&H-*C.albicans* on Chrome agar, I- on SB agar

Table 3.3: Colonial morphology of isolated strains from the mastitis positive milk samples

S. No	Microbes	Color	Shape	Texture
1	*E.coli* MacConkey agar	Dark pink	Circular	Small shiny, Smooth Mucoid Colonies
2	*S. aureus* Blood agar	Golden, Yellow and clear zone of hemolysis on blood agar	Round	Large shiny, Smooth Colonies
3	*C.albicans* Chrome Agar	Dark Green on Chrome Agar	Button shaped, oval	Large Smooth, Slimy

Cellular Morphology of MDR pathogens

Under microscope, *E.coli* showed rods and retained counterstain safranin pink rods of Gram-negative *E.coli* **Figure 3.5A**, *S .aureus* retain crystal violet color with round cluster of cells **Figure 3. 5B** and *C.albicans* also found Gram positive spheres with attached buds and mycelium. Most candida organisms appear as gram-positive, football shaped morphology, candida species are evident even under 10X microscope power, although 100X oil immersion is best to confirm the isolation as shown in the **Figure 3.5C.**The *Candida* grow well on Sabouraud Agar at 37°C, forming colonies within 24–48 h. Colonies were opaque, often white or yellowish, and at first usually smooth.

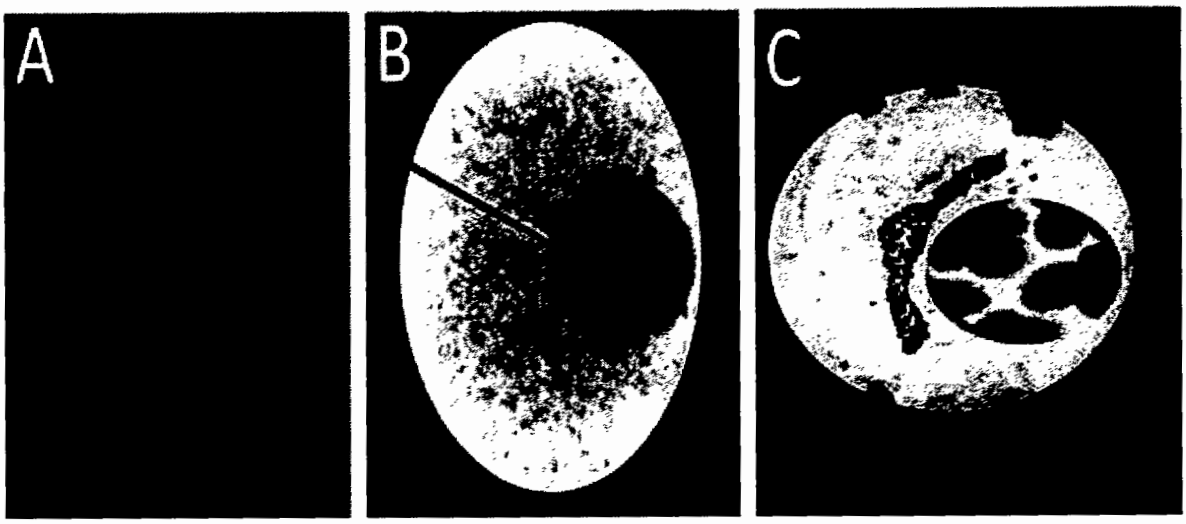

Figure 3.5: Microscopy of mastitis causing MDR pathogens,

Key: A- MDR *E.coli*, B- MDR *S. aureus*, C, MDR *C.albicans*.

Isolated microbes were confirmed by conventional biochemical tests, Coagulase and catalase tests were positive while cytochrome oxidase was negative for all isolates of *S. aureus*. All *E.coli* strains were found indol positive and catalase positive and *C.albicans* has given negative indol test results and positive catalase test as shown in the **Table 3.4**.The rapid identification test for *E.coli* produced number from API 20E was 5144552 as shown in **Tables 3.5** and for Gram-positive isolates of *S. aureus* 6736153 (**Tables 3.6**) while *C.albicans* generated API 20C number 6172174 as described in the **Table 3.7**.

Table 3.4: Conventional biochemical tests to identify isolated microbes from the milk sample of infected animals

S. No	Tests	*E.coli*	MRSA	*C.albicans*
1	**Indol test**	+ve	-ve	-ve
2	**Catalase test**	+ve	+ve	+ve
3	**Citrate test**	-ve	+ve	-ve
4	**Coagulase**	-ve	+ve	-ve
5	**Urease**	-ve	+ve	-ve
6	**Triple sugar iron**	+ve	+ve	+ve
7	**Oxidase**	-ve	-ve	+ve
8	**Motility**	+ve	-ve	-ve
9	**Germ tube**	-ve	-ve	+ve

Table 3.5: Analytical Profile Index (API 20E) performed for the identification of *E.coli*

Test	**Active Ingredient**	**QTY (mg/cup)**	**Reaction/enzyme**	***E.coli***
ONPG	2-nitrophenyl-BD-galactopyranoside	0.223	B-galactosidase (ortho 2-nitrophenyl-BD-galactopyranosidase	**+ve**
ADH	L-arginine	1.9	Arginine dihydrolase	**+ve**
LDC	L-lysine	1.9	Lysine decarboxylase	**+ve**
ODC	L-ornithine	1.9	Ornithine decarboxylase	**+ve**
CIT	Trisodium citrate	0.756	Citrate utilization	**+ve**
H_2S	Sodium thiosulphate	0.075	H_2S Production	**+ve**
URE	Urea	0.76	Urease	**-ve**
TDA	L-trytophan	0.38	Tryptophan deaminase	**-ve**
IND	L-tryptophan	0.19	Indol Production	**+ve**
VP	Sodium pyruvate	1.9	Acetoin production (vongesproskauer)	**-ve**
GEL	Gelatin (bovine origin)	0.6	Gelatinase	**-ve**
GLU	D-glucose	1.9	Fermentation/oxidation (glucose)	**+ve**
MAN	D-mannitol	1.9	Fermentation/oxidation (mannitol)	**+ve**
INO	Inositol	1.9	Fermentation/oxidation (inositol)	**-ve**
SOR	D-sorbitol	1.9	Fermentation/oxidation (inositol)	**+ve**

RHA	L-rhmnose	1.9	Fermentation/oxidation (rhamnose)	+ve
SAC	D-sucrose	1.9	Fermentation/oxidation (saccharose)	+ve
MEL	D-melibiose	1.9	Fermentation/oxidation (melibiose)	+ve
AMY	Amygdalin	1.9	Fermentation/oxidation (amygdalin)	-ve
ARA	L-arabinose	1.9	Fermentation/oxidation (arabinose)	+ve
OX	Oxidase		Cytochrome oxidase	-ve

Table 3.6: Analytical Profile Index (API Staph) performed for the identification of *S. aureus*

Test	**Active Ingredient**	**QTY (mg/cup)**	**Reaction/enzyme**	***S. aureus***
O	Negative control	0.223		**-ve**
GLU	D-glucuse	1.56		**+ve**
FRU	D-fructose	1.4		**+ve**
MNE	D-mannose	1.4		**+ve**
MAL	D-maltose	1.4		**+ve**
LAC	D-lactose	1.4		**+ve**
TRE	D-trehalose	1.32		**+ve**
MAN	D-mannitol	1.36		**+ve**
XLT	Xylitol	1.4		**-ve**
MEL	D-melibiose	1.32		**-ve**
NIT	Potassium nitrate	0.08	Reduction of nitrates to nitrites	**+ve**
PAL	ß-Naphthyl phosphate	0.024	Alkaline phosphates	**+ve**
VP	Sodium pyruvate	1.94	Acetyl-methyl-carbinol production	**+ve**
RAF	D-raffinose	1.56	D-raffinose	**-ve**
XYL	D-Xylose	1.4	D-Xylose	**-ve**
SAC	D-saccharose	1.32	D-saccharose	**+ve**
MDG	Methyl-D-glucopyranoside	1.28	Methyl-D-glucopyranoside	**-ve**
NAG	N-acetyl-glucosamine	1.28	N-acetyl-glucosamine	**+ve**
ADH	L-arginine	1.904	Arginine dihydrolase	**+ve**
URE	Urea	0.76	Urease	**+ve**

Table 3.7: Representing results of API 20C for *C.albicans*

Test	**Active Ingredient**	***C.albicans***
Glu	Glucose	**+ve**
Gly	Gylcerol	**+ve**
KDG	2-Keto-D-gluconate	**+ve**
LA	L-Arabinose	**-ve**
XYL	Xylitol	**+ve**
ANL	Adonitol	**+ve**
DX	D-Xylose	**-ve**
Gla	Glactose	**+ve**
INS	Inositol	**-ve**
SBL	Sorbitol	**-ve**
MDG	Methyl-D-Glycoside	**+ve**
NADG	N-Acetyle-D-Glucosamine	**+ve**
CL	Cellibiose	**-ve**
LAC	Lactose	**-ve**
MAL	Maltose	**+ve**
DSAC	D-Sucrose	**+ve**
THL	Trehalose	**+ve**
MLZ	Melezitose	**-ve**
SAC	Sacharose	**+ve**
RAN	Raffinose	**-ve**
OX	Oxidase	**+ve**

AST of *E.coli* strains of milk samples positive CMT

Antibiotic sensitivity profiling of all the isolated strains has done by disc diffusion. Disc diffusion method was the primary tool to classify the strains as a MDR and ESBL producing *E.coli* strains. Results showed (**Figure 3. 6**) that *E.coli* had found highly resistant to a broad range of antibiotics. Most resistant and inefficient antibiotics were observed Ampicillin (100%), Augmentin (100%), Ciprofloxacin (99%)and Tetracycline (98%). The resistance pattern exhibited by Imipenem and Meropenem was much lesser but still susceptibility against MDR strains is vulnerable as shown in the **Figure 3.7**.

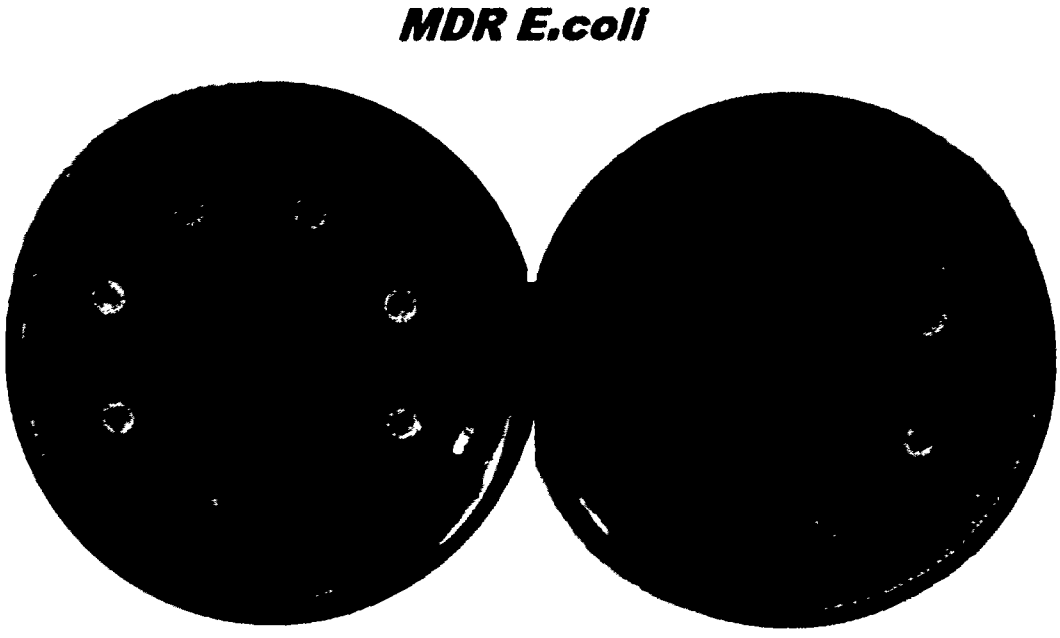

Figure 3.6 Antibacterial sensitivity testing of isolated strains of *E.coli* (N=155):

1-Ceftazidime (CAZ) 30µg, 2-Cefazolin (KZ) 30µg, 3-Cefoxitin (FOX) 30µg, 4-Imipenem (IPM) 10 µg, 5-Ceftriaxone (CRO) 30µg, 6-Ampicillin (AMP) 10µg, 7- Meropenem (MEM) 10 µg, 8- Ciprofloxacin (CIP) 5µg, 9-Augmentin (AMC) 20µg, 10Gentamicin (CN) 10 µg, 11-Doxycycline (DO) 30µg ,12-Norfloxacin (NOR) 30µg, 13-Fosfomycin (FOS) 10 µg, 14-Tetracycline (TE) 30µg, 15-Trimethoprim/Sulfamethoxazole (SXT) 30 µg

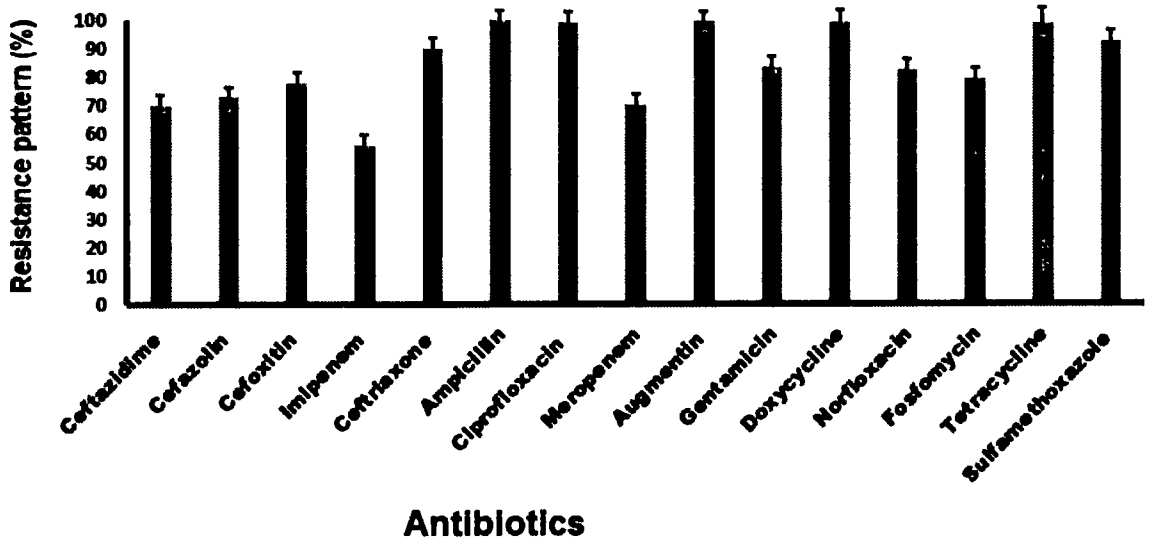

Figure 3.7 Antibiotic resistance profile of MDR *E.coli* strains of isolated from the milk samples of cattle infected with mastitis

AST of MDR *S.aureus* strains of milk samples positive CMT

The prevalence of drug resistance pattern among the *S. aureus* isolates was also determined by AST, which included a number of conventional broad-spectrum antibiotics commonly used to treat *S. aureus* and other Gram-positive strains **(Figure 3.8)**. AST revealed 73 potential MRSA out of the quarantined 118 *S. aureus*. In the suspected MRSA strains showed resistance to Augmentin (100%), fluoroquinolone CIP (96%), Ampicillin (91.6%), Cefotaxime (75%), Imipenem (75%), the narrow-spectrum beta-lactam antibiotic of the penicillin class OXA (61%), Meropenem (51.6 %) and the second-generation cephamycin antibiotic FOX (30%) and the narrow-spectrum beta-lactam antibiotic of the penicillin class OXA (61%),resistance against MDR *S. aureus* has been shown in the **Figure 3.9**.

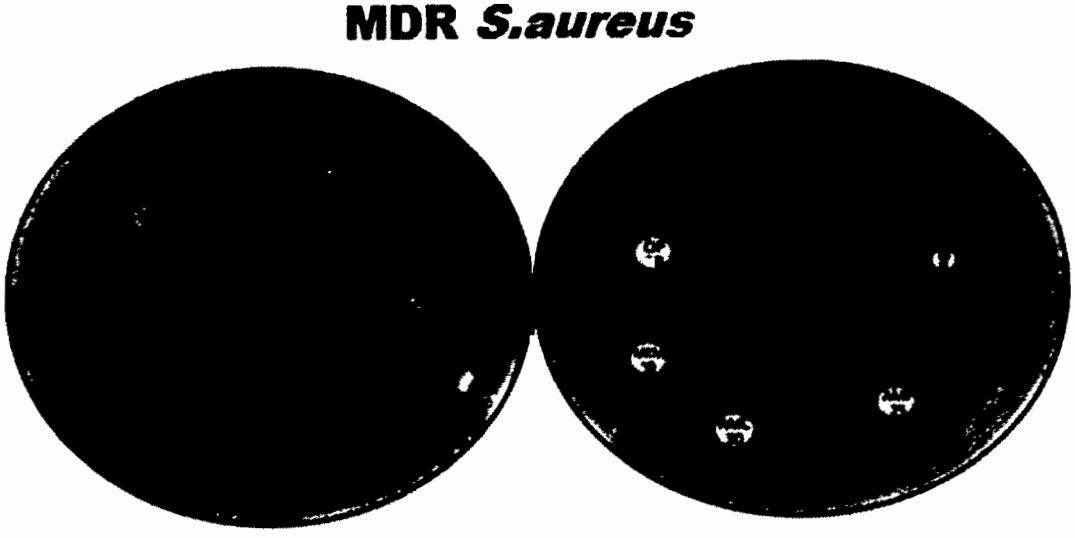

Figure 3.8 Sensitivity of *S. aureus*against different conventional antibiotics,

1-Ceftazidime (CAZ 30 µg), 2-Cefazolin (KZ 30 µg), 3-Cefotaxime (CTX 30 µg), 4- Imipenem (IPM 10 µg), 5-Cefoxitin (FOX 30 µg), 6-Ceftriaxone (CRO 30 µg), 7-Aztreonam (ATM 30 µg), 8-Ampicillin (AMP 25 µg), 9-Meropenem (MEM 10 µg), 10-Ciprofloxacin (CIP 5 µg), 11-Oxacillin (OX 1 µg), 12-Augmentin (AMC 30 µg).

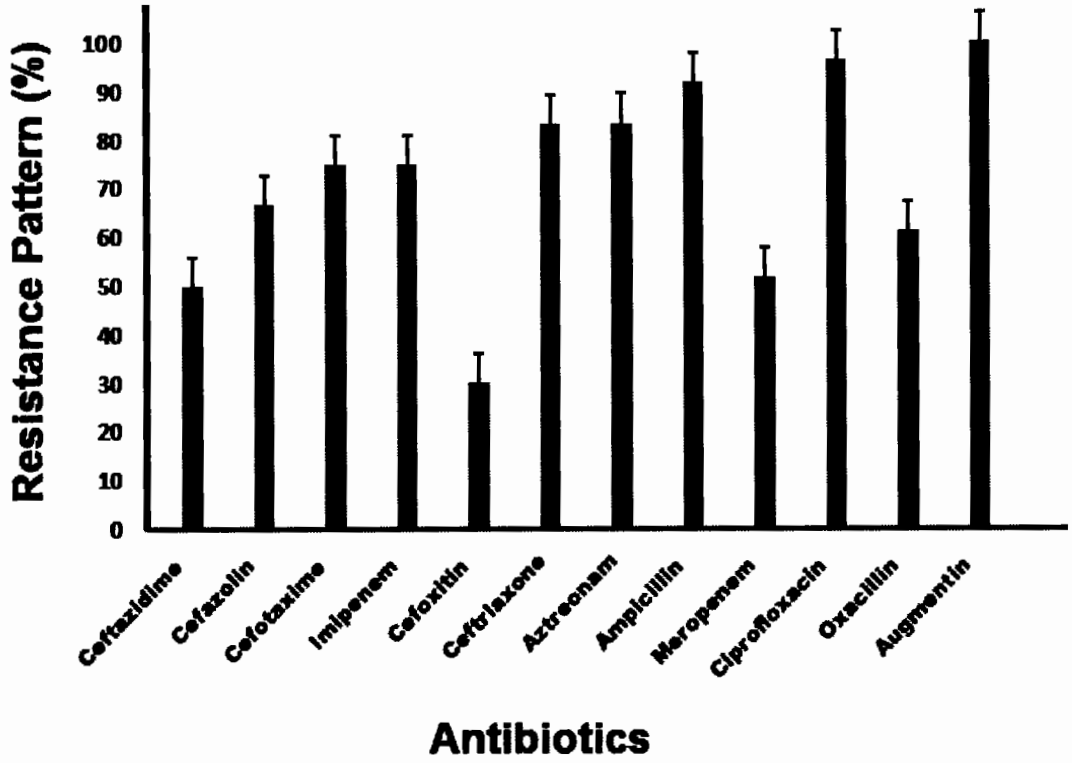

Figure 3.9 Antibiotic resistance profile of strains of *S. aureus* isolated from the mastitis positive milk samples.

AST of *C. albicans* strains of milk samples positive CMT

The antibiotic sensitivity pattern of *C. albicans* was presented in **Figure 3.10.** Most resistant antibiotics were Fluconazole (93%), Itraconazole (83%), Amphotericin B (76%), Anidulafungin (60 %) and Nystatin (59 %) while Ciclopirox (36%), Clotrimazole (35%), Voriconazole (20%), Ketoconazole (25%) and Voriconazole (20%) were found still effective against MDR strains of *C .albicans* as shown inthe **Figure 3.10**. As shown inthe **Figure 3.11**resistance frequency of MDR *C.albicans* strains isolated from the milk samples of cattle suffered from mastitis which clearly showed the ineffectiveness of Fluconazole, Itraconazole and Nystatin.

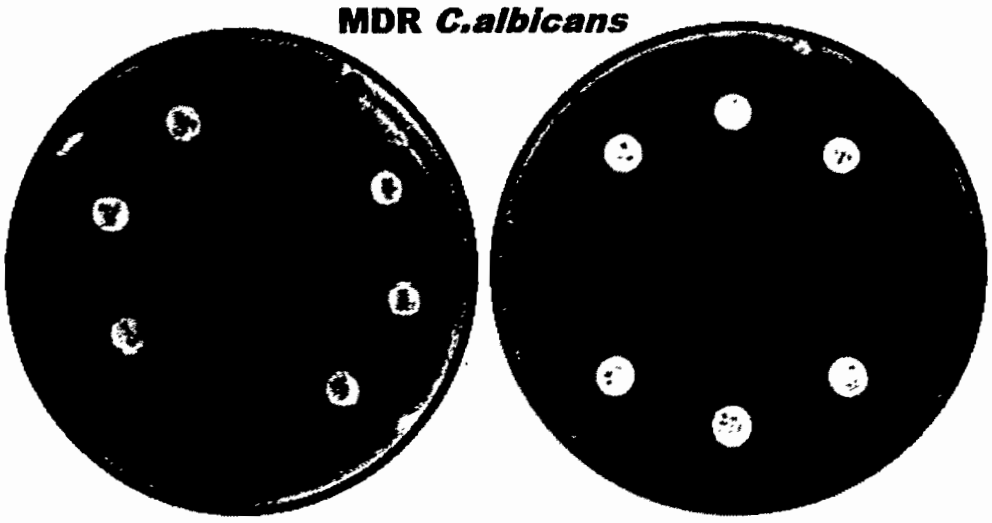

Figure 3.10 Antibiogram of MDR isolates of *C.albicans*,

Key:1-Amphotericin B, 2- Fluconazole,3- Ketoconazole, 4-Itraconazole, 5-Voriconazole 6-Nystatin, 7- Ciclopirox, 8- Caspofungin, 9-Flucytosine ,10-Posaconazole,11-Anidulafungin,12-Clotrimazole.

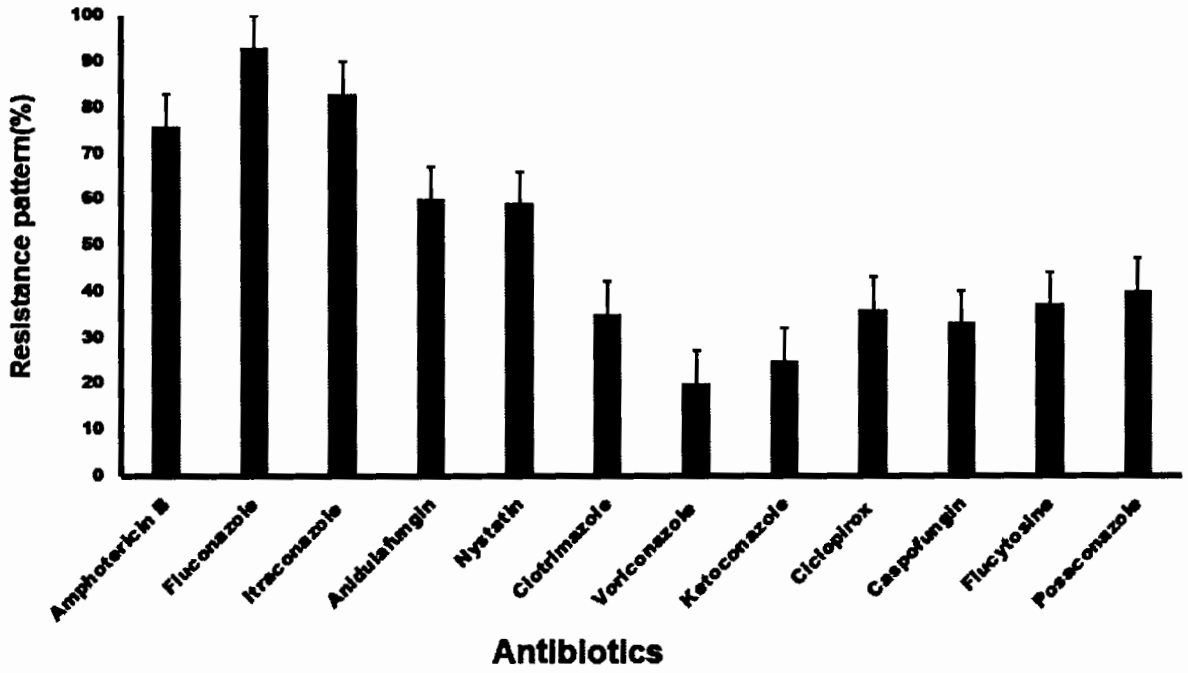

Figure 3.11 Resistance spectrum of MDR *C.albicans* strains detained from the milk samples of cattle infected with mastitis.

Drug resistance in the isolated microbial species

On the basis of drug resistance profile pathogens were assigned to Multidrug resistant (MDR), Pand drug resistant (PDR), and while Methicillin resistant *S. aureus* (MRSA) and Extended spectrum Beta Lactamases (ESBL) switching is also attributes of resistance to specific class of antibiotics as shown in the **Figure 3. 12.** Increasing resistance and limited treatment therapy is raising voice to find the solution for the emerging resistant Gram-negative and Gram positive pathogens found in the cattle suffering from mastitis.

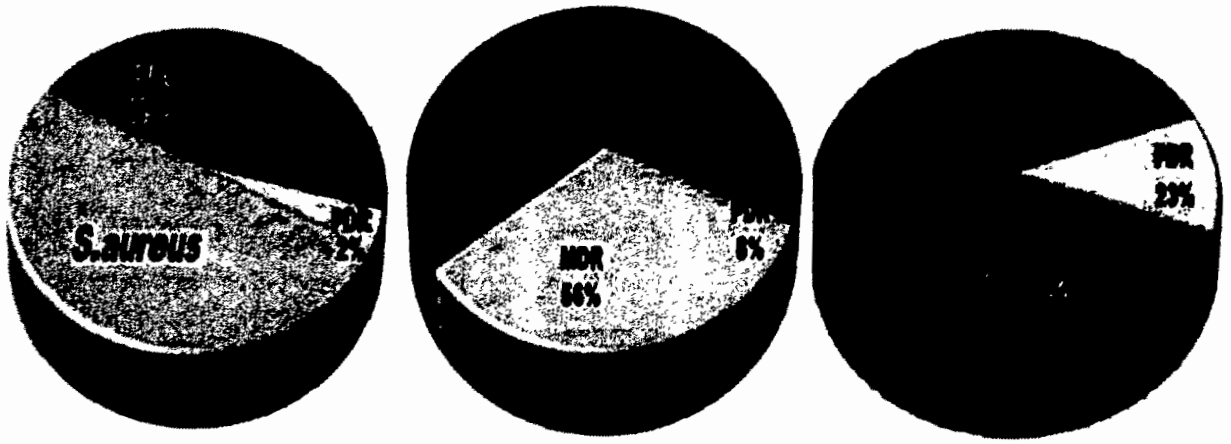

Figure 3.12: Incidence of drug resistance in the highly prevalent causative agents of mastitis.

Detection of Antibiotic Resistant Genes

To avoid false positive MRSA strains, PCR detection of the *mecA* gene was performed as shown in the **Figure 3.13d**. The *mecA* gene is known to confer *S. aureus* resistance to methicillin .It is worth mentioning that the recommended susceptibility breakpoints for the 30-μg FOX disk test used to detect *mecA*-mediated resistance in *S. aureus* has been changed in January 2007 by CLSI from ≤19 mm and ≥20 mm to ≤21 mm and ≥22 mm .The amplification of *mec*A gene is prescribed as a gold standard in the detection of this resistance.Subsequently, genotyping allowed to confirm only 35 (47.94%) MRSA from the 73 suspected MRSA based on AST basis.

Gram negative rods of *E.coli* showed highest resistance to large number of antimicrobials agent used in this study. Particularly,β-lactams, *E.coli* have 100% resistant to Ampicillin (100%), Augmentin (100%)and this resistance properties associated with 100%, 85% and 70% prevalence of bla_{TEM}, bla_{SHV} and bla_{CTX} respectively as shown in the **Figure 3. 13 a-c**. This is may be due to the ability of many of the *Enterobacteriaceae* to have intrinsic resistance to β-lactams by releasing β-lactamaseswhich break the β-lactam ring and stop the action of antibiotic. SHV, CTX, TEM, are the most dominant β - lactamases in Gram-negative bacteria. In the current study, blaTEM found in all isolates (100%).

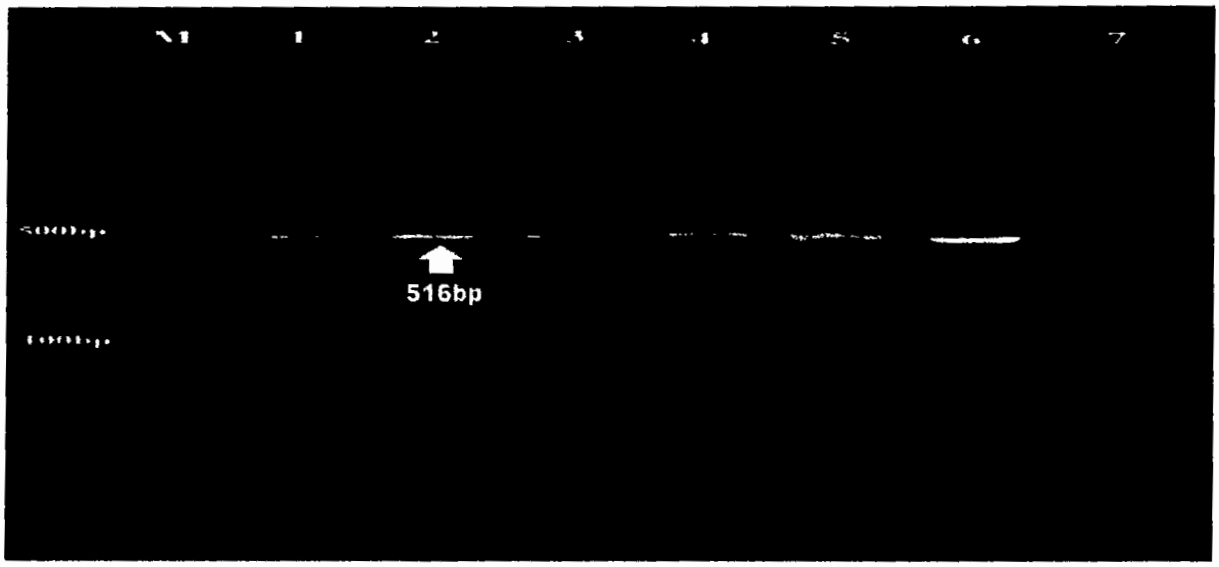

Figure 3.13a: Amplification of ESBL genes (bla TEM) by PCR analysis in ESBL *E.coli* causing mastitis

Key: M- 100bp ladder; 1-PC, 2-7 test samples of *bla* TEM.

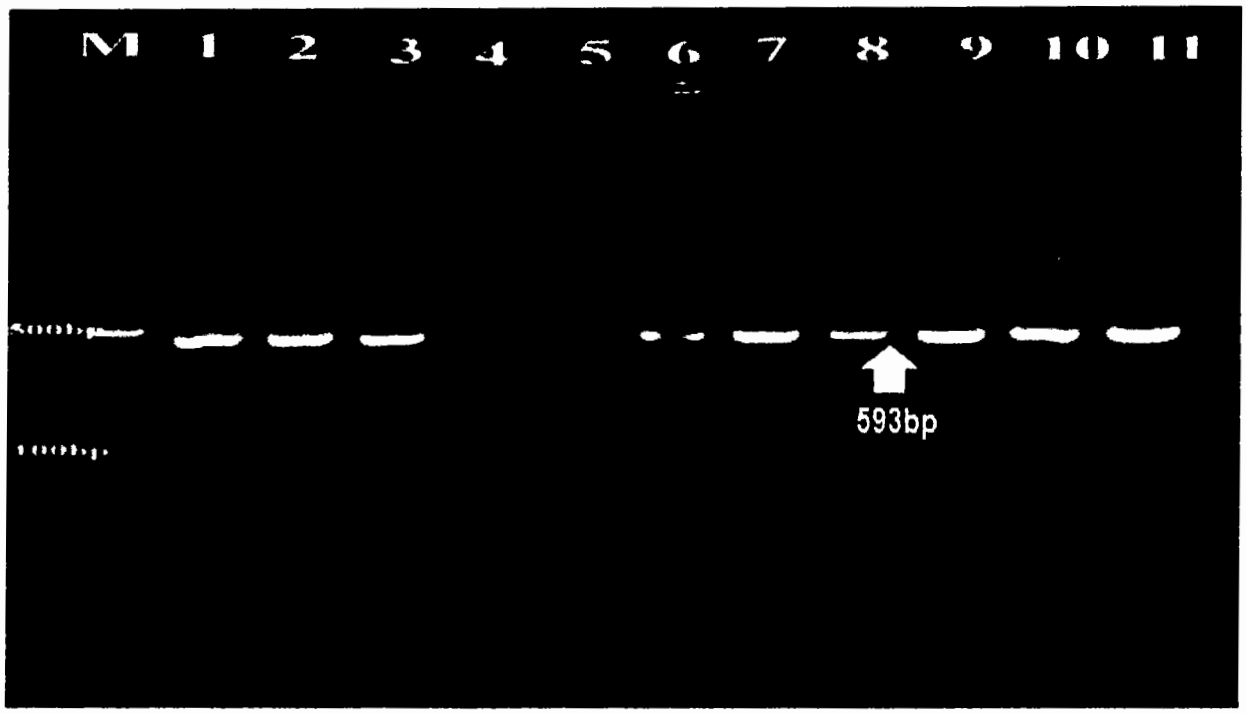

Figure3. 13 b: Amplification of ESBLgenes (CTX genes) by PCR in *E.coli* causing mastitis

Key: M- 100bp ladder; 1-PC, CTX genes.

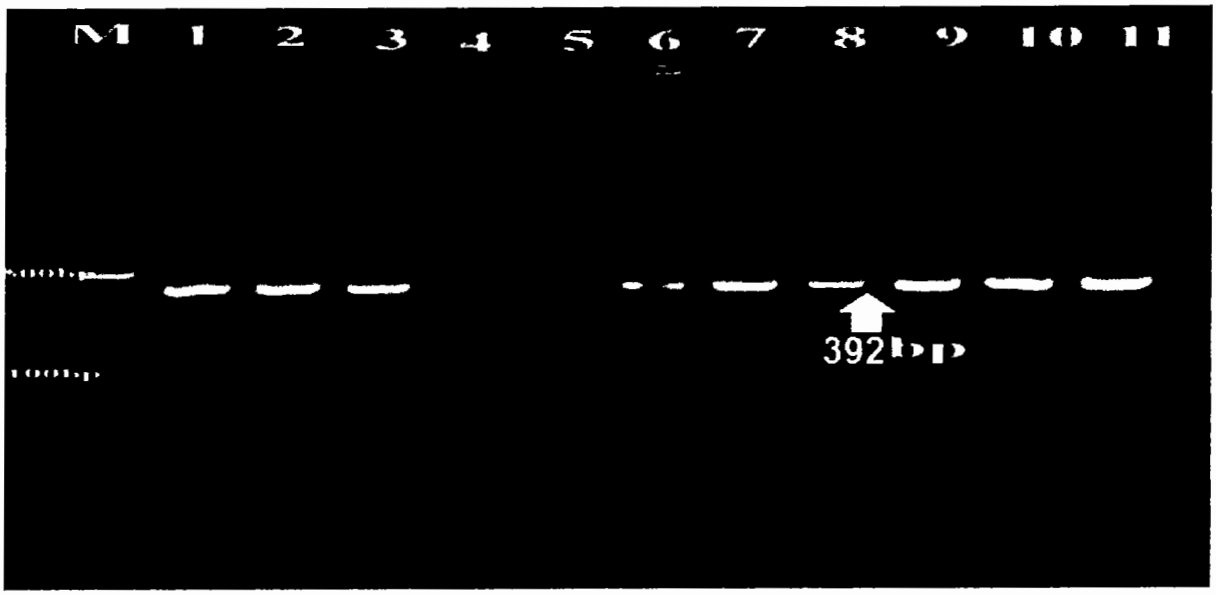

Figure 3. 13 c: Gel electrophoresis image displaying amplification of ESBL *E.coli* fragment using blaSHV primer (392).

Key: M- 100bp ladder; 1-PC, 2-11 test samples of *bla*SHV.

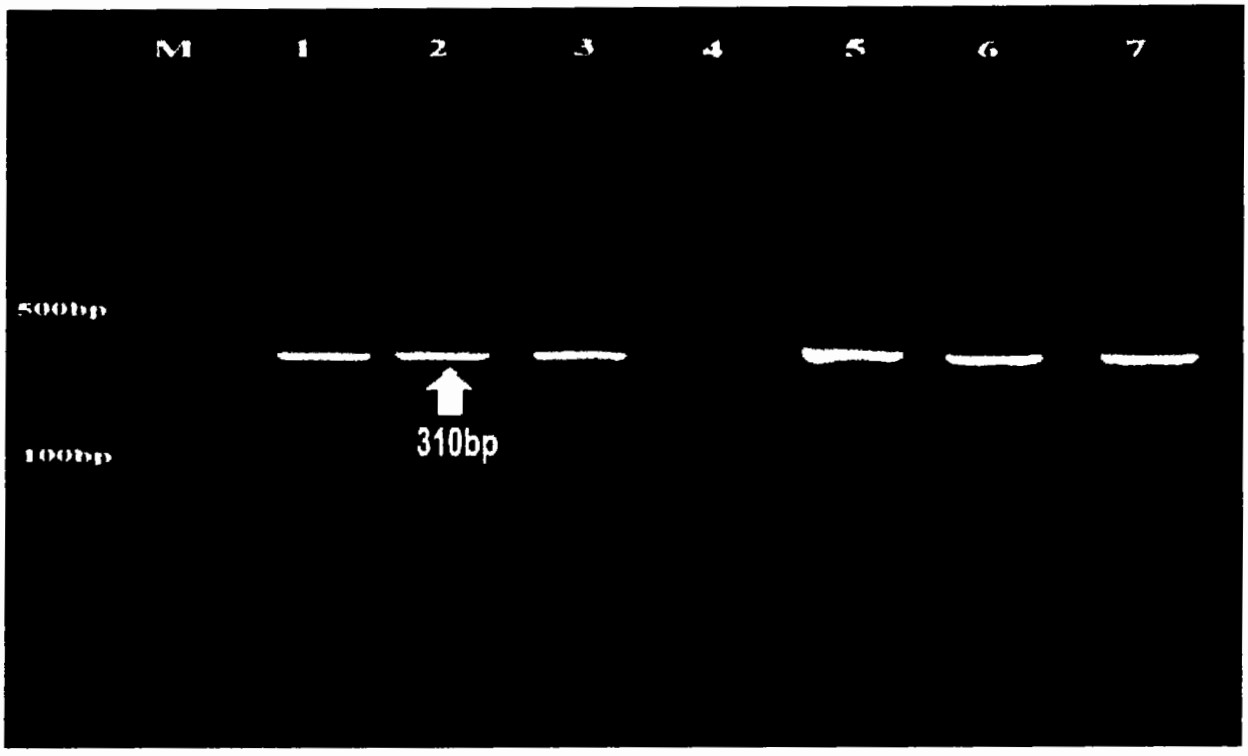

Figure 3. 13 d: A-Amplification of *mec*A gene (310bp) by PCR in suspected MRSA.

Key: M- 100bp ladder; 1-NC, 2-PC, 3-7 test samples, included a PC (MRSA strain ATCC 43,300), a NC (*S. aureus* strain ATCC 25923).

3.3. Conclusion

Mastitis is causing economic problem in the dairy industry and treatment revolution for suitable antimicrobial drugs is highly required to control the infection. Moreover, the antibiotic susceptibilities of isolated MDR pathogens from mastitis positive samples were observed periodically. Screening of resistance genes in MDR pathogens, ESBL genes in *E.coli* and *mecA* genes in MRSA, whichplay key role about limiting the emergence of resistance and subsequently decrease the risk of dissemination of resistant MDR isolates through the food chain.

CHAPTER 4

GREEN SYNTHESIS OF METALLIC OXIDES NPs BY USING AQUEOUS EXTRACT OF M. CONCANENSIS LEAVES AND BLACK CARDAMOM SEEDS

4.1. Introduction

Medicinal plants have historically proven their value as a source of molecules with therapeutic potential, and nowadays still represent an important pool for the identification of novel drug leads. In the past decades, pharmaceutical industry focused mainly on libraries of synthetic compounds as drug discovery source. They are comparably easy to produce and resupply and demonstrate good compatibility with established high throughput screening platforms (Luseba & Tshisikhawe, 2013). However, at the same time there has been a declining trend in the number of new drugs reaching the market, raising renewed scientific interest in drug discovery from natural sources.

M .concanensis is the medicinal herb and the versatile use of moringa plant is been reported such as a medicinal product, practical food source, nutraceutical and water purifying agent. It is used for the treatment of variety of diseases including paralysis, menstrual pain, high blood pressure skin tumors, joint pain , inflammation ,liver and kidney disease indicating its immense importance in health care industry(Balamurugan et al., 2015). *M. concanensis* is found to be effective against inflammation and well known medicinal plant. Reactive oxygen species-promoting substances such as phytol constitute a promising novel class of pharmaceuticals for the treatment of rheumatoid arthritis and possibly other chronic inflammatory diseases i.e. mastitis which is inflammation of udder (Balamurugan et al., 2015) .

Many chemical methods are chosen for synthesizing NPs because of their quick reaction time and their capability to produce monodispersed NPs (Smitha et al., 2008). They have few disadvantages such as the high price of the process and not being environment friendly since

they make lots of pollution in the environment because of using toxic solvents and reducing agent (Naraginti & Li, 2017) .To avoid these drawbacks, green chemistry approaches have been employed for production of NPs which is simple, convenient, less energy-intensive, eco-friendly and minimize the usage of unsafe materials, and maximize the efficiency of the process (Gross & Kalra, 2002; Raveendran et al., 2003).

Moringa plant has gained much importance in green chemistry due to its therapeutic applications in agriculture, medicine, and industries. *Amomumsubulatum* (Black cardamom) seeds have studied for various research purposes but for NPs synthesis not much explored. Although it is highly regarded as a ''Queen'' of species, is a perennial herbaceous crop belonging to the family *Zingiberaceae*(Pura Naik et al., 2004). This plant is distributed chiefly in Africa and Tropical Asia, and cultivated in swampy places (e.g. Nepal) across hills around water streams for its subsequent uses in cooking, folklore and Ayurvedic medicine (Agnihotri & Wakode, 2010). Here in, a biogenic one step procedure for the preparation of metallic oxide NPs to enhance the morphological, structural, and optical properties of NPs using *M. concanensis* aqueous extract and black cardamom seeds exract.

4.2. GC-MS analysis of M .concanensis and A. subulatum (Black cardamom) Selected for the Synthesis of Nanoparticles

GC-MS employed for the analysis of phytochemicals in the *M .concanensis*leaves extract and Black cardamom seeds extract. It is evident from the GC-MS chromatogram with peak area as shown in the figure (**Figure 4. 1 and 4.2**) all fractions have a complex chemical composition, retention time and structural formula .

The active phytocompounds with their retention time (RT), molecular formula and specific reference number in the aqueous leaves extract of *M. concanensis* presented in the **Table 4.2.**

Aqueous leaves extract contained following phytochemicals i.e.Pyridine-3-carboxamide (32.23%), Phytol (22%), Callitrisic acid (14%), Hexadecanoic acid (11%), Ethyl benzene (9%), Benzene, 1,3-dimethyl- (5%) , 1,2-Benzenedicarboxylic acid (3%), alpha -Amyrin (4%),p-Xylene(0.1%) ,2,6-Octadien-1-ol (2%), 3,7-dimethyl- (1%), Phenol 2,4-bis(1,1-dimethyleth...(11%) ,2,6-Octadien-1-ol, 3 (8%),7-dimethyl- acetate (11.2%), (E)-Bicyclo[3.1.1]heptane (1.23%), 3,5-bis(1,1-dimethylethyl)-4-hydroxy-, methyl ester, (11.98%).

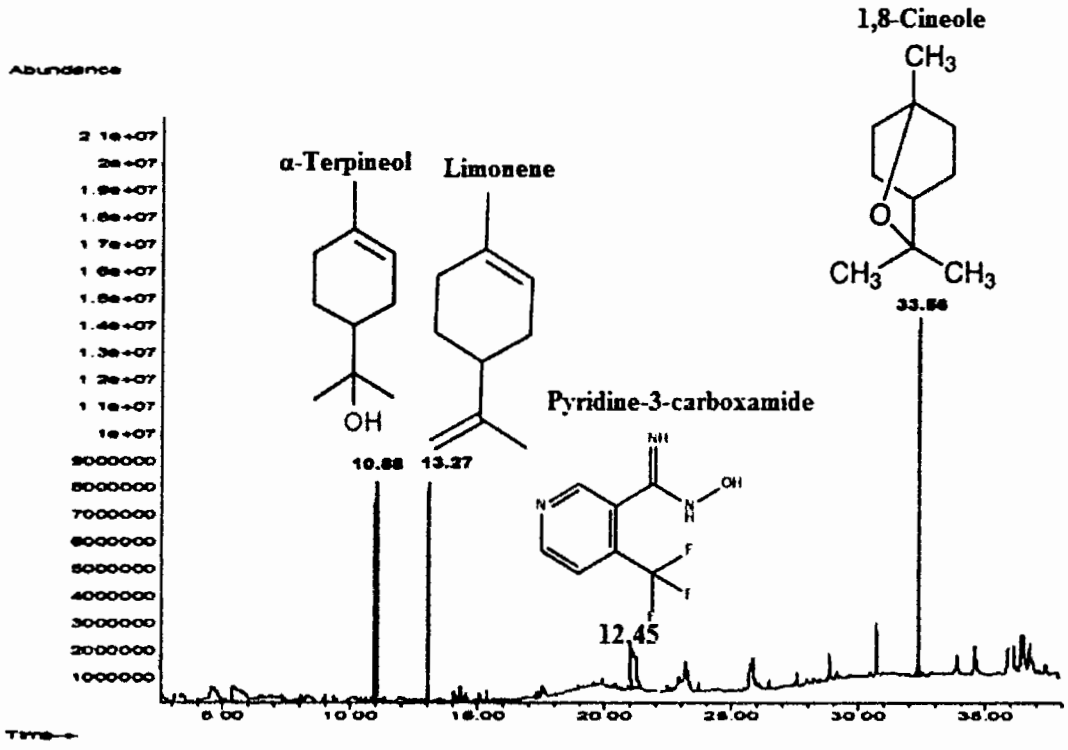

Figure 4.1 GC-MS spectrum of aqueous extracts of Black Cardamom seeds.

Black cardamom seeds extract were enriched by following phytocompounds i.e. 2,6-Octadienal,3,7-dimethy-,(15.48%), 2-Nitro-I-naphthol (15.58%), 7-Oxabicyclo[4.1.0] heptane, 1-(15.84%), Tridecanoic acid (15.94%), 1,8 Cineole (33.56%), α-Terpineol (10.88%), Limonene(13.27%), α-Pinene (1.64%), β Pinene (6.46%) as shown in the **Table 4.1.**

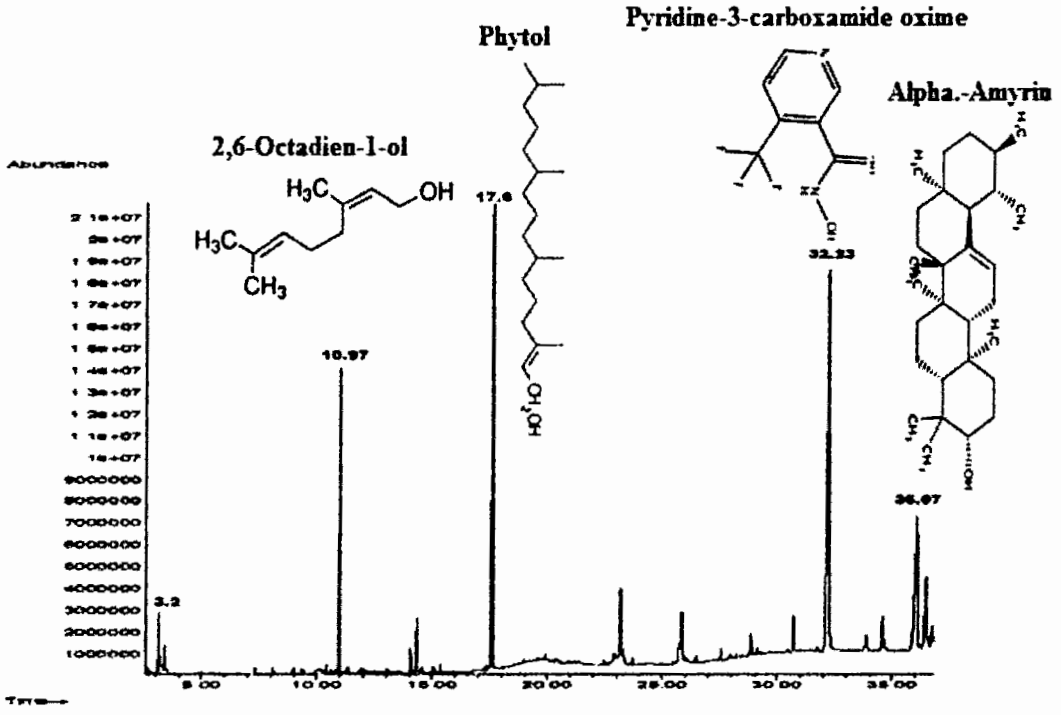

Figure 4.2 GC-MS analysis of aqueous extracts of *M. concanensis* leaves.

Table 4.1: Phytocompounds revealed by GC-MS chromatogram of Black Cardamom seeds extract.

Compounds	RT	Area %	Cas #
Quinoline, 2,7-dimethyl-	12.33	0.13	000093-37-8
Isolongifolene, 7,8-dehydro-8a-hydroxy-	12.50	0.07	1000151-49-2
Tricyclo[20.8.0.0(7,16)]triacontane,1(22),7(16)-diepoxy—	12.78	0.09	1000155-90-3
Tricyclo[6.3.3.0]tetradec-4-ene,10,13-dioxo- RCL T297321	12.95	0.09	078046-17-0
2-Dodecanol	13.51	0.06	010203-28-8
2-Heptanone, 4-methyl-	14.12	0.06	006137-06-0
Calarene epoxide	14.51	0.12	1000151-46-0
Androst-7-ene, (5.alpha.)-	14.79	0.06	054411-76-6
Phenanthrene, 7-ethenyl-1,2,3,4,4a,4b,5,6,7,8,8a,9-dodecahydro-1,1,4b,7-tetramethyl-, (4aS,4bR,7S,8aR)-	15.19	0.14	055255-56-6
Benzenepropanoic acid, 3,5-bis(1,1-dimethylethyl)-4-hydroxy-, 2-[3-[3,5-bis(1,1-dimethylethyl)-4-hydroxyphenyl]-1-oxopropyl]hydrazide	15.36	0.08	006386-38-5
2,6-Octadienal, 3,7-dimethyl-, (E)	15.48	0.04	000106-26-3
2-Nitro-1-naphthol	15.68	0.13	000607-24-9

7-Oxabicyclo[4.1.0]heptane, oxiranyl	15.84	0.11	089128-14-3
Tridecanoic acid	15.94	0.16	000638-53-9
1,8-Cineole	33.56	10.07	110983-42-1
α-Terpineol	10.88	3.3	000596-84-9
Limonene	13.27	0.32	073669-46-2
α-Pinene	1.64	2.11	038754-94-8
Pyridine-3-carboxamide, oxime, n-(2-trifluoromethylphenyl)-	12.45	0.71	288246-53-7
β-Pinene	6.46	1.5	000117-77-1

Table 4.2 Various compounds were studied by GC-MS analysis of *M. concanensis* leaf extract.

Compounds	**RT**	**Area%**	**Ref#**	**CAS#**
Ethylebenzene	3.07	0.25	4962	000100-41-4
Benzene, 1,3-dimethyl-	3.14	2.27	4977	000108-38-3
p-Xylene	3.37	0.98	4954	000106-42-3
2,6-Octadien-1-ol, 3,7-dimethyl-, (E)-	7.31	0.16	25591	000106-24-1
Phenol, 2,4-bis(1,1-dimethyleth...	10.42	0.14	60203	000096-76-4
2,6-Octadien-1-ol, 3,7-dimethyl-, acetate, (E)-	10.97	6.20	53388	000105-87-3
Bicyclo[3.1.1]heptane, 2,6,6-trimethyl-, (1α,2β,5α	14.04	04 0.44	16409	006876-13-7
3,5-bis(1,1-dimethylethyl)-4-hydroxy-, methyl ester	15.36	0.18	113228	006386-38-5
Phytol	17.60	22.17	115538	000150-86-7
Callitrisic acid	22.93	1.22	117818	005155-70-4
Hexadecanoic acid	23.18	4.93	132706	023470-00-0
1,2-Benzenedicarboxylic acid	23.70	0.21	105069	004376-20-9 81
Pyridine-3-carboxamide oxime	32.23	0.23	106566	288246-53-7
alpha.-Amyrin	36.75	0.95	161264	000638-95-9

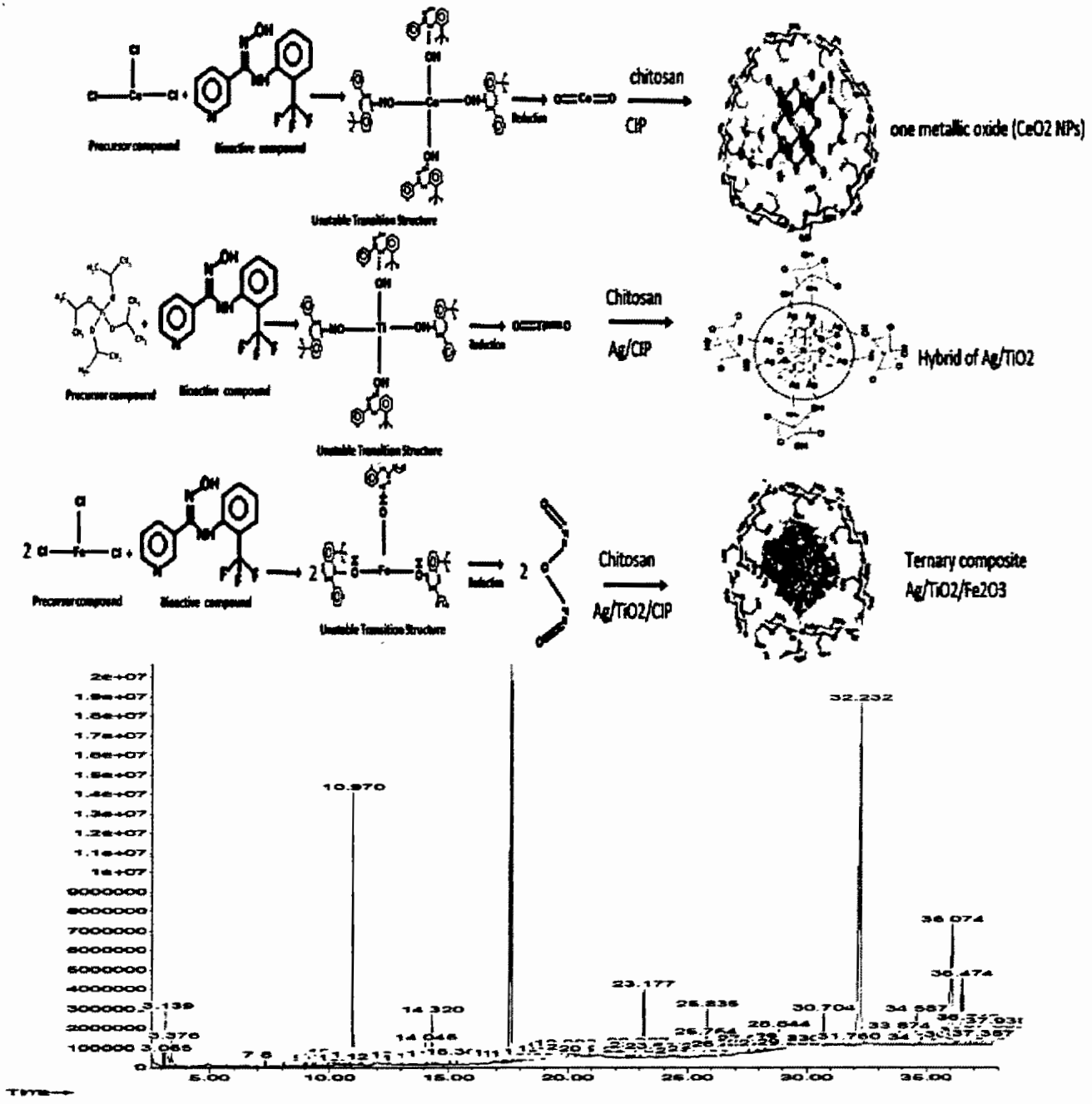

Figure 4.3 GC-MS spectrum phytocompound (Pyridine-3-carboxamide, oxime,

n-(2-trifluoromethylphenyl)-) proposed as precursor for the synthesis of respective metallic oxides Ag, TiO_2, CeO_2, Fe_2O_3 NPs interact by Redox reactions.

In the green synthesis of leaves, extracts were utilized in exchange to the chemical reagents as a potential reducing agent due to its antimicrobials as shown in the **Figure 4.3.** All these applications were because of the phytochemicals such as alkaloids, tannins, flavonoids, saponins, triterpenoids, and anthraquinones intrinsic in Moringa leaf extracts.

4.3. Conclusion

Medicinally important plants were selected and analyzed their phytochemicals by GC-MS analysis. To combat MDR pathogens, nanoparticles of the following metallic oxides were synthesised: Ag NPs, CeO_2 NPs, TiO_2 NPs, and Fe_2O_3 NPs, all of which are deemed generally recognised as safe materials (GRAS). Metallic oxide nanoparticles were made utilising aqueous extracts of Moringa concanensis leaves and Amomum subulatum, which are selected medicinal important plants. New hope of Nanotechnology is providing therapeutic alternative to conventional antibiotics.

CHAPTER 5

NANOMATERIAL A: CHITOSAN COATED GREEN SYNTHESIZED TiO_2 NANOPARTICLES

5.1. Introduction

Mastitis is the most common and the most prevalent and costly disease of dairy industry worldwide and the most common reason in which animals are treated with antibiotics (Harmon, 1995). All the diseases were under control in the past few decades are now difficult to treat because of MDR pathogens. The magnitude of antimicrobial resistance in the Gram negative bacteria is increasing, whereas efforts of all the communities are required to confront the challenges of treatment options (Lago et al., 2011). It poses a major public health risk due to transmission possibility of zoonotic bacteria or their toxin along with antibiotic resistance genes (Seegers et al., 2003).

The antimicrobial activities of metallic nano-particles are well established and several methods to study bactericidal effects have been reported. Although very few studies are encountered on coating of metallic nano-particles and application against drug resistant pathogens. However, nano-particles such as titanium oxides, gold, nickel, cobalt, silver oxides and copper oxide are demonstrating superior antimicrobial activity. There is acute need in the development of unique and new antibacterial materials with biocompatibility and sturdy antimicrobial capability against drug resistant microorganisms and treatment strategies which can control bacterial growth by the improved mechanisms(Thorley & Tetley, 2013). The significance of nanomaterials due to their unique physicochemical properties as compared to bulk particles make them efficient, effective and promising candidate for currently antimicrobial agent. The metal based nanomaterials have great resistant potential in front of microorganisms (Sosnik et al., 2010).

Titanium dioxide has been received great interest in many applications as the decomposition of pollutants in air, water purification, self-cleaning, and killing pathogenic bacteria. Titanium dioxide have prospective properties i.e. photocatalytic activity, hydrophilicity, stability, harmless electrical, optical, magnetic, electro-optical, and magneto-optical and high production yield therefore it has been used extensively in different field of science (Matsunaga et al., 1988 ;Saravanan et al., 2018).

Antimicrobial activity of TiO_2 was reported first time in 1985 by Matsunaga and colleagues. They observed under illumination with near UV light that microbial cells could be killed by the contact with a TiO_2–Pt catalyst (Matsunaga et al., 1985). According to literature highly reactive oxygen species (ROS) are considered to be the key species in the photocatalytic disinfection process. Reactive oxygen species (ROS), •OH, $•O_2^-$ and H_2O_2 are capable of mineralizing pollutants. All three ROS exhibit bactericidal activity but some studies have emphasized that nanoparticles might be performed as electron traps and hinder the rate of recombination of e^-/h^+ pair by tuning the band gap value. This assists the creation of ROS and improves the antibacterial activity (Kubacka et al., 2012). To enhance stability of NP they could be coated with biocompatible polymers. Chitosan is a good biocompatible polymer by exhibiting high biological, antimicrobial activities and homeostatic effect which strengthens the stability of nanoparticles (Yuan et al., 2016).

Numerous studies have been formerly reported on the antimicrobial activity of TiO_2 NPs to show the sway of concentration and size over its antibacterial properties. Although much progress has been made in preparation of TiO_2 NPs, there is a need of biopolymer based TiO_2 composites for loftier activity which is eco-friendly and non-toxic. There are many preparatory methods to synthesize TiO_2 NPs, agglomeration between the nanoparticles is the main drawback of these methods. To avoid this agglomeration between cationic nanoparticles, it is necessary to induct the suitable coating materials so various stabilizers have been reported such as polyvinyl

pyrrolidone, polyvinyl alcohol and polyaniline. Moreover, biopolymers based coating materials are now becoming popular like pectin, cellulose, chitosan, and starch which can stabilize the metal nanoparticles through electrostatic interaction between the functional group of polymers and nanoparticles(Dickinson, 2017) . Mainly chitosan biopolymer receives much more attraction because of its excellence in biocompatibility, biodegradability and intrinsic antimicrobial ability (Yuan et al., 2016). Chitosan is a polysaccharide self-possessed of glucosamine and N-acetyl glucosamine linked with a β-1-4- glycosidic linkage and is mostly acquired by deacetylation of vastly copious chitin. Chitosan has ability to chelate metal nanoparticles originates from the presence of both amino ($-NH_2$) and hydroxyl (–OH) groups in its glucosamine unit (Yuan et al., 2016). TiO_2 NPs has been considered as generally recognized as safe (GRAS) additive in medical devices and biomaterials, hence it has been found attractive material for efficient adhesiveness and bactericidal activities (Kochkodan et al., 2008).

The aim of the present study is to introduce a new and unique CS-NPs coated TiO_2NPs which were prepared by the modified ionic gelation method. The TiO_2 nanoparticles coated with chitosan biopolymer has endorsed its antibacterial activity against MDR strains of *E.coli* causing mastitis. Subsequently, the synthesized CS-NPs coated TiO_2 NPs were scrutinized using x-ray diffractometer (XRD), FTIR spectroscopy, transmission electron microscopy (TEM), scanning electron microscopy (SEM) and their corresponding energy dispersive X-ray analysis (EDX), UV Vis analysis, Zeta potential, particle size distribution. To evaluate antibacterial potential several standard antimicrobial tests were conducted including disc diffusion method, growth kinetics, flow cytometryand biocompatibility was analyzed by MTT assay and hemolysis studies. There is passionate hope for battling against gram-negative MDR/PDR strains of *E.coli* causing mastitis in the livestock animals.

5.2. Results

5.2.1. Structural Characterization of Synthesized Nanomaterials

5.2.1.1. XRD Analysis

XRD measurements were presenting the crystalline size and nature of synthesized nanomaterials. **Figure 5. 1A** indicates the XRD profile of, TiO_2 NPs. XRD pattern of TiO_2 results represents the (101), (004), (200), (105), (211) and (204) plane indices that are corresponding to crystalline anatase phase .In the graph characteristic peaks indicate the anatase phase of TiO_2 without any indication of other diffraction peaks as a impurity. There is a strong peak in the diffractogram of chitosan at 21.8°, indicating the high degree of crystallinity of chitosan as shown in **Figure 5.1B** (a).In the **Figure 5.1B** (b) TiO_2 coated with CS-NPs are comprised of a dense network structure of interpenetrating polymer chains cross-linked to each other by TPP counter ions .It is clear in the **Figure 5.1B** (b) TiO_2 maintained its structure during coating by showing its similar characteristic peaks and plane indices.

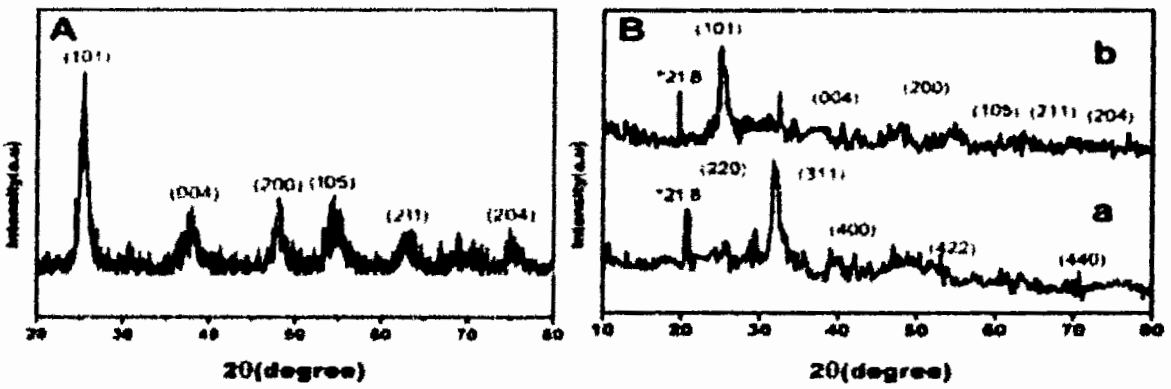

Figure 5.1 XRD patterns of synthesized nanomaterials

Key :(A) TiO_2 NPs, **(B)** line **(a)** represent the chitosan and **(b)** CS-NPs coated TiO_2 NPs

5.2.1.2. SEM and EDX Analysis

In the **Figure 5.2(A)** SEM photographs of TiO_2 showed spherical appearance while CS-NPs coated TiO_2 NPs photograph is shown in **Figure 5.2 (B)**. It was clearly seen from the image that nanoparticles presented spherical and agglomerated morphology and size of nanoparticles were comprised of the diameter ranging from 19-75 nm. SEM confirmed the size of chitosan NPs 19-25nm, TiO_2 NPs 35-50nm and CS-NPs coated TiO2 NPs with size ranging from 65-75nm (Kubacka et al., 2012). The relevant data of EDX is listed in **Table 5.1**. **Figure 5.2 (C-D)** indicates the signals of Ti and O which confirmed the synthesis of CS-NPs coated TiO2 NPs and TiO_2 NPs.

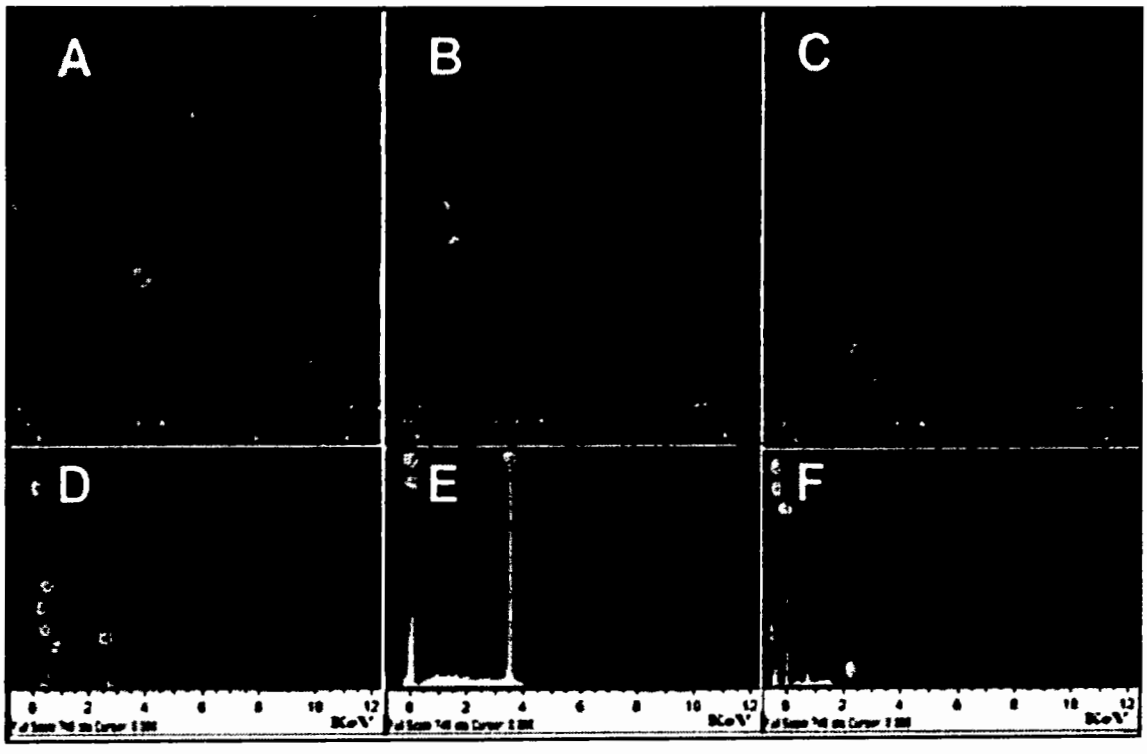

Figure 5.2: SEM and EDX data of synthesized formulations.

Key: **(A)** TiO_2NPs **(B)**CS-NPs coated TiO_2NPs **(C)** Chitosan NPs **(D)** EDX of Chitosan NPs **(E)** EDX ofTiO_2 NPs **(F)** CS-NPs coated TiO_2 NPs.

Table 5.1: EDX results of synthesized nanomaterials.

Samples	**Weigh%**							
Elements	**Ti**	**O**	**C**	**Na**	**Ti**	**O**	**C**	**Na**
TiO_2 NPs	50.78	49.22	-	-	25.63	74.37	-	-
CS-NPs coated TiO_2 NPs	2.52	55.30	26	12.04	0.85	0.61	34.71	8.40
Chitosan NPs	-	40.57	43.72	-	-	49.75	50.42	-

5.2.1.3. UV Vis Study

UV-Vis spectrum of the TiO_2nanoparticles, chitosan and CS-NPs coated TiO_2 NPs are exhibited in the **Figure 5.3A** and **5.3B** respectively. From the spectra, the absorption power of TiO_2 NPs, chitosan NPs and CS-NPs coated TiO_2 NPs was in the red area which described that the CS-NPs coated TiO_2 active in the visible light due to the existence of chitosan with TiO_2 nanoparticles. Moreover it was due to surface modification of TiO_2 by chitosan which shifted the absorption edge in visible range. The absorbance spectrum consists of two bands, one at around 220nm and other band around 320nm.The band around 220nm is assigned to tetra-hedral isolated Ti present in the sample and the band around 300–400nm arises due to charge-transfer from the valence band (mainly formed by 2p orbitals of the oxide anion) to the conduction band (mainly formed by 3d t_{2g} orbitals of the Ti^{4+}cations). This band further confirms the existence of the anatase phase of $TiO_2$and an obvious red shift towards the Vis portion of light could be attributed to addition of chitosan contents which possesses the small band gap value. This improvement in UV-Visible light absorption is demonstrating that the major portion of solar light could be successfully utilized.

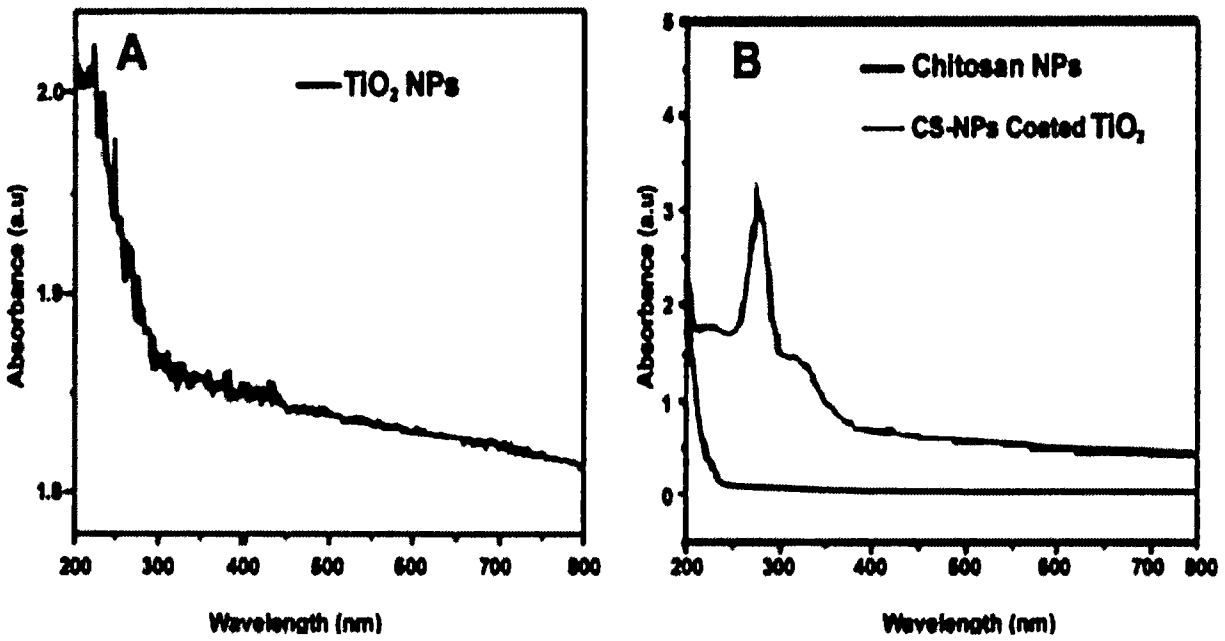

Figure 5.3: UV-Vis absorbance spectra of synthesized formulations.

Key: (A) TiO_2 NPs**(B)** Chitosan and CS-NPs coated TiO_2 NPs.

Colloidal samples of the three phases were analyzed using UV–vis transmission measurements. Extrapolation of the reflectance versus wavelength curves shown in **Figure 5.4 (A, B)**. Results in the following estimates of the band gap energy 3.21 eV for anatase phase of TiO_2 observed. It is clearly seen that TiO_2 nanoparticles are respondent only to the UV region of light due to having wide band gap energy value. UV spectrum of chitosan manifests the absorption peak at 202 nm. In case of CS-NPs coated TiO_2NPs considerably improvement was observed in absorption spectrum in UV-Vis light region. An obvious red shift towards the Vis portion of light could be attributed to the addition of chitosan content which possesses the small band gap value.

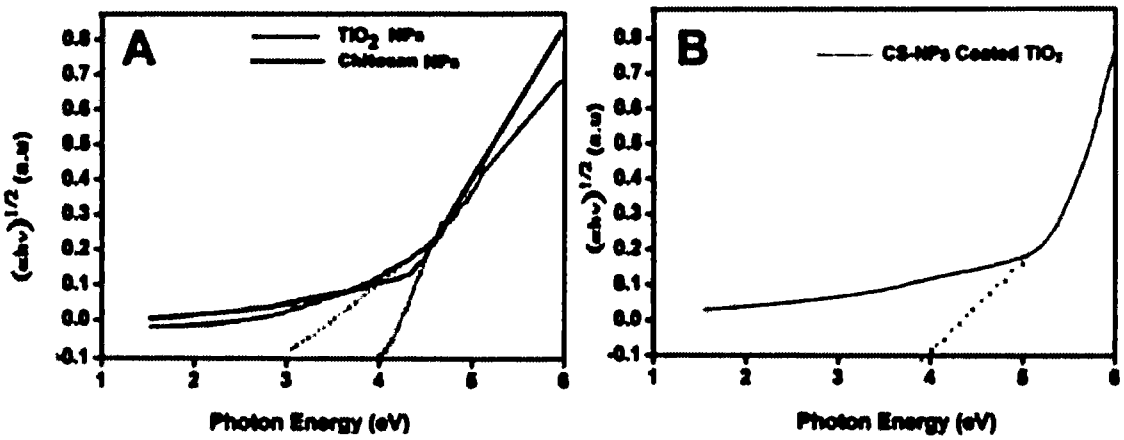

Figure 5.4 Calculations of band gap of synthesized formulations.

Key: (A) TiO_2 NPs and Chitosan NPs **(B)** CS-NPs coated TiO_2 NPs.

5.2.1.4. FT-IR Analysis

The FTIR spectra of TiO_2NPs, Chitosan and CS-NPs coated TiO2 NPs were expressed in **Figure 5.5**. FTIR spectrum of pure TiO_2NPs (**Figure 5.5B**) exhibited the emergence of absorption characteristic peaks at 3408cm-1 is belonged to superposition of the hydroxyl groups (O–H) that is the evidence of coordination of water molecule to Ti4+ cations and signature at 1603 cm-1 can be attributed to and C=O stretching vibration due to butyl group, organic species as starting precursor solutions and adsorbed water molecules on the surface of the nanomaterials. The absorption band cantered at 2928 cm-1 is assigned to the C–H stretching vibrations. The absorption band in the range of 766-610 cm-1 is related to the Ti–O bonding which authenticates the formation of titanium dioxide. The FTIR spectrum of the chitosan (**Figure 5.5A**) exhibits a sharp absorption peaks for 3423 cm-1 and 1636 cm-1 are related to availability of free –OH group of water molecule and C=O carbonyl moieties groups. The peak at 1018 cm-1 is corresponding to a stretching vibration from C–O–C bonds of epoxy or alkoxy. The signature at 1269 cm-1 and 1419cm-1 is attributed to C–O and the CH–OH bonds. FTIR investigation of CS-NPs coated TiO_2NPs is shown is **Figure 5.5C**.FTIR spectrum of pure TiO_2 exhibited the emergence of absorption characteristic peaks at 3408cm^{-1} is belonged to superposition of the hydroxyl groups while FTIR spectrum of the chitosan exhibits a sharp absorption peaks for 3423 cm-1 and 1636 cm-1 were related to availability of free –OH group of water molecule and C=O carbonyl moieties groups.

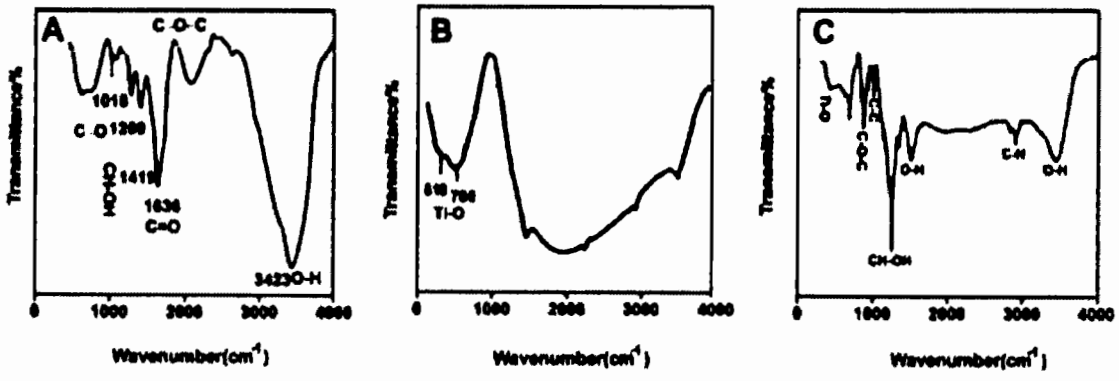

Figure 5.5 FTIR analysis of prepared nanomaterials (A) Chitosan NPs (B) TiO_2 NPs(C) CS-NPs coated TiO_2 NPs.

5.2.1.5. Zeta Potentials

The Zeta potentials of TiO_2 NPs, chitosan and CS-NPs coated TiO_2 NPs were -150.5 ± 0.8, 75.6 ± 1.0, and 95 ± 1.65 mV, respectively. The Zeta potential of prepared CS-NPs coated TiO_2 NPs were 95 ± 1.65 mV. These results provided evidence of successful coating of chitosan on the surface of TiO_2 NPs and suggested that the samples were stable during the storage period. The interaction among chitosan and TiO_2NPs in water solution was possibly promoted by the electrostatic force as chitosan carried positive charges, whereas TiO_2 NPs were negatively charged. Furthermore the amine groups of chitosan were protonated to ammonium thus adding the positive charges to chitosan. This phenomenon facilitated the surface coating of TiO_2 by chitosan and also prevented the aggregation of CS-NPs coated TiO_2 NPs (**Figure 5.6**).

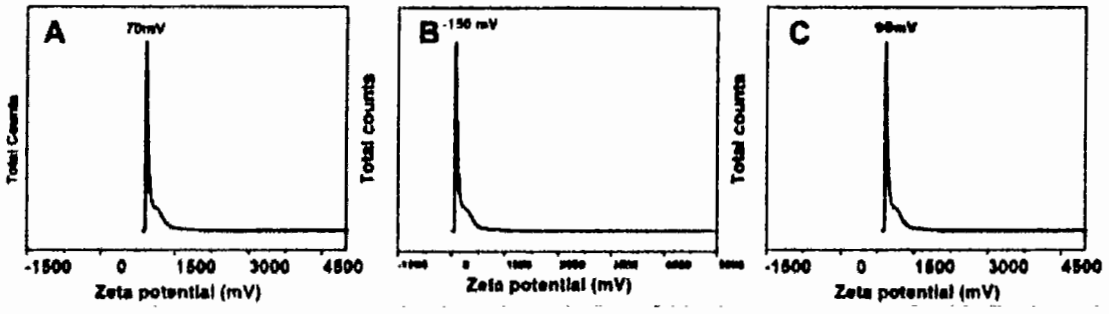

Figure 5.6 Expression of Zeta potentials of prepared nanomaterials (A) Chitosan NPs (B) TiO_2 NPs(C) CS-NPs coated TiO_2 NPs.

5.2.1.6. Encapsulation efficiency of CS-NPs coated TiO2 NPs

The encapsulation efficiency of CS-NPs coated TiO_2 NPs in the CS system was found as 85% ± 1.59.

5.2.2. Antibacterial effect and MIC determination of CS coated TiO_2 NPs on MDR strain of *E.coli.*

In the study, most prevalent mastitis causing strains were found to be *E.coli, S .aureus* and *C.albicans*. Therefore antimicrobial potential of synthesized nanomaterial A was screened against these strains. The synthesized nanomaterial A was found to be most active against *E.coli* as compared to *S. aureus* and *C.albicans* on the basis of zone of inhibition as shown in the **Table 5.2**. *E.coli* displayed largest zone measured as 21mm, *S .aureus*presented 16mm of diameter and*C.albicans*was found to exhibit 12mmof ZI after interaction of 24hrs with nanomaterial. Hence *E.coli* was selected as model organism for detailed antibacterial analysis of nanomaterial A, CS coated TiO_2 NPs.

Table 5.2 MIC determinations of synthesized nanomaterials against mastitis causing pathogen

Nanomaterials	**MIC determination (µg /ml)**		
	MRSA	*E.coli*	*C .albicans*
CS Coated TiO_2 NPs	15	0.78	28
CS NPs	64	75	9.57
TiO_2 NPs	78	67	98

Antibiotic resistant profiling of *E.coli* strain is shown in **Figure 5.7(a ,b)** that showed strain is found to be pandrug resistant strain as against total 14 antibiotic tested *E.coli* strain showed resistance against all antibiotics. Interestingly our synthesized formulation worked against pan drug resistant *E.coli* and killed this resistant strains zones of observation were quite promising as seen in **Figure 5.7C**. All of three nano formulations are effective against PDR *E.coli* but the most potent activity was noticed against CS-NPs coated TiO_2 NPs, previous studies reported antibacterial potential of TiO_2 and chitosan .Data of zones of inhibition is presented in **Table 5.3**. MIC values of CS coated TiO_2 NPs was found to be 0.78µg/ml which was lowest among all the nanomaterials tested against microbes causing mastitis.

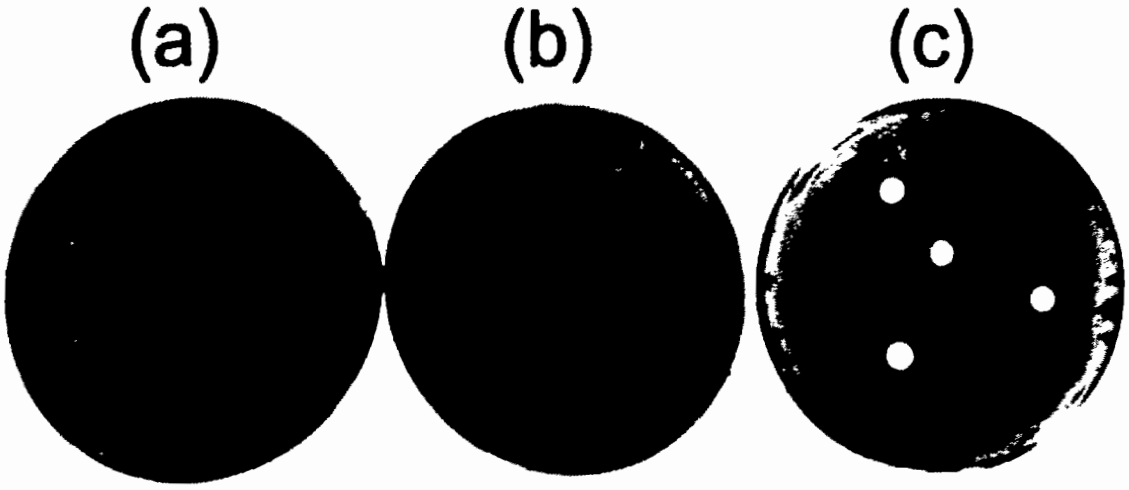

Figure 5.7 Antibiotic sensitivity profiling of isolated *E.coli* strain and antibacterial activity ofsynthesized nanoformulations (a and b) different antibiotics discs

Key: 1-AX Amoxicillin,2-CN Gentamicin,3-CRO Ceftriaxone ,4-AMC Augmentin ,5-AMP Ampicillin,6-F Nitrofurantoin,7-SXT Trimethoprim/Sulfamethoxazole,8-CIP Ciprofloxacin,9-MEM Meropenem, 10-IPM Imipenem,11-FOT Cefotaxime, 12-TZP Tazobactam,13-FEP Cefepime,14-CAZ Ceftazidime (c) Antibacterial activity of synthesized materials A-chitosan NPs, B- TiO_2 NPs, C-control, D-CS-NPs coated TiO_2 NPs.

Table 5.3: Zone of inhibition and SD values of formulated nanoformulations

Antimicrobial agents	**Zone of Inhibition (mm)**	
	(ATCC 8739)	***E.coli***
CS-NPs coated TiO_2 NPs	29mm± 2.45	21mm± 0.039
TiO_2 NPs	23mm± 1.67	16mm± 2.8
Chitosan NPs	9mm± 0.58	4mm± 1.32
DMSO (Control)	NZ	NZ

5.2.3. Growth curve kinetics of MDR *E.coli* strain

According to the present study CS-NPs coated TiO_2 NPs were found highly active in combating PDR strain of *E. coli* than TiO_2NPs. However, CS-NPs coated TiO_2 NPs effectively dropped the OD value and prominently inhibit the growth of superbugs. Based on the above results it could be observed the prospective enhancement in antibacterial activity of proposed CS-NPs coated TiO_2 NPs as shown in **Figure 5.8**. The superior antimicrobial activity of the CS-NPs coated TiO_2 NPs is also evidenced by the growth curve, which exhibited stronger antibacterial ability against PDR *E. coli*. The antibacterial ability of chitosan was higher than that of TiO_2 NPs during the first few hours. However, the difference became insignificant over the following 5 hours. Thereafter, TiO_2 NPs exhibited higher activity than the chitosan.

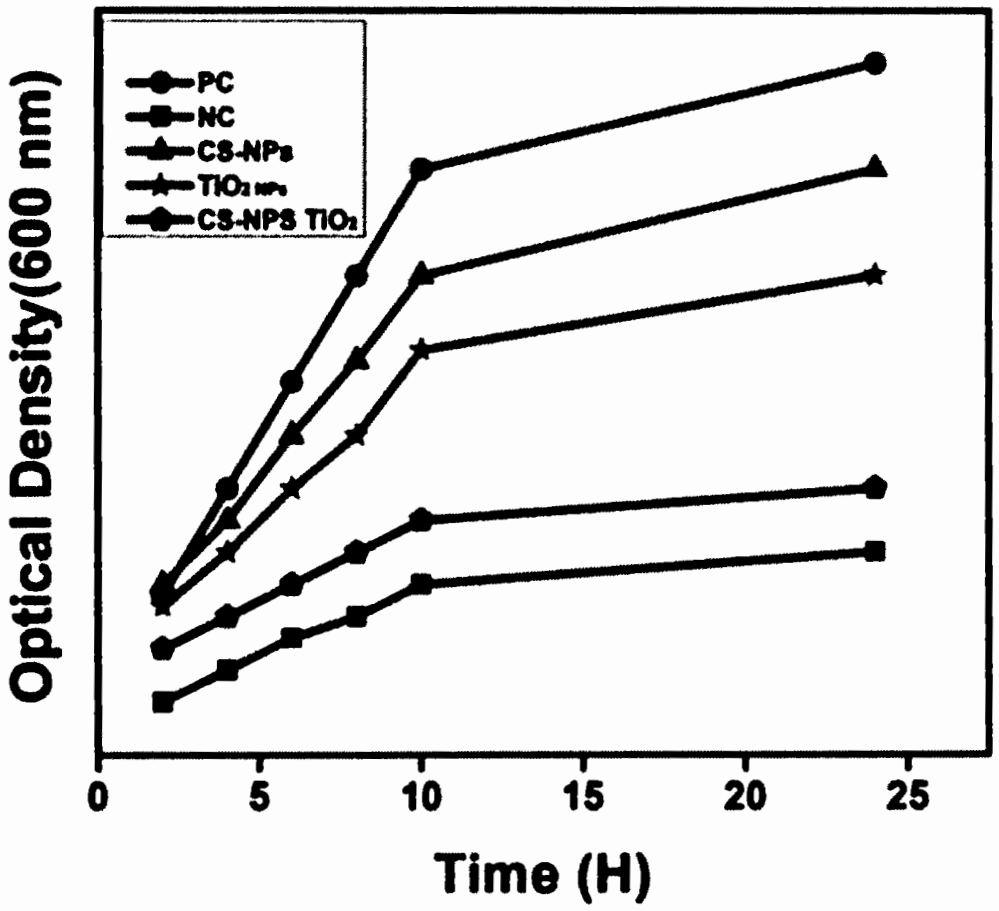

Figure 5.8: Growth kinetics of *E.coli* at the MIC for 24 hours. CS-NPs coated TiO_2 NPs control the bacterial growth effectively.

5.2.4. Hemolysis Assay

The synthesized formulations were found nontoxic to red blood cells of cow as all formulations at all tested concentrations did not lyse red blood cells as shown in **Figure 5.9**.

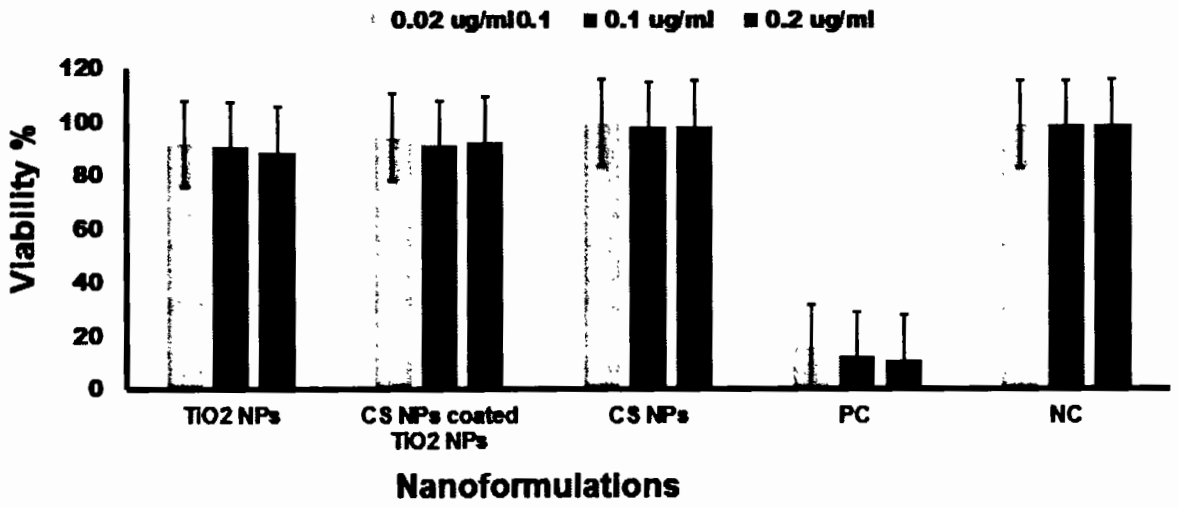

Figure 5.9: Hemolysis study of CS-NPs coated TiO_2 NPs after exposure to RBCs of cow blood.

Key: PC. Positive control, Triton, NC. Negative control, PBS.

5.2.5. MTT assay for Cytotoxicity Analysis

The cytotoxicity data exhibited in **Figure 5.10** clearly indicates that the CS-NPs coated TiO_2 NPs, CS NPs and TiO_2NPs did not show any toxicity on BMGE cell line of bovine at various concentrations. Results indicate that the cell viability remain maintained with the increase in concentrations of various prepared nanoformulation and particularly CS-NPs coated TiO_2 NPs didn't show any cytotoxicity on the BMGE cell line. Celecoxib was taken as positive control and significantly reduced cell viability at tested concentration ranges while PBS as negative control. All findings clearly suggest non toxicity of CS-NPs coated TiO_2 NPs may be attributed to controlled release of TiO_2 and coating of chitosan biopolymer.

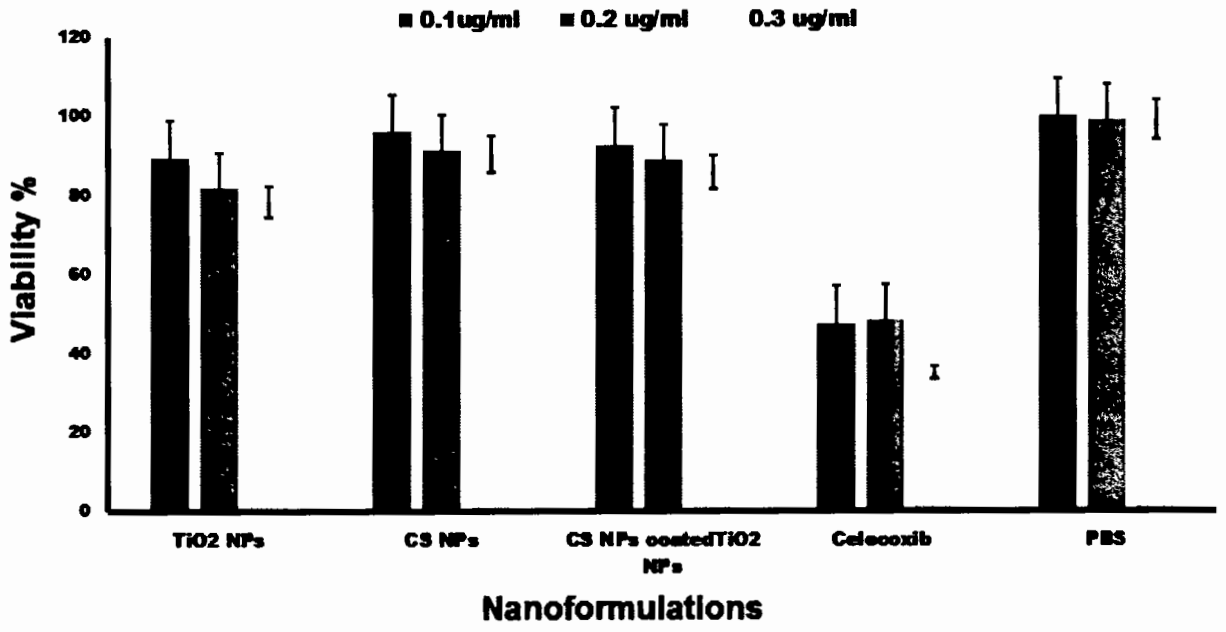

Figure 5.10 Cytotoxicity analysis of CS-NPs coated TiO_2 NPs, CS-NPs and TiO_2 NPs after exposure to BMGE cell line of bovine.

5.2.6. CS-NPs coated TiO_2 NPs altered morphology and structure of MDR *E.coli.*

Morphological changes in the integrity of bacterial cells were observed after treatment with MIC (0.78µg/ml) of CS-NPs coated TiO_2 NPs by TEM analysis of MDR *E.coli* strain. Expected destruction of bacterial cells was captured after 3-6 hours of incubation. It is evident from the results (**Figure 5.11**) CS-NPs coated TiO_2 NPs completely lysed the MDR *E.coli* cells and lost their integrity. Moreover, it was observed that shape of bacillus was no more maintained so become agglomerated which may became the ultimate cause of cell death.

Figure 5.11 Effect on cellular morphology of MDR *E.coli* after treatment with CS-NPs coated TiO_2 NPs at various interval of time by TEM microscopy.

Key A: control **B:** 3 hrs of incubation **C:** 6 hrs of incubation.

5.2.7. Flow cytometer analysis of CS-NPs coated TiO_2 NPs treated *E.coli.*

To further strengthen the molecular mechanism mediated by the newly developed Nanomaterial A, as we use a double-staining (PI/Annexin V) method and calculated the number of alive cells by a statistical gating approach using FACS before and after treating *E.coli* strains by CSNPs coated TiO_2NPsat MIC (0.78 µg/mL) at 37 °C and at various intervals of time (i.e. 0 hrs, 6 hrs) **(Figure 5.12)**. Such assay aims to determine both the necrotic death (by PI staining) as well as the early and late apoptosis (by AnnexinV) and ultimate death in the selected populationdensity (Hussain et al., 2012). Thereby, the death rate was negligible and late apoptosis (1.98% ± 0.03) in untreated cells (NC) **(Figure 5.12A)**, whereas the late apoptosis was found 55.79 % ± 1.52 after 6 hrs **(Figure 5.12 B)** of incubation after treatment with the nanoformulation.

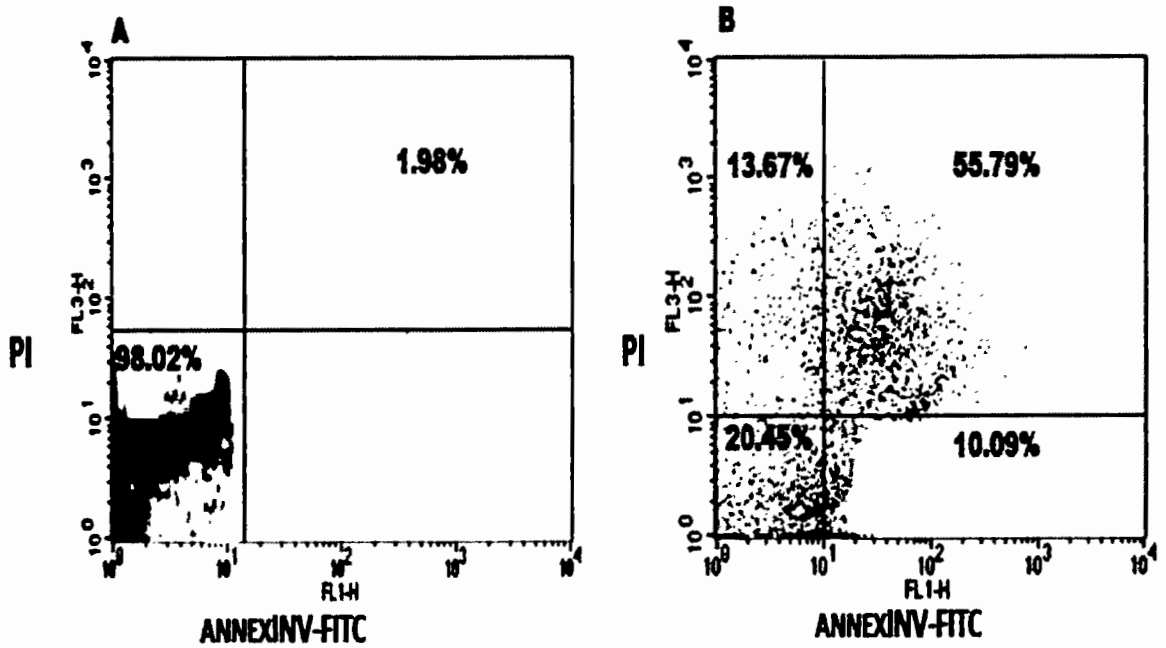

Figure 5.12 Death rate of *E.coli* cells by FACS exposed to CS NPs coated TiO_2 NPs at MIC,

Key: A- Untreated *E.coli* (NC); B- 6 hrs post-treatment of *E.coli.*

5.2.8. General mechanism for the destruction of bacterial cells by CS-NPs coated TiO_2 NPs.

To overcome resistance mechanism, coating of chitosan content on TiO_2 NPs can significantly improve the bactericidal effect against PDR pathogens of veterinary origin. The distinctive physical and chemical characteristics of nanomaterials contribute collectively in a synergistic manner to expose a novel, exceedingly efficient antibacterial nano interface. Since the chitosan itself holds the antibacterial effect against both Gram-negative and Gram-positive bacteria (Banerjee et al., 2010). In the **Figure 5.13** proposed mechanism of action has been shown to describe the destruction of bacterial cell. Mechanism mainly follows three steps i.e. 1st step preceded after the attachment and penetration in the bacterial cells may occurs which was facilitated by chitosan coating. In the 2nd step generation of ROS occurred after the interaction of MDR *E.coli* with CS-NPs coated TiO_2NPs. The generation of cations by the oxidation of TiO_2 NPs and reactive oxygen radicals (ROS) are followed by the dispersion of chitosan coated nanomaterials into the growth medium under incubation during the antibacterial activity against microorganism. Fundamental steps during the generation of ROS (•O2 –, •OH and H_2O_2) are given [eq (1) – eq (5)] under irradiation of UV-Vis light. In the 3rd step lysis of bacterial cell took place due to ROS stress by damaging cellular content like cell wall, cell membrane, DNA and inhibits protein synthesis.

$$TiO_2 + hv \longrightarrow TiO_2(h+ + e^-) \quad (1)$$

$$H_2O \longrightarrow H+ + OH^- \quad (2)$$

$$H+ + OH^- \longrightarrow \bullet OH \quad (3)$$

$$H+ + H_2O \longrightarrow \bullet OH + H^+ \quad (4)$$

$$e^- + O_2 \longrightarrow \bullet O^{2-} \quad (5)$$

TiO_2/Ba hybrid Nano clusters effectively reduced cell for both Gram positive and Gram negative bacteria. The improvement in cytotoxic reaction of Ba doped TiO_2 nanoparticles was attributed

to widening of band gap energy that significantly increase their capability to persuade ROS generation. ROS interfere with proteins, lipids of cell membrane, enzymes and DNA, oxidize them and produce the more oxidative stress of ROS (Vijayalakshmi & Sivaraj, 2016). The synergistic expression including to disruption of cell membrane and oxidative stress of ROS on cell results into improvement of the antibacterial activity of unique combination of TiO_2 with coating of biocompatible chitosan (Haldorai & Shim, 2014). This system is more efficient for gram –ve bacteria as compared to gram +ve and efficiently inhibit the growth at MIC concentration of proposed CS-NPs coated TiO_2 NPs .

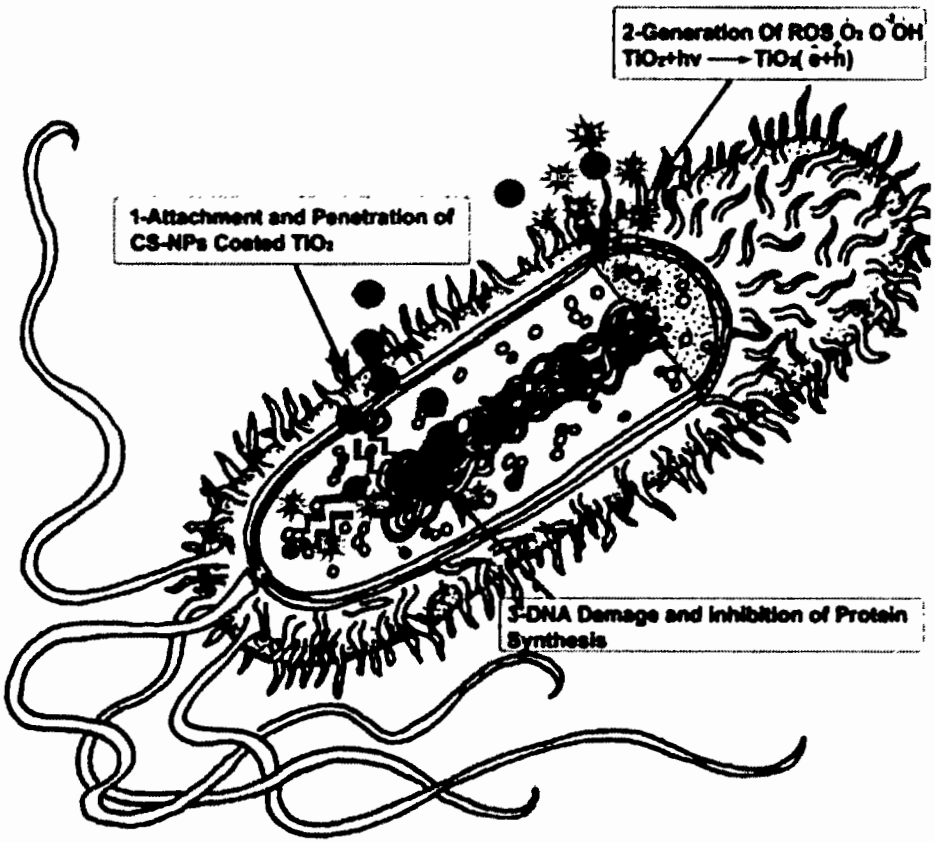

Figure 5.13: Proposed antibacterial mechanism of action of CS-NPs coated TiO_2 NPs.

5.3. Conclusion

TiO_2 NPs were synthesized by using green route and synthesized TiO_2 NPs nanoparticles were coated with nanoparticles of chitosan to combat PDR bacterial pathogens of *E.coli* causing mastitis in the livestock animals.The findings of current study revealed that synthesized formulation has superior antibacterial activity against PDR *E.coli* that has opened a new window for the alternate treatment strategy against super bugs by surface modification of TiO_2 NPs via CS-NPs. Present evaluation further confirmed coating of TiO_2 NPs with chitosan nanoparticles is found very effective as CS-NPs coated TiO_2 showed strong activity evident by increase in size of zone of inhibition. Synthesized CS-NPs coated TiO_2 was found bactericidal at MIC concentration of 0.78µg/ml as lysed cells were observed by TEM. The hemolytic and cytotoxicity studies of CS-NPs coated TiO_2 NPs showed its non-toxicity to the bovine mammary gland epithelial cells. Hence very stable, nontoxic, spherical shape CS-NPs coated TiO_2 was synthesized having potential to kill an alarming pathogen i.e. MDR/PDR strain of *E.coli* in veterinary region and this could be added in alternate antimicrobial agents for livestock industry.

CHAPTER 6

NANOMATERIAL B: CIPROFLOXACIN CONJUGATED CHITOSAN ENCAPSULATED GREEN SYNTHESIZED CERIUM OXIDE NANOPARTICLES (CIP-CeO_2/CS NPS)

6.1. Introduction

Nanomaterilas have recently attracted much attention because are considered as a valuable solution to strongly combat MDR strains (Ma et al., 2017). A wide range of metal and metal oxide-based nanomaterials have recently been directly integrated in antibacterial applications and have demonstrated remarkable results. Nanomaterials possessed a high surface area-to-volume ratio and unique physicochemical properties which contribute to effective antimicrobial activities (Batool et al., 2020; Wang et al., 2017). Thereby, NPs, especially metallic/inorganic NPs such as silver (Ag), gold (Au) copper (Cu), cerium (Ce), or Zinc (Zn) NPs (Hemeg, 2017; Slavin et al., 2017), have showed up benefits to treat microbial infections (Uzair et al., 2020).

Cerium- and cerium oxide-based nanomaterials have garnered considerable attention as alternative to antibiotics because of its unique functional mechanism, cerium oxide nanoparticles with decreased toxicity work as potent antibacterial agents (Qi et al., 2020).Cerium dioxide (CeO_2), a rare-earth material belongs to lanthanide series , has a variety of properties at the nanoscale and widely applied pharmacological agents (Charbgoo et al., 2017) due to their lower toxicity to mammalian cells and unique antibacterial mechanism, CeO_2 NPs have also been widely applied in biomedical sciences such as in antitumor, anti-inflammation (Huang et al., 2018) and antibacterial activities (Arumugam et al., 2015). CeO_2 have shown promising approaches to circumvent the existing problems of drug-resistant bacteria and served as excellent antibacterial agents in biology and medical sciences in comparison with other metal oxides (Zhang et al., 2019). Therefore, various cerium- and cerium oxide-based nanomaterials including doping metal ions (Atif et al., 2019), antibacterial element Au/Ag decorations (Wang et al.,

2014), nanocontainers(Gagnon et al., 2015) and dopants (Bomila et al., 2018) were developed to optimize antimicrobial performance as well as physical and biological properties (Liu et al., 2019).

Nanomaterials have high surface area-to-volume ratio and unique physicochemical properties which contribute to effective antimicrobial activities (Batool et al., 2020; Wang et al., 2017). Thereby, NPs, especially metallic/inorganic NPs such as silver (Ag), gold (Au) copper (Cu), cerium (Ce), or Zinc (Zn) NPs (Hemeg, 2017; Slavin et al., 2017), are consider effective to treat microbial infections (Uzair et al., 2020).

Nevertheless, activities of metallic NPs against pathogens-causing mastitis have been poorly explored while CeO_2 NPs have exhibited strong bactericidal effects against both Gram-positive and Gram-negative bacteria (Arumugam et al., 2015).Importantly, a recent shift from physical and/or chemical NPs synthesis toward green NPs synthesis is observable and preferable because plants extracts are used as reducing and capping agents (Uzair et al., 2020). Thereby, phytogenic synthesis of NPs is an user-friendly, cost-effective, safe and eco-friendly method that does not require multiple purification steps that use toxic solvents (Uzair et al., 2020). For instance, Maqbool et al. recently reported the greenly synthesis of CeO_2 NPs from *Oleaeuropea* leaf extract and their antimicrobial potential against model Gram-positive and negative ATCC strains (Maqbool et al., 2016).

Furthermore, the possibility to load one or multiple drug combinations into NPs and nanocomposites/nanohybrids leads to a highly complex antimicrobial mechanism of action, to which bacteria are unlikely to develop resistance (Huh & Kwon, 2011). Thereby, some previous studies described the direct conjugation of ampicillin, streptomycin and kanamycin to AuNPs(Saha et al., 2007). The resulting complexes elicited lower MIC than the free drug counterparts against both Gram-negative and Gram-positive bacteria (Saha et al., 2007).

Polymeric NPs have not been deeply explored for mastitis treatment yet, even though they can concomitantly act as antimicrobial agents and nanocarriers, then allowing the design of powerful therapies (Lam et al., 2018). Natural polymers such as chitin, CS, alginate, gelatin, and collagen

are used for many medical applications due to their good biodegradability and biocompatibility (Sung et al., 2010). CS can be easily synthesized and CS-based nanomaterials are being applied in most important biomedical fields (e.g. tissue engineering and regenerative medicine, controlled-drug delivery and targeting) (Iqbal et al., 2020a).Besides its well-known biocompatibility and biodegradability, CS is non-toxic to humans and animals (Sung et al., 2010). The goal of an efficient and safe drug/compound delivery system is to provide the best theranostic efficiency with a minimal therapeutic dosage which can be maintained during a specific time until the drug concentration is released to the target site(Menaa, 2013) .This requires not only a suitable material to hold the drug, and later release it, but also a biocompatible material, with high absorption rate. Fortunately, the development of drug delivery nanocarriers of tunable size and well-defined surface properties, are allowing to control the adsorption and release of drugs in a predictable manner (Wang et al., 2006).

The goal of our present research study is to contribute to the better management of mastitis in dairy cattle, by developing an original organic/inorganic nanocarrier of antibiotics. For such purpose, we report here the encapsulation of CIP into CeO_2/CS NPs we biologically synthetized *via* green route using *Amomumsubulatum* (aka BC) seeds extract and ionic gelation method. This highly regarded as a ''Queen'' of species, is a perennial herbaceous crop belonging to the family *Zingiberaceae*(Pura Naik et al., 2004). This plant is distributed chiefly in Africa and Tropical Asia, and cultivated in swampy places (e.g. Nepal) across hills around water streams for its subsequent uses in cooking, folklore and Ayurvedic medicine (Agnihotri & Wakode, 2010). To the best of our knowledge, CIP-CeO_2/CS NPs drug system has never been developed and tested for its antimicrobial potential.

6.2. Results

The modern trends in the nanomedicines favor green route of synthesis NPs instead of physical or chemical methods. Indeed, the biosynthesis of NPs is increasingly regarded as a rapid, ecofriendly, and easily scaled-up technology.

In the present study, CeO_2 NPs were prepared by using aqueous seed extract of BC as reducing agent .Then, CeO_2 NPs were coated with CS and encapsulated with CIP via ionic gelation method. The NPs were purified by calcination. All the green synthesized nanomaterials CeO_2 NPs, CS NPs, CeO_2 NPs, and the newly developed CIP-nanohybrid carrier were compared either with CIP or between them in terms of physical-chemical and biological characterizations. The goal was to propose a novel nanomaterial that could be safe and more efficient than CIP alone currently used as a conventional antibiotic.

6.2.1. Physical characterizations of synthesized nanomaterials

Besides, XRD technique was used to examine the crystal phases, and the crystallinity of the green synthesized nanomaterials **(Figure 6.1a)**, CIP-CeO_2/CS NPs **(Figure 6.1c)** and CeO_2/CS NPs **(Figure 6.1d)** correspond to Bragg reflections with 2θ values of 28.6, 33.02, 47.4, 55.3, 59.01, and 69.4. These Bragg reflections were identical based on their orientations and were respectively indexed to (111), (200), (220), (311), (222), (400) crystal planes of cubical structure typical found in NPs CeO_2[NPJCPDS34-0394] .XRD of CS showed a signal at $2\theta = 19.63°$ (220) **(Figure 6.1b)**. The amorphous nature of CS appeared clearly in the spectrum and has been obtained most likely during the intercalation of bulk chitosan with TPP. The location of the peaks was compared to literature values and the presence of CeO_2/CS NPs was confirmed. The diffraction peaks were well-defined with high intensity and narrow width which indicates that the resulting biosynthesized NPs were highly crystalline. Further, no reflection related to any impurity was detected in the pattern, up to the detection limit of the XRD diffractometer, which defined the prepared NPs as pure. Also, the data strongly suggest that CS incorporation in CeO_2 NPs did not change the crystallinity of the composite. However, the CeO_2/CSnanocomposite **(Figure 6.1d)** displayed a higher intensity spectrum compared to that of CeO_2 NPs **(Figure 6.1a)**.

The average crystallite size of NPs was found to be $\sim 7.9 \pm 1.3$ nm, $\sim 10.63 \pm 1.4$ nm, $\sim 5.9 \pm 0.09$ nm, $\sim 7.1 \pm 0.2$ nm in CeO_2 NPs, CS NPs, CeO_2/CSNPs, and CIP-CeO2/CS composite respectively, based on the Debye-Scherrer's equation centered about most strong diffraction

signal of 28.6° (111). Interestingly, it is worth noting that the small sized nanostructure of fabricated samples was shown be very effective for inactivation of bacterial growth.

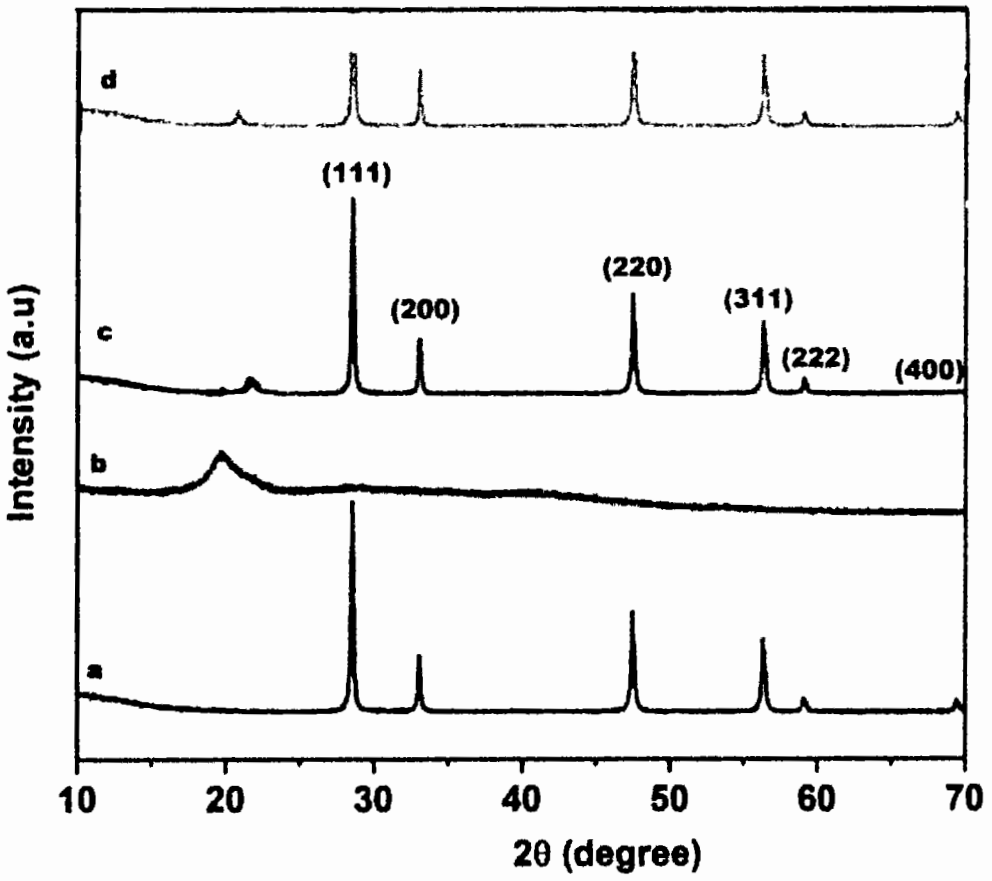

Figure 6.1 XRD spectra related to green synthesized nanomaterials,

Key:-

(a) CeO_2 NPs

(b) CS NPs

(c) CIP-CeO_2/CS NPs

(d) CeO_2/CS NPs

6.2.2. SEM and TEM of Green Synthesized Nanomaterials

To examine the nanostructure surface morphology (i.e. shape), size of CeO_2 NPs, CS NPs, CeO_2/CS NPs and CIP-CeO_2/CS NPs, we used one of the most versatile instrument, FE-SEM **(Figure 6.2)** along with EDX (EDS) analysis **(Table 6.1)** to check the elemental chemical composition of these nanomaterials. Moreover, TEM was used to offer unparallel detail (at near-atomic resolution) of the internal nanostructure, which is valuable when considering the small size of the NPs **(Figure 6.2)**. Eventually, to confirm the crystalinity of the nanohybrid of interest, we performed XRD analyses **(Figure 6.1)**.

Thereby, SEM micrograph of CeO_2 NPsdepicted some mixed small fluffy, spherical as well as few elongated edges of particles, which were extremely amassed and agglomerated **(Figure 6.2A)**. The SEM micrograph of CS **(Figure 6.2B)** exhibited less agglomerated spherical particles than CeO_2 NPs, suggesting the anti-aggregation role of CS when coated into CeO_2 NPs **(Figure 6.2C)**, most likely because CS enhanced the dispensability in the solution. The SEM micrograph of CIP-CeO_2/CS revealed less agglomerated secondary particles with large grooves and voids **(Figure 6.2D)**. These materials with huge voids are beneficial for the attachment of foreign materials and are then expected to contribute to enhance the antibacterial activity.

Elemental mapping and quantitative composition of the same fabricated nanomaterials was investigated. As expected, EDX spectrum of CeO_2 NPs indicated the peaks of O, C and Ce **(Figure 6.2A and Table 6.1)**. Also, EDX spectrum of CS displayed peaks of O and C **Figure 6.2B and Table 6.1)**. The presence of O, C and Ce in the EDX spectrum of CeO_2/CS NPs **(Figure 6.2C and Table 6.1)** and CIP-CeO_2/CS NPs **(Figure 6.2D and Table 6.1)** demonstrated that the nanohybrid has been prepared successfully. Peaks related to C did arise due to the depositing sample on carbon tape. Quantitative elemental compositions of the prepared samples are summarized in **Table 6.1**. The bottom-up approach, in which the metal ions could be reduced to synthesize nanoparticles presence of capping ligands, preferably used .green synthesis is gaining more attention instead of the physical and chemical synthesis methods.In the present

study natural seeds of black cardamom reduced to cerium oxide NPs and chitosan biopolymer reported in many studies for biocompatible and biodegradable used for encapsulation via simple ionic gelation method using even acetic acid.

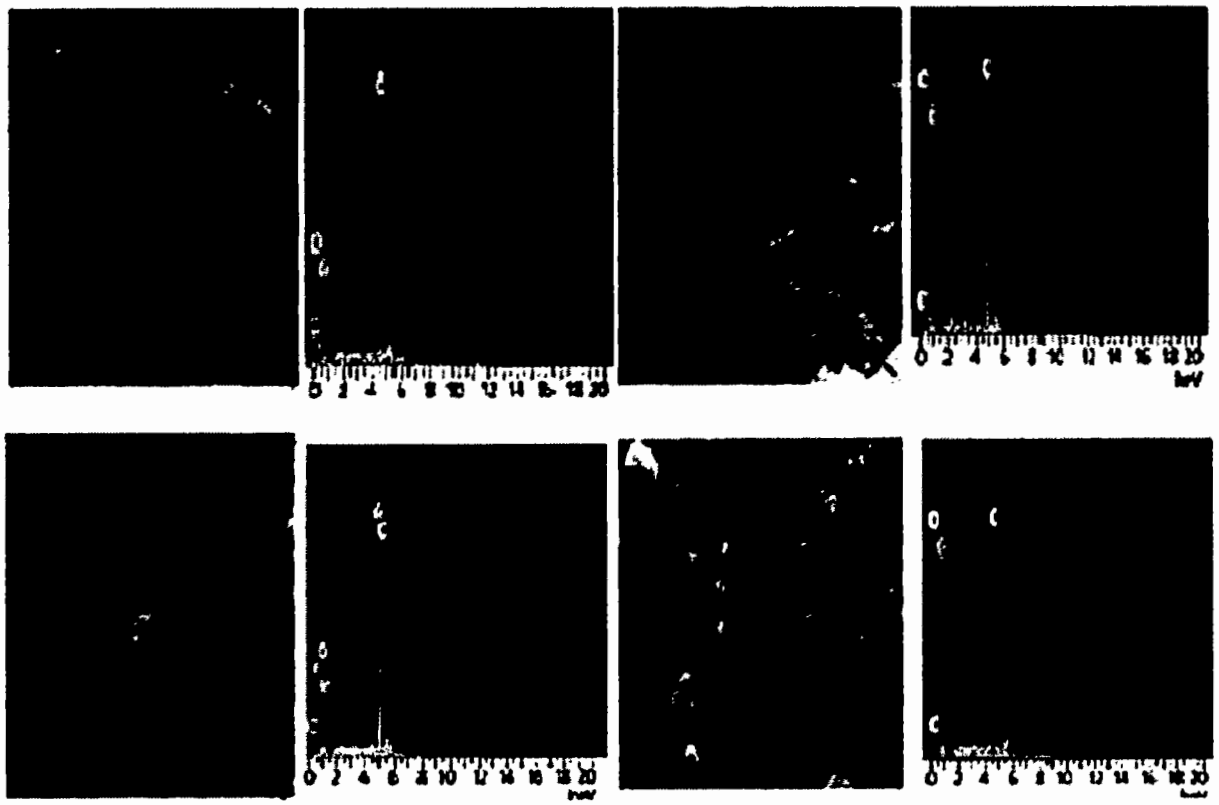

Figure 6.2 FESEM micrographs (left) and EDX spectra (right) of green synthesized nanomaterials

Key:-

(A) CeO_2 NPs

(B) CS NPs

(C) CeO_2/CSNPs

(D) CIP-CeO_2/CS composite

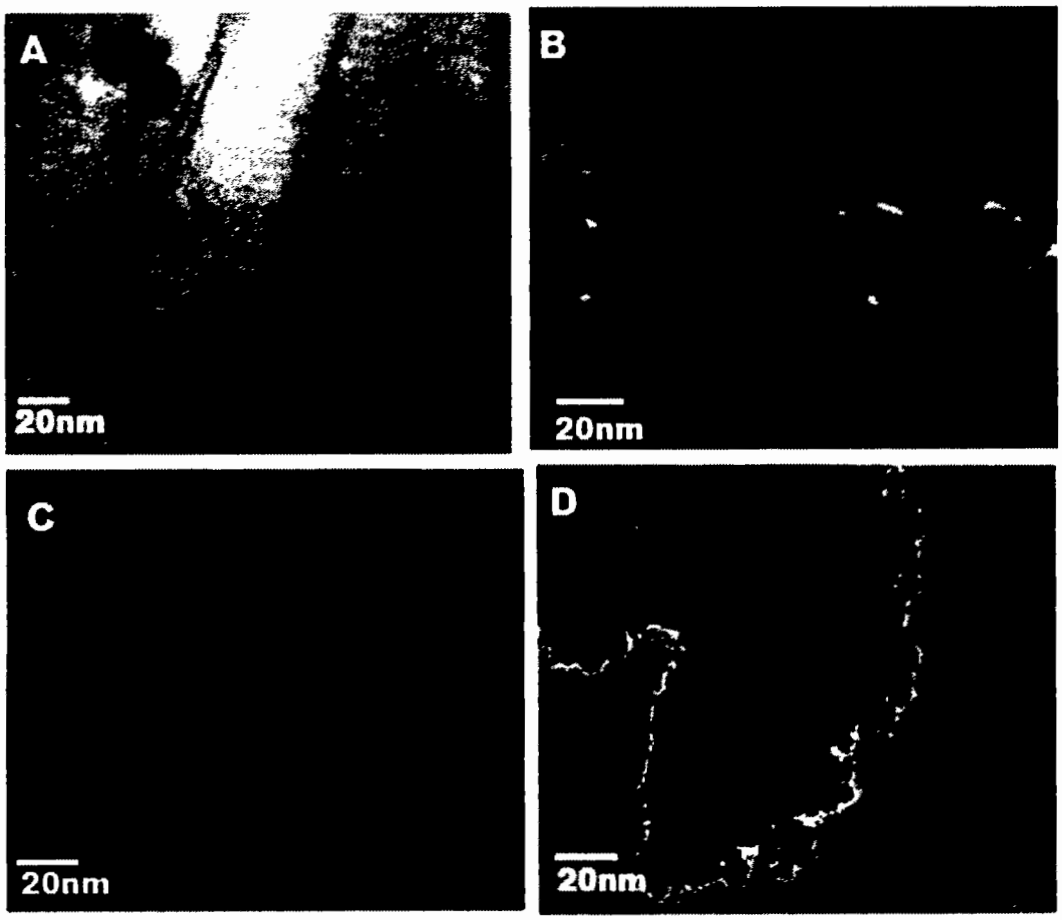

Figure 6.3 TEM images of green synthesized nanomaterials,

Key:-

(A) CeO_2 NPs

(B) CS NPs

(C) CeO_2/CS NPs

(D) CIP-CeO_2/CS NPs

Table 6.1: Elemental chemical composition of the synthesized nanomaterials.

Elements	**CeO_2 NPs**	**CS**	**CeO_2/CSNPs**	**CIP-CeO_2/CSNPs**
C	4.02	64.27	12.50	9.52
O	18.37	35.73	45.29	34.05
Ce	77.61	-	39.56	55.44

Further, the TEM micrograph of CeO_2 NPs showed mixed quasi-spherical particles and some elongated particles **(Figure 6.3A)**. TEM micrographs of CS **(Figure 6.3B)** and CeO_2/CS NPs **(Figure 6.3C)** clearly displayed round spherical NPs. The TEM micrograph of CIP-CeO_2/CS NPsdepicted agglomerated spherical morphology of secondary particles **(Figure 6.3D)**. These TEM data are consistent with our previous SEM analyses. The average diameter of CeO_2 NPs, CS NPs , CeO_2/CS NPs and CIP-CeO_2/CS NPs ranged from ~6-10 nm which was also confirmed by XRD analysis. The average particle size (PS) was found in the present study was 45nm ±0.87 nm, 35±1.0 nm, 65±0.37nm and 40± 0.91 nm in (A) CeO_2 NPs, (B) CS NPs, (C) CeO_2/CSNPs, and (D) CIP-CeO2/CS composite respectively.

6.2.3. FTIR spectroscopic analysis of green synthesized nanomaterials

In a further step, the surface adsorption of functional groups on NPs was investigated by FTIR enabling the *in-situ* analysis of interfaces. To identify functional groups involved in the stabilization of NPs, FTIR spectroscopy was performed on BC seeds extract used as control **(Figure 6.4a)**, CeO_2 NPs **(Figure 6.4b)**, CS NPs **(Figure 6.4c)**, CIP **(Figure 6.4d)**, CIP-CeO_2/CSNPs, **(Figure 6.4e)**, and CeO_2/CSNPs **(Figure 6.4f)**.

Various phytochemicals present in these extracts are considered to provide the action of capping and stabilizing agents that aid the formation of CeO_2 and CeO_2/CS NPs. Substance-specific vibrations of the molecules lead to the specific signals obtained by IR spectroscopy in the range of 400–4000 cm^{-1}.

Consistently, a prominent peak attributed to hydroxyl (-OH) group is observed in the wavelength range 3500-3200 cm^{-1} in all spectra **(Figures 6.4a-6.4f)**, which is an important functional group of phenolic compounds. In plant **(Figure 6.4.a)**, characteristic FTIR signals at 1634 cm^{-1} and 1050 cm^{-1} belong to NH_2 and C=O stretching vibrations from amine group and butyl group respectively. In CeO_2 NPs **(Figure 6.4b)**, the spectral region between 949-517cm^{-1} revealed bending vibrations of Ce–O and O–Ce–O which confirms the successful formation of CeO_2 NPs. In CS NPs **(Figure 6.4c)**,CIP-CeO_2/CSNPs **(Figure 6.4e)** and CeO_2/CSNPs **(Figure 6.4f)**, the FTIR peak at 1264 cm^{-1} is assigned to the bending vibrations of C–C–C from ketone, whereas the signals at the spectral region 1625-1640 cm^{-1} indicate NH_2 vibrations. Also, in CIP-CeO_2/CSNPs **(Figure 6.4e)**, the peaks in the spectral region of 712-509 cm^{-1} indicate the new surface Ce-C-F linkage, that is known to be very beneficial for efficient antibacterial activity.In CIP **(Figure 6.4d)**, the FTIR signals observed specifically at 1711 cm^{-1} and 1613 cm^{-1} are associated with C=O and C–H vibrations, respectively. The peak centered at 1019 cm^{-1} is ascribed to C–F bending vibrations as shown in the **Table 6.2**.

Table 6.2: FTIR spectral assignments of green synthesized nanomaterials

Materials	**Wavenumber (cm^{-1})**	**FTIR Assignment (functional groups)**	**Name (corresponding)**	**Reference**
BC (seed extract)	3500-3200	-O-H-	Hydroxyl group	(Jamila et al., 2020)
CeO_2 NPs	949-517	Ce–O and O–Ce–O	Cerium and oxygen linkages	(Leung et al., 2015)
CS NPs	1625-1640	NH_2	Amino groups	(Zafar et al., 2020)
CeO_2/CSNPs	1625-1640	NH_2	Amino groups	(Zafar et al., 2020)
CIP-CeO_2/CSNPs	712-509	Ce-C-F linkage	Cerium linked, Carbon, and Fluorine atoms of the drug	(Staff, 2010)
CIP	1019	C–F	Carbon and Fluorine atoms	(Sasikumar, 2013)

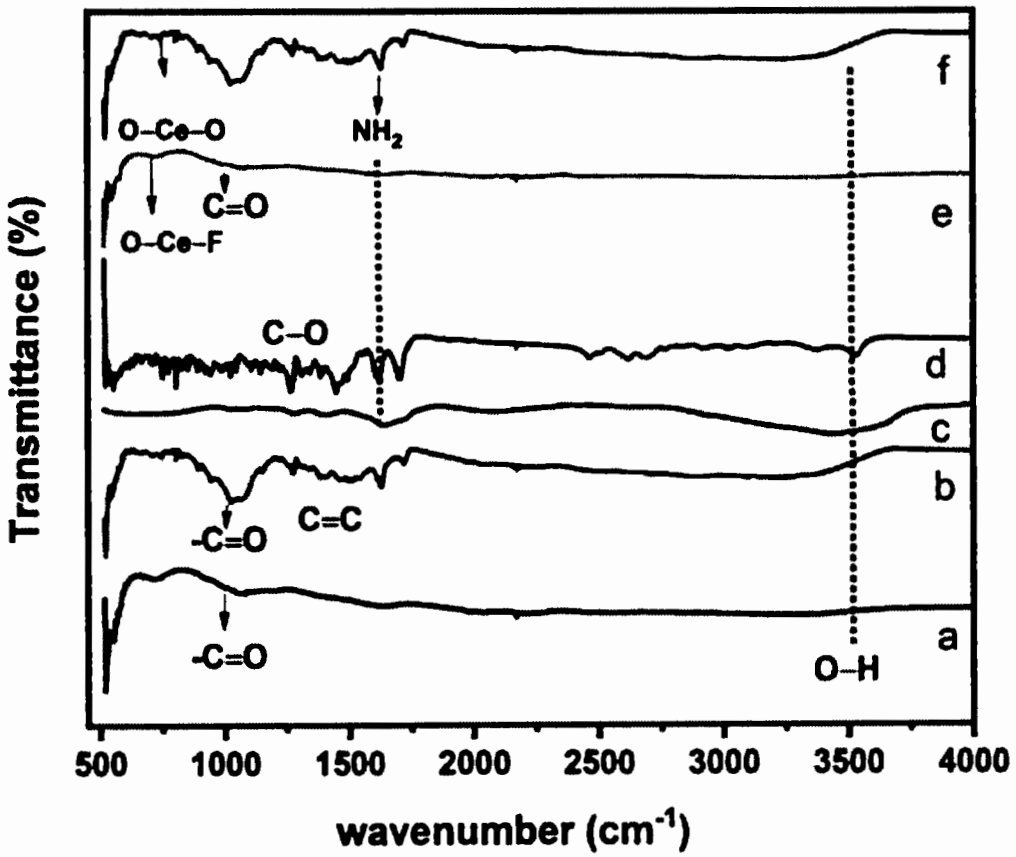

Figure 6.4: FTIR spectra of synthesized nanomaterials

Key:-

(a) BC seed extract

(b) CeO_2 NPs

(c) CS NPs

(d) CIP alone

(e) CIP-CeO_2/CSNPs

(f) CeO_2/CSNPs

6.2.4. Zeta Potential Study of Synthesized Nanomaterials

The surface charge of all biosynthesized nanomaterials (i.e. CeO_2 NPs, CS NPs, CeO_2/CSNPs, CIP-CeO_2/CSNPs, CeO_2/CSNPs) was measured by ZP in the water which used as solvent **(Figure 6.5)**. Zeta potential is the electrical potential at the slipping plane (i.e. interface which separates mobile fluid (e.g. water) from fluid that remains attached to the surface) .In the previous study chitosan-coating reaction, the zeta-potential was measured as +50 mV, suggesting that chitosan has the ability to stabilize cerium system and caused increase in dispersity.

Although CeO_2 NPs showed an unstable stability with the negative ZP value of -123 ± 1.58mV **(Figure 6.5a)**. CS NPs showed a high stability with a positive ZP value of +45± 0.12 mV **(Figure 6.5b)**. CeO_2/CSnanocomposite showed an excellent stability with a ZP of +62 ± 0.74 mV **(Figure 6.5c)**. CIP-CeO_2/CSdrug nanocarrier showed the best stability with a ZP of +110 ± 0.65mV **(Figure 6.5d)**. Thus, since the negative zeta potential value shifted from negative to positive zeta potential in the presence of NH_2 groups of CS, we can conclude that, in water, the surface charge was clearly influenced by the surface coating by CS.

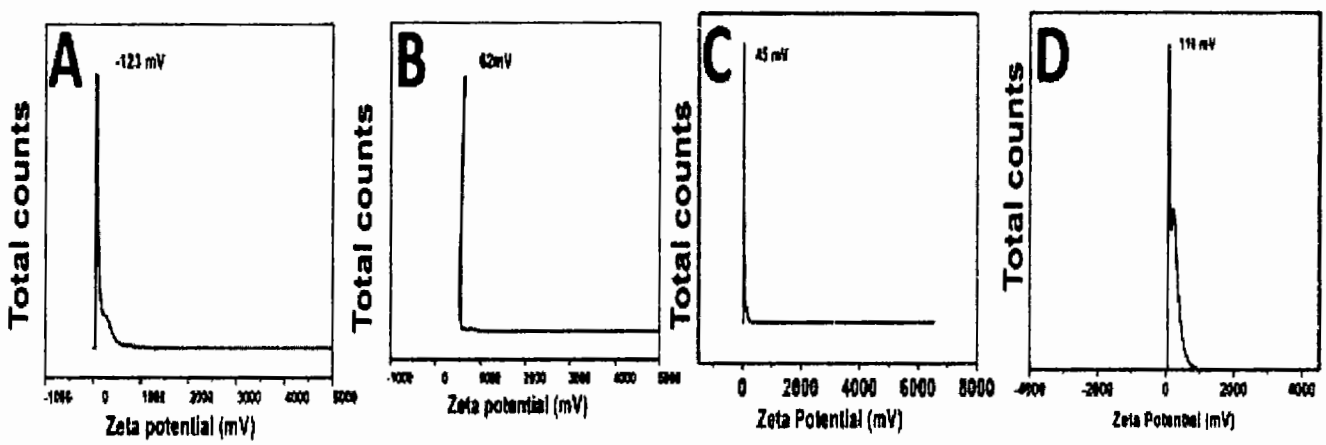

Figure 6.5 Zeta potential analysis of green synthesized nanomaterials, (a) CeO_2 NPs (b), CS NPs, (c) CeO_2/CS NPs (d) CIP-CeO_2/CS NPs .

6.2.5. Encapsulation efficiency of CIP-CeO_2/CS NPs

The encapsulation efficiency of CIP-CeO_2/CS NPs was calculated 75% ± 2.08 which confirmed successful encapsulation of biocompatible polymer chitosan to stabilize the metallic oxide nanoparticle CeO_2 NPs and reverse its polarity to assess its antibacterial activity against MRSA strains.

Taken together, the data revealed that the NPs were successfully prepared via green route using BC seeds extract. Their structure, molecular interactions and elemental composition were confirmed. The biocompatible CIP-CeO_2/CSNPs were pure, small (<50 nm), well distributed), quasi-spherical, displaying large voids, and crystalline in nature. Eventually, all these physical-chemical characteristics were found ideal for testing them as potential anti-bacterial.

6.2.6. In-Vitro antibacterial activity of nanomaterial B (CIP-CeO_2/CS NPs)

The most prevalent mastitis causing strains were found to be *E.coli, S .aureus* and *C.albicans* from the mastitis positive milk samples. Therefore antimicrobial potential of synthesized nanomaterial B was tested against isolated MDR strains and synthesized nanomaterial B was noted efficient against Methicillin Resistant *S. aureus* (MRSA) at very low concentration (8 µg/mL) of nanomaterial B while *E.coli* and *C.albicans* respond at higher concentrations. Hence MRSAwere selected as model organism and these selected strains were also found to be positive for *mec*A genes.

Antibacterial activity of green synthesized nanomaterial B (CIP-CeO_2/CSNPs) was evaluated by using disc diffusion method at various concentrations i.e. MIC (8 µg/mL) and at 2MIC against MDR strains and measured the respective ZI on agar plate. The data at MIC (i.e. OX (900 µg/mL) FOX (650 µg/mL), CIP 700 µg), and to NC (i.e. DMSO 10µl) has shown in the **(Figure 6.6 and Table 6. 3)**.

Interestingly, CIP-CeO_2/CSNPs presented the most significant effect by forming the largest ZI of 12 mm ± 0.45 and 17 mm ± 2.89 against MRSA at MIC and 2MIC values, respectively **(Figure 6.6A and 6.6B)**. Thus, the antibacterial activity of the tested NPs was concentration dependent.

Other pure nanomaterials exhibited inherent antibacterial activities but were not as effective as CIP-CeO_2/CSNPs **(Table 6.3)**. Importantly, OX, FOX and CIP pure antibiotic were not exerting an antibacterial activity onMRSA (all the strains resistant to Oxoid disc of CIP 5μg, OX 1 μg, FOX 30μg) at their MIC values.

The excellent anti-MRSA activity exerted by CIP-CeO_2/CSNPs, compared to CIP alone on mecA-positive MRSA can be explained by the size, the specific surface area, the polar surface, the morphology and the cross-linking of doped materials (e.g. CS). Moreover, electrostatic attraction between negatively charged bacterial cells and positively charged CIP-CeO_2/CSNPs, as confirmed by zeta potential charge value 110±0.65mV, is crucial for the antibacterial activity. Such interaction is not only able to inhibit the bacterial growth but also generate ROS, which molecular mechanism is known to lead to MRSA cell death. CIP-CS based nanohybrid strongly suggest an enhanced antibacterial mechanism thanks to the incorporation/surface coating of CS to CeO_2 NPs by ionic gelation method and the CIP conjugation which penetration into the bacterial cells is enhanced considering the thick cell wall of resistant MRSA isolates.Taken together, the greenly synthesized CIP-CeO_2/CSNPs showed brilliant antibacterial activity against MRSA strains and thus, provided an alternative treatment therapy to treat *S. aureus* -induced mastitis infection which remains a challenge for veterinarians.

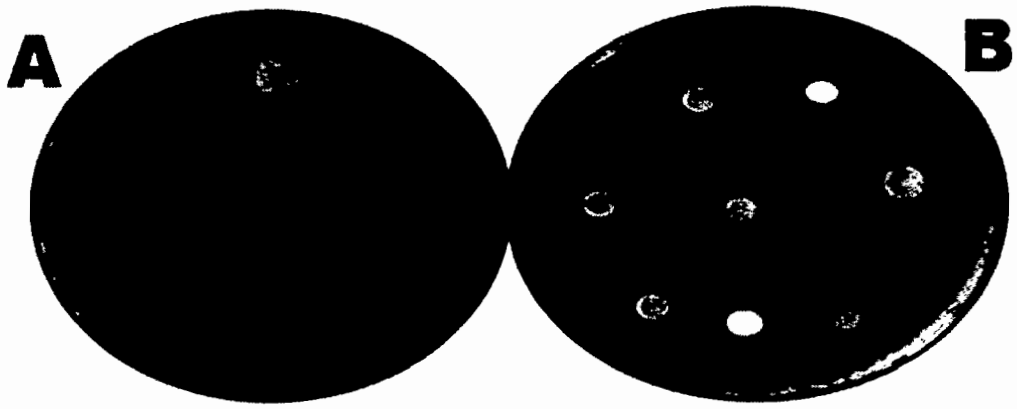

Figure 6.6: Sensitivity of mec*A*-positive MRSA to nanomaterials;

Key: (A) 1-CIP-CeO_2/CSNPs at MIC (8 µg/mL), 2-CeO_2 NPs (8 µg/ml), 3-CS NPs (8 µg/ml),4-CIP (5 µg Oxoid disc) and 5-NC (DMSO);**(B)** 1-NC, 2-FOX (30 µg Oxoid), 3-CS (200 µg/ml), 4-CeO_2NPs (350 µg/ml) 5-CeO_2/CSNPs (75 µg/ml) ,6-OX(1 µg Oxoid), 7-CIP-CeO_2/CSNPs at MIC (8 µg/mL) ,8-CIP (5 µg Oxoid).

Table 6.3: Zone of Inhibition induced (after 24hrs) by the green synthesized NPs against mecA-positive MRSA.

Antibacterial Agents (Putative of Confirmed)	**Zone of Inhibition (mm)**	
	At MIC	**2MIC**
CIP-CeO_2/CSNPs	12±0.45	17± 2.89
CeO_2 NPs	4±0.11	9± 0.27
CS NPs	2±0.08	5± 0.19
Ciprofloxacin	-	-
DMSO (NC)	-	-
CeO_2/CSNPs	5±1.03	11± 2.09
Cefoxitin	-	-
Oxacillin	-	-

6.2.6.1. Killing kinetics of Synthesized Nanomaterial B against MRSA

A more instinctive approach was considered to study the proficiency of the CIP-CeO_2/CSNPs. Indeed, the MRSA growth was further characterized by monitoring the viable cell counts using the classic colony counting method. Each mecA-positive MRSA strain was inoculated on the blood agar plates containing various concentrations (μg/mL) of the CIP-loaded nanocarrier (0, 8 (MIC), 16 (2MIC), 32 (4MIC)). Cell viability rates were then investigated at different time intervals (6, 12 and 24 hrs) by counting the CFU ratios of the respective treatments to the controls (**Figure 6.7**). Blood agar plates without drugs were used as the PC and those without MRSA culture were used as NC. Remarkably, after CIP-CeO_2/CSNPs treatment, the formation of bacterial colonies was reduced in a concentration and time-dependent manner as compared to PC. In particular, CIP-CeO_2/CSNPs exerted a significantly lethal effect on MRSA colonies at the concentration of 32 μg/mL (4 MIC) right after 6 hrs of incubation.

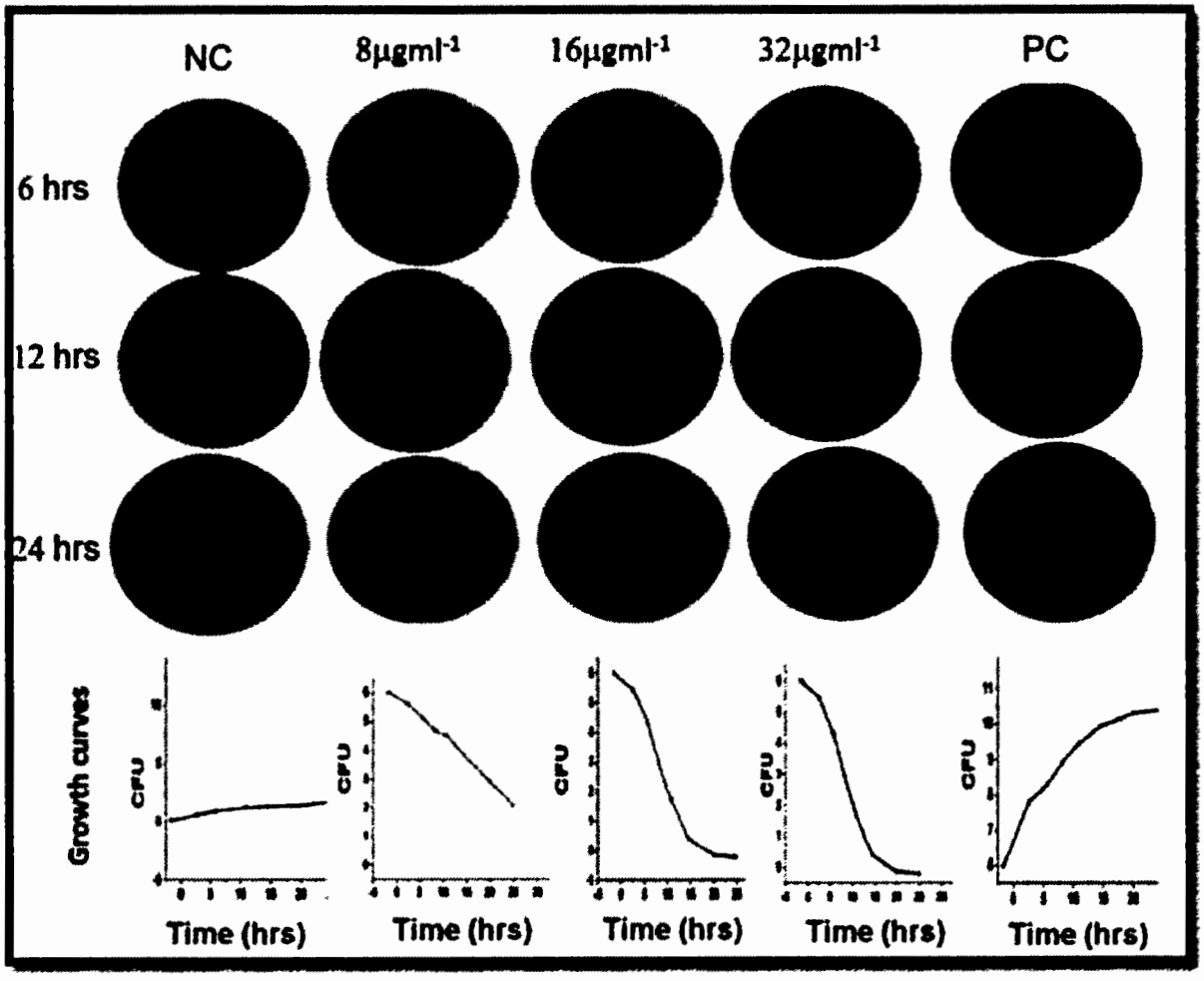

Figure 6.7: Killing kinetics of MRSA isolates treated with nanomaterial B, CIP-CeO_2/CS NPs.

Key:-

PC, Positive control is untreated MRSA

NC, Negative control is only sterile NB (without inoculation of MRSA)

6.2.6.2. Morphological alterations in MRSA induced by Nanomaterial B (CIP-CeO_2/CS NPs)

Expectedly, the morphological changes occurred MRSA isolatestreated by CIP-CeO_2/CSNPsat MIC (8 µg/mL) when monitored by SEM **(Figure 6.8)**. The negative control (untreated MRSA) showed round and smooth MRSA morphology identical to what observed at 0 hrs after treatment by CIP-CeO_2/CSNPs**(Figure 6.8a)**. Slightly deformation was visible after 4 hrs in the spherical structure of treated-MRSA **(Figure 6.8b)**, which was accentuated at 8 hrs **(Figure 6.8c)** to reach an abrupt change at 12 hrs **(Figure 6.8d)**. At 12 hrs post-treatment, the drastic MRSA morphological change suggested typical wrinkled lysed cells releasing their cytosolic content which demonstrated the potent antibacterial effect of the new developed CIP nanoformulation.This effect is most likely mediated through the electrostatic interaction between the positively charged NPs and the negatively charged MRSA cell wall, which subsequently induce ROS species and ultimately cause inhibition of bacterial cell growth cell death free radical stress is sufficient enough

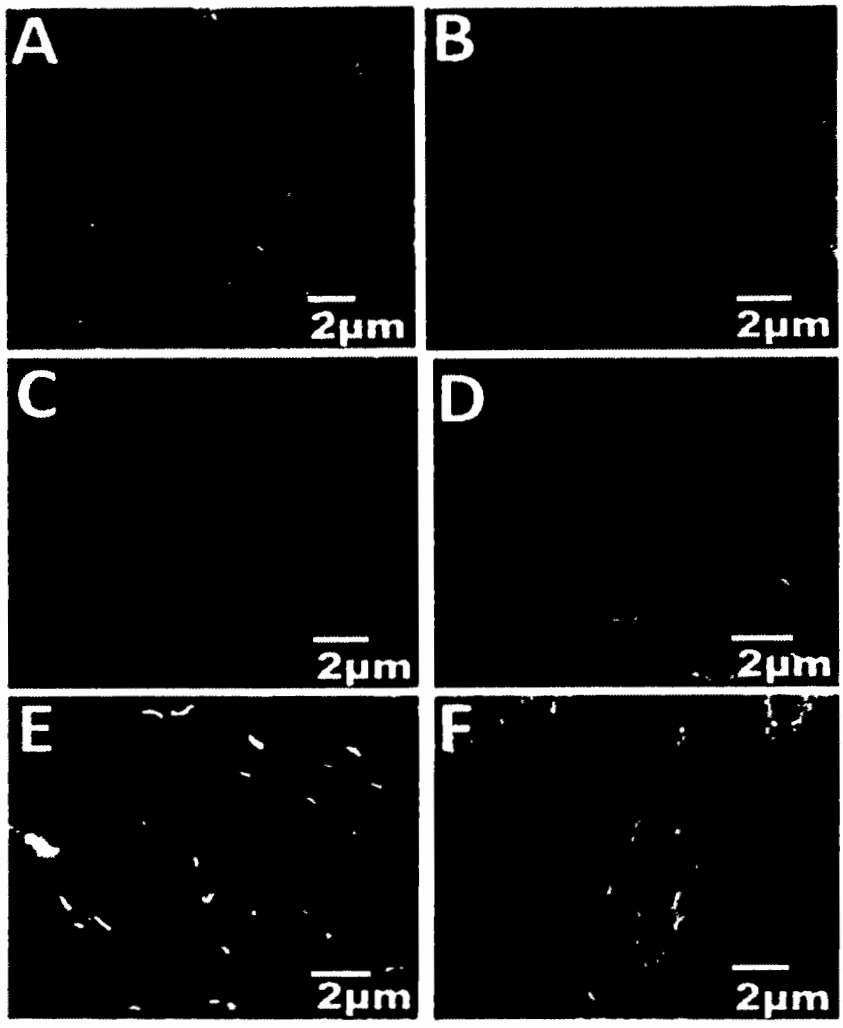

Figure 6.8: SEM micrographs showing morphological changes of MRSA isolates aftertreatment with nanomaterial B CIP-CeO_2/CSNPs using MIC (8 μg/mL) at various times intervals.

Key:-**(A)** 0 hrs; **(B)** 4 hrs; **(C)** 8 hrs; **(D)** 12 hrs; **(E)** Negative control (Untreated culture); **(F)** Positive control (CIP 5μg commercial disc sensitive strains).

6.2.6.3. Screening of Anti-MRSA potential of Nanomaterial B under Flow Cytometry

To further strengthen the antibacterial potential of nanomaterial B (CIP-CeO_2/CSNPs) double-staining (PI/Annexin V) method of flow cytometer and calculated the number of alive cells by a statistical gating approach using FACS before and after treating MRSA strains with CIP-CeO_2/CSNPsusing MIC (8 µg/mL) value at 37 °C for various intervals of time (i.e. 0 hrs, 6 hrs, and 12 hrs) **(Figure 6.11)**. Such assay aims to determine both the necrotic death (by PI staining) as well as the early and late apoptosis (by AnnexinV) and ultimate death in the selected populationdensity (Hussain et al., 2012). Thereby, the death rate was negligible (0.9% ± 0.62) in untreated cells (NC) **(Figure 6.11A)**, whereas the death rate increased in a time dependent manner, with 1.23% ± 0.52 , 40.33% ± 1.79 ,87.04% ± 3.92 after 0hrs **(Figure 6.11B)**, 6 hrs **(Figure 6.11C)** 12 hrs **(Figure 6.11D)**, of incubation after treatment with the CIP-Nanoformulation. It was clearly observed a shift from AnnexinV-stained cells at 0 hrs after treatment to a mixed of AnnexinV/PI stained cells 6 hrs after treatment with CIP-nanoformulation at MIC **(Figure 6.11C).** It can be observed that CIP-CeO_2/CSNPscompromised the cell wall integrity of MRSA cells, thereby favoring the PI permeability and uptake which led to intercalation of PI in the dsDNA and the shift in PI fluorescence.

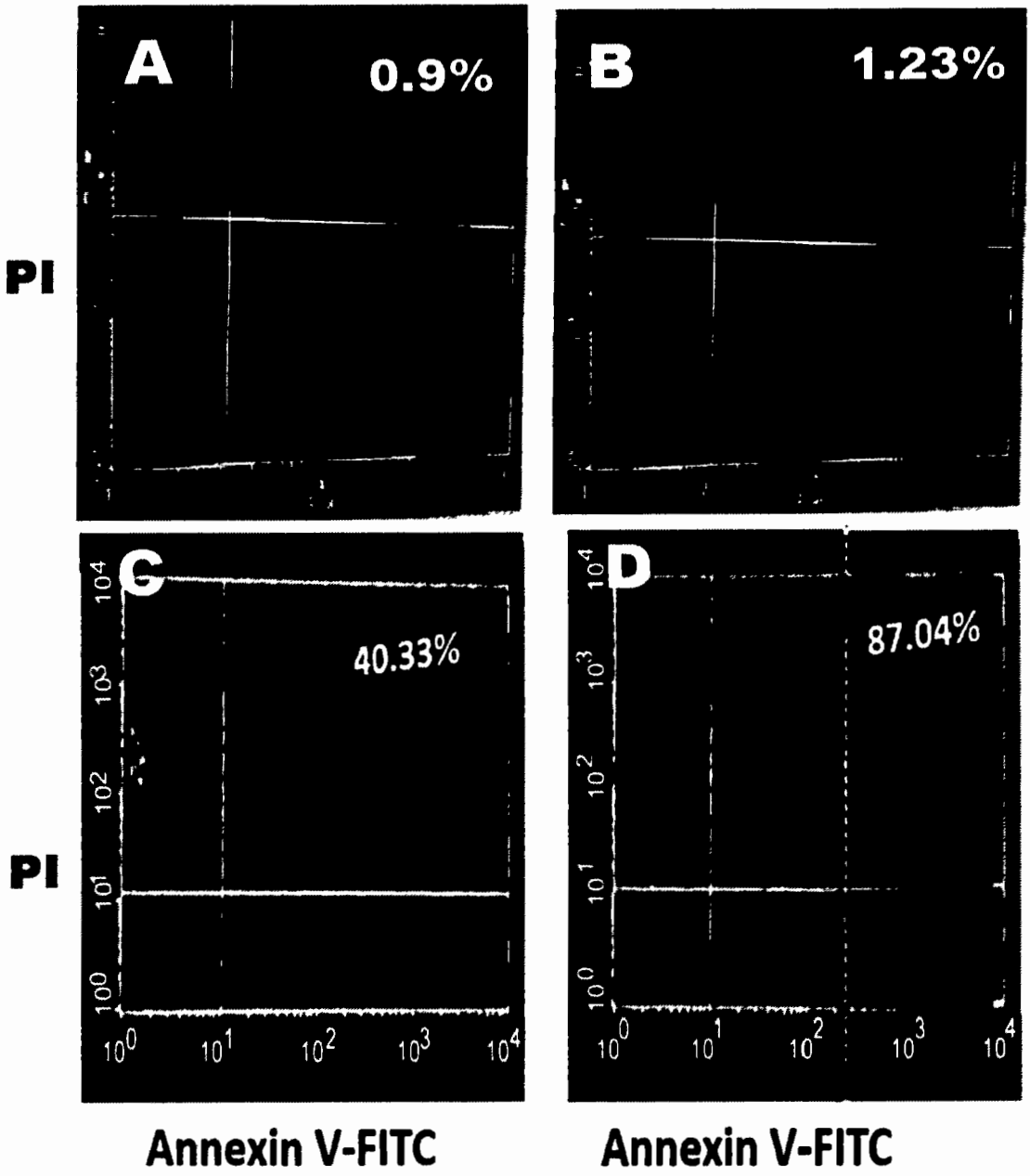

Figure 6.9 Death rate of MRSA cells by FACS exposed to CIP-CeO2/CS NPs at MIC (8 μg/mL)

A-Untreated MRSA (NC);

B- 0 hrs post-treatment,

C- 6 hrs post-treatment;

D- 12 hrs post-treatment.

6.2.7. In-Vitro Biocompatibility Analysis of Synthesized Nanomaterials

The cytotoxicity of the synthesized nanomaterials was studied by MTT assay against Bovine mammary gland epithelial cell line. Importantly, exposure of BMGE cell lines to CeO_2 NPs CS NPs, CeO_2/CSNPs and CIP-CeO_2/CSNPs at various concentrations showed percent viability of mammalian cells as compared to PBS treated cells ($p<0.05$) negative control and Celecoxib which was positive control(**Figure 6.12**). It was found that bovine cells showed concentration dependent viability such as at MIC excellent viability was found and by decreasing concentration cells become more viable as described in **Figure 6.12**. Only green synthesized CeO_2 NPs had a minimal enhanced cytotoxicity compared to that of CIP-CeO_2/CSNPs and CS NPs ($p<0.05$).

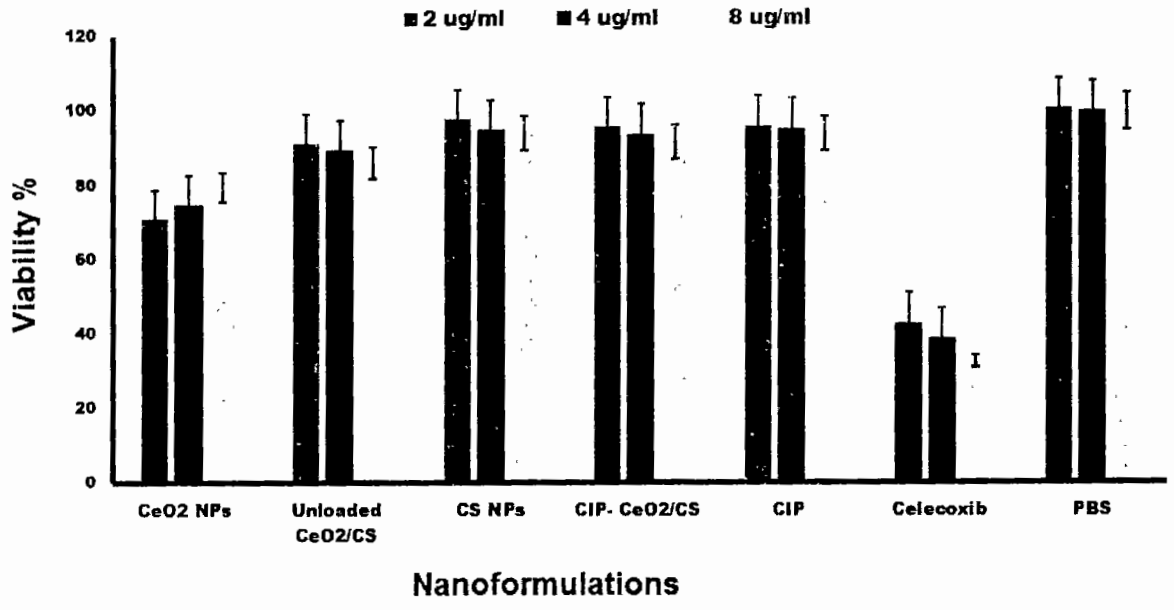

Figure 6.10: Cytotoxicity analysis at various concentrations on BMGE cell line by MTT assay after 24hrs of treatment with synthesized nanomaterials, PBS (100µL) was negative and Celecoxib served as positive control.

One of the important aspects for the *in-vivo* application of nanomaterials is the hemocompatibility, as the injected nanomaterials interact firstly with RBCs before the immune cells. Therefore, the hemolysis assay and RBCs morphology are considered an important feature for preclinical study. Hence, potential hemolytic activity of CeO_2 NPs, CSNPs, CeO_2/CS NPs, and CIP-CeO_2/CSNPs using hemolysis assay on the RBCs of cow **(Figure 6.13)**.The data revealed negligible hemolytic activity of CIP-CeO_2/CSNPs at the MIC value (8 µg/mL) compared to the positive control triton 100X 9 (7% viable RBCs) While CeO_2 NPs, CeO_2/CS NPs, CIP and CSNPs also did not induce hemolysis at various concentrations .CS NPs was even meaningfully not different from PBS (99% viable cells) used at NC ($p>0.05$).

Altogether, the greenly synthesized CIP-CeO_2/CSNPs are safe, noncytotoxic and hemocompatible to mammalian cells, favoring their use for *in-vivo* applications.

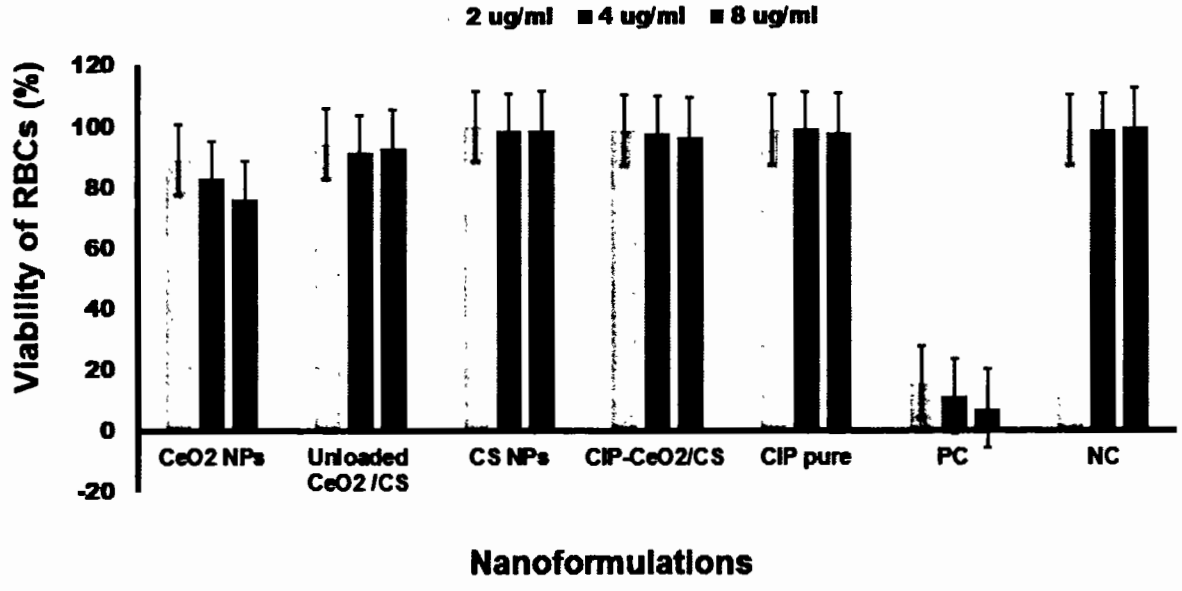

Figure 6.11: Hemolytic effect of synthesized nanomaterials at various concentrations exposed to RBCs (incubation at 37^0C).

Key:-

NC, PBS was used as a negative control

PC, Triton X-100 was used as Positive control.

6.2.8. Ex-vivo antibiotic release from nanomaterial B, CIP- CeO_2/CS

The ex-vivo antibiotic release profile of CIP from the CIP- CeO_2/CS nanocomposite were presented in **Figure 6.12**. The CIP- CeO2/CS nanocomposite exhibited the highest cumulative drug release (88%± 1.09) at the 8hrs of incubation study (37 °C), which was compared to the control value of CIP (91%± 1.14) alone during 24 hrs. The drug release studies revealed that the cross-linked network structure could effectively reduce the antibiotic (e.g. ampicillin sodium) release rate and its burst effect following a Fickiadiffusion.The important criteria for developing an effective delivery system is to ensure the sustained release of the encapsulated drug into the physiological environment.

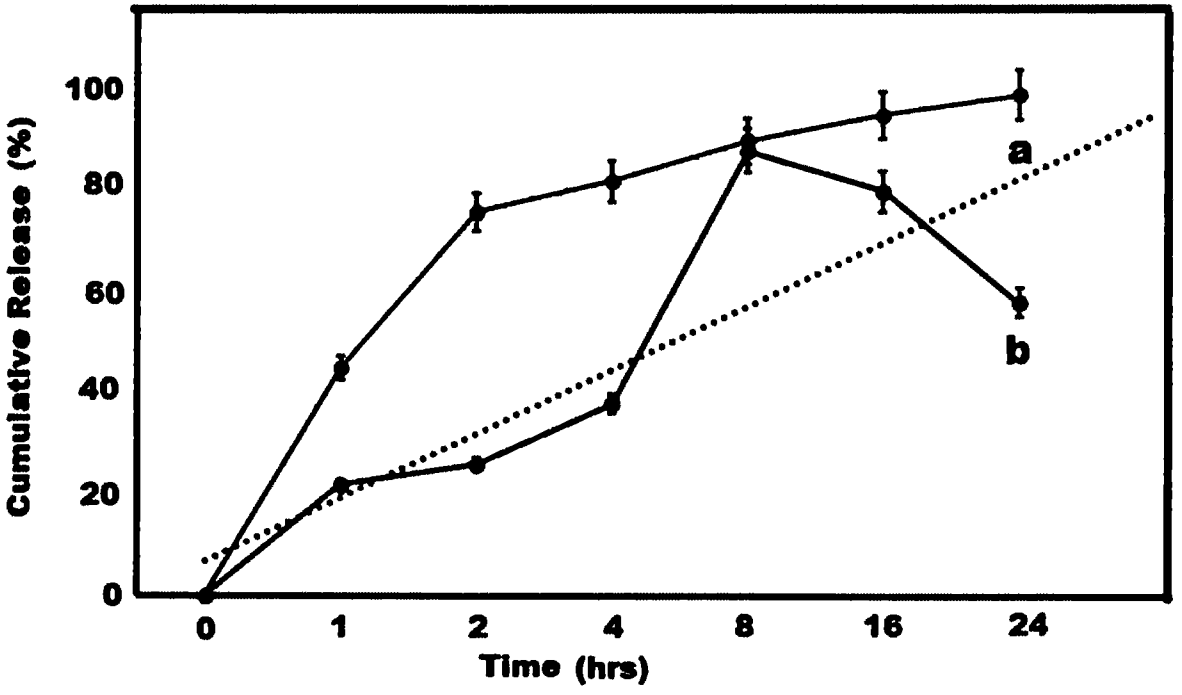

Figure 6.12 The ex-vivo antibiotic release profile of CIP from the CIP- CeO_2/CS nanocomposite in PBS (pH 7.4, 37 °C) a, control CIP alone, b; CIP- CeO_2/CS.

6.2.9. Proposed mechanistic insight to the antibacterial action of CIP-CeO_2/CSNPs

The chitosan has different theories for structural modification with metallic ion but it is mainly due to the amine group (Mohandas et al., 2018). The Nitrogen atom of amine group has free lone pair that made it reactive for antibacterial activity and structural interaction with CeO_2 NPS. Antibacterial activity of CIP-CeO_2/CSNPS was tested against MRSA which has Gram-positive cell wall. Both Gram-positive and negative bacteria have negatively charged cell wall, a characteristic that is hypothesized to influence the interactions between the cell walls of the bacteria and positively charged Ce +3/Ce +4 ions released from CIP-CeO_2/CSNPS (Nagarwal et al., 2009; Slavin et al., 2017). After the interaction of CIP-CeO_2/CSNPS and MRSA, generation of ROS may trigger several reactions which are toxic to MRSA (e.g. oxidation of bacterial cell wall's lipids, cell membrane deformation enhancing its porosity for ions and drug uptake, inhibiting DNA synthesis and protein synthesis by interfering ribosomal subunit complex) (Assali et al., 2017). It was previously found that CeO_2 NPs was more toxic to Gram positive compared to Gram negative due to its higher affinity with proteins and peptidoglycans (Arumugam et al., 2015). Further, the mechanism of action of CIP-CeO_2/CSNPsdepend on the site of action whether it interact with the MRSA by internalization process or not. For non-internalized CIP-CeO_2/CSNPs, direct contact of the nanocomposite and the cell membrane occurs, initiating antibacterial activity by generating ROS stress (Arumugam et al., 2015; Lin et al., 2005) membrane disruption with nutrient transport functions (Lin et al., 2005). In contrast, as shown in the **(Figure 6.13)** when CIP-CeO_2/CSNPs is internalized after causing lysosomal injury, oxidative stress increased, and compromised membrane integrity and subsequent cell death occur (Lin et al., 2005; Moon et al., 2007; Xia et al., 2008).

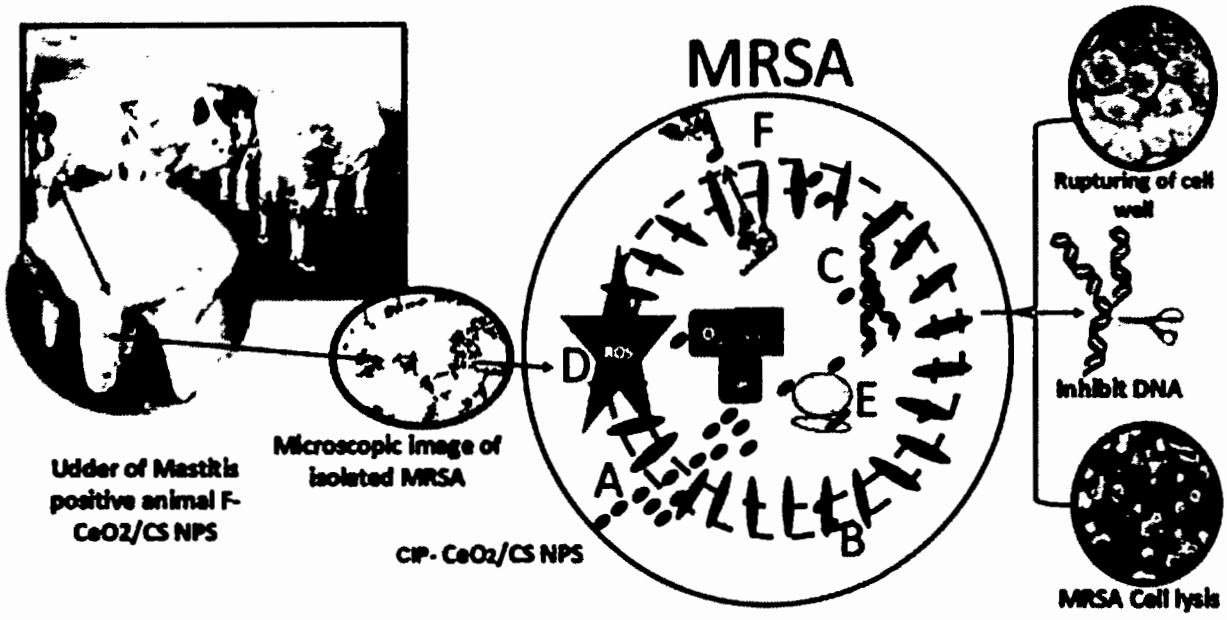

Figure 6.13 Putative molecular and cellular mechanisms of CIP-CeO_2/CS NPs mediated anti-MRSA activity.

Key: A- Attachment and penetration; B- ROS production; C- Oxidation cell wall component; D- Inhibition of DNA synthesis; E- Inhibition of ribosomal assembly; F- Inhibition of protein synthesis.

6.3. Conclusion

MRSA isolated from many infected milk samples were confirmed by disc diffusion method and concealed *mecA* gene in its genome was revealed by PCR. An alternative approach was designed to bypass the resistance mechanism of MRSA by introducing nanomaterials conjugated with at least one large spectrum synthetic antibiotic. The present study introduced a novel composition of biocompatible, biodegradable, and safe inorganic/organic NPs using CeO_2/CS elements in which the potent fluoroquinolone antibiotic CIP was encapsulated. The novel CIP-loaded CeO_2/CS nanocomposite was synthetized for the first time via a green route using Black cardamom, a traditional medicinal plant. Physical characterizations (i.e. SEM, TEM, XRD, FTIR) of CIP-CeO_2/CSNPs confirmed its nanosize with uniform spherical morphology, its efficient synthesis and antibiotic encapsulation, as well as its high stability. Importantly, the anti-MRSA activity of CIP-CeO_2/CSNPs at MIC value (8 μg/ml) was strong and efficient in comparison to the CIP alone, as confirmed by the disc diffusion and the broth microdilution methods. The bacterial cell death occurred in a time and concentration dependent manner eventually increasing ROS stress as observed by SEM, FACS (PI/Annexin V double staining). Eventually, our data clearly showed formation that CIP-CeO_2/CSNPsare nontoxic to bovine mammary gland epithelial cells and nonhemolytic when using RBCs of cow, which flapped green signal for its *in-vivo* applications.

CHAPTER 7

GREEN SYNTHESIS OF NANOMATERIAL C, CIPROFLOXACIN LOADED-Ag/TiO2/CS NANOHYBRID

7.1. Introduction

The use of antibiotics in the treatment of animal infection and the enhancement of animal health are the main driving force behind the development of antimicrobial resistance in animal husbandry (Kimera et al., 2020; Ventola, 2015). Drug resistance has been attributed to over use or misuse of antibiotics in the cattle to treat mastitis whereas MDR (multidrug resistant) strains induced mastitis cattle, are the major cause of economic loss in the dairy industry, and is more likely due to irrational use of antibiotics in dairy industry(Pereira et al., 2014).In addition, traditional antibiotics have been less effective in the treatment of infectious diseases in dairy cattle. In this context, there is an urgent need for the production of biocompatible antibacterial formulations that could regulate bacterial growth by means of improved and efficient mechanisms (Abid et al., 2021).

Bimetallic NPs have received a lot of interest in the last decade in terms of study and technology because of their distinctive optical, electrical, magnetic, and catalytic capabilities, which are often identifiable from monometallic counterparts. Bimetallic NPs can have a range of morphologies and are made by mixing two different types of metal NPs.They are frequently made by reducing two metal ions simultaneously while using proper stabilising tactics including steric hindrance and electrostatic repulsive forces. The reduction rates of the two metal precursor components can be adjusted during synthesis to produce bimetallic NPs with the desired size, shape, structure, morphology, and metal distribution.Such bimetallic NPs are designed to have a synergistic antibacterial impact, and systems whose antibacterial efficacy has recently been explored include Ag–Au, Ag–Cu, Fe–Ag, and Cu–Ni (Perdikaki et al., 2018).Ag–Pt–TiO2 NPs prepared by Sol–gel against *C. albicans*,*E. coli*,*S. aureus* using 16 >256μg cm−3 studied by Jurek et al., 2015(Zielińska-Jurek et al., 2015).

In the New York State a study reported about 82% of milk fed to calves contained residues of antibiotics (Van Vleck Pereira et al., 2016). Subsequent research studied the effect of the

intake of antimicrobial-containing raw milk and identified an increased incidence of antimicrobial resistance in *E. coli* strains of milk/dairy origin (Ventola, 2015). The rise of the antimicrobial resistance is considered a "ticking time bomb" although the WHO has called for a global reduction in veterinary antibiotics to phase out the use of medicinally essential antibiotics by the food industry because of scientific evidence that antimicrobial resistance strains were found in live stocks (Agga et al., 2015; Shrivastava et al., 2018) .

Ciprofloxacin is a fluoroquinolone class antimicrobial, widely used for a wide range of infections, including those caused by *E.coli* but resistance is reported against it (Anderson et al., 1998; van der Putten et al., 2018).

Nanotechnology is a possible response to antimicrobial resistance, which could promote creativity and create a new generation of antibiotic therapies for potential medicines. Sustaining existing antibiotic activity through novel formulation using nanotechnologies can increase the therapeutic longevity of anti-infection action of existing antibiotics that are no more effective against MDR strains. There is credible evidence of the effective use of nanotechnologies as antimicrobials (Kumar et al., 2018). Metal oxide NPs as antimicrobial agents demonstrated relatively high efficiency to combat MDR strains. Metal-based nanomaterials, such as silver nanoparticles (AgNPs) and titanium, have attracted immense attention because of their excellent efficiency against MDR bacteria owing to their electronic, optical, and catalytic properties (Slavin et al., 2017). In addition, it is relatively simple to synthetize AgNPs, and the mass production of metal oxide based Ag-nanohybrids is cost-effective (Kandi & Kandi, 2015) .The antimicrobial activity of TiO_2 was first reported by Matsunaga and colleagues in 1988 (Matsunaga et al., 1988). Under near-UV light illumination, microbial cells could be destroyed by contact with a TiO_2–Pt (Gnanaprakasam et al., 2015). Nanomaterials based on chitosan have gained considerable interest in the biomedical field due to their unusual biodegradability, biocompatibility, protection and antimicrobial properties (Kravanja et al., 2019) .This powerful biopolymer is capable of enhancing the stability of AgNPs and Ag-based nano-hybrids (Marta et al., 2015). CS-based composite nanomaterials have been reported as highly effective antibacterial agent, and found wide applications including in drug delivery, tissue engineering, wound healing and antibacterial activity (Abd Elgadir et al., 2015). There are many ways to develop new drug

delivery systems using liposomes, polymer-drug conjugates, lipid-based nanoparticles and copolymeric cells, which could improve the drug delivery (Thu et al., 2015).

Recently, the plant-mediated green synthesis of silver nanoparticles has grown into a unique and novel field of nanotechnology. It has gained importance because of its eco-friendly and cost efficiency with lower toxicity as compared to chemical method (Zhang et al., 2016). The reduction properties of plant secondary metabolites are responsible for the enhanced ability of plant extracts to produce nanoparticles with enhanced properties (Basiuk & Basiuk, 2015). *M. concanensis* nimmo is a medicinal herb with versatile use in pharmaceutical products, antibacterial agent, food source and water purifying agent and is used for the treatment of variety of diseases including paralysis, menstrual pain, high blood pressure, skin tumors, liver and kidney disease as well as to treat inflammation of joints indicating its immense importance in health care industry (Anbazhakan et al., 2007; Balamurugan et al., 2015).

Considering the urgent need for new clinical interventions to control global issue of AMR, a unique ciprofloxacin loaded-TiO_2/Ag/CS nanohybrid was synthesized by green approach using *M. concanensis* leaves extract. AgNPs and TiO_2NPs were prepared by *M. concanensis* leaves extract, as a reducing and stabilizing agent. Incorporation of AgNPs onto the surface of TiO_2nanomaterials was performed by wet chemical impregnation technique. The CS encapsulation of TiO_2/Ag composite followed after coupling with CIP by ionic gelation method. Physical characterizations were performed by the routine state-of-the-art techniques of microscopy and spectroscopy. Ciprofloxacin loaded-TiO_2/Ag/CS nanohybrid was tested for its efficacy against MDR strains of *E.coli*-causing mastitis in the cattle by various standard antimicrobial assays indicating strong antibacterial potential of synthesized nanohybrid. Eventually, we assessed the possible sustained release of the ciprofloxacin from the hybrid material by drug release kinetics study. Cytotoxicity was evaluated by MTT assay for veterinary application using bovine mammary gland cell lines.

7.2. RESULTS

7.2.1. Physical Characterization of the Green Synthetized nanomaterials

7.2.1.1. XRD Analysis

XRD pattern of TiO_2NPs**(Figure 7.1a)**represented the(101), (004), (200), (105), (211) and (204) plane indices that corresponds to crystalline anatase phase as supported by (JCPDSNo.84-1285).The XRD peaks of AgNPs **(Figure 7.1b)** shows the (111), (200), (220), and (311) crystallographic planes at $2\theta^{\circ}$ = 38.18°, 44.25°, 64.72°, and 77.40°leading to face-centered cubic metallic silver crystals.It can be inferred that Ag ions (Ag^{+}) are strongly reduced by the *M. concanensis* leaf extract during the synthesis process .Any diffraction peak related to silver oxides was not observed. In Ag/TiO_2nanocomposite**(Figure 7.1c)**,the characteristic XRD peaks show the anatase phase of TiO_2 and the face-centered cubic silver content without any sign of any other diffraction peaks as impurity. In CSNPs **(Figure 7.1d)**, the characteristic XRD peak was indicated at 21.8° crystallinity and purity of chitosan in the nano structure.The XRD profile of Ag/TiO_2/CS nanohybrid **(Figure 7.1e)**, The XRD profile of CIP-Ag/TiO_2/CS nanohybrid**(Figure 7.1f)** revealed the diffraction peaks of anatase TiO_2 ,Ag , and CS .It is observed that the diffraction peaks of this nanocarrier are shifted to high angle region which indicated that foreign material i.e. CS and CIP inserted the stress on the lattice of host material (Ag/TiO_2). It is also noted that leading peak of Ag at 38.18° overlapped with the

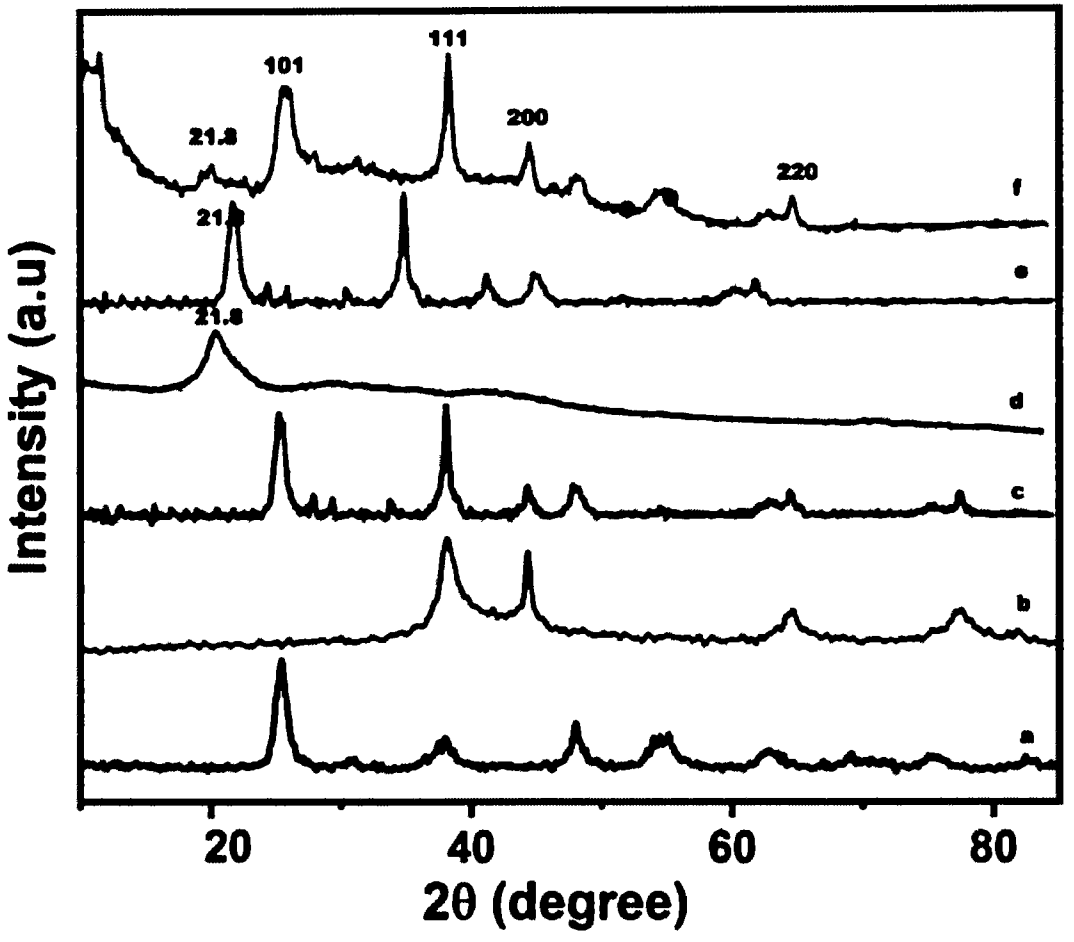

Figure 7.1: XRD patterns of greenly synthetized nanomaterials.

Key: (a) TiO_2 NPs (b) AgNPs (c) Ag/TiO_2 nanocomposite (d) CS NPs (e) Ag/TiO_2/CS nanohybrid and (f) CIP-Ag/TiO_2/CS nanohybrid.

Peak of TiO_2 at 38° and suppressed the signal of TiO_2.The crystalline particle size of nanoformulations is measured about the peaks centered at (101) of anatase TiO_2 and (111) of Ag by using the Scherrer's equation. The PS and the crystalline size of the newly developed drug nanocarrier were 19 nm± 1.98 and0.9821±0.76 Å in average and all other characterized NPs.

7.2.1.2. FESEM and TEM of Nanomaterial C, CIP-Ag/TiO_2/CS nanohybrid

Texture and morphological analyses of greenly synthesized TiO_2NPs, AgNPs, Ag/TiO_2 nanocomposite and CIP-Ag/TiO_2/CS nanohybrid were determined by FESEM **(Figure**

7.2).TiO_2NPs, AgNPs and Ag/TiO_2 nanocomposite the nanostructures showed uniform round spherical morphology (Bokare et al., 2013) as illustrated in FESEM micrographs represented by **Figure 7.2A, 7.2B and 7.2C** respectively. The particle size of TiO_2NPs, AgNPs, Ag/TiO_2 nanocomposite CSNPs and CIP-Ag/ TiO_2/CS nanohybrid, showed from 25-55 nm, 22-40 nm, 19-35 nm and 19-75 nm, respectively. This also tentatively confirms the particles size observed from XRD analyses. Agglomerated and spherical AgNPs were well dispersed throughout the surface of TiO_2 **(Figure 7.2B)**.Also, it can be remarkably observed from the Ag/TiO_2 nanocomposite that AgNPs are incorporated on the surface of TiO_2 **(Figure 7.2C)**. It is noted that there is no distinction between the TiO_2NPs and AgNPs in Ag/TiO_2 nano-composite. Eventually, it was clearly seen that the biopolymer CS anchored the whole surface of spherical Ag/TiO_2 nanocomposite **(Figure 7.2D)**. After CS grafting, it was perceived that AgNPs remained segregate onto TiO_2 surface **(Figure 7.2D)**.

EDX analysis was done to investigate the elemental distribution of the four nanostructures **(Figure 7.2)**. **Figure 7.2A** displayed the Ti and O signals supporting the TiO_2 NP synthesis. **Figure 7.2C** revealed the peaks corresponding to the Ti, O and Ag in Ag/TiO_2nanocomposite. It was cleared from the signal that 1.2 wt% nominal content of Ag was closed to its stoichiometric value of 2.0 wt% solution of AgNPs exploited for the fabrication of Ag/TiO_2 nanocomposite. The signal of C in Ag/TiO_2nanocomposite can be ascribed to the carbon substrate/grid. No additional peaks were observed which indicated the purity level of the synthesized nanoformulations **Figure 7.2B** showed elemental profile of AgNPs which determined the sharp signal of Ag element. Finally synthesized CIP-Ag/ TiO_2/CS nanohybrid elemental spectrum was shown in the **Figure 7.2D** which displayed the peak signals corresponding to TiO_2, Ag, TiO_2/Ag and CS, other peaks or modifications in signal intensity may be attributed to incorporation of CIP.

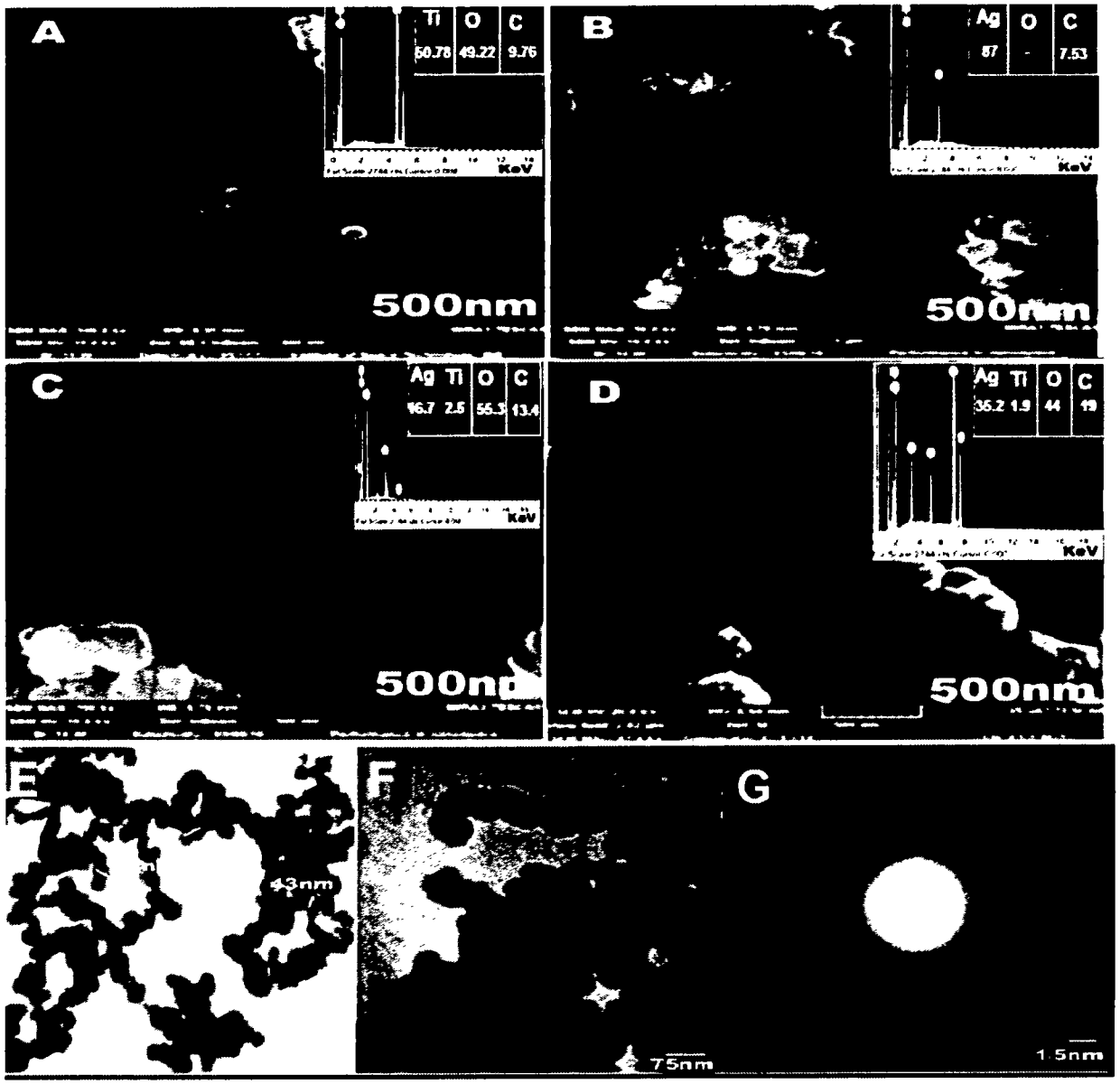

Figure 7.2 FESEM images of nanomaterials,

Key: (A) TiO_2NPs (B) AgNPs, (C) TiO_2/Ag nanocomposite (D) CIP-Ag/TiO_2/CS nanohybrid TEM analysis (E) TiO_2/Ag composite (F) CIP-Ag/TiO_2/CS nanohybrid and (G) SAED.

The TEM results confirmed the outcomes of FESEM analysis, as shown in the **Figure 7.2E and 7.2F** round and spherical morphology was depicted, while purity of the newly developed CIP-TiO_2/Ag/CS nanohybrid was observed by SAED as shown in the **Figure 7.2G**.The particles size of Ag/TiO_2 composite and CIP-Ag/TiO_2/CS nanohybrid was 47 -75nm and 20 - 80nm respectively The SAED pattern of the prepared CIP-Ag/TiO_2/CS nanohybrid

demonstrated Ag/TiO_2 contained a face-centered cubic crystalline phase. SAED pattern further exhibits discrete circular diffraction rings corresponding to anatase phase of TiO_2 NPs. Moreover SAED showed less agglomeration which further supported the facts that phytocompounds of leaf extract of moringa and chitosan contribute their role.

7.2.1.3. FTIR Analysis of Synthesized Nanomaterials

FTIR spectra of TiO_2NPs, AgNPs, CSNPs, Ag/TiO_2 nanocomposite, unloaded Ag/TiO_2/CS Nanohybrid and CIP-Ag/TiO_2/CS Nanohybrid are displayed in **Figure 7.3.** The FTIR spectrum of pure TiO_2**(Figure 7.3a)** exhibited emerging characteristic peaks of absorption at 3408cm^{-1} which belongs to superposition of the hydroxyl groups (O–H) that evidences the coordination of water molecule to Ti^{4+}cations. The absorption band cantered at 2928 cm^{-1} is assigned to C–H stretching vibrations. The signature at 1603 cm^{-1} can be attributed to C=O stretching vibrations due to the butyl group, organic species as starting precursor solutions and adsorbed water molecules on the surface of the nanoformulations. The absorption band in the range of 766-610 cm^{-1} is related to the Ti – O bonding that authenticates the formation of TiO_2.The FTIR spectrum of AgNPs **(Figure 7.3b)** revealed the characteristic peak at 3424 cm^{-1} corresponding to O–H stretching vibrations of adsorbed water molecules. The peaks at 2919 cm^{-1} and 2841 cm^{-1} indicated alkanes (C–C) stretching vibrations. The signature that appeared at 1625 cm^{-1} is attributed to bending vibrations of alkene group.The peak at 1099 $cm^{-1}$was assigned to the asymmetric and symmetric C=O stretching vibrations due to carbonyl group present in leaf extraction. Alkanes, alkenes and carbonyl groups of leaves extraction are mainly involved in the reduction of Ag^+ to AgNPs. The FTIR spectrum of TiO_2/Ag nanocomposite **(Figure 7.3c)** displayed bands ranges in the region from 800 to 530 cm^{-1}that are attributed to Ti–O stretching mode and Ti–O–Ag/Ag–O–Ti linkage. The FTIR spectrum of CS **(Figure 7.3d)** exhibited a high absorption peak of 3423 cm^{-1} and 1636 cm^{-1} due to the availability of a free –OH group from water molecules, amino group and a C=O carbonyl moiety group. The value at 1018 cm^{-1} corresponded to the throttle vibration of the C–O–C bond of epoxy or alkoxy. The signature at 1269 cm^{-1} and 1419 $cm^{-1}$was due to C–O and CH–OH bonds. The FTIR study of unloaded Ag/ TiO_2/CS **(Figure 7.3e)** characteristic peaks of metal components and CS differential peaks were prominently showed in the spectrum. Moreover the binary junction of Ti –O and Ag metals was also displayed in the

spectrum. The FTIR of CIP-Ag/ TiO_2/CS nanohybrid **(Figure 7.3f)** showed peaks at around 1010 cm^{-1} and 1600 cm^{-1} that are correlated with aromatic bending and stretching. It is clear that the absorption peak centered at 596 cm^{-1} is due to the metal oxygen metal (Ti–O–Ag) mode of vibration.

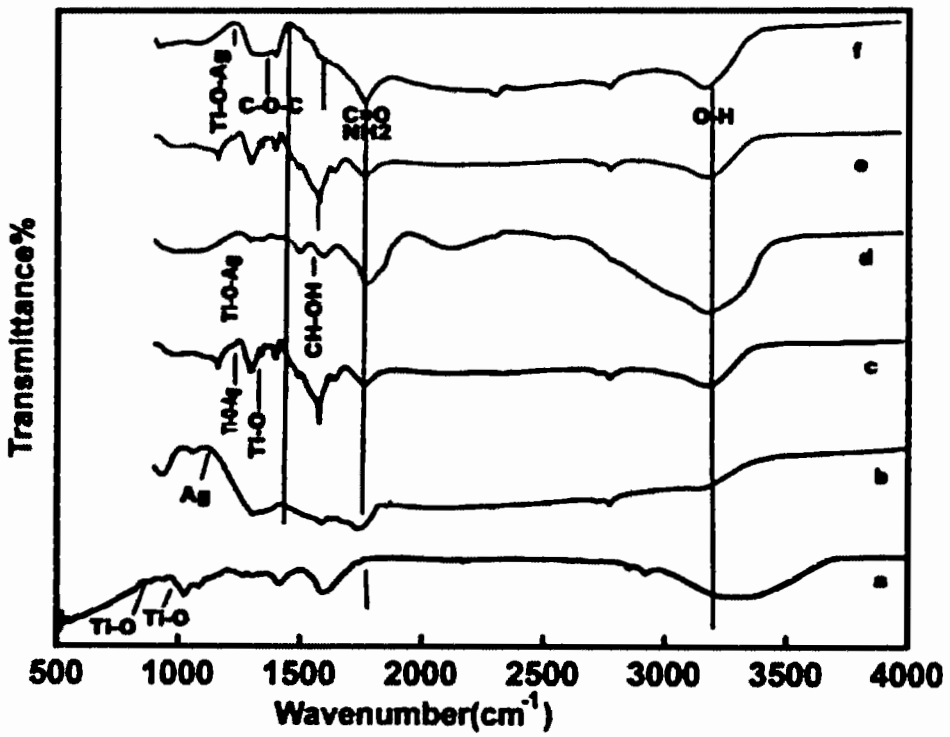

Figure 7.3 FTIR spectrum of green synthesized nanomaterials,

Key:(a) TiO_2 NPs (b) AgNPs (c) Ag/TiO_2nanocomposite (d) CS NPs (e) unloaded Ag/ TiO_2/CS Nanohybrid and (f) CIP-Ag/ TiO_2/CS Nanohybrid.

7.2.1.4. Zeta Potential Analysis

Zeta potential is the capacity of suspended particles to affect their stability and the zeta potential greater than 30mV or less than-30mV can be distributed permanently in the medium.The zeta potential values of AgNPs **(Figure 7.4a)**, TiO_2NPs **(Figure 7.4b)**, TiO_2/Ag nanocomposite**(Figure 7.4c)** and CSNPs **(Figure 7.4d)** were -110, -123 mV, -200 mV and 35.12 mV, respectively. The newly synthesized CIP-Ag/ TiO_2/CS nanohybrid showed good stability with a zeta potential value of 67.45mV **(Figure 7. 4e)**.

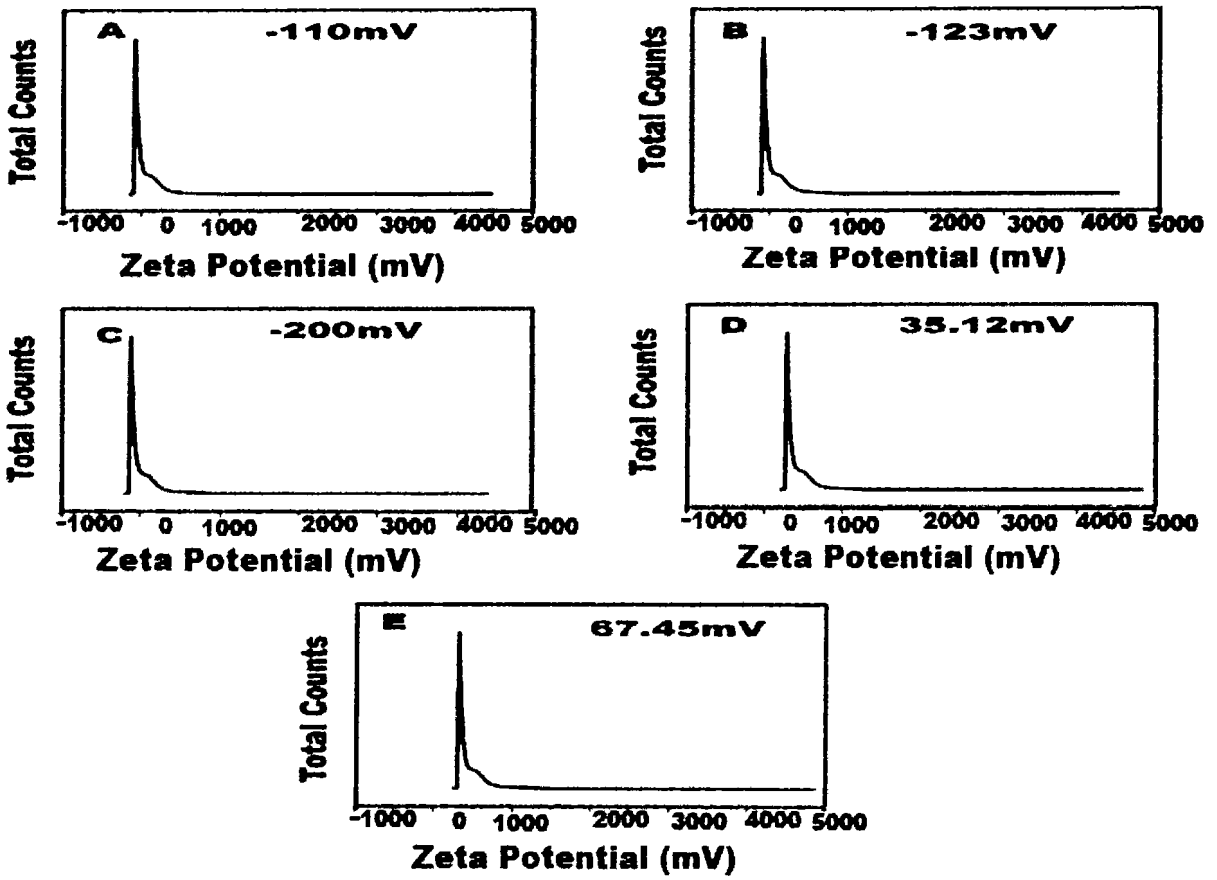

Figure 7.4 Zeta potential of green synthesized nanoformulations,

Key: (A) TiO_2 NPs, (B) Ag NPs, (C) Ag/TiO_2 nanocomposite, (D) CS, (E) CIP-Ag/TiO_2/CS nanohybrid.

7.2.2. Encapsulation efficiency of CIP-Ag/TiO_2/CS nanohybrid

The encapsulation efficiency of CIP-Ag/TiO_2/CS nanohybrid in the CS system was found as 90% ± 2.07 which was excellent to deliver target antimicrobial agents at the site of infection.

7.2.3. Antibacterial activity of greenly synthesized nanomaterial C, CIP-Ag/ TiO_2 /CS

Antibacterial activity of synthesized nanomaterial C was tested against isolated MDR strains of *E.coli*, *S. aureus* and *C.albicans* from the mastitis positive milk samples. Antibacterial activity was screened by disc diffusion method and it was studied that nanomaterial C was effective against *E.coli* strains as compare to *S. aureus* and *C.albicans* strains. On the basis of MIC determination, nanomaterial C was found proficient to inhibit the growth of MDR *E.coli* at lowest concentration 0.0512 µg/mL as shown in **Figure 7.5 A&B**. As *E. coli* was considered to be MDR on the basis of a resistant pattern against synthetic antibiotics that are generally used for the cure of mastitis. The ciprofloxacin was considered most efficient drug but according to the present study it has lost its efficacy, *E.coli* strains have developed resistance against this drug and become super bugs by showing resistance against all the recommended values of MIC by employing E-strip method. The CIP-Ag/ TiO_2/CS nanohybrid was found most efficient and active antimicrobial agent, means of zones of inhibitions of *E.coli* produced by nanoformulations were measured.

As shown in the **Table 7.1** dose dependent antibacterial property of chitosan, Ag/TiO_2 nanocompositeandciprofloxacin loaded CS nanohybrid was observed. CIP-Ag/ TiO_2 /CS nanohybrid exhibited highest zone of inhibition of 23mm± 1.185 by using 0.2048µg/ml of CIP-Ag/ TiO_2/CS nanohybrid which is an admirable antibacterial activity.

Table 7.1: Zone of inhibition, SD values of synthesized nanoformulations and synthetic antibiotic at various concentrations against MDR *E.coli.*

Antimicrobial Agents	**Concentrations (µg/mL) and Zone of Inhibitions (mm)**		
	MICs	**MICsX2**	**MICsX3**
Loaded CIP-TiO_2/Ag/CS	15 ± 1.06	18 ± 0.98	23± 1.185
UnloadedTiO_2/Ag/CS	7± 0.03	9 ± 0.10	10 ± 1.35
Ag/TiO_2 Nanocomposite	5 ± 0.12	7 ± 0.14	9 ± 1.76
TiO_2 NPs	2 ± 0.11	9 ± 1.05	11 ± 0.40
Ag NPs	3.5± 0.02	8± 1.13	12± 1.79
CS NPs	1 ± 0.17	3± 0.90	7± 0.64
CIP	0.9 ± 0.03	2± 0.48	5± 0.58
DMSO	-	-	-

7.2.3.1. Killing kinetics Study of nanomaterials against MDR *E.coli*

According to the current findings CIP-Ag/TiO_2/CS nanohybrid is highly effective in combating MDR *E. coli* as reflected in **Figure 7.6** which presented killing kinetic curve. The growth of MDR *E.coli* was ceased by CIP-Ag/TiO_2/CS nanohybrid within 6-8hrs of incubation by reducing the OD values close to the negative control of study (autoclaved nutrient broth) as shown in **Figure7.6**. Antibacterial activity was remarkable as observed in this study by the synthesized nanoformulations particularly CIP-Ag/TiO_2/CS nanohybrid halted the growth of *E.coli* within few hours of exposure. The findings showed a mutual antibacterial activity of ciprofloxacin with the Ag/ TiO_2/CS composite.

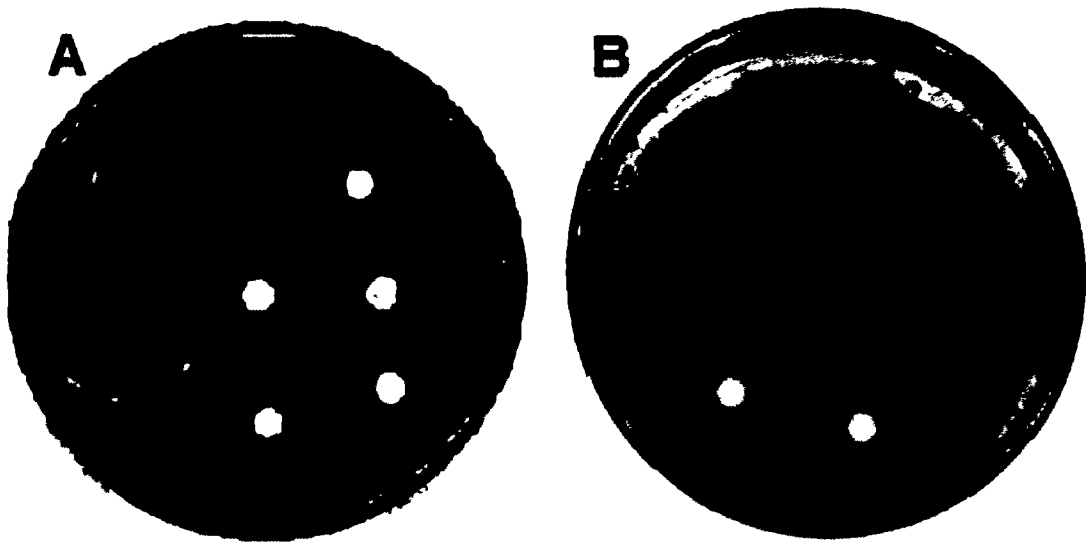

Figure 7.5 Antibacterial activity of nanomaterial C, (A) Zone of inhibition exhibited by synthetic and prepared antimicrobial agents, (B) ZIs shown by synthesized nanoformulations at respective MICs.

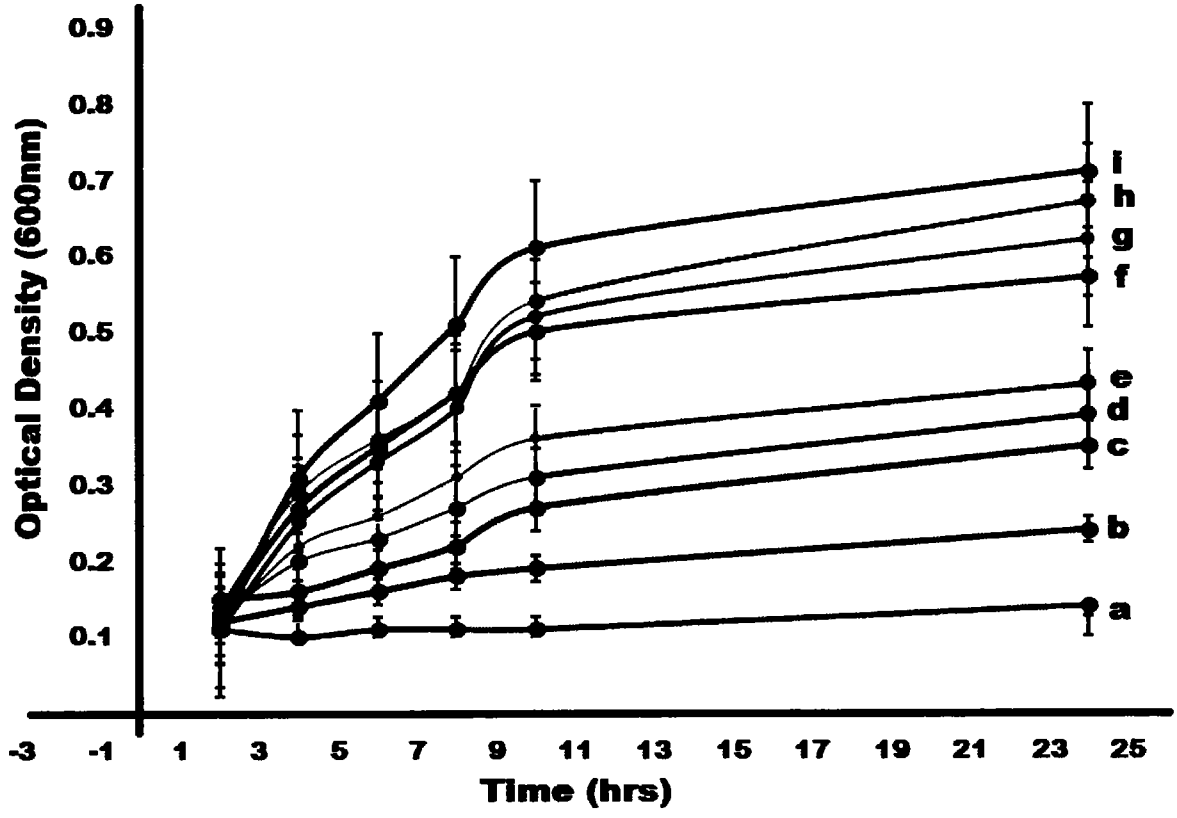

Figure 7.6 Killing kinetics curves for MDR *E. coli* at 0.0512µg/mL (MIC),

Key: (a) NC (pure NB), (b)CIP-Ag/ TiO_2/CS nanohybrid (c) unloaded Ag/TiO_2/CS, (d) Ag/TiO_2, (e) AgNPs, (f) TiO_2NPs; (g) CS, (h) CIP (i)PC (positive control *E.coli* in broth).

7.2.4. *E. coli* cell morphology alterations mediated by CIP-TiO_2/Ag/CS nanohybrid

FE-SEM and TEM is been used to visualize the CIP-TiO_2/Ag/CS nanohybrid-induced potential morphological alterations on MDR *E. coli* using respective MIC. After treating the bacterial cells with CIP-Ag/ TiO_2/CS nanohybrid cytolysis in *E. coli* cells can be seen in **Figure 7.7 and 7.8**. In the control group (untreated) cells shown intact, uniform, and plump morphology as seen in **Figure 7.7A and 7.8A**; however, after 6 hrs of treatment, the surface of the previously healthy *E.coli* cells showed deep rill like folds which led to the detachment of membrane from the cell wall (**Figure 7.7B and 7.8B**). Almost all cells have low density regions in their center, which clearly indicates cytoplasm was damaged by the nanohybrid and outer membrane was disintegrated but the cytoplasmic shape was still maintained

(**Figure 7.7B and 7.8B**). CIP alone was tested against *E.coli* strains and results were concluded in the (**Figure 7.7D, 7.8E and 7.7F**), by the FE-SEM and TEM (**Figure 7.8D, 7.8E and 7.8F**).

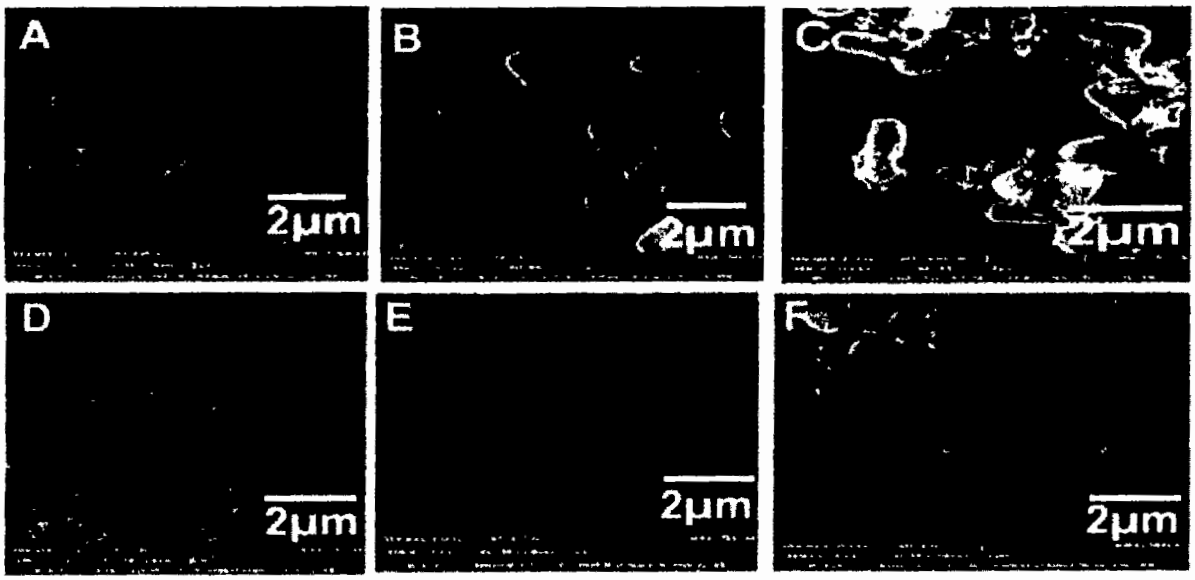

Figure 7.7: FESEM micrographs displaying morphological changes in MDR *E. coli* cells treated with CIP-Ag/TiO_2/CS nanohybrid at MIC (0.0512 μg/mL) and at different intervals of time.

Key: (A) Untreated MDR *E.coli* cells; **(B)** MDR *E.coli* cells after 6 hrs of incubation;**(C)** MDR *E.coli* cells after 12 hrs of incubation;**(D)** *E.coli* with CIP at 0hrs; **(E)** CIP at 6hrs and **(F)** CIP at 12hrs culture of *E.coli.*

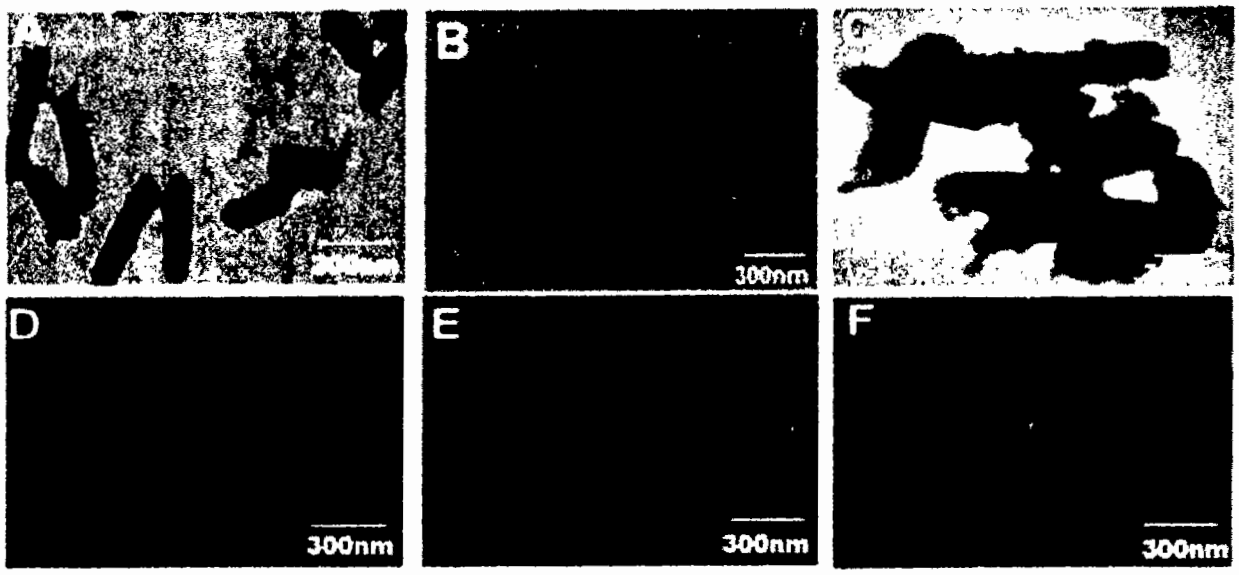

Figure 7.8: TEM micrographs displaying Ultrastructural changes in MDR *E. coli* cells treatedwith CIP-Ag/TiO_2/CS Nanohybrid at MIC (0.0512 µg/mL) and at different intervals of time.

Key:**(A)** Untreated MDR *E.coli* cells; **(B)** MDR *E.coli* cells after 6 hrs of incubation **(C)** MDR *E.coli* cells after 12 hrs of incubation. **(D)** *E.coli* with CIP at 0hrs; **(E)** CIP at 6hrs and **(F)** CIP at 12hrs of *E.coli* treatment.

7.2.5. Live/Dead Assessment of CIP-Ag/ TiO_2/CS Nanohybrid-Treated Bacteria by Flow Cytometry

Antibacterial activity of synthesized nanomaterial C, CIP-Ag/ TiO_2/CS was double checked by live/dead assay using flow cytometry. *E.coli* exhibited increased cell membrane damage and cell inclusion leaking when treated with CIP-Ag/ TiO_2/CS nanohybrid, as confirmed by flow cytometry analysis. Annexin V-FITC and PI dyes were used to reveal stages of apoptosis in the *E.coli* cells after interacting with CIP-Ag/TiO_2/CS nanohybrid. Phosphatidylserin is a phospholipid abundant in the internal surface of the plasma membrane that is exposed to calcium-dependent signals in the outer leaflet during early apoptosis. PI, an intact impermeable dye can only pass via the cells until it is weakened or dead. In connection with PI, we have obtained a rapid and reliable analysis of cellular structural damage based on a flow cytometric analysis. These result showed that untreated cell population in the right upper quadrant late apoptotic cells which was found 0.19% and 99.81% cells were live in the lower left quadrant as shown in the **Figure 7.9A.** In the treated cells findings were highlighting the efficacy of nanomaterial C by displaying 67.87% of late apoptotic cells and 32.13% live cells as shown in the **Figure 7.9B.** Late apoptosis occurred when nanohybrid penetrated in the *E.coli* cells instigated death as PI dye is permeable to dead cells only. The *E.coli* cells in the late apoptotic stage were sensitive to Annexin V-FITC dye showing the damaged cell membrane and leakage of content was confirmed by PI binding. it was observed that cell death caused by CIP-Ag/ TiO_2/CS nanohybrid displays initially higher late apoptotic attributes. Cohesively, data show that CIP-Ag/ TiO_2/CS nanohybrid increased the permeation of the *E.coli* cells, potentially leading to cell harm or death.

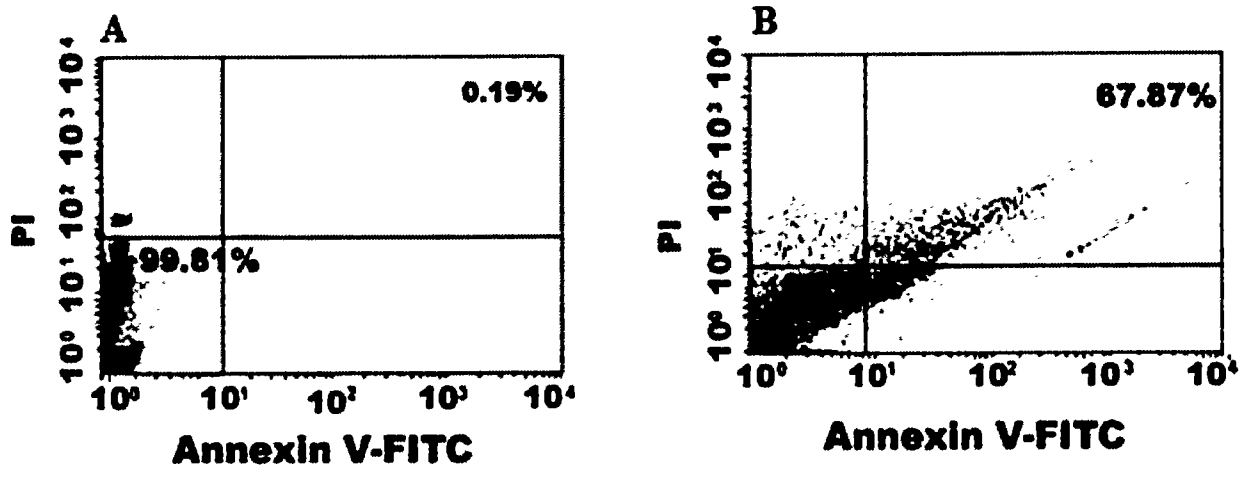

Figure 7.9 Flow cytometer data nanohybrid-induced cell death. A-control (untreated), B-CIP-Ag/TiO_2/CS nanohybrid-treated *E.coli* cells.

7.2.6. Ex-vivo Antibiotic release study CIP-Ag/ TiO_2/CS nanohybrid

The ex-vivo drug release profile of CIP from the CIP-Ag/ TiO_2/CS nanohybrid presented in **Figure 7.10**. The CIP-Ag/TiO_2/CS nanohybrid demonstrated the cumulative drug release (89%± 2.43) at 8th hrs of incubation, which was compared to the control value of CIP (94%± 1.97) during 24 hrs. The result has confirmed that the drug conjugated with Ag/TiO_2/CS nanoparticles and encapsulated in chitosan nanoparticles has improved stability in the acid medium and sustained and prolonged release of the drug. This stability and regulated release is due to chitosan encapsulation and most possibly due to the hydrophilic nature of chitosan. The antibiotic ciprofloxacin was trapped within the polymer matrix of chitosan, which supported the slow release of drugs through the diffusion process. Taken together, it was noted that burst CIP release at 8 hours, followed by a sustained release in next 24 hours.

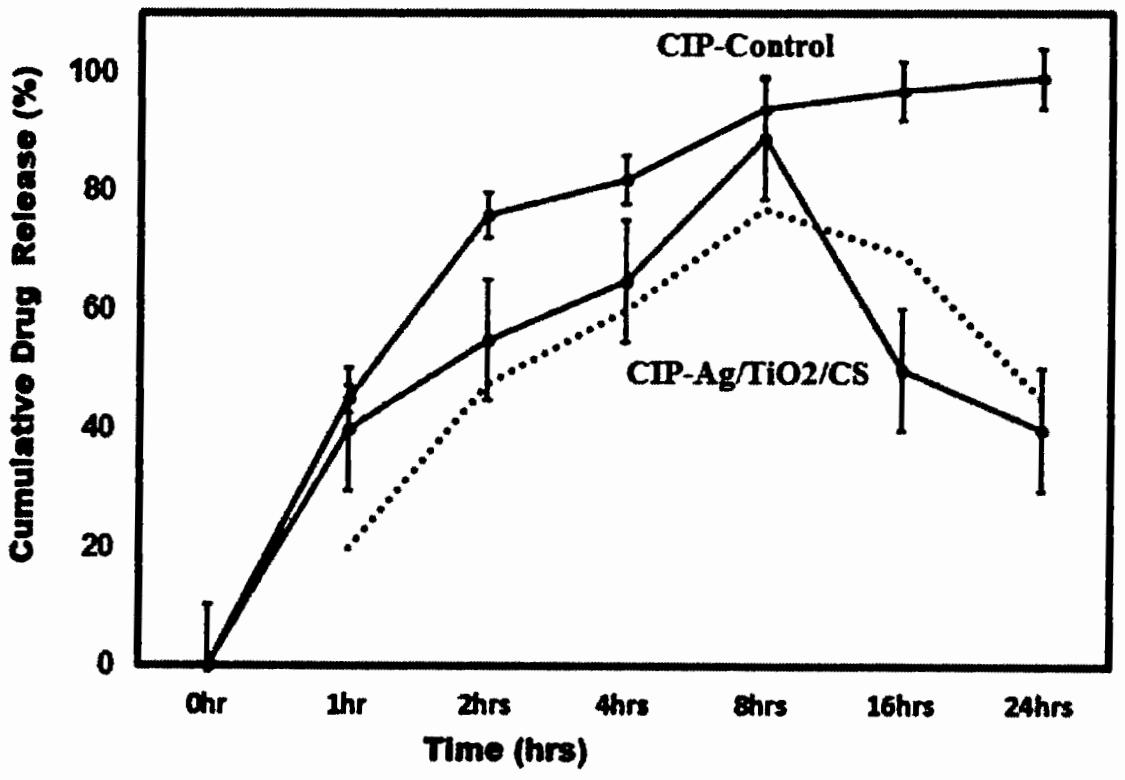

Figure 7.10 Ex-Vivo antibiotic release profile of CIP-Ag/ TiO_2 /CS Nanohybrid in PBS (pH 7.4, 37 °C).

7.2.7. Ex-vivo Biocompatibility Analysis of CIP-Ag/TiO2/CS nanohybrid on Mammalian Cell lines and RBCs

A- MTT Assay using BMGE Cells

Since most nanoparticles are semi-or totally synthetic, in vivo toxicity is critical. Particularly if the nanoparticle contains an antibiotic in a formulation that can affect the normal metabolism of antibiotics this may reduce the toxicity profile of the antibiotic allows safer use of these drugs. Potential cytotoxicity at various concentrations (0.02, 0.1 and 0.2 µg/mL) was being analyzed on primary cultures of proliferating bovine mammary gland epithelial cells (BMGE).It was found BMGE cells metabolically viable and proliferating after treatment, in a dose-dependent manner with synthesized nanoformulations which were Ag NPs, TiO_2 NPs, and TiO_2/Ag nanocomposite, CS NPs, CIP pure, Ag/ TiO_2 /CS Nanohybrid and CIP-Ag/ TiO_2/CS nanohybrid. The cells treated with PBS were used as a negative control and celecoxib drug was used as positive control. As shown in **Figure 7.11**, viability of BMGE cells was calculated 95.23% at lowest concentration (0.02 µg/mL) while 93.08% cells were viable at highest concentration of CIP-Ag/TiO_2/CS nanohybrid (0.2 µg/mL).The viability pattern using different concentration of synthesized nanoformulations exhibited in **Figure 7.11**. The current study deep-rooted the biocompatibility of synthesized nanoformulation for BMGE cells by displaying good viability pattern.

The good viability of BMGE cells in the presence of CIP-Ag/TiO_2/CS nanohybrid is likely due to the indirect exposure of cells to Ag/TiO_2 that is safeguarded by biocompatible polymer of chitosan nanoparticles whereas ciprofloxacin is already approved safe drug.

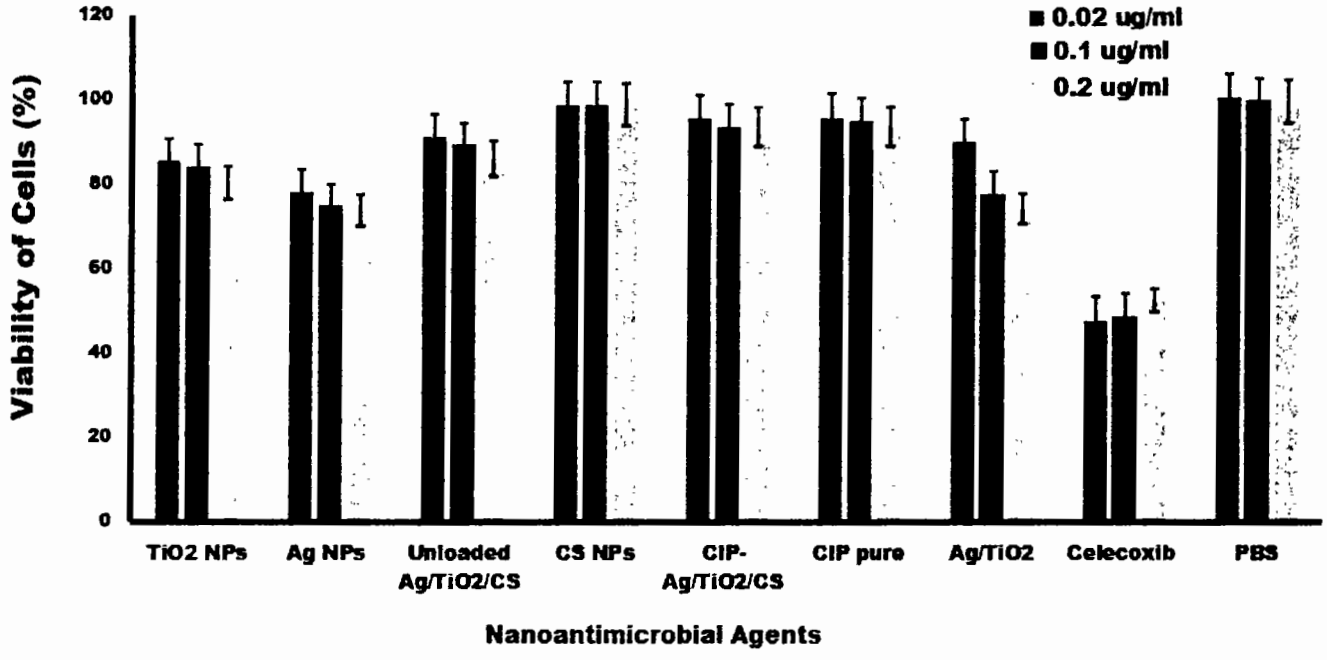

Figure 7.11: Biocompatibility analysis is of nanomaterials at various concentrations.

Key:-

A-PC, Celecoxib

B-NC, PBS

B- Hemolysis Assay using RBCs of Cow

Blood tissue encounters directly or indirectly with nanoparticles and able to transport nanoparticles to other cells, tissues, and organs. For this reason, it is highly required to study the toxicity on blood, mainly erythrocytes. Hemolysis assay was designed to study toxicity on RBCs after exposure to all green synthesized nanomaterials at various concentrations (0.02, 0.1 and 0.2 µg/mL). Nanomaterials were allowed to interact for 2hrs of incubations and findings were displayed in the **Figure 7.12**. Furthermore, study revealed that RBCs were viable after exposure to Ag NPs, TiO_2, Ag/TiO_2, Unloaded Ag/TiO_2/CS NPs, CIP pure, and CS NPs. It was apparent that CIP-Ag/TiO_2/CS nanohybrid treated RBCs were more viable (98.23 %) caused no release of hemoglobin from RBCs when results compared with positive control Triton.

Hence, newly synthesized CIP-Ag/TiO_2/CS nanohybrid showed negligible hemolysis of RBCS and proposed hemocompatibility, biocompatibility and nontoxicity of CIP-Ag/TiO_2/CS nanohybrid for human and animal cells as well.

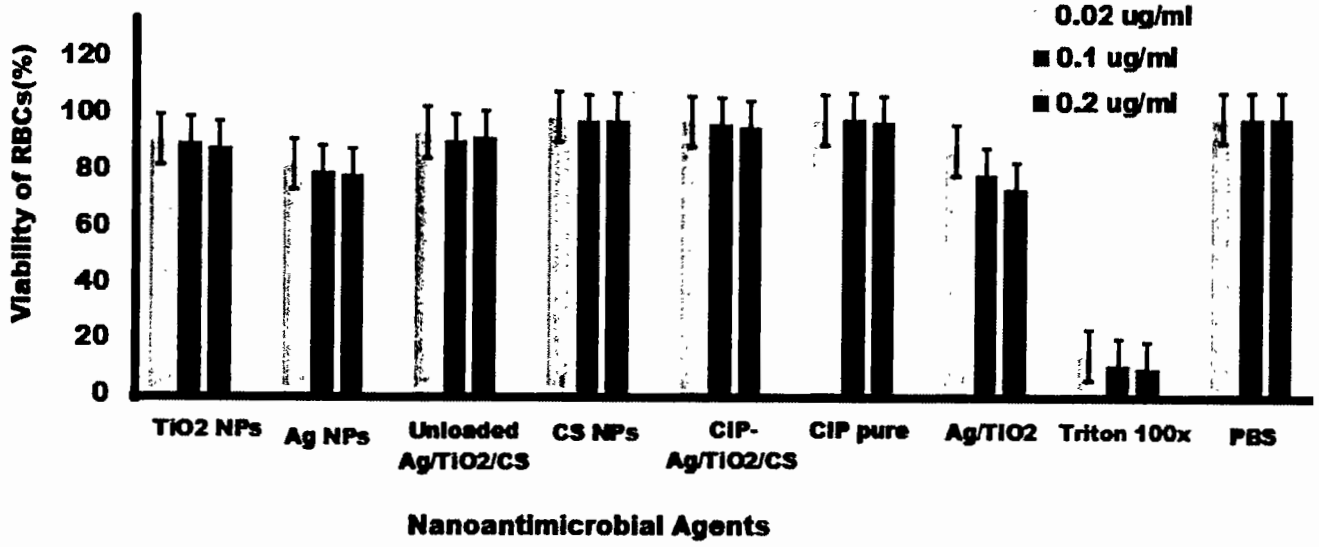

Figure 7.12 Study of hemolysis potential of nanomaterials on RBCs of cow at various concentrations,

Key:-A-PC, Triton 100X, B-NC, PBS

7.2.8. Proposed CIP-TiO_2/Ag/CS nanohybrid-mediated antibacterial activity mechanism

Taken together, the current data underline a possible mechanism mediated by CIP-Ag/ TiO_2/CS Nanohybrid involved an initial step of adhesion of the particles to the cell wall, followed by its destruction of the cell wall (detachment from the outer membrane) to penetrate and disrupt the cell integrity ultimately leading to apoptotic cell death. Thereby, as compared to CIP alone, the enhanced bactericidal effect could be attributed to a synergistic effect of CIP with TiO_2/Ag nanocomposite, moreover the surface charges modification of CIP-Ag/ TiO_2 /CS Nanohybrid by the biocompatible CS doping. Previous studies (Marta et al., 2015; Vijayalakshmi & Sivaraj, 2016) reported that TiO_2/Ba hybrid nanoclusters effectively reduced cell count for both Gram-positive and Gram-negative bacteria. Besides, it was reported that CS can enhance the permeability of the cell membrane *via* the interaction of anionic groups on the cell (Shahriar et al., 2019). The presence of –NH bond is important for antimicrobial activity of CS (Rabea et al., 2003).

Then, CIP anchored to CS trigger liberation of Ag^+ from the nanohybrid material, enhancing Ag^+ penetration/entrance into the cell through the cell membrane and subsequently enhancing the ROS levels leading to cell death (Qian et al., 2011). Meantime, it is known that TiO_2 further disrupt the barrier properties of the outer membrane of the bacteria by ROS. CIP is an exceeding energetic antibiotic against diverse microorganisms and effectively causes double-stranded DNA (dsDNA) breaks and inhibits the DNA gyrase (Campolis et al., 1988).Eventually, the synergistic action of each entity of the newly biosynthesized nanohybrid has led to the disruption of the cell membrane and ROS-mediated oxidative stress resulting into the improvement of the antibacterial activity **(Figure 7.12).**

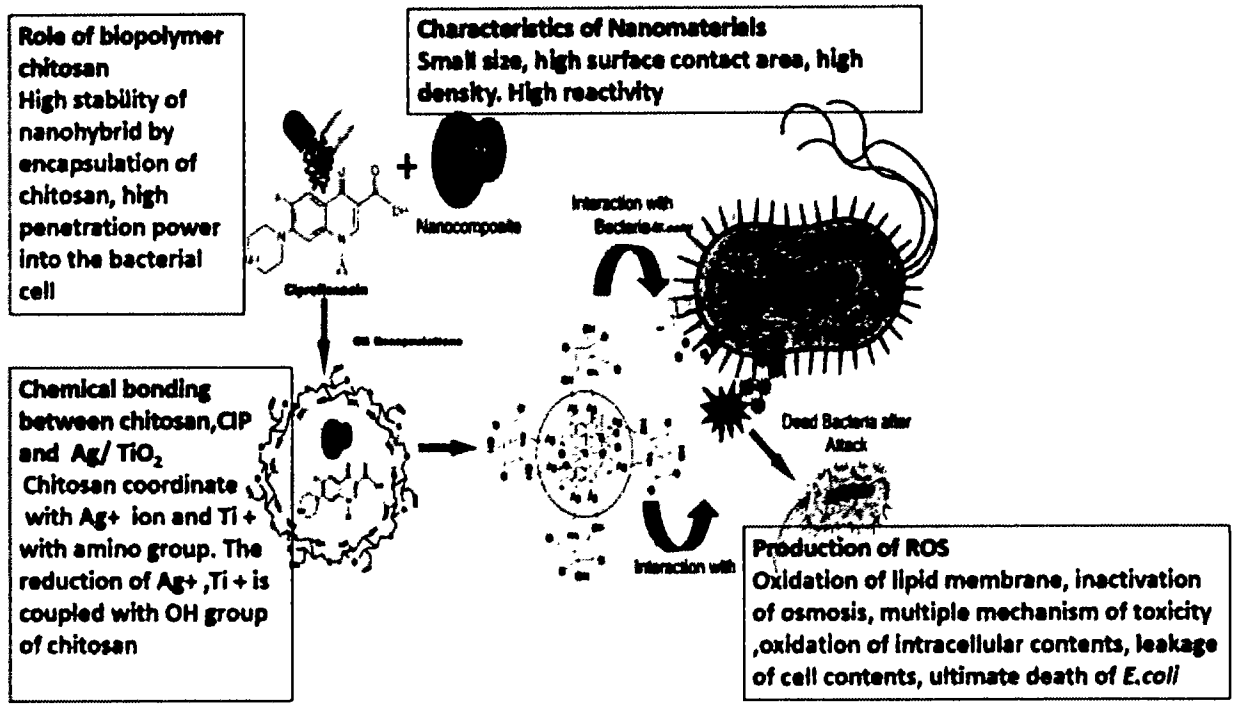

Figure 7.13: Putative CIP-TiO2/Ag/CS nanohybrid-mediated cellular and molecular bactericidal mechanism.

The green synthesized CIP-Ag/TiO_2/CS nanohybrid have been prepared by using unique leaves extract of *Moringa concanensis* which is less explored for the synthesis of nanoparticles. This newly developed CIP-Ag/TiO_2/CS nanohybrid is not reported to treat mastitis caused by MDR *E.coli* .The nanoparticles obtained in the study had small particle size (20-40nm), suitable polarity (67.45 mV) due to chitosan encapsulation which may increase the drug penetration into the MDR *E.coli* cells as evident by flow cytometry and improve its antibacterial activity to overcome resistance mechanism. The results showed that CIP-Ag/TiO_2/CS nanohybrid con successfully inhibit the growth of MDR *E.coli* strikingly with lowest MIC value than MIC of ciprofloxacin itself. It was anticipated that CIP-Ag/TiO_2/CS nanohybrid could be applied broadly in the treatment of livestock infectious diseases (mastitis) as an alternative therapeutic agent in the field of medicine due to highly biocompatibilities.

7.3. Conclusions

This research was conducted to improve the effectiveness of existing groups of antibiotics (ciprofloxacin) and to reduce dosage and mitigate associated toxicity. The study illustrates the successful development of CIP-Ag/ TiO_2/CS nanohybrid. The green synthesized CIP-Ag/TiO_2/CS nanohybrid exerted excellent antibacterial activity at relatively very low MIC, compared to ciprofloxacin alone. The synthesis of Ag/ TiO_2 occurred through reduction of *M. concanensis* leaves extract followed by ionic gelation method for conjugation of CIP and CS encapsulation. The excellent rapid anti *E.coli* activity was exhibited by the synthesized nanohybrid formulation. Flow cytometry revealed cell membrane damage leading to cell lysis as confirmed by SEM and TEM as major morphological alterations were seen in *E.coli* cells. Drug released kinetics exhibited sustained drug release from the nanohybrid. The nanohybrid was proved to be safe and nontoxic on bovine mammary gland epithelial cells and RBCs of cow.

CHAPTER 8

NANOMATERIAL D: GREEN SYNTHESIZED CIP-Ag/TiO_2/ Fe_2O_3/CS TERNARY COMPOSITE

8.1. Introduction

Microbial resistance to numerous conventional antibiotics trigger by MDR pathogens have recently become a major cause of morbidity and mortality around the world. This has prompted efforts to produce novel, alternative antibacterial materials that address the problem of multidrug-resistant pathogens. To tackle MDR bacteria, a variety of different strategies have been developed. Several in vitro investigations have shown that combinations of essential oils/plant extracts, conventional antibiotics/plant extracts, and phytochemicals/antibiotics have considerable antibacterial activity.

Nanotechnology has become widespread alternative therapeutic agents due to advantageous physicochemical features, such as antibacterial properties and remarkable biocompatibility, nanotechnology using nanoscale materials, specifically multimetallic nanoparticles (NPs), has sparked attention(Arora et al., 2020). Dairy farmers believe that mastitis is one of the major reasons for economic fluctuation that ultimately affect the national economy (Ashraf & Imran, 2020). Due to emergence of MDR strains cost to treat infection has become difficult and expensive (Nielsen, 2009).

Bimetallic and multimetallic NPs possess a promising potential as antimicrobial agents and have the tendency to exert significant contribution in livestock industry. Further researches are made for the synthesis of highly effective agents based on bimetallic or multimetallic combinations is being carried out in a systematic fashion. To bind multimetallic species, porous support is used in terms of encapsulation, which also increases surface area. Targeted outcome of these studies has the delivery of novel, efficient, and robust nanostructured systems able to significantly contribute toward battling the major problem of bacterial spread and antimicrobial resistance. The developed materials engineered to fit the targeted

applications, be provided in various formulations, and be ready to be applied on various surfaces (Arora et al., 2020).

Nanoparticles (NPs) are emerging as promising tools to help mitigate the rise of antimicrobial resistance (Zhang et al., 2016). Metallic oxide nanoparticles can encapsulate and deliver antimicrobial agents to improve drug pharmacokinetic and pharmacodynamics profiles, ultimately resulting in improved treatment outcomes (Bankier et al., 2018). Sustained drug release formulations decrease dosing frequencies and simplify dosing regimens, which can improve passivity and subsequently reduce resistance development rates from mismanaged drug use (Bikiaris et al., 2007; Wang et al., 2017). Targeted NPs can be especially effective at improving therapies by binding to and accumulating at sites of infections (Lu et al., 2017). Targeted NP delivery elevates the local concentrations of antibiotics in close proximity to bacteria, which increases drug antimicrobial activities. Targeted delivery can also reduce off-target side-effects, and enable or revive the use of older-generation antibiotics. For the green synthesis of metallic oxide NPs, medicinal important plants have been used extensively (Singh et al., 2018). Moringa species are famous as they contain various phytoconstituents such as alkaloids, saponins, tannins, steroids, phenolic acids, glucosinolates, flavonoids and terpenes. The diversity of these phytochemicals in the genus contributes to its numerous pharmacological uses. About 110 compounds were identified from the genus. Recently, isothiocyanates have become a major research interest of Moringa for their various biological activities such as their anticancer, antidiabetic, antimicrobial, and anti-inflammatory effect (Padla et al., 2012; Waterman et al., 2015) Among the 13 species, research is limited to *Moringa oleifera*, *Moringa stenopetala*, *Moringa concanensis*, and *Moringa peregrine*(Abd Rani et al., 2018).

The Iron oxide (III) is a very stable oxide, it crystallizes in hexagonal form and is found in nature as the mineral hematite α-Fe_2O_3. The Fe_2O_3 NPs bactericidal effect against *E. coli* and *S. aureus* has been reported, where an increase of this effect is observed, as the concentration of iron oxide NPs increases. In the presence of iron-oxide nanoparticles at 0.15 mg/mL, the largest reduction was seen when compared to other concentrations (0.01 mg/mL, 0.05 mg/mL, and 0.1 mg/mL). In comparison to *E. coli* and *P. aeruginosa*, *S. aureus* showed the

greatest inhibition at 0.15 mg/mL of iron-oxide nanoparticles (Thukkaram et al., 2014). Another study reports on the bactericidal activity of nanostructured hematite against a variety of Gram-positive and Gram-negative bacteria; *P. aeruginosa*, *S. aureus*, *K. pneumoniae*, *Lysinibacillussphaericus* and *Bacillus safensis*(Jiménez et al., 2019).

Noble metals such as Ag, Au, Pt, and Pd deposited on TiO_2 surfaces enhance the antimicrobial activity of TiO_2 NPs. This is mainly due to the noble metals acting as electron traps, which promote interfacial charge transfer processes in the composites (S. Li et al., 2018; Zielińska-Jurek et al., 2015).Thus, highly efficient antimicrobial agent that are modified with incorporation of noble metals can be prepared to combat AMR issue. Moreover, the anatase TiO_2 nanoparticles on the surface of the Fe_2O_3 exhibit high antimicrobial activity due to their large specific surface area and high crystallinity (Saranya et al., 2020). Ag nanoparticles, which are well deposited on the surface of the Fe_2O_3-TiO_2 composite by a green synthesis route, combine with TiO_2 to form the Ag– Fe_2O_3-TiO_2 heterostructure. The heterostructure can improve the lethal properties against MDR pathogens causing mastitis infection(Mohamed et al., 2019; Razani et al., 2017). Chitosan is well known biopolymer with excellent antimicrobial and antioxidant properties due to presence of amino groups which act as scavenger of free hydroxyl radicals .The degree of deacetylation further increases its antioxidant and antimicrobial property. The CS encapsulation of antibiotics metallic oxide NPs protect them from external environmental factor which degrade antibiotics and NPs, before site of action. Chitosan encapsulation can also mask toxicity of NPs and enhance its antibacterial potential (Raza et al., 2020).

Ciprofloxacin belongs to fluoroquinolones class, commonly prescribed for a wide variety of infections, including those caused by Gram positive and Gram negative. Present study mainly consider CIP as target drug to retrieve its antibacterial potential which was lost due to misuse or excessive use in order to treat mastitis.

Mechanism of action of CIP triggered ,When CIP binds with DNA gyrase form complex with DNA, the single-stranded DNA breaks cannot be re-ligated and thus accumulate, leading to double-stranded DNA breaks. A similar mechanism is hypothesized for topoisomerase IV (Anderson et al., 1998; van der Putten et al., 2018). Development of resistance produced by

bacterial strains against ciprofloxacin is due to mutations in genes producing ciprofloxacin target proteins and efflux pump regulators, resulting in efflux pump overexpression. However, the basis of ciprofloxacin resistance is not yet fully understood.

From the above facts, there is serious need of new and safe therapeutic agent which can bypass the resistance mechanisms in order to combat MDR pathogens such as *E.coli*, MRSA and MDR *C.albicans* .The present study proclaims a new and unique Ciprofloxacin loaded Ag/TiO_2/ Fe_2O_3/ CS nanohybrid system which principally based on eco-friendly mode of synthesis. AgNPs, TiO_2 NPs and Fe_2O_3 were prepared by *M. concanensis* aqueousleaves extract, as a reducing agent. Incorporation of AgNPs onto the surface of TiO_2 and Fe_2O_3 nanomaterials was performed by wet chemical impregnation technique, eventually CS encapsulation by ionic gelation method. Physical characterizations were performed by standard tools of microscopy and spectroscopy. Ciprofloxacin loaded Ag/TiO_2/ Fe_2O_3/ CS nanohybrid was tested for its antimicrobial potentials against various MDR strains of *E.coli*, MRSA and *C. albicans* causingmastitis in the cattle. Ultimately, *Invivo* antimicrobial efficiency of such biocompatible hetero-nanosystem was assessed in induced infection model in rabbits.

8.2. Results

8.2.1. XRD Analysis

XRD profile of synthesized nanomaterials, pure CIP and leaves extract powder have been shown in the **Figure 8.1**. The XRD patterns of synthesized nanostructure were clearly presented the insight of fabricated products. **Figure 8.1a** shows the diffraction peaks of pure ciprofloxacin with the occurrence of dominant signals at 2θ of 12 ^{0}, 20 ^{0}, 29 ^{0},30^0,31^0,35^0,39^0. As shown in the **Figure 8.1b** plant extract expressed many small and weak signal in the spectrum while irregular shaped peaks at 2θ ° = 19.5 and broader dominant peak at 29 were expressed more prominently. The XRD of pure Fe_2O_3 **(Figure 8.1c)** showed dominant signals at 2θ of 24°, 33°, 36° 41° 49°, 54° 58° 63° 64° corresponds to Fe_2O_3 (012) (104) (110), (113), (024) (115), (112), (214), (300) were well matched with JCPDS Card No. (00-001-1053). The XRD peaks of Ag NPs **(Figure 8.1d)** showed the (111), (200), (220), and (311) crystallographic planes at 2θ ° = 38.18°, 44.25°, 64.72°, and 77.40°leading to face-centered cubic metallic silver crystals.The XRD of pure TiO_2 **(Figure 8.1e)** represents the (101), (004), (200), (105), (211) and (204) plane indices that corresponding to crystalline anatase phase as supported by (JCPDSNo. 84-1285). XRD profile of chitosan **(Figure 8.1g)** drug loaded encapsulated Ag/TiO_2nano-hybrid system possesses the diffraction peaks of Ag, anatase TiO_2 (Lei et al., 2012) and chitosan. It is also noted that leading peak of Ag at 38.18° overlapped with the peak of TiO_2 at 38° and suppressed the signal of TiO_2. Moreover the XRD of CIP-Ag/TiO_2/ Fe_2O_3/ CS Ternary composite which confirming the characteristic peak of chitosan at 21.8^0, dominant peak of TiO_2 at 2θ ° = 29^0, 44.2^0, significant appearance of Fe_2O_3 at 2θ ° = 33^0,36^0,49^0,54^0 and dominant signal of Ag NPs at 64^0 were observed in the **Figure 8.1h**. The noticeable region in the CIP-Ag/TiO_2/ Fe_2O_3/ CS Ternary composite was presence of Fe-Ag-Ti linkages of heterojunction.17–21. XRD analysis further extended the findings of CIP-Ag/TiO_2/ Fe_2O_3/ CS Ternary composite by exhibiting the diffraction peaks shifting was found in the ternary composite to high angle region that specifies the impregnation of foreign material i.e. chitosan and ciprofloxacin supplements the strain on the crystalline matrix of metallic oxides.

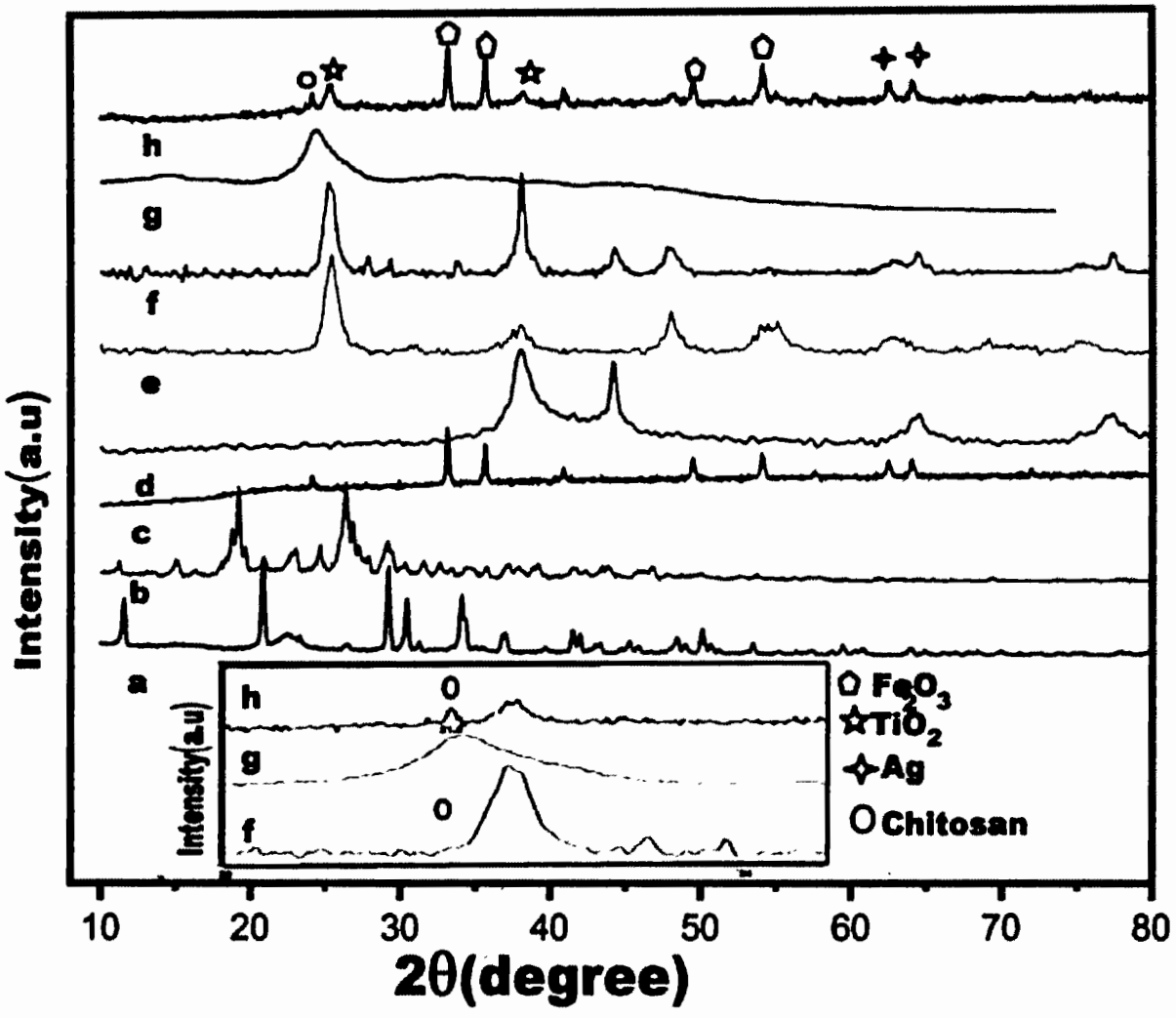

Figure 8.1 XRD spectrum of synthesized nanomaterials,

Key: Ciprofloxacin (a), pure plant powder (b), pure Fe_2O_3 (c), pure Ag NPs (d), pure TiO_2 NPs (e), Ag/TiO_2 nanohybrid (f), pure chitosan NPs (g), CIP-Ag/TiO_2/ Fe_2O_3/ CS (h).

8.2.2. SEM and EDX Analysis

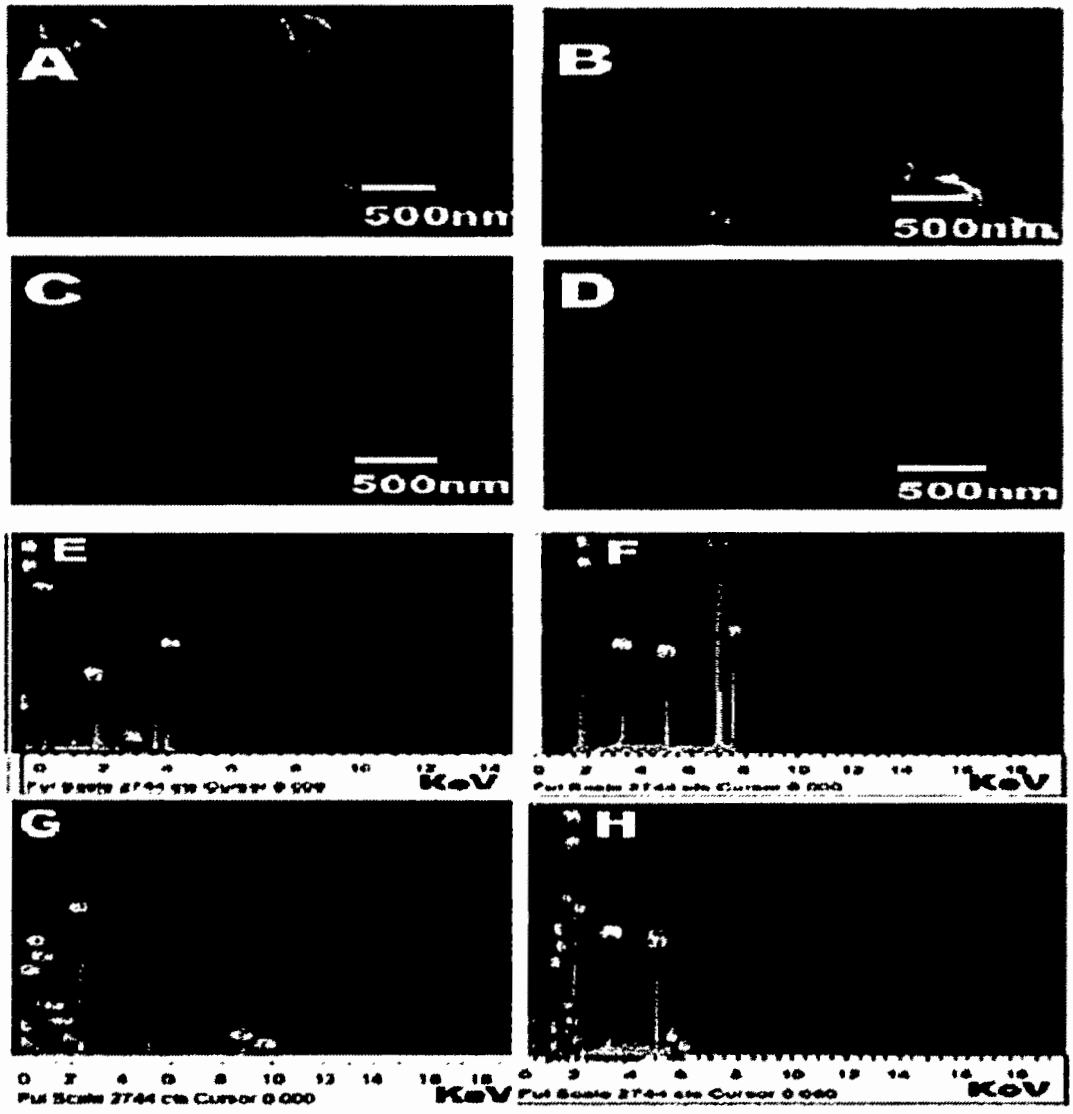

Figure 8.2 SEM analysis of synthesized nanomaterials,

Key: Pure chitosan NPs (A), Ag/TiO_2 nanohybrid (B), Fe_2O_3 (C) and CIP-Ag/TiO_2/ Fe_2O_3/ CS Ternary composite (D). EDX spectra of prepared nanomaterials, chitosan NPs (E), Ag/TiO_2 nanohybrid (F), Fe_2O_3 (G) and CIP-Ag/TiO_2/ Fe_2O_3/ CS Ternary composite(H).

The **Figure 8.2** represents the SEM photographs of chitosan, green synthesized Ag/TiO_2 nano-hybrid, pure Fe_2O_3 NPs and CIP-Ag/TiO_2/ Fe_2O_3/ CS Ternary composite. SEM confirmed the size of chitosan NPs 23-30nm, Ag/TiO_2 NPs 25-40nm , Fe_2O_3 nanorods diameter of

2-6nm and CIP-Ag/TiO_2/ Fe_2O_3/ CS Ternary composite ranging from 5-7nm. The spherical and agglomerated morphology of both chitosan and Ag/TiO_2 hybrid was presented in the **Figure 8.2Aand 8.2B** respectively. SEM analysis further revealed the surface morphology of Fe_2O_3 nanorods as shown in the **Figure 8.2C** .It is clearly seen (**Figure 8.2D**) in green synthesized CIP-Ag/TiO_2/ Fe_2O_3/ CS Ternary compositethat Ag NPs and Fe_2O_3 are incorporated on the surface of TiO_2. Ag NPs are not integrated into the lattice of crystalline TiO_2. It is noted that there is no distinction between the TiO_2, Fe_2O_3 and Ag NPs in Ag/TiO_2 / Fe_2O_3 nano-hybrid. Furthermore it is clearly seen from the image that chitosan anchored the whole surface of nanorods Ag/TiO_2 / Fe_2O_3 and selected antibiotic CIP.

EDX analysis was used to investigate the elemental distribution of synthesized TiO_2 NPs and green synthesized Ag/TiO_2 nano-hybrid. The relevant data of EDX is listed in **Table 8.2**. **Figure 8.2E** indicates the signals of Ti and O which confirmed the synthesis of TiO_2 NPs. The peaks corresponding to the Ti, O and Ag (**Figure 8.2E**) designate the Ag/TiO_2 nano-hybrid. It is cleared from the signal that 1.2 wt% nominal content of Ag that is close to its stoichiometric value of 2.0 wt% solution of Ag NPs exploited for the fabrication of Ag/TiO_2nano-hybrid. No additional peaks are observed which indicates the purity level of synthesized nanomaterials. The appearance of the signal of C in Ag/TiO_2 nano-hybrid can be ascribed to the carbon substrate/grid.

8.2.3. TEM study

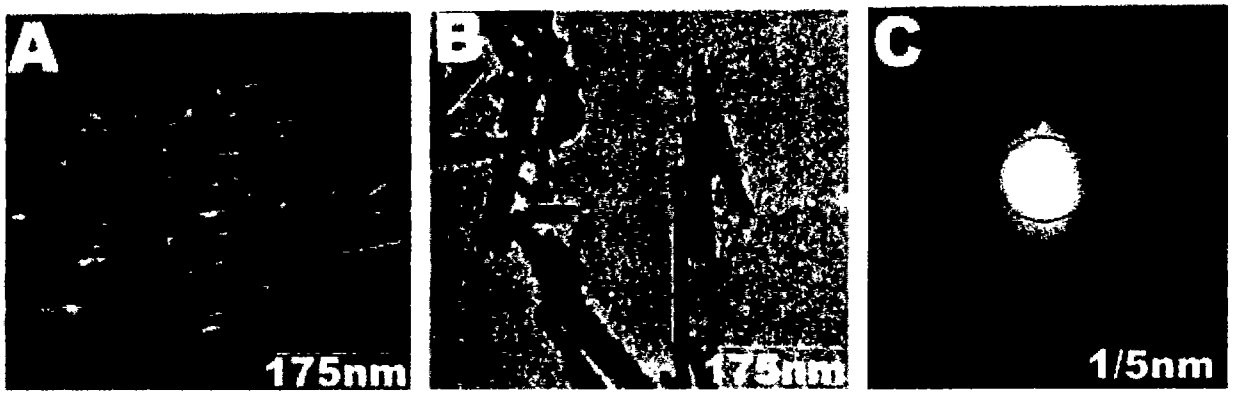

Figure 8.3 TEM images of synthesized nanomaterial

Key:-

A-Ag/TiO_2/Fe_2O_3

B-CIP-Ag/TiO_2/ Fe_2O_3/ CS Ternary composite

C- SAED pattern of CIP-Ag/TiO_2/ Fe_2O_3/ CS Ternary composite

The morphological display of prepared materials are further analyzed by TEM images. **Figure 8.3** represents TEM images of Ciprofloxacin conjugated CIP- Ag/TiO_2/ Fe_2O_3/ CS Ternary composite and Ag/TiO_2/ Fe_2O_3 at different nano scales. TEM image of Ag/TiO_2/ Fe_2O_3 (**Figure 8.3A**) showed mixed elongated nanorods which was consistent with FESEM findings. TEM image of Ciprofloxacin loaded Ag/TiO_2/ Fe_2O_3/ CS Ternary composite (**Figure 8.3B**) depicted nanorods shaped morphology with average diameter ranges ~6-10 nm as also confirmed by XRD analysis. The purity of CIP- Ag/TiO_2/ Fe_2O_3/ CS Ternary composite was presents in the (**Figure 8.3C**) by SAED.

8.2.4. FTIR Analysis

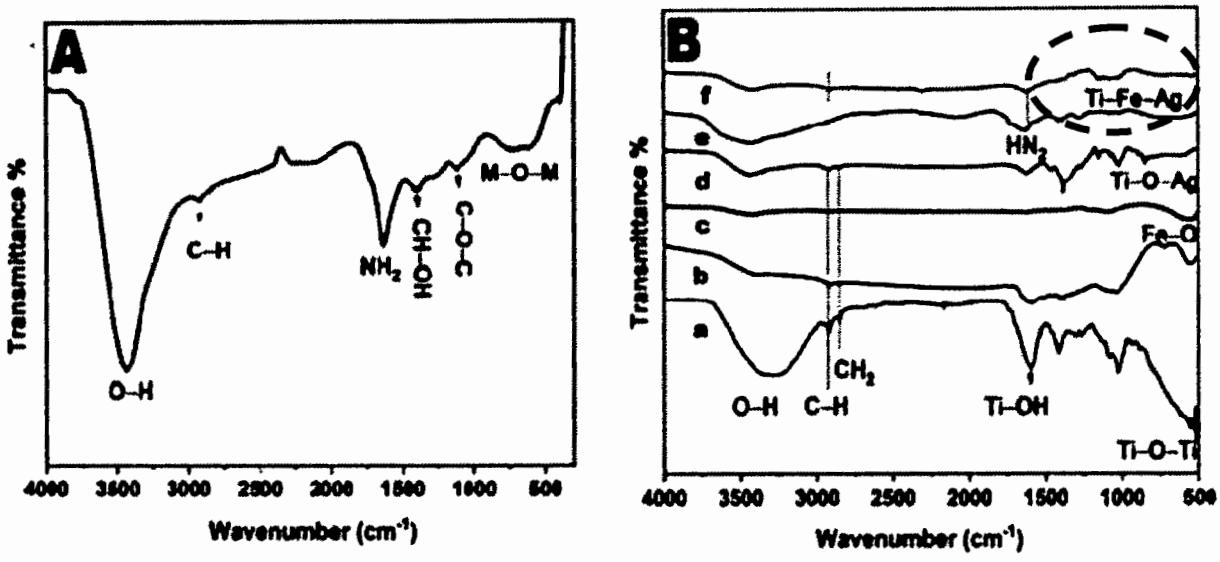

Figure 8.4 :FTIR of M. concanensis leaves and synthesized nanomaterials,

Key:-

A- *M. concanensis* leaves

B-a, TiO_2 (a),

b- Fe_2O_3

c- Ag

d- Ag/TiO_2 nanohybrid

e- Chitosan

f- CIP-Ag/TiO_2/ Fe_2O_3/ CS Ternary composite.

FTIR spectra of synthesized nanomaterials were recorded in the range of 500–4000 cm−1 are shown the **Figure 8.4**. As shown in the **Figure 8.4A** the peak patterns appeared in the regions of 499 to 1074 cm−1 metallic oxide region and broad peaks appeared at 3450 cm−1 and 1650 cm−1 corresponds to –OH and NH_2 group stretching and bending vibrations mode. The FTIR spectrum of pure TiO_2 (**Figure 8.4B(a)**) exhibits the emergence of absorption characteristic peaks at 3408cm^{-1} belongs to superposition of the hydroxyl groups (O–H) that is the evidence of coordination of water molecule to Ti^{4+}cations and signature at 1603 cm^{-1} can be attributed to and C=O stretching vibration due to butyl group, organic species as starting precursor solutions and adsorbed water molecules on the surface of the nanomaterial. The absorption band cantered at 2928 cm^{-1} is assigned to the C–H stretching vibrations. The absorption band in the range of 766-610 cm-1 is related to the Ti – O bonding that authenticates the formation of titanium dioxide. As shown in the **Figure 8.4B (b)** the band corresponding to Fe-O stretching mode of Fe_2O_3 is observed at 560 cm−1.and 700cm-1 The FTIR analysis of Ag nanoparticles (**Figure 8.4B (c)**) interprets the characteristic peak at 3424 cm^{-1} corresponding to O–H stretching vibration of adsorbed water molecules. The peaks at 2919 cm^{-1} and 2841 cm^{-1} indicate alkanes (C=C) stretching vibration. Signature appeared at 1625 cm^{-1} is attributed to bending vibration of alkene group (Li et al., 2018).In case of Ag/TiO_2 hetero system (**Figure 8.4B (d)**) bands ranges in the region from 530 to 800cm^{-1} are attributed to Ti–O stretching mode and Ti–O–Ag/Ag–O–Ti linkage respectively. The FTIR spectrum of chitosan exhibits a high absorption peak of 3423 cm-1 and 1636 cm-1 due to the availability of a free –OH group and NH_2 moiety group of chitosan monomers molecules respectively (**Figure 8.4B (e)**). The value at 1018 cm-1 corresponds to the throttle vibration of the C–O–C bond of epoxy or alkoxy. The signature at 1269 cm-1 and 1419 cm-1 is due to C–O and CH–OH bonds. Peaks at around 1010 and 1600 cm-1 in nano-hybrid spectra have been correlated with benzene rings which indicates presence of Ciprofloxacin conjugation with metallic oxide ternary heterojunction (**Figure 8.4B (f)**). It is clear that the absorption peak centered at 596 cm-1 is due to the metal oxygen metal (Ti–O–Ag) mode of vibration. where Fe-O stretching mode was clearly observed in the spectra. The peak at 1074 cm−1 is due to the stretching vibration Fe-Ti-Ag and the strong band below 700 cm−1 is assigned to Fe-O-Ti and Fe-O-Ag stretching mode. The peak at 1099 cm^{-1} represents asymmetric and

symmetric C=O stretching vibration due to carbonyl group present in leaf extraction. Alkanes, alkenes and carbonyl groups of leaves extract which encountered the reduction of Ag^+, Ti^+ and Fe^{+3} to Ag,TiO_2 and Fe_2O_3NPs. The reduction in the intensity of all the peaks was observed in case of composites after the incorporation of Fe_2O_3 and Ti-O bond of TiO_2, was found to be shifted to 525 cm−1 after the incorporation of chitosan and ciprofloxacin. The linkages further confirmed the blending of organic and inorganic materials which presents tight junctions of ternary composites.

8.2.5. UV-Vis Analysis

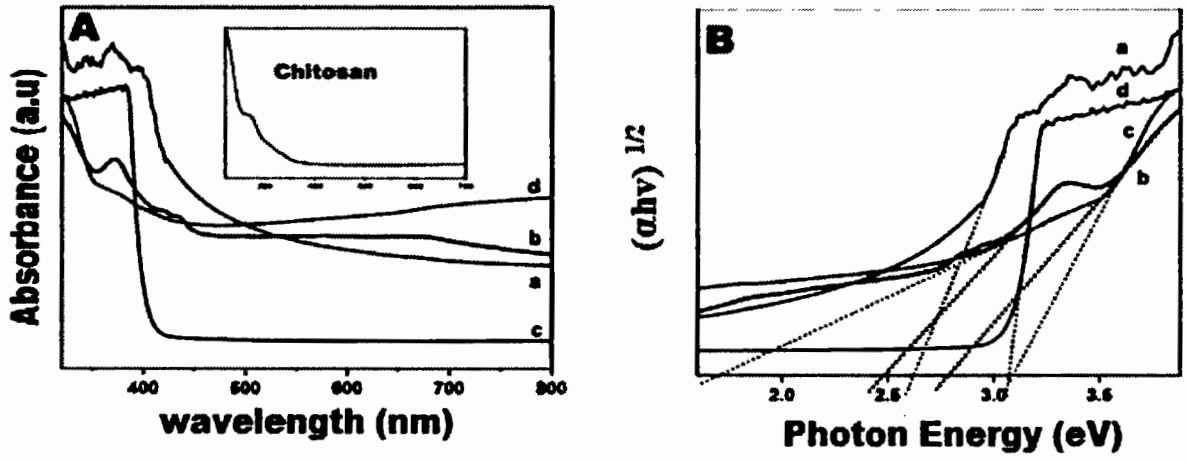

Figure 8.5: UV –Vis analysis (A) and corresponding Tauc plot of synthesized nanomaterials,

Key: *M. concanensis* leaves (a), Fe_2O_3 (b), CIP (c), CIP-Ag/TiO_2/ Fe_2O_3/ CS Ternary composite (d).

In UV-Vis profile of TiO_2, the absorption edge relative to O^{2-}– Ti^{4+} responsible for charge transition at 300–390 nm in anatase TiO_2 and absorption spectrum of chitosan NPs showed (Inset of **Figure 8.5A**) single band centered at 280nm. The optical band gap values were determined by using Tauc plot as shown in the **Figure 8.5B** (a, b, c and d). The band gap energies for plant 2.7, Fe_2O_3 2.4, drug 3.2 and CIP-Ag/TiO_2/ Fe_2O_3/ CS Ternary composite have displayed transition energies between1.3 and 3.1eV which are corresponding to the charge transition from O^{2-}– Fe^{4+} and O^{2-}– Fe^{3+} respectively .Having large band gap value

(3.12 eV) of TiO_2; light absorption is restricted only in UV region. Surface modifications of Ag/TiO_2 by incorporation of chitosan and ciprofloxacin could strongly enhance the absorption in whole UV-Vis region. The reduced band values in CIP- CIP-Ag/TiO_2/ Fe_2O_3/ CS Ternary composite are noted .The clusters of Fe^{2+} and Fe^{3+} in different regions of host Ag/TiO_2 act as the electron trappers, firmly inhibited the recombination process and proliferate the absorption in visible region. These clusters are also responsible for generation of oxygen vacancies below the conduction bands of TiO_2 and reduced the band gap values of CIP-Ag/TiO_2/ Fe_2O_3/ CS Ternary composite samples. In CIP-Ag/TiO_2/ Fe_2O_3/ CS Ternary composite integration of Fe_2O_3 is fruitful in absorption of light in visible region by existence of oxygen moieties, fast electronic transition properties and innovative connection between Ag–O-Ti-O–FeO is very supportive in the antimicrobial activity.

8.2.6. Zeta Potential Analysis

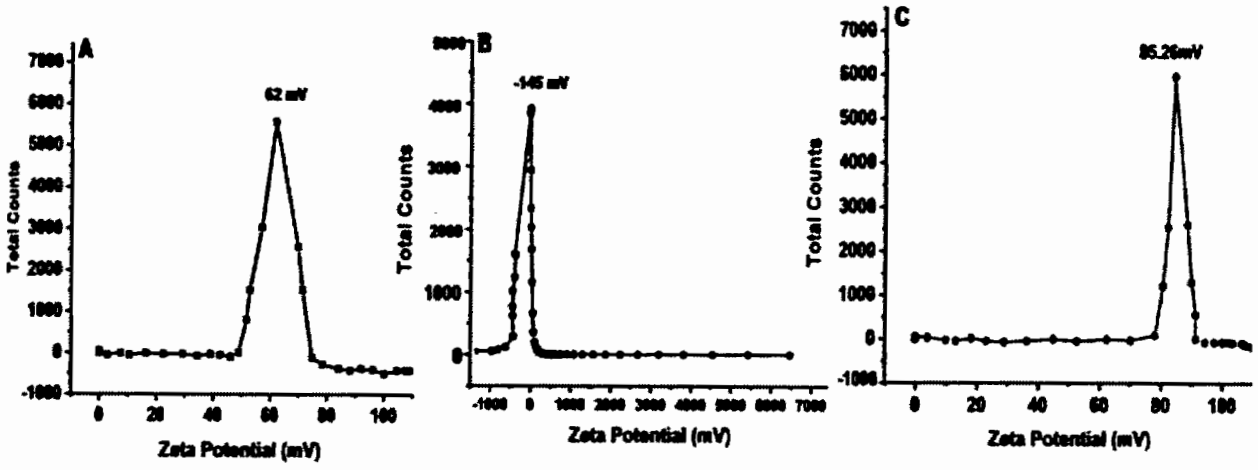

Figure 8.6: Zeta potential of synthesized nanomaterials

Key:-

A-Chitosan NPs

B-Fe_2O_3

C-CIP-Ag/TiO_2/ Fe_2O_3/ CS Ternary composite

The surface charge of Chitosan NPs, Fe_2O_3 and CIP-Ag/TiO_2/ Fe_2O_3/ CS Ternary composite was determined by zeta potential investigation in the aqueous medium62± 0.03mV,-145 ± 2.74mV and 85.26± 0.12 respectively as shown in the **Figure 8.6**. Chitosan exhibited highly stable 62 ± 0.03mV.while the zeta potential value of 85.26 ± 0.12 mV support the highly stable feature of CIP-Ag/TiO_2/ Fe_2O_3/ CS Ternary composite **Figure 8.6C**. In water, surface charge was clearly influenced by the surface coating, being negative in the case of pure Fe_2O_3 while it became positive in the presence of NH_2 groups of chitosan .When came in contact with chitosan superficial charge -145 ± 2.74mV was changed to the higher positive potential which confirmed the successful encapsulation by completely shielding the original surface charge of Fe_2O_3.

8.2.7. Encapsulation efficiency of CIP-Ag/TiO_2/ Fe_2O_3/ CS Ternary composite

The encapsulation efficiency of CIP-Ag/TiO_2/ Fe_2O_3/ CS Ternary compositein the CS system was found as 94% ± 1.26.

8.2.8. Antimicrobial evaluation of CIP-Ag/TiO_2/ Fe_2O_3/ CS Ternary composite

The antimicrobial evaluation was performed by disc diffusion method , each disc contained MIC values of CIP-Ag/TiO_2/ Fe_2O_3/ CS Ternary compositeand Ag/TiO_2 nanohybrid to disclose their antimicrobial potential against antibiotic resistant strains of *C.albicans*, Gram negative MDR *E.coli* and Gram positive MRSA strains which are responsible for mastitis. The disc holding CIP-Ag/TiO_2/ Fe_2O_3/ CS Ternary composite offered excellent antimicrobial activity against MDR pathogens as shown in the **Table 8.1 and 8.2**. The zone of inhibition was observed was observed 33mm ± 1.40 against MDR *E.coli*, 28 mm ± 1.45 against *C.albicans* and 22mm ± 0.06 was recorded against MRSA by using corresponding MIC values as shown in the **Figure 8.7A, B and C**.

The synthesized CIP-Ag/TiO_2/ Fe_2O_3/ CS Ternary composite showed excellent antibacterial activity which predominantly depend on morphology, size, surface area specifically, polar surface, and cross linking of doped materials. Moreover, electrostatic attraction between negatively charged bacterial cells and positively charged CIP-Ag/TiO_2/ Fe_2O_3/ CS Ternary compositeis fundamental step for the antimicrobial reactions. This interaction is not only able to inhibit the growth of microbes but also induces the production of ROS, which ultimately

lead to cell death. The growth of *C.albicans* was more affected by the CIP-Ag/TiO_2/ Fe_2O_3/ CS Ternary composite treatment as compared to Gram-negative MDR *E.coli*. Most importantly, the antibacterial activity was improved significantly in comparison to the CIP-Ag/TiO_2/ CS as confirmed by the disc diffusion method due to incorporation of Fe_2O_3 as antibacterial activity principally depends on morphology.Nano encapsulation of chitosan on the surface of Ag/TiO_2/Fe_2O_3 ternary heterojunction amplified antibacterial potential and by increasing concentrations as shown in the **Table 8.1** enhancing the antimicrobial activity against resistant strains of MRSA,MDR *E.coli* and *C.albicans*. The successful synthesis of CIP-Ag/TiO_2/ Fe_2O_3/ CS Ternary composite was confirmed by FTIR diffraction signals of ternary composite. The zeta potential value 85.26± 0.12 supported stability and super reactivity of ternary structure against the MDR pathogens. In the present study biogenic engineered CIP-Ag/TiO_2/ Fe_2O_3/ CS Ternary compositeshowed brilliant antibacterial activity against tested strains and launching an alternative therapeutic agent to cure mastitis which has been become challenge for both developed and under developing countries.

Table 8.1: Zone of inhibitions of synthesized CIP-Ag/TiO_2/ Fe_2O_3/ CSTernary composite were recorded at various concentrations

Antimicrobial Agents	**Concentrations (µg/mL) and Zone of Inhibitions (mm)**		
	MICs	**MICs1/2**	**MICsX2**
MDR *E.coli*	**33 ± 1.40**	**14 ± 0.98**	**39± 1.185**
MRSA	**22 ± 0.06**	**19 ± 0.10**	**34 ± 1.35**
MDR *C.albicans*	**28± 1.45**	**20 ± 0.14**	**32 ± 1.76**
DMSO	-	-	-

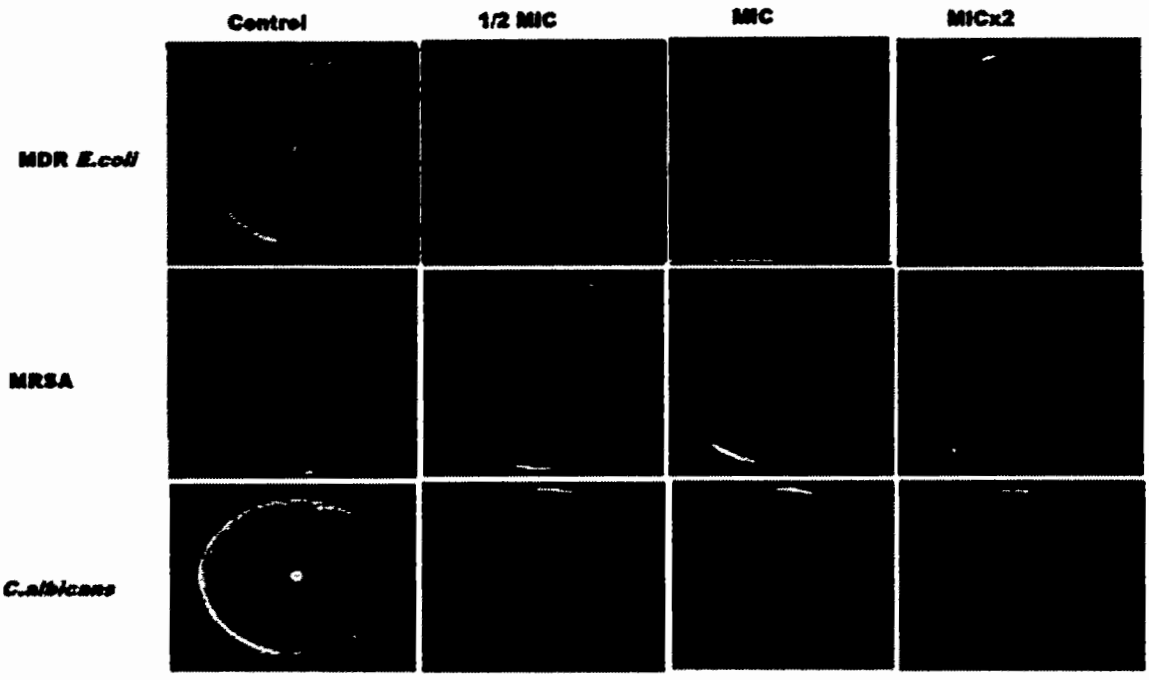

Figure 8.7 Antimicrobial activity of green synthesized nanomaterial D, CIP-Ag/TiO_2/ Fe_2O_3/ CS Ternary composite

Key:-

(A) *C.albicans* ,

(B) MDR *E.coli*

(C) MRSA strains

(D) Control (DMSO)

Table 8.2 The MIC values of synthesized Nanomaterials

Nano antimicrobial Agents	**MIC determination (µg /ml)**		
	MRSA	*E.coli*	*C .albicans*
CIP-Ag/TiO_2/ Fe_2O_3/ CS Ternary composite	0.112	0.022	0.004
Ag/TiO_2/Fe_2O_3 composite	10.14	8.07	9.57

8.2.8.1. Killing kinetics of mastitis causing MDR strains

The colloidal nature of microbial growth allows indirect detection of their growth by monitoring turbidity and optical density of aqueous suspensions containing synthesized nano antimicrobial agents. In the current study CIP-Ag/TiO_2/ Fe_2O_3/ CS Ternary composite was found highly effective and efficient in combating the growth of MDR strains of, MRSA, MDR E. *coli* and *C. albicans* as shown in the **Figure 8.8A, B and C** respectively. The growth kinetic curve of **Figure 8.8A** presented reduction in OD value of MRSA after 6hrs of incubation. However the growth of MDR *E.coli* was controlled prominently by CIP-Ag/TiO_2/ Fe_2O_3/ CS Ternary compositeas shown in the **Figure 8.8B**. The Anti-candida proficiency of CIP-Ag/TiO_2/ Fe_2O_3/ CS Ternary compositewas much higher than pure nanomaterials due to strong synergistic effect of constituent metallic oxides and encapsulation of chitosan as demonstrated in the **Figure 8.8C** the growth of *C.albicans* significantly inhibited. In the growth curves positive and controls were consider to validate the findings.

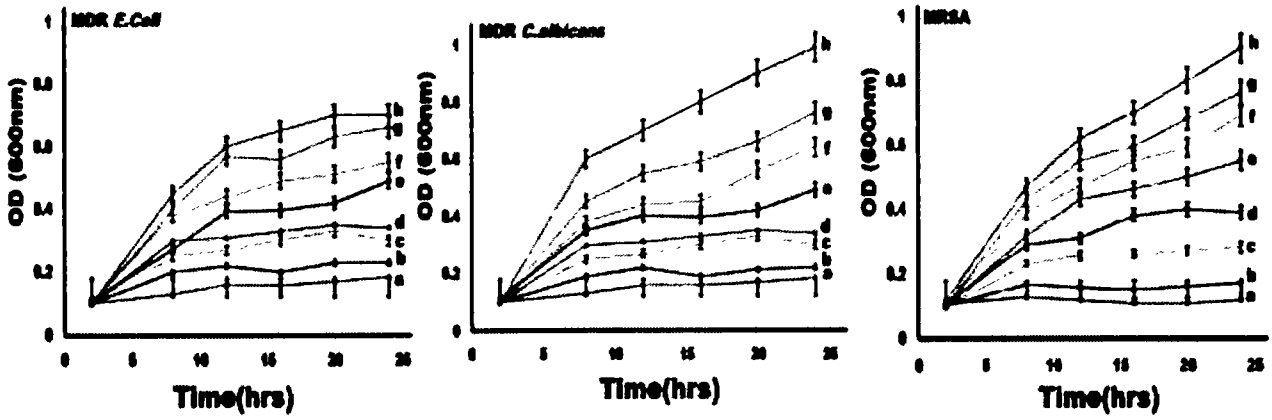

Figure 8.8 Killing kinetics of green synthesized nanomaterials against MDR *E.coli*, *C.albicans* and MRSA,

Key: a- NC, b- CIP-Ag/TiO_2/ Fe_2O_3/ CS Ternary composite, c- Ag/TiO_2/ Fe_2O_3/ CS, d- Ag/TiO_2/ Fe_2O_3, e-Fe_2O_3 nanorods, f- CS NPs , g-Ciprofloxacin, and h- PC

8.2.8.2. Flow cytometry of cultures after interaction with CIP-Ag/TiO2/ Fe2O3/ CS Ternary composite

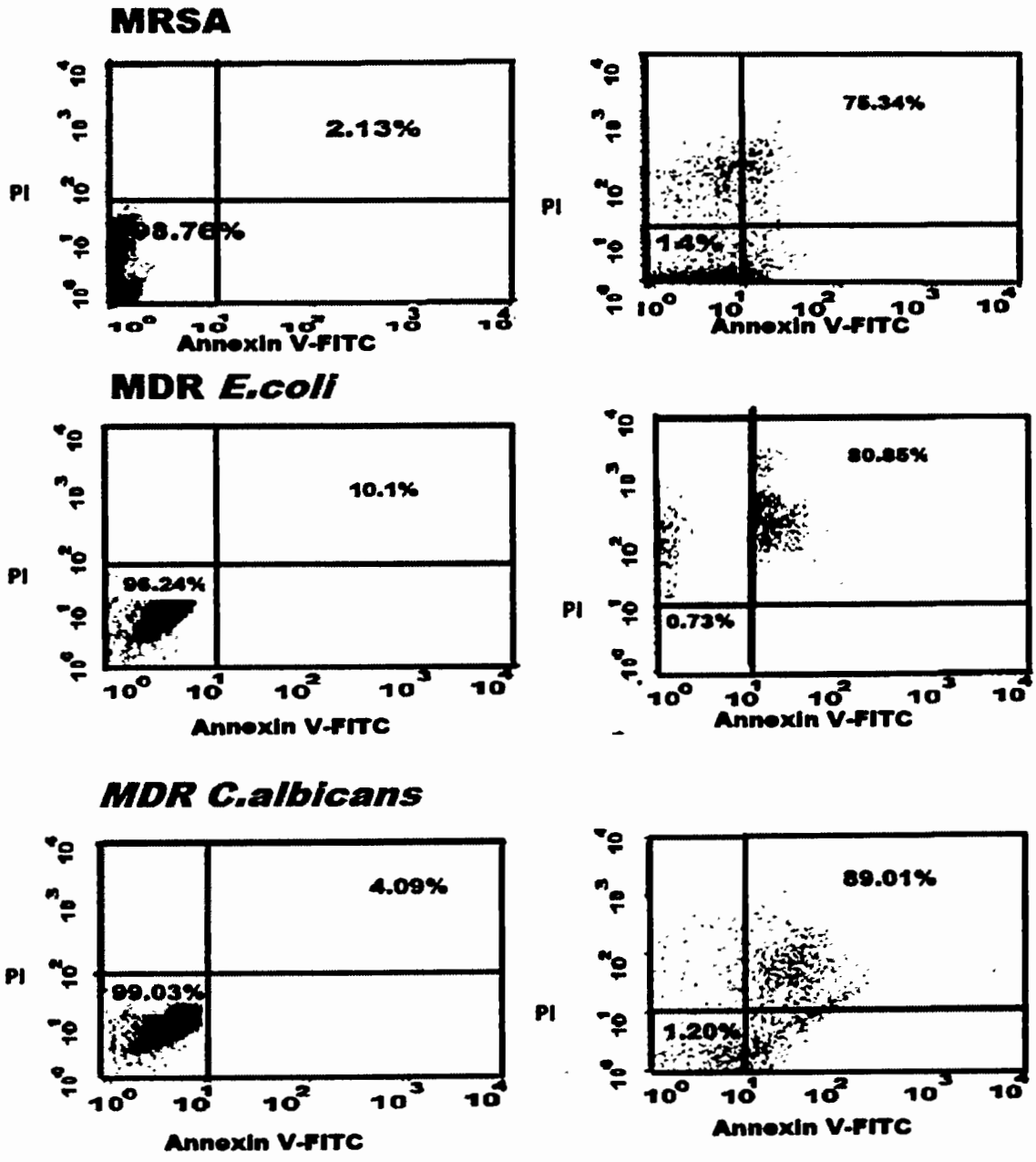

Figure 8.9 Flow cytometry outcomes of CIP-Ag/TiO_2/ Fe_2O_3/ CS Ternary composite treated MDR pathogens.

Antimicrobial study was explained with more intense detailed analysis by undergoing flow cytometry of MRSA strains, MDR *E.coli* and *C.albicans* after interacting CIP-Ag/TiO_2/ Fe_2O_3/ CS Ternary composite at MIC value, allowing 6hrs of incubation time to assess the early apoptosis, late apoptosis and death rate in the selected population density. As shown in the **Figure 8.9**, for 0hrs of incubation as control 98.76% cells were alive and sustainable while the survival rate of MRSA isolates after 6hrs of incubation was 14% and death of 75.34%. The antimicrobial potential revealed in the **Figure 8.9** at the 6hrs of aging with CIP-Ag/TiO_2/ Fe_2O_3/ CS Ternary composite, causing cell death of MDR *E.coli* strains about 80.85%. In the **Figure 8.9** showed excellent anti candida activity of combined effect of all constituent nanoantimicrobial agents after incubation with CIP-Ag/TiO_2/ Fe_2O_3/ CS Ternary composite induces changes in the morphology and cells cycle causing death of 89.01%, which was detected using special dyes. The PI fluorescent dye, which is not cell wall permeating, is generally used to detect dead cells in the population. The CIP-Ag/TiO_2/ Fe_2O_3/ CS Ternary composite mode of action disrupt the integrity of the cell by damaging cell wall and membrane, which enhances the PI permeability and uptake into the cell and leads to intercalation with the DNA that result in a shift in PI fluorescence.

8.2.8.3. Morphological Changes in Mastitis Causing Pathogenic Microbes after Exposure to Ternary Composite

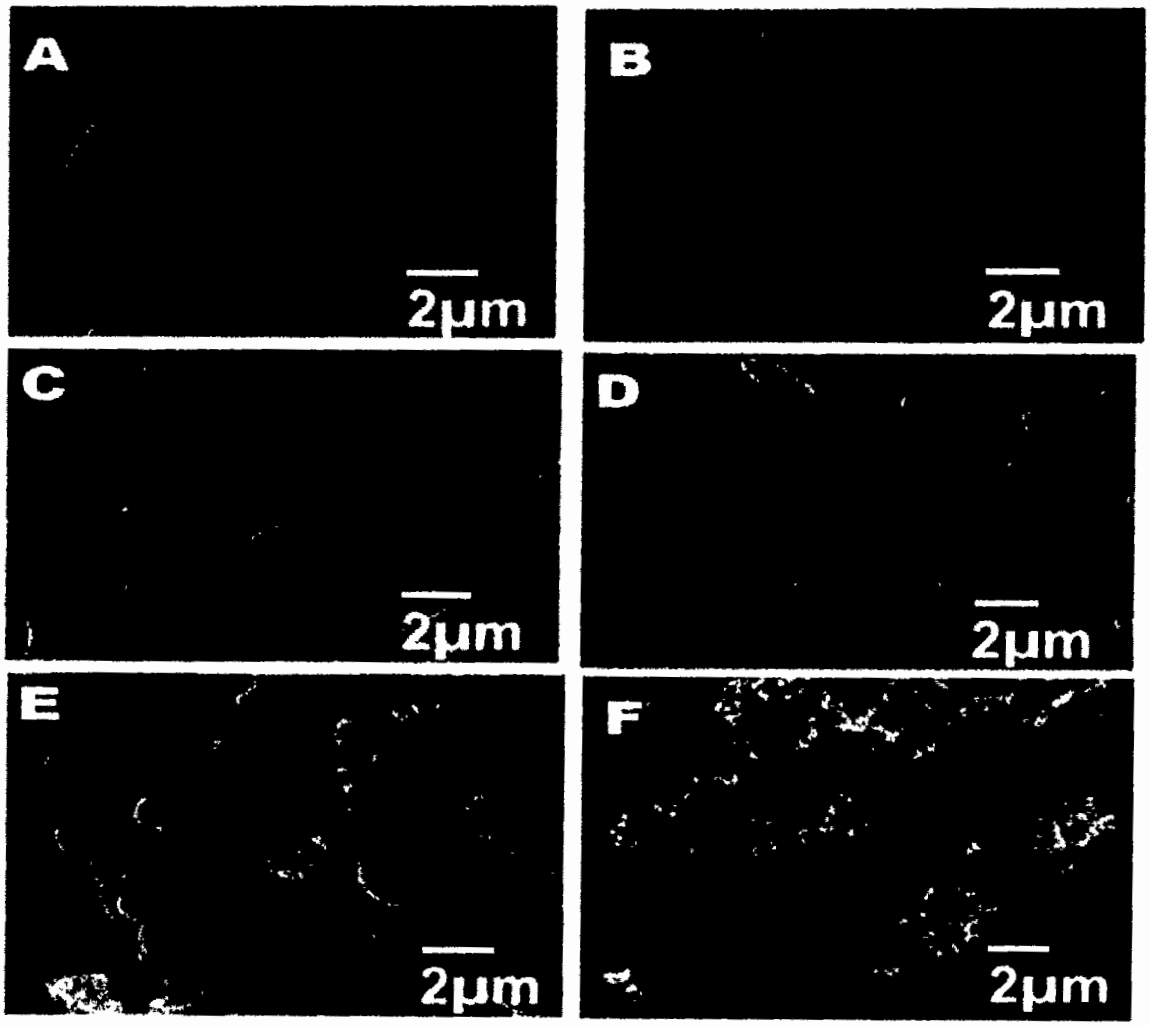

Figure 8.10 Morphological alteration induced by CIP-Ag/TiO_2/ Fe_2O_3/ CS Ternary Composite at respective MIC value,

Key:-

A- *C.albicans* control, B- treated *C.albicans* (0.004 µg /ml)

C- MDR *E.coli* control, D –treaded *E.coli* (0.022 µg /ml)

E-MRSA strains control, F- treated MRSA (0.112 µg /ml)

Results of MIC values revealed that CIP-Ag/TiO_2/ Fe_2O_3/ CS Ternary composite showed an increased rate of toxicity against G– rods of *E.coli.* The SEM study was applied to further investigate the morphological changes in the *C.albicans*, MDR *E.coli*, and MRSA and after exposure to CIP-Ag/TiO_2/ Fe_2O_3/ CS Ternary composite. In this regard controlled group showed intact cells, cell wall and membrane presenting uniform morphology (**Figure 8.10A, C, and E**), which means the cellular proliferation of remained normal. The microbial cultures after exposure to CIP-Ag/TiO_2/ Fe_2O_3/ CS Ternary composite at the 6 hrs of incubation viewed under SEM analysis for observing destruction of *C.albicans* (**Figure 8.10B**),MDR *E.coli* (**Figure 8.10D**) and MRSA strains (**Figure8.10F**). MDR *E.coli* (**Figure 8.10D**) showed remarkable changes in the morphology as many were detached from outer membrane and cellular fragments were seen clearly. The prominent morphological changes could be seen for *C. albicans*(**Figure 8.10B**) almost all the cells have low density regions in their center, which clearly indicates that cytoplasm was damaged and outer membrane was disintegrated by CIP-Ag/TiO_2/ Fe_2O_3/ CS Ternary composite. The morphological changes incurred in the MRSA cells when encountered with CIP-Ag/TiO_2/ Fe_2O_3/ CS Ternary composite as shown in the **Figure 8.10F** the deformation in the spherical structure of MRSA. This proposes lysis of bacterial cells with release of cytosolic content and wrinkled cells upon their interaction with CIP-Ag/TiO_2/ Fe_2O_3/ CS Ternary composite. Results revealed that strong bonding between MRSA and CIP-Ag/TiO_2/ Fe_2O_3/ CS Ternary composite is responsible for the profound antibacterial activity .The zeta potential value of CIP-Ag/TiO_2/ Fe_2O_3/ CS Ternary compositeis positive while bacterial cell wall is negatively charged ,this established electrostatic attachment and prompt ROS production which ultimately cause inhibition of microbial growth and eventually caused cell death .

8.2.8.4. Antibiofilm activity

Biofilm formation in the infections caused by MDR *E.coli* played important role in enhancing pathogenicity and drug resistance.Currently, biofilm infection therapy is a complex challenge for clinicians. Antibiotic treatment is insufficient in combating against biofilm-related infections. Biofilm treatment can include the elimination of infected foreign bodies, the choice of well penetrating and sensitive antibiotics and early administration of high dosage

antibiotics/combinations.Antibiofilm activity of synthesized nanoformulations has been shown in the **Figure 8.11**. The synergistic effect of metallic oxides in the ternary composite of CIP-Ag/TiO_2/ Fe_2O_3/ CS Ternary composite successfully inhibited biofilm of MDR *E.coli* studied at various time interval 24, 48 and 72 hrs of incubation. It can be seen from the **Figure 8.11** CIP alone failed to inhibit biofilm of pathogenic strains of *E.coli*.

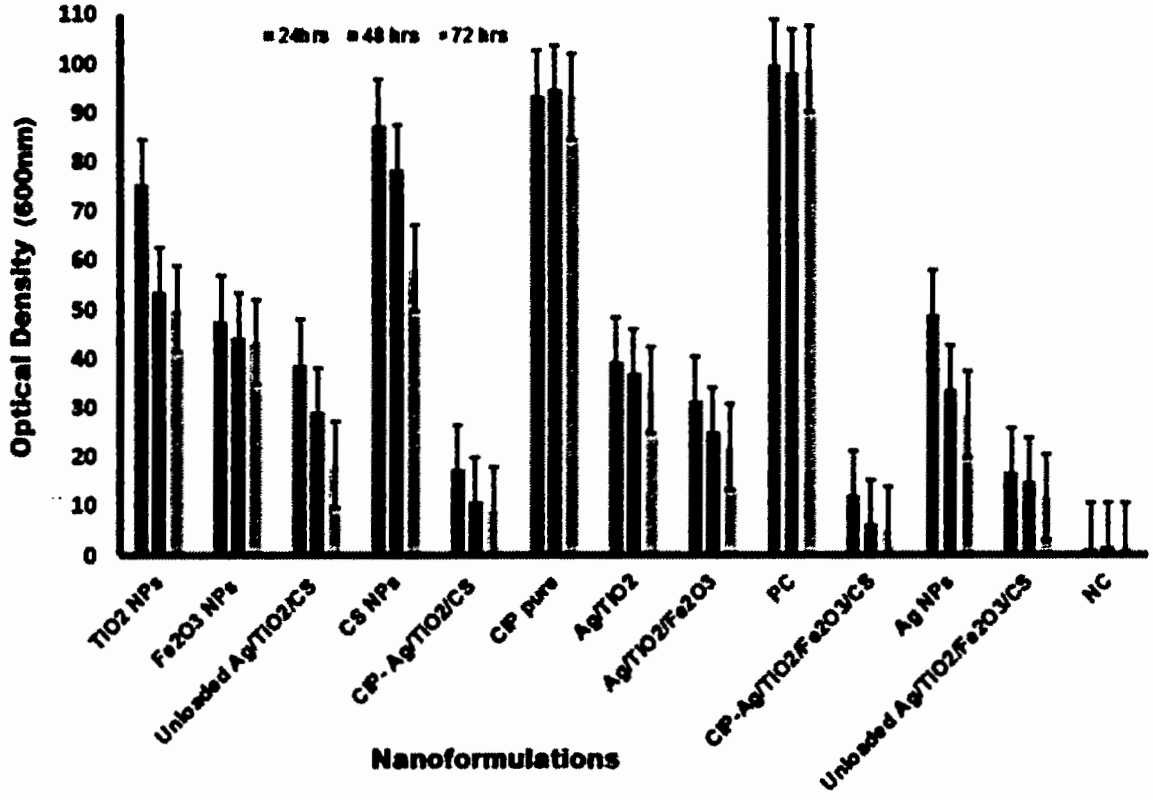

Figure 8.11 Inhibition of biofilm activity of MDR *E.coli* after treatment with green synthesized nanomaterials.

8.2.9. Cytotoxicity analysis

The cytotoxicity evaluation of the prepared nanomaterials was studied by MTT assay against Bovine mammary gland cell lines. As described in the **Figure 8.12A** positive control, BMG cell lines after treated with anticancer drug Celecoxib showed small round cells with shrinkage after blocking normal functioning. CIP-Ag/TiO_2/ Fe_2O_3/ CS Ternary composite was found safe and nontoxic to BMG cell line as shown the **Figure 8.12B** can be compared with negative control (untreated) **Figure 8.12C**.

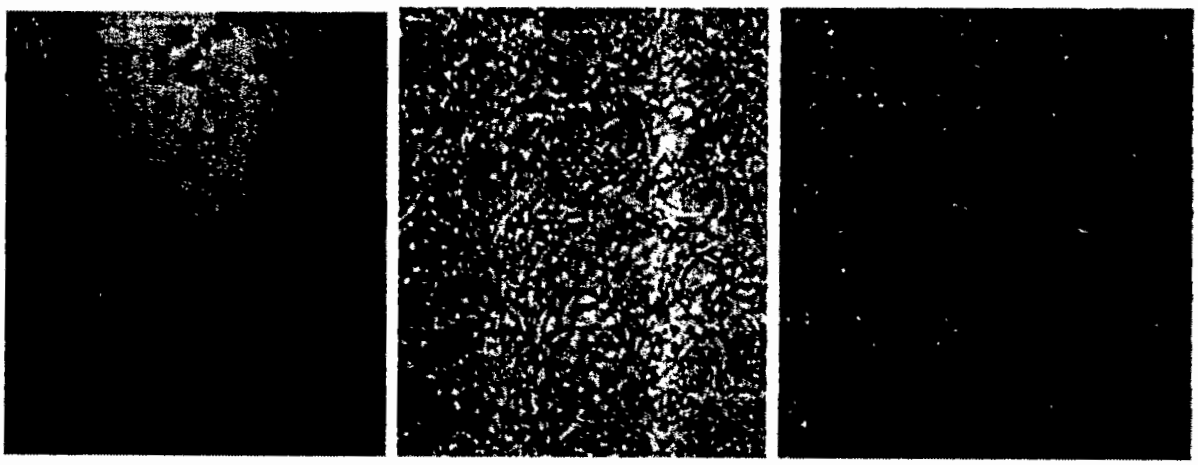

Figure 8.12 Cytotoxicity evaluation of CIP-Ag/TiO2/ Fe2O3/ CS Ternary composite on Bovine mammary gland cell lines

Key:-

A-PC treated with Celecoxib

B-BMGE Cell line treated with CIP-Ag/TiO_2/ Fe_2O_3/ CS Ternary composite

C-NC untreated cells

The relative percentage viability of mammalian cells at various concentrations (0.02, 0.1 and 0.2 μg/mL) of synthesized nanoformulations was being analyzed on primary cultures of proliferating bovine mammary gland epithelial cells (BMGE).The relative percentage viability of mammalian cells was found more viable and safe after interaction with CIP-Ag/TiO_2/ Fe_2O_3/ CS Ternary composite at all tested concentrations may be chitosan encapsulations as shown in the **Figure 8.13**.

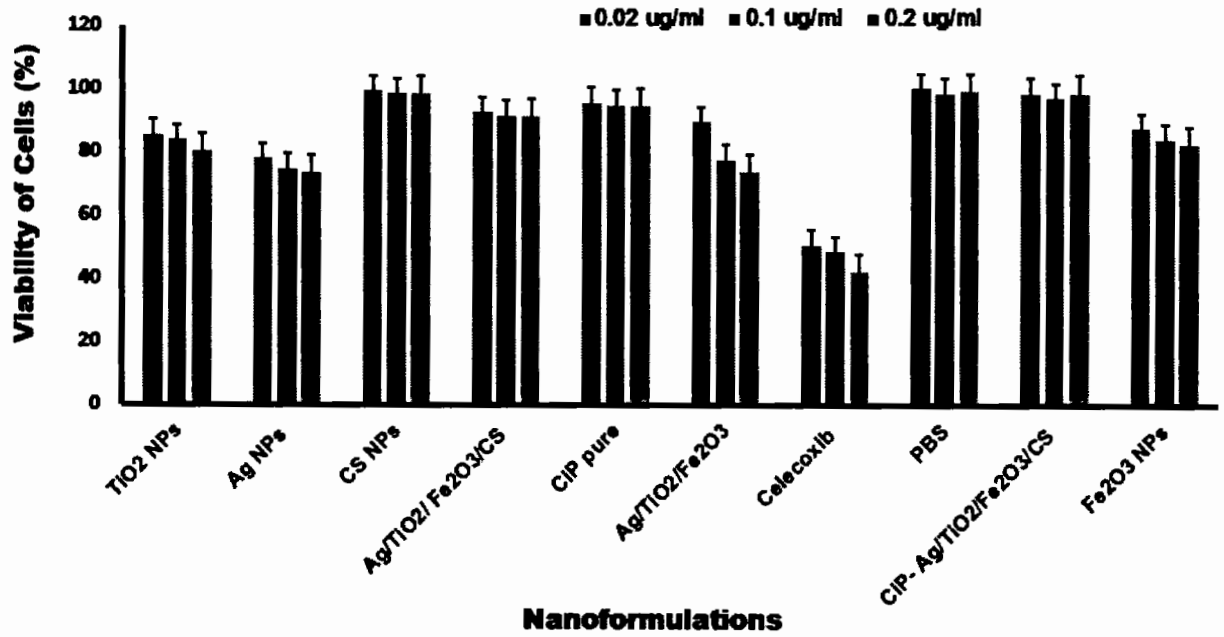

Figure 8.13 Viability of mammalian cells after interaction with synthesized nanoformulations at various concentrations.

BMG cell lines after treating with CIP-Ag/TiO_2/ Fe_2O_3/ CS Ternary composite exhibited excellent viability of cells and posed ternary composite nontoxic for mammalian cells. The CIP-Ag/TiO_2/ Fe_2O_3/ CS Ternary composite was found safe and biocompatible as compare to positive control (Celecoxib). Moreover the cytotoxicity of CIP-Ag/TiO_2/ Fe_2O_3/ CS Ternary composite, chitosan NPs, Ag NPs, TiO_2 NPs, Ag/TiO_2 nanohybrid, Fe_2O_3 and PC at various concentrations have been shown in the **Figure 8.13**. The cells treated at lowest concentrations were more viable and stable as compare to higher concentrations of nano antibacterial agents included in the study.

8.2.10. Hemolysis of CIP-Ag/TiO2/ Fe2O3/ CS Ternary composite

Hemocompatibility isone of the important aspects for the *in-vivo* application of nanomaterials as the injected nanomaterials interact firstly with RBCs before the immune cells. Therefore, the hemolysis assay was performed for preclinical study. Hence, the potential hemolytic activity of Fe_2O_3 NPs, CSNPs, CIP,Ag/TiO_2/ Fe_2O_3, Ag/TiO_2/ Fe_2O_3/ CS and CIP-Ag/TiO_2/ Fe_2O_3/ CS ternary compositewas examined on the RBCs of cow (**Figure 8.14).** The results have revealed negligible hemolytic activity of CIP-Ag/TiO_2/ Fe_2O_3/ CS ternary composite as compared to the positive control Triton 100X showed significant hemolysis and negative control PBS which did not induce hemolysis. It was observed CS NPs was also not meaningfully different from PBS. CS as nontoxic and hemocompatible making it highly useful for biomedical applications such as in antimicrobial delivery metallic-based nanocarriers thanks to its good interactions with metal oxide.

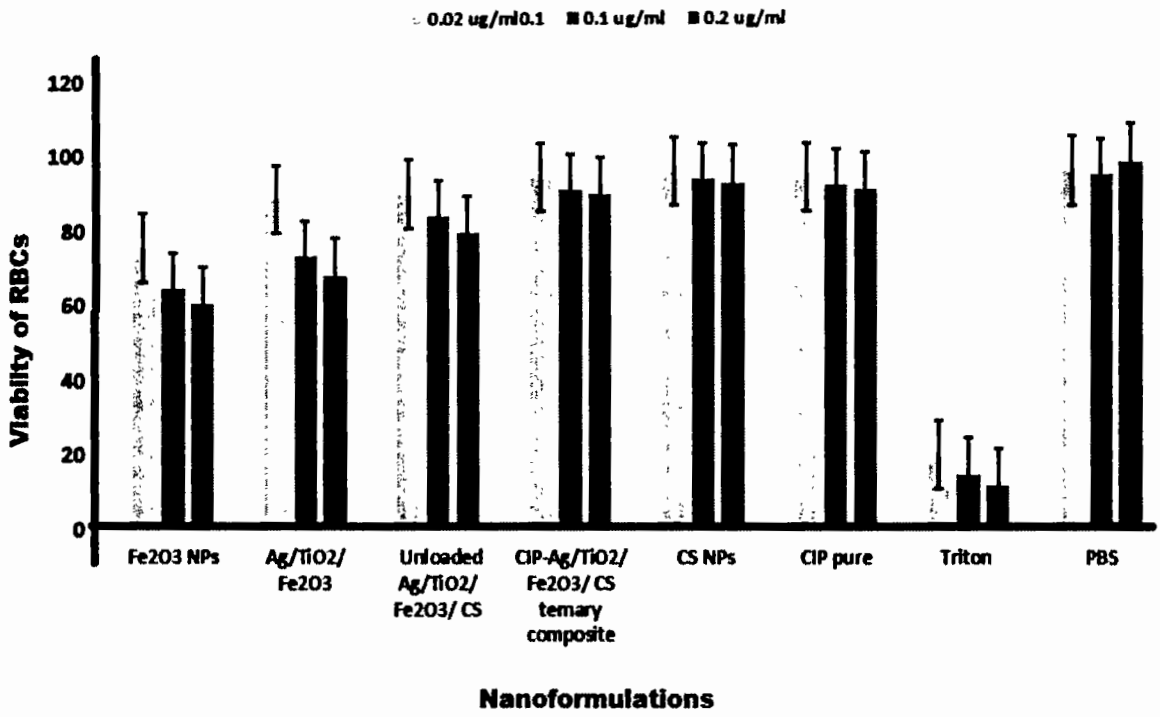

Figure 8.14 Hemolytic potential of green synthesized nanoformulations on the RBCs of healthy cow

Key:-

PBS was used as a negative control (NC)

Triton X-100 was used as Positive control (PC)

8.2.11. Invivo antibacterial activity of CIP-Ag/TiO_2/ Fe_2O_3/ CS Ternary Composite

Rabbit was selected as animal model to investigate *Invivo* antibacterial activity of green synthesized nanomaterial D, CIP-Ag/TiO_2/ Fe_2O_3/ CS Ternary composite. The *E.coli* strains were selected to induce infection in the rabbit model and CFU was analyzed to observe the antibacterial potential of CIP-Ag/TiO_2/ Fe_2O_3/ CS Ternary composite at various time intervals on the media plates of MH and Blood agar as shown in the **Figure 8.15**. The CFU was counted after treatment period of 24hrs whereas CFU remarkably decreased after 24hrs and 48 hrs of treatment and infection was completely controlled as no colonies of *E.coli* were obtained on both MH and Blood agar plates as shown in the **Figure 8.15**. Thereduction

of colonies after increasing time interval 24, 48 and 72 hrs of post treatment in the rabbit model and findings were compared with positive and negative controls. Infection is completely controlled in the test group treated with CIP-Ag/TiO_2/ Fe_2O_3/ CS Ternary composite and showing no viable colony on blood and MH agar plates at 72 hrs at lowest value of MIC, indicating that the cells were killed.

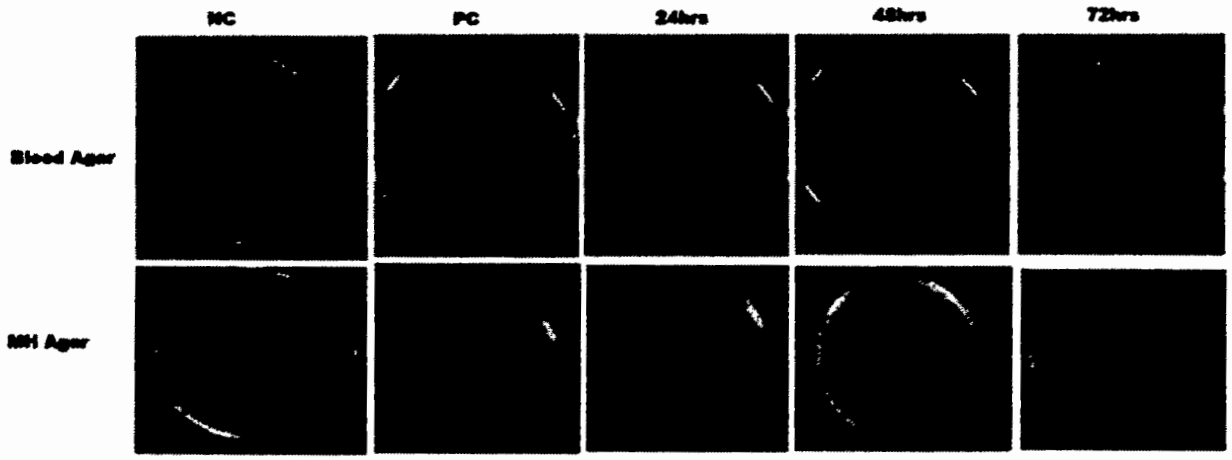

Figure 8.15 Invivo antibacterial activity of nanomaterial D, CIP-Ag/TiO2/ Fe2O3/ CS Ternary composite,

Key:-

PC (positive control) containing *E.coli* without any treatment

NC (negative control) only broth

For the *Invivo* study, different parameters of renal and hepatic function were also evaluated after treatment with CIP-Ag/TiO_2/ Fe_2O_3/ CS Ternary composite. These parameters included urinary volume, concentrations of proteins, glucose levels and creatinine levels.

The **Figure 8.16** has demonstrated that urine volumes, glucose levels, total proteins, and creatinine levels (**Figure 8.16**) in the urine, are similar to the values obtained for the treatment group of CIP-Ag/TiO_2/ Fe_2O_3/ CS Ternary composite. In addition, no significant differences were observed between the groups of rabbits treated with CIP-Ag/TiO_2/ Fe_2O_3/ CS Ternary composite, and the control groups in the parameters tested to evaluate hepatic function albumin (**Figure 8.17A**), ALT (**Figure 8.17B**), and AST (**Figure 8.17C**) concentrations in blood plasma.

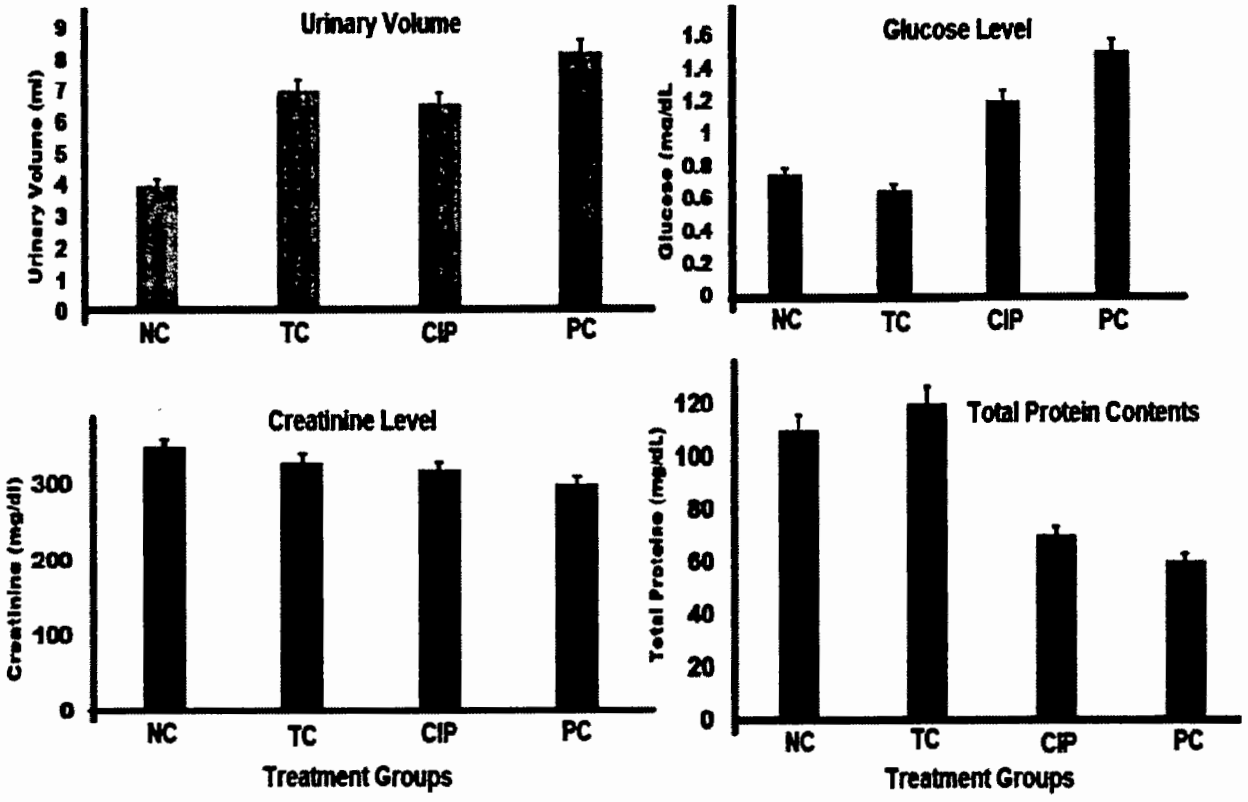

Figure 8.16 Renal functioning of Rabbit model animal for induced infection after treatment withNC (negative control),TC (CIP-Ag/TiO_2/ Fe_2O_3/ CS Ternary composite), CIP (ciprofloxacin)PC (positive control).

The appearance and characteristics of the vital organs kidney ,liver and heart were studied between the treated group of rabbit including positive control and negative control in the experiment. The suitable functioning of its organs is very important to achieve a healthy balance maintaining the composition of its internal environment. This is largely achieved with the correct functioning of organs such as liver kidney and heart as shown in the **Figure 8.18.**Thus, the CIP-Ag/TiO_2/ Fe_2O_3/ CS ternary compositemanufactured in the study did not cause any adverse or toxic effects in the nephrons and renal function of the animals treated.

The concentration of ALT and AST and the concentration of albumin of the treated groups with CIP-Ag/TiO_2/ Fe_2O_3/ CS Ternary composite were similar to the values of control groups **Figure 8.17- 8.18**.

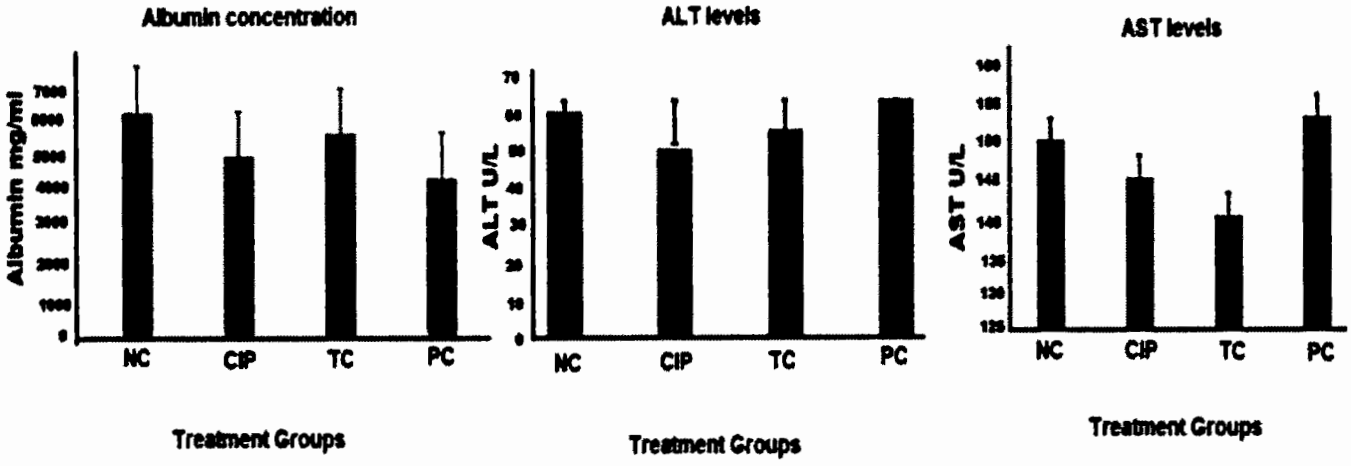

Figure 8.17: Hepatic functioning of Rabbit model animal for induced infection after treatment

Key:-

NC (Negative control),

TC (CIP-Ag/TiO_2/ Fe_2O_3/ CS Ternary composite),

CIP (Ciprofloxacin)

PC (Positive control).

Thus, the CIP-Ag/TiO_2/ Fe_2O_3/ CS Ternary compositeobtained in this study did not have any adverse or toxic effects in the hepatic function.

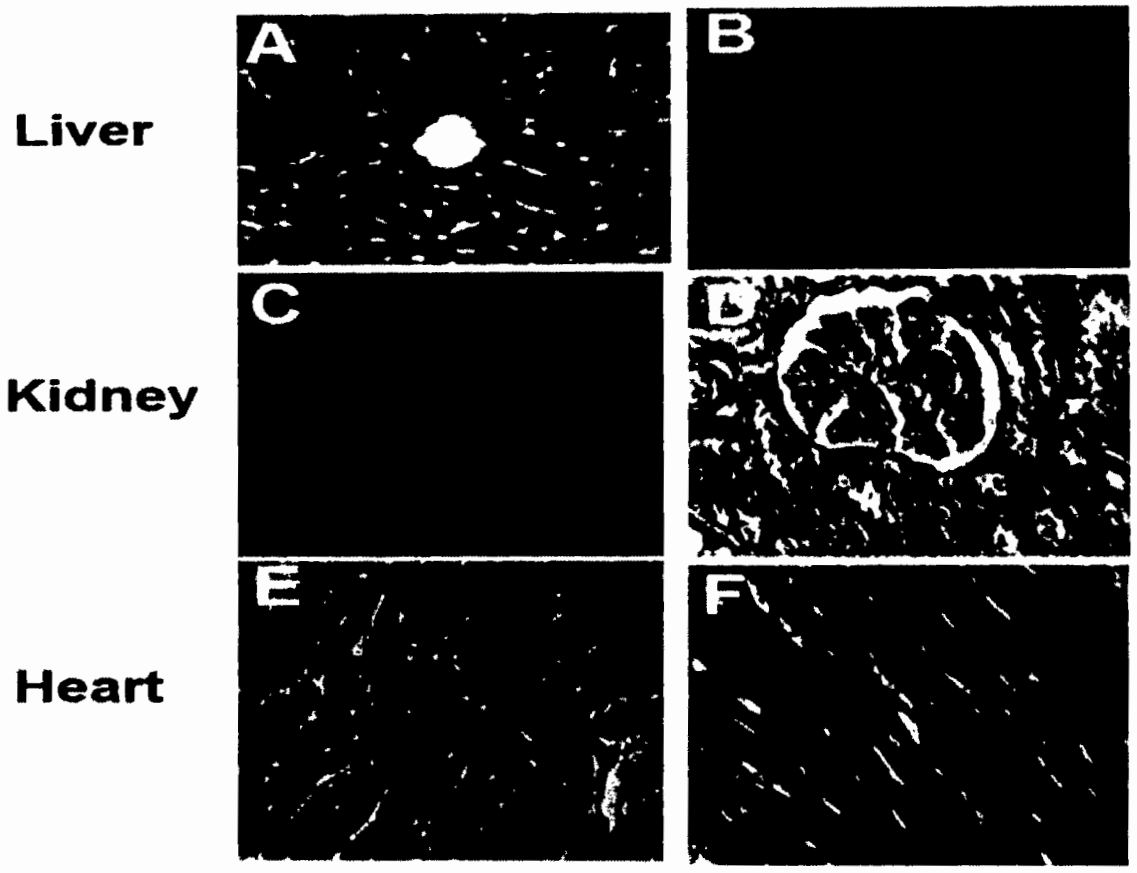

Figure 8.18 Effect of nanomaterial D, on the vital organs of rabbit model after treatment with CIP-Ag/TiO_2/ Fe_2O_3/ CS ternary composite

Key:-

A-Cellular morphology of untreated hepatocytes tissues

B-Cellular morphology of hepatocytes tissues treated with nanomaterial D

C-Cellular morphology of untreated renal tissues

D-Cellular morphology of renal tissues treated with nanomaterial D

E-Cellular morphology of untreated cardiac tissues

F-Cellular morphology of treated with nanomaterial D cardiac tissues

8.2.12. Invivo Antibiotic release kinetics of Nanomaterial D, CIP-Ag/TiO2/ Fe2O3/ CS Ternary Composite

Invivo drug release pattern of CIP from the In vitro drug's release pattern CIP from the CIP-Ag/TiO_2/ Fe_2O_3/ CS ternary composite was estimated by using UV-Vis Spectrometry by maintaining the diffusion gradient in the donor and receptor containing PBS (pH 7.4, 37 °C) during 0,1,2,4,8,16,24,hrs. The results of *Invivo* drug release studies from CIP-Ag/TiO_2/ Fe_2O_3/ CS ternary composite were depicted in **Figure 8.19**. The CIP-Ag/TiO_2/ Fe_2O_3/ CS ternary composite exhibited highest active drug release (89% ± 0.57) at the 8^{th} hrs , which was remarkable in the 24hrs of release study when compared to control (CIP alone) showing 90% ± 0.78 release kinetics from the skin. In the present study, it was observed that rate of drug release was increase progressively during first 8hrs of experiment and then decrease gradually till 24hrs.

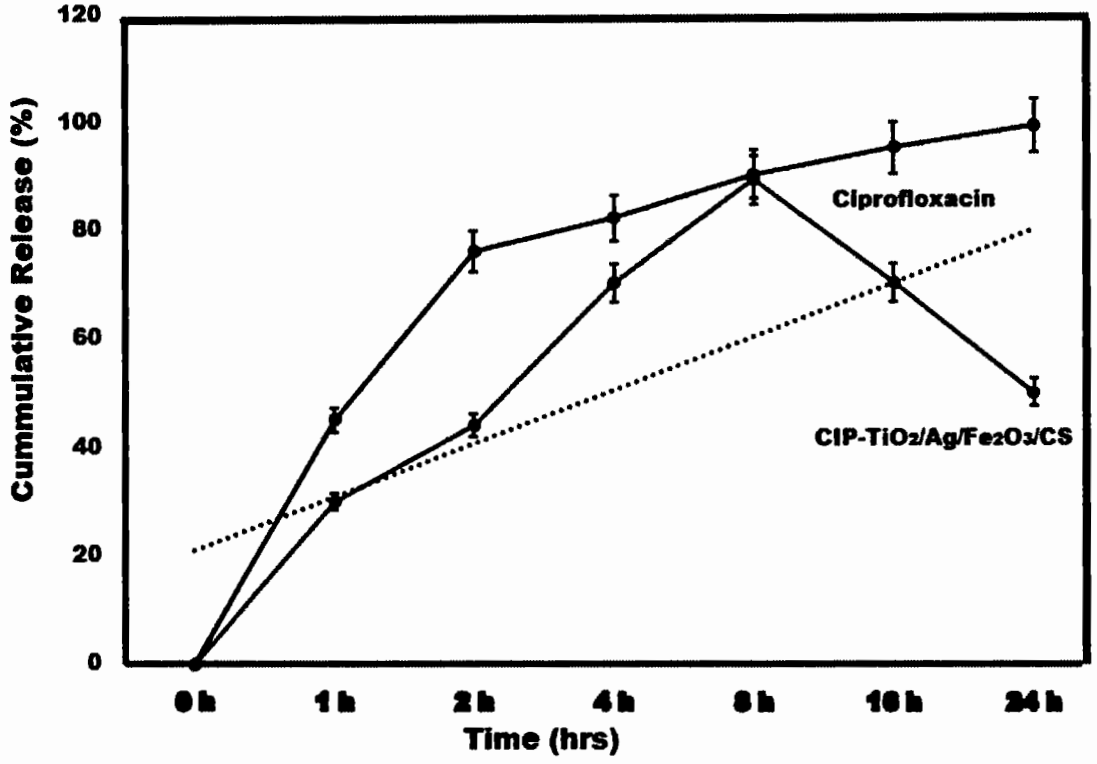

Figure 8.19: In-vivo Ciprofloxacin release profile from chitosan encapsulation, drug release spectrum of CIP-Ag/TiO_2/ Fe_2O_3/ CS ternary compositewith CIP (Ciprofloxacin) taken as control.

8.2.13. Antimicrobial mechanism CIP-Ag/TiO_2/ Fe_2O_3/ CS ternary composite

The antimicrobial activity of proposed CIP-Ag/TiO_2/ Fe_2O_3/ CS ternary composite was found excellent and successfully inhibit the growth MDR pathogens of veterinary origin. The encapsulation of chitosan further enhances the antimicrobial potential by triggering the destruction pathways after occupying metabolic machinery of MDR pathogens. The incorporation of Fe_2O_3 nanorods content in the Ag/TiO_2 composite to form ternary metallic oxide material conjugated with ciprofloxacin which further encouraged antimicrobial effect with improved morphology. The distinctive physical and chemical characteristics of nanomaterials contribute collectively in a synergistic manner to expose a novel, exceedingly efficient antibacterial nano interface of CIP-Ag/TiO_2/ Fe_2O_3/ CS ternary composite. As chitosan showed intrinsic antimicrobial effect against both Gram-negative and Gram-positive

bacteria. The generation of silver cations by the oxidation of Ag NPs (Birla et al., 2009) and reactive oxygen radicals (ROS) are produced by the chelation of chitosan ,Ti+ and Fe+3 into cell of Microbes which imbalance of ions and homeostasis of the internal environment. In the **Figure 8.20** crucial stages of cell death are as follows, attachment and penetration by Vander wall's force of attraction between charged surfaces of microbes, which are negatively charged and CIP-Ag/TiO_2/ Fe_2O_3/ CS ternary composite is positively charged. The generation of ROS ($^{\bullet}O_2^-$, $^{\bullet}OH$ and H_2O_2) may occur after the release of metallic ions in the cytosol. These free radicals are toxic to the cells as they have a strong ability to damage cellular constituent's i.e. damage cell wall, cell membrane, inhibit DNA synthesis and protein assembly which eventually leading cause of cell death of MDR *E.coli*, MRSA and *C.albicans.*

Proposed mechanisms have been comprehensively include release of toxic ions as well as oxidative stress, lipid peroxidation, cell membrane damage, enzyme inhibition, and proteolysis (Bokare et al., 2013). A definitive study demonstrating the requirement of Ag ion release for Ag-NP antibacterial activity (Huang et al., 2017). Alternatively, for the catalytic production of reactive oxygen species (ROS) is a commonly proposed mechanism of action. This mechanism is based on the catalytic properties of metallic oxide. Specifically, Fe_2O_3 nanorods are showing transition states from Fe +4 to Fe +3 in optical properties and band gap is highly in the favor of antimicrobial action.

As CIP-Ag/TiO_2/ Fe_2O_3/ CS ternary composite has nanorods with sharp edges that could effectively inhibit enzyme activity through binding to the enzyme without protein denaturation. They suggest that specific edges or vertices of the shape allowed binding and conformational frustration of the enzyme. Interestingly, this specific shape of small length nanorods was much more effective in inhibiting bacterial growth than spherical morphology. This suggests that CIP-Ag/TiO_2/ Fe_2O_3/ CS ternary composite interact with cell membrane and provide a mechanical disruption of the membrane .This results in loss of membrane integrity, dissipation of ion gradients, arrest of cellular metabolism, and ultimately cell death via lysis .

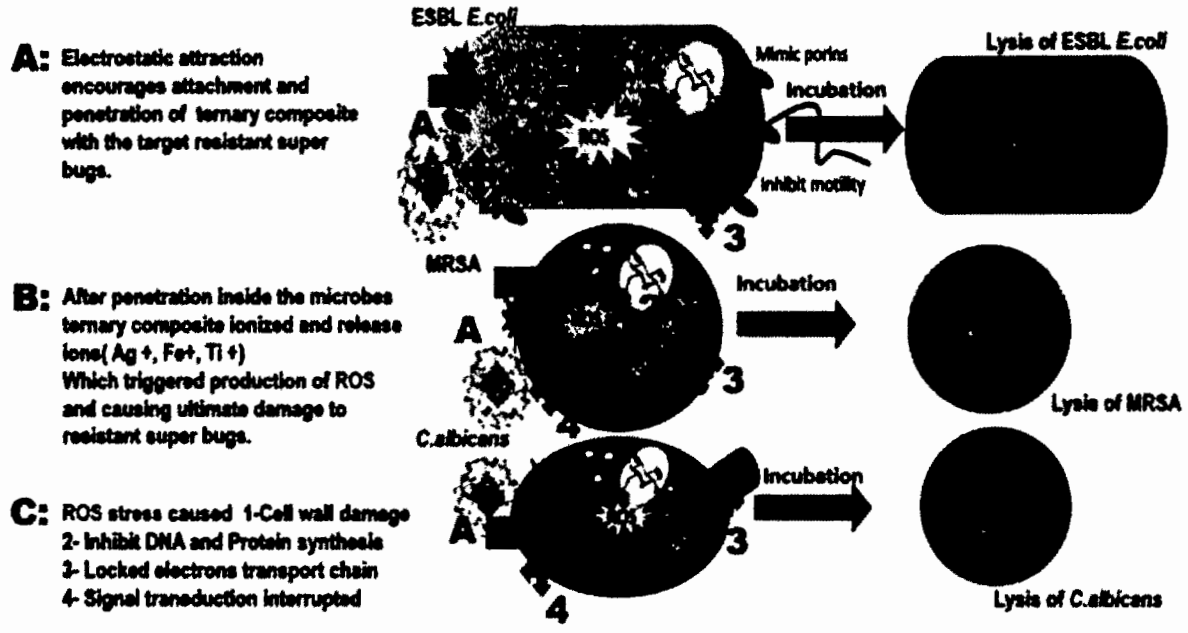

Figure 8.20: Proposed mechanism of antimicrobial action of biologically synthesized CIP-Ag/TiO_2/ Fe_2O_3/ CS ternary composite.

Conclusion

The primary goal of this research is to create a safe and nontoxic broad spectrum CIP-Ag/TiO_2/ Fe_2O_3/ CS ternary composite to tackle MDR strains that cause mastitis in cattle. In comparison to CIP alone, this study demonstrates the effective synthesis of a CIP-Ag/TiO_2/ Fe_2O_3/ CS ternary composite with significant antibacterial activity at comparatively low MICs. The synthesis of Ag/TiO_2/ Fe_2O_3/ occurred through reduction of *M. concanensis* leaves extract followed by ionic gelation method for conjugation of CIP and CS encapsulation. The CIP-Ag/TiO_2/ Fe_2O_3/ CS ternary composite was proved to be safe and nontoxic on bovine mammary gland epithelial cells and RBCs. Invivo antimicrobial evaluation was performed on rabbit model of induced infection and CFU counts revealed no visible growth at 72 hrs of post treatment .Moreover vital function of kidney and liver remained in equilibrium as in negative control. Histopathological study of heart, kidney and

liver further suggested the safety and nontoxicity of CIP-Ag/TiO_2/ Fe_2O_3/ CS ternary composite.

CHAPTER 9

DISCUSSIONS

The lack of advancement of new antibiotics and suboptimal concentrations exposure may be associated with possible reasons due to which treatment inefficiency occurs. Deploying novel treatment strategies is inevitable by searching for new systems that consider various growth forms, eschewing falling into the post-antibiotic era, and impacts of antibiotics that are not effective to treat resistant microbes. Bacteria can easily adapt to the environment by developing various resistance mechanisms and virulence factors (Breser et al., 2018).It is a challenge for pharmaceutical industry worldwide to respond more efficiently and faster to the unfortunate increasing speed of bacterial adaptations to the environment.

Higher rates of multidrug resistance have been reported to control the mastitis (Breser et al., 2018).Bovine mastitis is most prevalent illness affecting quantity and quality of milk production in dairy cows that lead to the financial losses to dairy industries. Mastitis can cause serious health problems when zoonotic pathogens are involved due to the accumulation of bacteria and toxins in milk. In recent years *Staphylococcus aureus*, *Escherichia coli,* and *Candida albicans* are nominated as high drug resistant pathogens causing infections in both animals and humans. These pathogens enter the cow's mammary glands by teat canal when natural immunity of cow is affected. They colonize and proliferate in the canal and release toxins to damage the mammary gland cells (Neculai et al., 2021).

The administration of various antibiotics like penicillin, tetracycline, gentamycin, and ampicillin via intramammary route has been the first choice of treatment against bovine mastitis but inappropriate and overuse of these antibiotics led to the resistance in bacterial species (Serwecińska, 2020). Current treatment failures to tackle multi drug resistant bacteria pose anxiety and it urges to increase the funding and research to navigate for new technologies and products for humans and animals.

The worldwide bovine mastitis market is estimated to reach USD 1.84 billion by the end of 2027. Nanotechnology based solutions are expected to lead towards an exciting future of the

global market to treat and control bovine mastitis. A report published by Fortune Business Insights entitled "Bovine Mastitis Market Size, Share & COVID-19 Impact analysis, by type (Clinical, and Sub-Clinical), by product (antibiotics, and others), by route of administration (Intra-mammary, and Systemic), by therapy (Lactating Period and Dry Period) and Regional Forecast, 2020–2027" stated that the market that was forecasted in 2019 at USD 1.23 billion is estimated to experience a 5.2% CAGR (compound annual growth rate) during 2020-2027. European market growth will be driven by an increasing number of business alliances to design new treatment strategies for bovine mastitis in various countries like Germany, France, and the UK (Neculai et al., 2021).

Nanotechnology has been considered as a substitute to resolve the issue of AMR and provide sustainable animal health to support the production of high-quality animal products. Various metallic nanoparticles have been reported against bovine mastitis infections and methicillin resistant bacteria (Serwecińska, 2020; Wady et al., 2014). Nanoparticles have been considered as potential delivery systems in the bovine mastitis treatment. This alternative therapy is gaining attention in organic dairy farms to control bovine mastitis due to its efficient antimicrobial activity, low cytotoxicity, and targeted delivery.

Various approaches have been designed for the synthesis and fabrication of nanomaterials. In top-bottom approaches, the desired bulk of materials break down into the particles in the nanosized range by mechanical milling/alloying and sputtering (Ahmed et al., 2016; Hodaei et al., 2015) are examples of methods for reducing the size of the particles. Many chemical methods are chosen for synthesizing NPs because of their quick reaction time and their capability to produce monodispersed NPs (Smitha et al., 2008). They have few disadvantages such as the high cost of the process, not being environment friendly, and cause lots of pollution in the environment because of using toxic solvents and reducing agents (Naraginti & Li, 2017).To avoid these drawbacks, green chemistry approaches have been employed for production of NPs which are simple, convenient, less energy-intensive, eco-friendly and minimize the usage of unsafe materials, and maximize the efficiency of the process (Gross & Kalra, 2002; Raveendran et al., 2003).

Medicinal plants have historically proven their value as a source of molecules with therapeutic potential, and nowadays still represent an important tool for the identification of novel drug leads. In the past decades, pharmaceutical industry focused mainly on libraries of synthetic compounds as drug discovery sources. They are comparably easy to produce and demonstrate good compatibility with established high throughput screening platforms (Luseba & Tshisikhawe, 2013). However, at the same time, there has been a declining trend in the number of new drugs reaching the market, raising renewed scientific interest in drug discovery from natural sources. *M .concanensis* is the medicinal herb and the versatile use of moringa plant is been reported such as a medicinal product, practical food source, nutraceutical, and water purifying agent. It is used for the treatment of variety of diseases including paralysis, menstrual pain, high blood pressure skin tumors, joint pain, inflammation, liver and kidney disease indicating its immense importance in the health care industry(Balamurugan et al., 2015). *M. concanensis* is found to be effective against inflammation and well-known medicinal plant. Reactive oxygen species-promoting substances such as phytol constitute a promising novel class of pharmaceuticals for the treatment of rheumatoid arthritis and possibly other chronic inflammatory diseases i.e. mastitis which is inflammation of udder (Balamurugan et al., 2015).

Moringa plant has gained much importance in green chemistry due to its therapeutic applications in agriculture, medicine, and industries. *Amomumsubulatum* (Black cardamom) seeds have been studied for various research purposes but these are not explored for the synthesis of nanoparticles. Although it is highly regarded as a ''Queen'' of species, is a perennial herbaceous crop belonging to the family *Zingiberaceae*(Pura Naik et al., 2004). This plant is distributed chiefly in Africa and Tropical Asia and cultivated in swampy places (e.g. Nepal) across hills around water streams for its subsequent uses in cooking, folklore, and Ayurvedic medicine (Agnihotri & Wakode, 2010). Herein, green synthesis procedure used for the preparation of metallic oxide NPs to enhance the morphological, structural, and optical properties of NPs using *M. concanensis* aqueous extract and black cardamom seeds extract.

GC-MS analysis revealed various compounds in plant extracts, present study reported twenty eight active compounds while the previous study revealed fifteen bioactive compounds in *M.*

concanensis from which some compounds like DL-3-4 Dimethyl-3,4- hexanediol (14.05%), 3,4 dimethyl 5 hexen 3 – of (14.05%), methyl ester (10.54%) were consistent with current findings (Balamurugan et al., 2015). Phytochemicals are acting as a reducing agent for the synthesis of nanoparticles. All the applications were as a result of the phytochemicals such as alkaloids, tannins, flavonoids, saponins, triterpenoids, and anthraquinones intrinsic in Moringa leaf extracts (Balamurugan et al., 2015).

Previous investigations had shown that bacteria or fungi as sole etiological agents were found in 15% and 14%, respectively. *Candida* yeast was isolated from 39% of the mixed infections, and in 11% of these cases, it was a sole infectious agent (Kaszak et al., 2012). Krukowski et al isolated fungi as pure cultures from 9.6% of investigated milk samples in the Lublin region in Poland, results found much similar to current findings (Krukowski et al., 2001). According to Casia dos Santos and Moacir Marin (dos Santos & Marin, 2005), the percentage of fungal isolation in surveys carried out in many countries varies considerably, with 6.1% rates described in Egypt(Awad et al., 1980), 1.3% in Denmark (AalbæK et al., 1994), and 12.07% in Brazil (Costa et al., 1993). Casia dos Santos and Moacir Marin (dos Santos & Marin, 2005) isolated fungi in 32% of the cases, and 17.3% of these were *Candida* spp. Biochemical results were in accordance with previous literature (Dudley et al., 2013). The rapid identification test for *E.coli* generated number from API20E was 5144552. Gram-positive MDR isolates of *S. aureus* were confirmed by biochemical tests. Indeed, coagulate and catalase tests were positive while cytochrome oxidase was negative for all isolates of *S. aureus* (Olson et al., 1970). When species level identification is desired, BioMerieux's API 20C has proven satisfactory.

MDR strains of *E.coli* were isolated from milk samples of cattle which were positive by CMT, on the MacConkey agar *E. coli* produced pink colored, smooth and round colonies **Figure 3.4A**. While ESBL differential media used to isolate ESBL *E.coli* strains from the isolated *E. coli* strains which produced purple to pink colonies **Figure 3. 4B**. The pink color indicated that *E.coli* is a Lactose fermenter(Dudley et al., 2013). The culture of milk on blood agar allowed to observe small round, and yellow-orange colonies of *S. aureus* **Figure 3. 4C**. Candida showed green color of colonies on chrome agar media **Figure 3.4D** which is differential media for candida spp isolation (Bhuyan et al., 2018) Morphology of isolated

microbes was summarized in the **Table 3.3.** All the biochemical results were in accordance with previous literature (Dudley et al., 2013). Isolated microbes were confirmed by conventional biochemical tests, Coagulase and catalase tests were positive while cytochrome oxidase was negative for all isolates of *S. aureus.* All *E.coli* strains were found indol positive and catalase positive and *C.albicans* has given negative indol test results and positive catalase test as shown in the **Table 3.4**(Olson et al., 1970). The rapid identification test for *E.coli* produced number from API 20E was 5144552as shown in **Tables 3.5** and for Gram-positive isolates of *S. aureus* 6736153 (**Tables 3.6**) while *C.albicans* generated API 20C number 6172174 as described in the **Table 3.7**.

Pathogenic strains were treated with commercial antibiotics that showed high resistance of these antibiotics to *Staphylococcus aureus*, *Escherichia coli,* and *Candida albicans.* In general, antibiotic therapy is considered ineffective. Clinical mastitis caused by *C. albicans* was treated with intramammarynystatin after being treated with various antibiotics for one month before culture and identification (Sinha et al., 1974) Six days after the beginning of nystatin treatment, milk returned to normal, inflammation subsided, and culture was negative.

Gram negative rods of *E.coli* showed highest resistance to large number of antimicrobials agents used in this study. Particularly, β-lactams, *E.coli* has 100% resistant to Ampicillin (100%), Augmentin (100%), and this resistance property associated with 100%, 85%, and 70% prevalence of bla_{TEM}, bla_{SHV}, and bla_{CTX}respectively.This is maybe due to the ability of many of the Enterobacteriaceae to have intrinsic resistance to β-lactams by releasing β-lactamases(Susić, 2004) which break the β-lactam ring and stop the action of antibiotic. SHV, CTX, TEM, are the most dominant β - lactamases in Gram-negative bacteria. In the current study, blaTEM was found in all isolates (100%) that agree with (Bailey et al., 2011; Younis et al., 2017) who reported that 97.1% of *E.coli* isolates (226) recovered from lambs affected with diarrhea. In this study, SHV was detected in 85% of the tested isolates which was higher than (Arabi et al., 2015) who reported 53.2% of ESBL producing isolates have bla_{SHV}. Also, (Tasli & Bahar, 2005) revealed SHV 74.3%. The bla_{CTX} is one of the most prevalent ESBLs genes. In this study, bla_{CTX} gene found gram negative bacteria (75%). The higher result recorded by (Geser et al., 2012) reported that 78 isolates (85.7%) had CTX- gene from *E.coli*,

E. cloacae, and *C.youngae* isolates taken from milk samples in Switzerland (Tinelli et al., 2012) .

Molecular characterization of MRSA strain has been performed. The *mecA* gene is known to confer *S. aureus* resistance to methicillin (Turutoglu et al., 2009). It is worth mentioning that the recommended susceptibility breakpoints for the 30-μg FOX disk test used to detect *mecA*-mediated resistance in *S. aureus* have been changed in January 2007 by CLSI from ≤19 mm and ≥20 mm to ≤21 mm and ≥22 mm (Lee, 2003; Saeed et al., 2014). The amplification of *mec*A gene is prescribed as a gold standard in the detection of this resistance (Melo et al., 2014; Morrissey et al., 2014).Subsequently, genotyping allowed to confirm only 35 (47.94%) MRSA from the 73 suspected MRSA based on AST basis. Previous studies reported an MRSA prevalence of 10.34% (Turutoglu et al., 2009) while we found a prevalence of 29.66% MRSA when compared to the number of *S. aureus* strains (N=118). This rate of occurrence in *mecA* gene suggests a high risk for transmission of AMR bacteria from milk or milk products to human populations (Kaszanyitzky et al., 2007; Turutoglu et al., 2009). Prevalence of β-lactam resistance genes was increasing in *S. aureus* isolates, where MRSA isolates possessed 16% concealed the mecA gene and many other responsible factors (Qu et al., 2019; Turutoglu et al., 2009). *In-vitro* and animal studies reported high cure rates for both methicillin-sensitive *S. aureus* (MSSA) and MRSA infections (Righter, 1987). Overall, 55.1% of all 1989 MRSA isolates (colonizing and infecting) were resistant to ciprofloxacin (Daum et al., 1990), which is now increasing exponentially. The presence of MRSA in bovine mastitis is a potential risk to other exposed cattle and farm workers, including veterinarians (Chandrasekaran et al., 2014; Kaszanyitzky et al., 2007). In general, the emergence and transfer of AMR bacteria or genetic determinants from animals to human populations *via* food chain is a growing concern (Chandrasekaran et al., 2014; Kaszanyitzky et al., 2007). The AMR to methicillin is due to the *mecA* gene, which encodes an alternative penicillin binding protein (i.e. PBPs such as PBP2) with decreased binding affinity to methicillin (Kaszanyitzky et al., 2007). In addition, homologs of less pronounced similarity to *mecA* (<70%) were found in *S. aureus* and *Macrococcuscaseolyticus* (Álvarez et al., 2011; Sakoulas et al., 2001; Tsubakishita et al., 2010)which are now named *mecB* and *mecC*, respectively (Ito et al., 2012; Sakoulas et al., 2001).Other parts of the *mec* gene complex

are *mecR1* and *mecI*, which encode a transcriptional repressor and a signal transduction protein involved in regulation of *mecA*(Ito et al., 2012). Meanwhile fluoroquinolones (e.g. CIP, levofloxacin) are well-established broad spectrum antibiotics with potent bactericidal activity against most common Gram-positive and Gram-negative pathogens (Naber et al., 2001). Among fluoroquinolones, CIP is one of the most widely prescribed to treat a variety of bacterial infections (Yang et al., 2010). Thereby, CIP, synthesized in 1981 as a second-generation antibacterial, was recently pointed out as the most consumed antibacterial agent worldwide and the fifth most commonly prescribed generic antibacterial in the USA (Acar & Goldstein, 1997; Staff, 2010). The excessive use, unnecessary administration, and consumption in irregular dose or with methods neither approved nor controlled by medical professionals, have undoubtedly contributed to the rapid advancement of bacterial resistance against CIP (Acar & Goldstein, 1997; Hart & Kariuki, 1998).

Current study presented eco-friendly green route of synthesis to synthesize nanomaterials i.e. nanomaterial A, nanomaterial B, nanomaterial C and nanomaterial D to combat MDR pathogenic strains that cause mastitis in cattle.

In this study, XRD analysis presenting the crystalline size and nature of green synthesized nanomaterial A, CS-NPs coated TiO_2 NPs. **Figure 5. 1A** indicated the XRD profile of, TiO_2 NPs. XRD pattern of TiO_2 results represents the (101), (004), (200), (105), (211) and (204) plane indices that are corresponding to crystalline anatase phase were in accordance with Kubacka et al (Kubacka et al., 2012).While SEM findings were also similar to Kubacka et al and the size of chitosan NPs 19-25nm, TiO_2 NPs 35-50nm and CS-NPs coated TiO_2 NPs with size ranging from 65-75nm (Kubacka et al., 2012). In the UV-visible analysis, absorbance spectrum ofgreen synthesized TiO_2NPs consists of two bands, one at around 220nm and other band around 320nm.The band around 220nm is assigned to tetra-hedral isolated Ti present in the sample and the band around 300–400nm arises due to charge-transfer from the valence band (mainly formed by 2p orbitals of the oxide anion) to the conduction band (mainly formed by 3d t_{2g} orbitals of the Ti^{4+}cations). This band further confirms the existence of the anatase phase of TiO_2(Qian et al., 2011; Saravanan et al., 2018). An obvious red shift towards the Vis portion of light could be attributed to addition of chitosan contents, which possesses the small band gap value. This improvement in UV-Visible light absorption is demonstrating

that the major portion of solar light could be successfully utilized. In case of CS-NPs coated TiO_2NPs considerably improvement was observed in absorption spectrum in UV-Vis light region. An obvious red shift towards the Vis portion of light could be attributed to the addition of chitosan content which possesses the small band gap value (Saravanan et al., 2018).

FTIR investigation of CS-NPs coated TiO_2NPs is shown is **Figure 5.5C**.FTIR spectrum of pure TiO_2 exhibited the emergence of absorption characteristic peaks at 3408cm^{-1} is belonged to superposition of the hydroxyl groups while FTIR spectrum of the chitosan exhibits a sharp absorption peaks for 3423 cm-1 and 1636 cm-1 were related to availability of free –OH group of water molecule and C=O carbonyl moieties groups. Our results of characterization were in accordance of reported work(Alagumuthu& Kumar, 2013; Saravanan et al., 2018). The Zeta potentials of TiO_2 NPs, chitosan and CS-NPs coated TiO_2 NPs were −150.5 ± 0.8, 75.6 ± 1.0, and 95 ± 1.65 mV, respectively. The Zeta potential of prepared CS-NPs coated TiO_2 NPs were 95 ± 1.65 mV. These results provided evidence of successful coating of chitosan on the surface of TiO_2 NPs and suggested that the samples were stable during the storage period. The interaction among chitosan and TiO_2NPs in water solution was possibly promoted by the electrostatic force as chitosan carried positive charges, whereas TiO_2 NPs were negatively charged. Furthermore the amine groups of chitosan were protonated to ammonium thus adding the positive charges to chitosan (Patil et al., 2007). This phenomenon facilitated the surface coating of TiO_2 by chitosan and also prevented the aggregation of CS-NPs coated TiO_2 NPs (**Figure 5.6**).The encapsulation efficiency of CS-NPs coated TiO_2 NPs in the CS system was found as 85% ± 1.59. Hanna and Saad also reported good encapsulation efficiency of CIP inside hydrogel made up of chitosan (Hanna & Saad, 2019).

Interestingly, synthesized formulation worked against pan drug resistant *E.coli* and killed this resistant strains zones of observation were quite promising as seen in **Figure 5.7C**. All of three nano formulations are effective against PDR *E.Coli*but the most potent activity was noticed against CS-NPs coated TiO_2 NPs, previous studies reported antibacterial potential of TiO_2 and chitosan (Haldorai & Shim, 2014; Jiang et al., 2013) .Data of zones of inhibition is presented in **Table 5.3**. MIC values of CS coated TiO_2 NPs was found to be 0.78µg/ml which was lowest among all the nanomaterials tested against microbes causing mastitis.Based on

the above results it could be observed the prospective enhancement in antibacterial activity of proposed CS-NPs coated TiO_2 NPs as shown in **Figure 5.8**. The superior antimicrobial activity of the CS-NPs coated TiO_2 NPs is also evidenced by the growth curve, which exhibited stronger antibacterial ability against PDR *E. coli*. The antibacterial ability of chitosan was higher than that of TiO_2 NPs during the first few hours. However, the difference became insignificant over the following 5 hours. Thereafter, TiO_2 NPs exhibited higher activity than the chitosan (Haldorai & Shim, 2014; Jiang et al., 2013).

The synthesized nanomaterials were found nontoxic to red blood cells of cow as all formulations at all tested concentrations did not lyse red blood cells as shown in **Figure 5.9** ,results were in accordance of previous findings (Mohammadi et al., 2019).Results indicate that the cell viability remain maintained with the increase in concentrations of various prepared nanoformulation and particularly CS-NPs coated TiO_2 NPs didn't show any cytotoxicity on the BMGE cell line. Celecoxib was taken as positive control and significantly reduced cell viability at tested concentration ranges while PBS as negative control. All findings clearly suggest non toxicity of CS-NPs coated TiO_2 NPs may be attributed to controlled release of TiO_2 and coating of chitosan biopolymer (Malvindi et al., 2014; Mohammadi et al., 2019).

It is evident from the results (**Figure 5.11**) CS-NPs coated TiO_2 NPs completely lysed the MDR *E.coli* cells and lost their integrity. Moreover it was observed that shape of bacillus was no more maintained so become agglomerated which may became the ultimate cause of cell death (Banerjee et al., 2010).A double-staining (PI/Annexin V) method and calculated the number of alive cells by a statistical gating approach using FACS before and after treating *E.coli* strains by CSNPs coated TiO_2 NPsat MIC (0.78 µg/mL) at 37 °C and at various intervals of time (i.e. 0 hrs, 6 hrs) **(Figure 5.12)**. Such assay aims to determine both the necrotic death (by PI staining) as well as the early and late apoptosis (by AnnexinV) and ultimate death in the selected populationdensity (Hussain et al., 2012). Thereby, the death rate was negligible and late apoptosis (1.98% ± 0.03) in untreated cells (NC) **(Figure 5.12A)**, whereas the late apoptosis was found 55.79 % ± 1.52 after 6 hrs **(Figure 5.12 B)** of incubation after treatment with the nanoformulation (Vanhauteghem et al., 2019).

Nanomaterial B of the current study, XRD technique was used to examine the crystal phases, and the crystallinity of the green synthesized nanomaterials. The main peaks found in CeO_2 NPs were matched with previous studies (Arumugam et al., 2015)**(Figure 6.1a)**, CIP-CeO_2/CS NPs **(Figure 6.1c)** and CeO_2/CS NPs **(Figure 6.1d)** correspond to Bragg reflections with 2θ values of 28.6, 33.02, 47.4, 55.3, 59.01, and 69.4. These Bragg reflections were identical based on their orientations and were respectively indexed to (111), (200), (220), (311), (222), (400) crystal planes of cubical structure typical found in NPs CeO_2[NPJCPDS34-0394].XRD of CS showed a signal at 2θ = 19.63° (220) **(Figure 6.1b)**. The amorphous nature of CS appeared clearly in the spectrum and has been obtained most likely during the intercalation of bulk chitosan with TPP. The location of the peaks was compared to literature values and the presence of CeO_2/CS NPs was confirmed. The diffraction peaks were well-defined with high intensity and narrow width which indicates that the resulting biosynthesized NPs were highly crystalline. Further, no reflection related to any impurity was detected in the pattern, up to the detection limit of the XRD diffractometer, which defined the prepared NPs as pure. Also, the data strongly suggest that CS incorporation in CeO_2 NPs did not change the crystallinity of the composite. This information is confirmed by Lin et al. who observed the same crystalline structure of the CeO_2 microspheres in presence or absence of CS (Lin et al., 2015). However, the CeO_2/CSnanocomposite **(Figure 6.1d)** displayed a higher intensity spectrum compared to that of CeO_2 NPs **(Figure 6.1a)**.

The average crystallite size of NPs was found to be $\sim 7.9 \pm 1.3$ nm, $\sim 10.63 \pm 1.4$ nm, $\sim 5.9 \pm 0.09$ nm, $\sim 7.1 \pm 0.2$ nm in CeO_2 NPs, CS NPs, CeO_2/CSNPs, and CIP-CeO_2/CS composite respectively, based on the Debye-Scherrer's equation centered about most strong diffraction signal of 28.6° (111). Interestingly, it is worth noting that the small sized nanostructure of fabricated samples was shown be very effective for inactivation of bacterial growth (Uzair et al., 2020). Thereby, SEM micrograph of CeO_2 NPsdepicted some mixed small fluffy, spherical as well as few elongated edges of particles, which were extremely amassed and agglomerated **(Figure 6.2A)**. The SEM micrograph of CS **(Figure 6.2B)** exhibited less agglomerated spherical particles than CeO_2 NPs, suggesting the anti-aggregation role of CS when coated into CeO_2 NPs **(Figure 6.2C)**, most likely because CS enhanced the dispensability in the solution. The SEM micrograph of CIP-CeO_2/CS revealed

less agglomerated secondary particles with large grooves and voids **(Figure 6.2D)**. These materials with huge voids are beneficial for the attachment of foreign materials and are then expected to contribute to enhance the antibacterial activity (Uzair et al., 2020).

Meantime, elemental mapping, and quantitative composition of the same fabricated nanomaterials was investigated. As expected, EDX spectrum of CeO_2 NPsindicated the peaks of O, C and Ce **(Figure 6.2A and Table 6.1)**. Also, EDX spectrum of CS displayed peaks of O and C **Figure 6.2B and Table 6.1)**. The presence of O, C and Ce in the EDX spectrum of CeO_2/CS NPs **(Figure 6.2C and Table 6.1)** and F-CeO_2/CS NPs**(Figure 6.2D and Table 6.1)** demonstrated that the nanohybrid has been prepared successfully. Peaks related to C did arise due to the depositing sample on carbon tape. Quantitative elemental compositions of the prepared samples were summarized in **Table 6.1**. A previous study observed different amount of elements in Ce02 NPs such as Cerium 52.52% Carbon 24.60% and Oxygen 21.50% in CeO_2 film containing chitosan (Tripathi et al., 2019). The bottom-up approach, in which the metal ions could be reduced to synthesize nanoparticles presence of capping ligands, preferably used .green synthesis is gaining more attention instead of the physical and chemical synthesis methods. There are many side effects reported by employing chemical method for the synthesis of NPs including consumption of toxic compounds (Uzair et al., 2020).In the present study natural seeds of black cardamom reduced to cerium oxide NPs and chitosan biopolymer reported in many studies for biocompatible and biodegradable used for encapsulation via simple ionic gelation method using even acetic acid (safe organic solvent) for acidic media(Mohandas et al., 2018). Further, the TEM micrograph of CeO_2 NPs showed mixed quasi-spherical particles and some elongated particles **(Figure 6.3A)**. TEM micrographs of CS **(Figure 6.3B)** and CeO_2/CS NPs **(Figure 6.3C)** clearly displayed round spherical NPs. The TEM micrograph of CIP-CeO_2/CS NPsdepicted agglomerated spherical morphology of secondary particles **(Figure 6.3D)**. These TEM data are consistent with our previous SEM analyses. In present study spherical morphology was reported similarly the literature also confirmed the spherical shape and nano size of CeO_2 NPs (Moon et al., 2007). The average diameter of CeO_2 NPs, CS NPs, CeO_2/CS NPs and CIP-CeO_2/CS NPs ranged from ~6-10 nm which was also confirmed by XRD analysis. The average crystalline size was estimated as 24 nm by XRD analysis and 5 nm for spherical structure using TEM

studies for CeO_2 NPs(Moon et al., 2007).The average particle size (PS) was found in the present study was 45nm ±0.87 nm, 35±1.0 nm, 65±0.37nm and 40± 0.91 nm in (A) CeO_2 NPs, (B) CS NPs, (C) CeO_2/CSNPs, and (D) CIP-CeO_2/CS composite respectively.

Various phytochemicals present in these extracts are considered to provide the action of capping and stabilizing agents that aid the formation of CeO_2 and CeO_2/CS NPs (Iqbal et al., 2020a). Substance-specific vibrations of the molecules lead to the specific signals obtained by IR spectroscopy in the range of 400–4000 cm^{-1}. Consistently, a prominent peak attributed to hydroxyl (-OH) group is observed in the wavelength range 3500-3200 cm^{-1} in all spectra **(Figures 6.4a-6.4f)**, which is an important functional group of phenolic compounds(Jamila et al., 2020). In plant **(Figure 6.4.a)**, characteristic FTIR signals at 1634 cm^{-1} and 1050 cm^{-1} belong to NH_2 and C=O stretching vibrations from amine group and butyl group (Acar & Goldstein, 1997; Arumugam et al., 2015), respectively. In CeO_2 NPs **(Figure 6.4b)**, the spectral region between 949-517cm^{-1} revealed bending vibrations of Ce–O and O–Ce–O (Leung et al., 2015), which confirms the successful formation of CeO_2 NPs. In CS NPs **(Figure 6.4c)**,CIP-CeO_2/CSNPs **(Figure 6.4e)** and CeO_2/CSNPs **(Figure 6.4f)**, the FTIR peak at 1264 cm^{-1} is assigned to the bending vibrations of C–C–C from ketone (Acar & Goldstein, 1997; Zafar et al., 2020), whereas the signals at the spectral region 1625-1640 cm^{-1} indicate NH_2 vibrations. Also, in F-CeO_2/CSNPs **(Figure 6.4e)**, the peaks in the spectral region of 712-509 cm^{-1} indicate the new surface Ce-C-F linkage, that is known to be very beneficial for efficient antibacterial activity (Staff, 2010). In CIP **(Figure 6.4d)**, the FTIR signals observed specifically at 1711 cm^{-1} and 1613 cm^{-1} are associated with C=O and C–H vibrations, respectively. The peak centered at 1019 cm^{-1} is ascribed to C–F bending vibrations as shown in the **Table 6.2**(Sasikumar, 2013; Zafar et al., 2020).

Zeta potential is the electrical potential at the slipping plane (i.e. interface which separates mobile fluid (e.g. water) from fluid that remains attached to the surface) .In the previous study chitosan-coating reaction, the zeta-potential was measured as +50 mV, suggesting that chitosan has the ability to stabilize cerium system and caused increase in dispersity(Zhao, 2018).Although CeO_2 NPs showed an unstable stability with the negative ZP value of -123 ± 1.58mV **(Figure 6.5a)**. CS NPs showed a high stability with a positive ZP value of +45± 0.12 mV **(Figure 6.5b)**. CeO_2/CSnanocomposite showed an excellent stability with a ZP of +62 ±

0.74 mV **(Figure 6.5c)**. CIP-CeO_2/CSdrug nanocarrier showed the best stability with a ZP of +110 ± 0.65mV **(Figure 6.5d)**. Thus, since the negative zeta potential value shifted from negative to positive zeta potential in the presence of NH_2 groups of CS, and in water the surface charge was clearly influenced by the surface coating by CS. This is in accordance with previous studies (Sendra et al., 2017).

The encapsulation efficiency of CIP-CeO_2/CS NPs was calculated 75% ± 2.08, which confirmed successful encapsulation of biocompatible polymer chitosan to stabilize the metallic oxide nanoparticle CeO_2 NPs and reverse its polarity to assess its antibacterial activity against MRSA strains. Interestingly, CIP-CeO_2/CSNPs presented the most significant effect by forming the largest ZI of 12 mm ± 0.45 and 17 mm ± 2.89 against MRSA at MIC and 2MIC values, respectively **(Figure 6.8A and 6.8B)**. Thus, the antibacterial activity of the tested NPs was concentration dependent. Other pure nanomaterials exhibited inherent antibacterial activities but were not as effective as CIP-CeO_2/CSNPs **(Table 6.4)**. Importantly, OX, FOX and CIP pure antibiotic were not exerting an antibacterial activity onMRSA (all the strains resistant to Oxoid disc of CIP 5μg, OX 1 μg, FOX 30μg) at their MIC values.The excellent anti-MRSA activity exerted by CIP-CeO_2/CSNPs, compared to CIP alone on mecA-positive MRSA can be explained by the size, the specific surface area, the polar surface, the morphology and the cross-linking of doped materials (e.g. CS). Moreover, electrostatic attraction between negatively charged bacterial cells and positively charged CIP-CeO_2/CSNPs, as confirmed by zeta potential charge value 110±0.65mV, is crucial for the antibacterial activity. Such interaction is not only able to inhibit the bacterial growth but also generate ROS, which molecular mechanism is known to lead to MRSA cell death (Burello & Worth, 2011; Xia et al., 2008). Also, it has been shown that the growth of the Gram-positive bacterium *S. epidermidis* was affected more by the CeO_2 NPs treatment as compared to the Gram-negative *P. aeruginosa*(Arumugam et al., 2015). Our data with CIP-CS based nanohybrid strongly suggest an enhanced antibacterial mechanism thanks to the incorporation/surface coating of CS to CeO_2 NPs by ionic gelation method and the CIP conjugation which penetration into the bacterial cells is enhanced considering the thick cell wall of resistant MRSA isolates (Assali et al., 2017).

Taken together, the greenly synthesized CIP-CeO_2/CSNPs showed brilliant antibacterial activity against MRSA strains and thus, provided an alternative treatment therapy to treat *S. aureus* -induced mastitis infection which remains a challenge for veterinarians (Batista et al., 2013; Kannan & Sundrarajan, 2014).

Expectedly, the morphological changes occurred MRSA isolatestreated by CIP-CeO_2/CSNPsat MIC (8 µg/mL) when monitored by SEM **(Figure 6.10)**. The negative control (untreated MRSA) showed round and smooth MRSA morphology identical to what observed at 0 hrs after treatment by CIP-CeO_2/CSNPs**(Figure 6.10a)**. Slightly deformation was visible after 4 hrs in the spherical structure of treated-MRSA **(Figure 6.10b)**, which was accentuated at 8 hrs **(Figure 6.10c)** to reach an abrupt change at 12 hrs **(Figure 6.10d)**. At 12 hrs post-treatment, the drastic MRSA morphological change suggested typical wrinkled lysed cells releasing their cytosolic content which demonstrated the potent antibacterial effect of the new developed CIP nanofromulation(Huang et al., 2017). This effect is most likely mediated through the electrostatic interaction between the positively charged NPs and the negatively charged MRSA cell wall, which subsequently induce ROS species and ultimately cause inhibition of bacterial cell growth cell death free radical stress is sufficient enough (Saravanakumar et al., 2018; Wang et al., 2014).

To further strengthen the antibacterial potential of nanomaterial B (CIP-CeO_2/CSNPs) double-staining (PI/Annexin V) method of flow cytometer and calculated the number of alive cells by a statistical gating approach using FACS before and after treating MRSA strains with CIP-CeO_2/CSNPsusing MIC (8 µg/mL) value at 37 °C for various intervals of time (i.e. 0 hrs, 6 hrs, and 12 hrs) **(Figure 6.11)**. Such assay aims to determine both the necrotic death (by PI staining) as well as the early and late apoptosis (by AnnexinV) and ultimate death in the selected populationdensity (Hussain et al., 2012). Thereby, the death rate was negligible (0.9% ± 0.62) in untreated cells (NC) **(Figure 6.11A)**, whereas the death rate increased in a time dependent manner, with 1.23% ± 0.52 , 40.33% ± 1.79 ,87.04% ± 3.92 after 0hrs **(Figure 6.11B)**, 6 hrs **(Figure 6.11C)** 12 hrs **(Figure 6.11D)**, of incubation after treatment with the CIP-Nanoformulation (Vanhauteghem et al., 2019).

Flow cytometry is a rapid and quantitative method for the analysis of membrane disruption analysis after antimicrobial treatment, and was used to reveal antibiotic-induced changes in

microbial energy metabolism (Maglica et al., 2015). The PI (red) fluorescent dye, which is not cell wall permeating, is generally used to detect necrotic dead cells in the population (García-Saucedo et al., 2011; Maglica et al., 2015). It was clearly observed a shift from AnnexinV-stained cells at 0 hrs after treatment to a mixed of AnnexinV/PI stained cells 6 hrs after treatment with CIP-nanoformulation at MIC **(Figure 6.11C).** It can be observed that CIP-CeO_2/CSNPscompromised the cell wall integrity of MRSA cells, thereby favoring the PI permeability and uptake which led to intercalation of PI in the dsDNA and the shift in PI fluorescence. These findings are consistent with previous studies regarding the toxicity of nanomedicines against bacteria. Indeed, Omolo et al. recently reported that polymeric-coated drug loaded nanovesicles had caused $98.5 \pm 1.49\%$ death in the selected population against MRSA strains (Omolo et al., 2018).

It was found that bovine cells showed concentration dependent viability at MIC excellent viability was found and by decreasing concentration cells become more viable as described in Figure 6.12. Only green synthesized CeO_2 NPs had a minimal enhanced cytotoxicity compared to that of CIP-CeO_2/CSNPs and CS NPs ($p<0.05$). Yet, a previous study reported that CeO_2 NPs tested in Jurkat human T lymphocytes showed no effects on the viability of cells and were found nontoxic (Caputo et al., 2017). Interestingly, CIP-CeO_2/CSNPs and CS NPs had very similar negligible cytotoxicity ($p>0.05$) and since CS NPs are known to be biocompatible and safe (Caputo et al., 2017), we can conclude that CIP-CeO_2/CSNPs as a safe therapeutic agent. Hence, potential hemolytic activity of CeO_2 NPs, CSNPs, CeO_2/CS NPs, and CIP-CeO_2/CSNPs using hemolysis assay on the RBCs of cow **(Figure 6.13)**.The data revealed negligible hemolytic activity of CIP-CeO_2/CSNPs at the MIC value (8 μg/mL) compared to the positive control triton 100X 9 (7% viable RBCs) While CeO_2 NPs, CeO_2/CS NPs, CIP and CSNPs also did not induce hemolysis at various concentrations. CS NPs was even meaningfully not different from PBS (99% viable cells) used at NC ($p>0.05$). According to the criterion in ASTM E2 S24-08 standard percent hemolysis > 5% indicates that synthesized CIP-CeO_2/CSNPs causes no damage to the RBCs (Choi et al., 2011). Previous studies reported CS as nontoxic and hemocompatible making it highly useful for biomedical applications such as in antimicrobial delivery metallic-based nanocarriers thanks to its good interactions with metal oxide (Guibal, 2004).

Altogether, greenly synthesizedCIP-CeO_2/CSNPs are safe, noncytotoxic and hemocompatible to mammalian cells , favoring their potential use for *in-vivo* applications.

The ex-vivo antibiotic release profile of CIP from the CIP- CeO_2/CS nanocomposite were presented in **Figure 6.14**. The CIP- CeO2/CS nanocomposite exhibited the highest cumulative drug release (88± 1.09) at the 8hrs of incubation study (37 °C), which was compared to the control value of CIP (91± 1.14) alone during 24 hrs. As described previously by Rao and Diwan, initial rapid dissolution of the hydrophilic polymer occurs when the prepared formulation is in contact with the hydrated skin, resulting in the accumulation of high amounts of drug in the skin surface and thus leading to saturation of the skin with drug molecules at all times (Rao & Diwan, 1998). While in the present study, most of the drug crossed the skin barrier and released in the fluid of receptor compartment.

The drug release studies revealed that the cross-linked network structure could effectively reduce the antibiotic (e.g. ampicillin sodium) release rate and its burst effect following a Fickia diffusion (Cui et al., 2018) The important criteria for developing an effective delivery system is to ensure the sustained release of the encapsulated drug into the physiological environment(Shahriar et al., 2019). Burst release is a phenomenon commonly observed in delivery devices of different forms and compositions (Shahzad et al., 2015). The burst effect may be favorable for certain indications or applications such as wound treatment and/or targeted delivery(Choo et al., 2016) .The previous study conducted by Iqbal et al using physiological-like conditions (Shahzad et al., 2015), showed that chitosan had lower drug release rate and smaller amount of drug burst release compared to that of free drug.(Iqbal et al., 2020b).

In this study, XRD profile of green synthesized nanomaterial C,CIP-Ag/TiO_2/CS nanohybrid**(Figure 7.1f)** revealed the diffraction peaks of anatase TiO_2 (Lei et al., 2012), Ag (Bokare et al., 2013), and CS (Yang et al., 2010). It was observed that the diffraction peaks of this nanocarrier are shifted to high angle region, which indicated that foreign material i.e. CS and CIP inserted the stress on the lattice of host material (Ag/TiO_2). It is also noted that leading peak of Ag at 38.18° overlapped with the Peak of TiO_2 at 38° and suppressed the signal of TiO_2.The crystalline particle size of nanoformulations is measured about the peaks centered at (101) of anatase TiO_2 (Lee et al., 1999) and (111) of Ag by using the Scherrer's

equation. The PS and the crystalline size of the newly developed drug nanocarrier were 19 nm± 1.98 and0.9821±0.76 Å in average and all other characterized NPs. XRD pattern of TiO_2NPs**(Figure 7.1a)**represented the(101), (004), (200), (105), (211) and (204) plane indices that corresponds to crystalline anatase phase as supported by (JCPDSNo. 84-1285) (Lei et al., 2012) results were in accordance with Lei et al findings of XRD spectrum.

The XRD peaks of AgNPs **(Figure 7.1b)**shows the (111), (200), (220), and (311) crystallographic planes at 2θ ° = 38.18°, 44.25°, 64.72°, and 77.40°leading to face-centered cubic metallic silver crystals (Georgekutty et al., 2008). It can be inferred that Ag ions (Ag^+) are strongly reduced by the *M. concanensis* leaf extract during the synthesis process. Any diffraction peak related to silver oxides was not observed. In Ag/TiO_2nanocomposite**(Figure 7.1c)**,the characteristic XRD peaks show the anatase phase of TiO_2 and the face-centered cubic silver content without any sign of any other diffraction peaks as impurity (Bokare et al., 2013). In CSNPs **(Figure 7.1d)**, the characteristic XRD peak was indicated at 21.8° crystallinity and purity of chitosan in the nano structure (Zafar et al., 2020).

TiO_2NPs, AgNPs and Ag/TiO_2 nanocomposite the nanostructures showed uniform round spherical morphology (Bokare et al., 2013) as illustrated in FESEM micrographs in the **Figure 7.2A, 7.2B and 7.2C** respectively. The particle size of TiO_2NPs, AgNPs, Ag/TiO_2 nanocomposite CSNPs and CIP-Ag/ TiO_2/CS nanohybrid, showed from 25-55 nm, 22-40 nm, 19-35 nm and 19-75 nm, respectively. This also tentatively confirms the particles size observed from XRD analyses. Agglomerated and spherical AgNPs were well dispersed throughout the surface of TiO_2 **(Figure 7.2B)**.Also, it can be remarkably observed from the Ag/TiO_2 nanocomposite that AgNPs are incorporated on the surface of TiO_2 **(Figure 7.2C)**. It was noted that there is no distinction between the TiO_2NPs and AgNPs in Ag/TiO_2 nano-composite. Eventually, it was clearly seen that the biopolymer CS anchored the whole surface of spherical Ag/TiO_2 nanocomposite **(Figure 7.2D)**. After CS grafting, it was perceived that AgNPs remained segregate onto TiO_2 surface **(Figure 7.2D)**. EDX analysis was done to investigate the elemental distribution of the four nanostructures **(Figure 7.2)**. **Figure 7.2A** displayed the Ti and O signals supporting the TiO_2 NP synthesis. **Figure 7.2C** revealed the peaks corresponding to the Ti, O and Ag in Ag/TiO_2nanocomposite. It was cleared from the signal that 1.2 wt% nominal content of Ag was closed to its stoichiometric value of 2.0 wt%

solution of AgNPs exploited for the fabrication of Ag/TiO_2 nanocomposite. The signal of C in Ag/TiO_2nanocomposite can be ascribed to the carbon substrate/grid. No additional peaks were observed which indicated the purity level of the synthesized nanoformulations **Figure 7.2B** showed elemental profile of AgNPs which determined the sharp signal of Ag element. Finally synthesized CIP-Ag/ TiO_2/CS nanohybrid elemental spectrum was shown in the **Figure 7.2D** which displayed the peak signals corresponding to TiO_2, Ag, TiO_2/Ag and CS, other peaks or modifications in signal intensity may be attributed to incorporation of CIP.

The TEM results confirmed the outcomes of FESEM analysis, as shown in the **Figure 7.2E and 7.2F** round and spherical morphology was depicted, while purity of the newly developed CIP-TiO_2/Ag/CS nanohybrid was observed by SAED as shown in the **Figure 7.2G**.The particles size of Ag/TiO_2 composite and CIP-TiO_2/Ag/CS nanohybrid was 47 -75nm and 20 - 80nm respectively (Yang et al., 2010). The SAED pattern of the prepared CIP-Ag/TiO_2/CS nanohybrid demonstrated Ag/TiO_2 contained a face-centered cubic crystalline phase. SAED pattern further exhibits discrete circular diffraction rings corresponding to anatase phase of TiO_2 NPs. Moreover SAED showed less agglomeration which further supported the facts that phytocompounds of leaf extract of moringa and chitosan contribute their role as previously explained in the literature by Senthilkumar et al. 2019, chitosan and silver nanoparticles were obtained by reducing *T. portulacifolium* extract and less agglomerated NPs were revealed by TEM analysis due to phytocompounds (Senthilkumar et al., 2019).Obtained polycrystalline diffraction rings of fabricated spherical NPs were in agreement with previous studies reported by Hussein et al 2021and Mohamed et al 2020 (Hussein et al., 2021; Mohamed, 2020).

FTIR spectra of TiO_2NPs, AgNPs, CSNPs, Ag/TiO_2 nanocomposite, unloaded Ag/TiO_2/CS Nanohybrid and CIP-Ag/TiO_2/CS Nanohybrid are displayed in **Figure 7.3.** The FTIR spectrum of pure TiO_2**(Figure 7.3a)** exhibited emerging characteristic peaks of absorption at 3408cm^{-1} which belongs to superposition of the hydroxyl groups (O–H) that evidences the coordination of water molecule to Ti^{4+}cations. The absorption band cantered at 2928 cm^{-1} is assigned to C–H stretching vibrations. The signature at 1603 cm^{-1} can be attributed to C=O stretching vibrations due to the butyl group, organic species as starting precursor solutions and adsorbed water molecules on the surface of the nanoformulations. The absorption band in the range of 766-610 cm^{-1} is related to the Ti – O bonding that authenticates the formation of

TiO_2(Li et al., 2018). The FTIR spectrum of AgNPs **(Figure 7.3b)** revealed the characteristic peak at 3424 cm^{-1} corresponding to O–H stretching vibrations of adsorbed water molecules. The peaks at 2919 cm^{-1} and 2841 cm^{-1} indicated alkanes (C–C) stretching vibrations. The signature that appeared at 1625 cm^{-1} is attributed to bending vibrations of alkene group (Li et al., 2018). The peak at 1099 $cm^{-1}$was assigned to the asymmetric and symmetric C=O stretching vibrations due to carbonyl group present in leaf extraction. Alkanes, alkenes and carbonyl groups of leaves extraction are mainly involved in the reduction of Ag^+ to AgNPs. The FTIR spectrum of TiO_2/Ag nanocomposite **(Figure 7.3c)** displayed bands ranges in the region from 800 to 530 cm^{-1}that are attributed to Ti–O stretching mode and Ti–O–Ag/Ag–O–Ti linkage (Bokare et al., 2013). The FTIR spectrum of CS **(Figure 7.3d)** exhibited a high absorption peak of 3423 cm^{-1} and 1636 cm^{-1} due to the availability of a free –OH group from water molecules, amino group and a C=O carbonyl moiety group. The value at 1018 cm^{-1} corresponded to the throttle vibration of the C–O–C bond of epoxy or alkoxy. The signature at 1269 cm^{-1} and 1419 $cm^{-1}$was due to C–O and CH–OH bonds (Li et al., 2018). The FTIR study of unloaded Ag/ TiO_2/CS **(Figure 7.3e)** characteristic peaks of metal components and CS differential peaks were prominently showed in the spectrum. Moreover the binary junction of Ti –O and Ag metals was also displayed in the spectrum. The FTIR of CIP-Ag/ TiO_2/CS nanohybrid **(Figure 7.3f)** showed peaks at around 1010 cm^{-1} and 1600 cm^{-1} that are correlated with aromatic bending and stretching. It is clear that the absorption peak centered at 596 cm^{-1} is due to the metal oxygen metal (Ti–O–Ag) mode of vibration.

Zeta potential is the capacity of suspended particles to affect their stability and the zeta potential greater than 30mV or less than-30mV can be distributed permanently in the medium (Zhao, 2018).The zeta potential values of AgNPs **(Figure 7.4a)**, TiO_2NPs **(Figure 7.4b)**, TiO_2/Ag nanocomposite**(Figure 7.4c)** and CSNPs **(Figure 7.4d)** were -110, -123 mV, -200 mV and 35.12 mV, respectively. The newly synthesized CIP-Ag/ TiO_2/CS nanohybrid showed good stability with a zeta potential value of 67.45mV **(Figure 7. 4e)**.It is worth mentioning that in relation to adhesion of NPs with bacteria, the surface charge or zeta potential is crucial since it was demonstrated that positively charged NPs will interact with negatively charged bacteria, and when these bacteria comes near positively charged NPs this

ultimately led to the penetration and destruction of bacteria (Hoseinzadeh et al., 2017; Wang et al., 2017).The encapsulation efficiency of CIP-TiO_2/Ag/CS nanohybrid in the CS system was found as 90% ± 2.07. Hanna and Saad also reported good encapsulation efficiency of CIP inside hydrogel made up of chitosan (Hanna & Saad, 2019).

Antibacterial activity by disc diffusion method as revealed by the zone of inhibitions of CIP-Ag/ TiO_2 /CS nanohybrid in the **Table 7.1**.On the basis of MIC determination, nanomaterial C was found proficient to inhibit the growth of MDR *E.coli* at lowest concentration 0.0512 µg/mL as shown in **Figure 7.5 A&B**.Enhancement of antibacterial activity was observed against *E.coli* and *S. aureus* when treated with titania nanoparticles co-dopped with silver nanoparticles in a previous study. Synergetic activity of the nanohybrid used as 10µg/ml and 20µg/ml concentration exhibited 7mm of zone of inhibition against both bacteria (Parvathi et al., 2020).In another study one-dimensional titanium dioxide (TiO_2) nanotubes (TNTs) doped silver (Ag) (% 5) were synthesized by two-step hydrothermal approach for evaluation of antibacterial studies. Disc diffusion method showed the zone of inhibition of nanoparticles against *E.coli* ATCC 25922 as 8mm when used as 25 µl suspension (10 mg ml-1) (Aydın et al., 2018). A study describes antibacterial and antifungal activity of chitosan PVA film encapsulated silver doppedtitania nanoparticles against various pathogenic strains. Significant zones of inhibition were observed, and they reported that chitosan and PVA improved antimicrobial activity due to their stability, mechanical strength and biocompatibility(Shende et al., 2018). By comparing results of present study to the previous literature, it is evident that green synthesized CIP-Ag/TiO_2/CS nanohybrid are strong antibacterial agents against MDR bacteria. Killing kinetic study of CIP-Ag/TiO_2/CS nanohybrid shows that after 6 hours of incubation growth of *E.coli* was inhibited as indicated in **Figure 7.6**. Results are compared with Silver/graphene oxide nanohybrid that inhibited the growth of pathogenic bacteria after 24 hours of incubation (Xiong et al., 2019). A study conducted by Li showed antibacterial attack of Ag NPs, TiO_2 NPs, Ag/TiO_2nanocomposite against MDR *E.coli* (Li et al., 2018) but activity was not as remarkable as observed in this study by the synthesized nanoformulations particularly CIP-Ag/TiO_2/CS nanohybrid halted the growth of *E.coli* within few hours of exposure. Current findings showed a mutual antibacterial activity of ciprofloxacin with the Ag/ TiO_2/CS composite. Previous study of Shahverdi and Colleagues

have observed improved antibiotic activity against the bacterial panel, using a combination of silver nanoparticles and FDA proven antibiotics (Shahverdi et al., 2007).

Morphology of MDR *E.coli* has been analyzed by FESEM and TEM before and after treatment with CIP-TiO_2/Ag/CS nanohybrid as noted in **the Figure 7.7 &7.8**. Before treatment intact, plump, and uniform cells are observed and after 6 hours of treatment with nanohybrid, it was indicated that cell membrane has been detached from cell wall, cytoplasm damaged and cell membrane disintegrated. In a previous study FESEM analysis of *E.coli* treated with Ag-TiO_2@PDA NRDs has been described, that showed the membrane damage of bacteria by these needle like nanorods and physical puncturing of bacterial cells. Various degrees of cell shrinkage have been reported (Guan et al., 2019). Flow cytometry analysis has been done to identify the rapid identification ofgreen synthesized nanomaterial C, CIP-Ag/TiO_2/CS nanohybrid internalized in the live bacterial cells. Results of nanohybrid show late apoptosis with 67.87% efficacy and early apoptosis with 32.13% efficiency as shown in the **Figure 7.9B**. Late apoptosis was due to the penetration of nanohybrid in *E.coli* cells. *E.coli* cells in the late apoptotic stage were sensitive to Annexin V-FITC dye showing the cell membrane damage and leakage of content that was confirmed by PI binding. Cell death caused by CIP-Ag/ TiO_2/CS nanohybrid shows late apoptotic attributes that confirm increased permeation of the *E.coli* cells by CIP-Ag/ TiO_2/CS nanohybrid,leading to cell harm or death. Results are comparable with a previous study in which TiO_2 @PDA NRDs have been designated as strong antibacterial agents with the ability of selectively bacterial membrane physical rupturing by Live/Dead Bacterial Viability fluorescence test (Guan et al., 2019). Late apoptosis occurred when nanohybrid penetrated in the *E.Coli*cells instigated death as PI dye is permeable to dead cells only(O'Brien-Simpson et al., 2016). The *E.coli* cells found in the late apoptotic stage as they were bind to Annexin V-FITC displayingimpaired and disturbed cell membrane while cytoplasmic contents released which was confirmed binding of PI with DNA. It was observed that cell death triggered by CIP-Ag/ TiO_2/CS nanohybrid mainly due to late apoptotic traits.

Ex vivo antibiotics release profile of ciprofloxacin from nanomaterial C presents the CIP release as (89± 2.43) after 8 hours of incubation that was compared to the control value of ciprofloxacin as (94± 1.97) during 24 hrs. Results show a burst release of CIP at 8 hours that

was followed by a sustained release in the next 24 hours. Findings of Shah and co-workers are in accordance with our findings as they described the release of moxifloxacin from chitosan nanocomposite.In another study drug release profile of ciprofloxacin HCl from ciprofloxacin-loaded CS nanoparticles has been studied at three different pH values. Small drug release was observed from chitosan nanoparticles and less than 12% drug was released after 96 hours. Amount of drug release was decreased by decreasing the pH. The free drug release was also evaluated by dialysis membrane and 100% of drug was permeated after 1 hour (Guan et al., 2019). Various studies reported the higher efficiencies of antibiotic loaded polymeric nanoparticles due to improved drug penetration in the bacterial cell, increased stability of drug due to conjugation with nanoparticles, and better drug delivery to the site of action (Fawaz et al., 1998).This study presented potent antibacterial activity of ciprofloxacin conjugated chitosan encapsulated silver titania nanohybrid against gram negative MDR *E.coli*. Gram-negative bacteria show resistance to antibiotics due to the cell wall in their structure. Some structures of the bacterial cell limit the penetration of the antibiotic. Gram negative bacteria have more negative charge on their cell wall that is the reason for chitosan adsorption on its cell wall and finally inhibiting the growth of bacteria (Sobhani et al., 2017). In a previous study strong antibacterial effects of chitosan on gram negative *E.coli* have been reported in terms of enzymes leakage (Sobhani et al., 2017; Xiao, 2021).

Previous study correlates with these findings, slow and sustained release of drug from the cross linked structure of polymers enclosing antibiotics was reported (Cui et al., 2018).The important requirements for designing an efficient delivery system is to ensure the continued and sustained release of the encapsulated drug to the biological system (Shahriar et al., 2019). The result has confirmed that the drug conjugated with Ag/TiO_2/CS nanoparticles and encapsulated in chitosan nanoparticles has improved stability in the acid medium and sustained and prolonged release of the drug. This stability and regulated release is due to chitosan encapsulation and most possibly due to the hydrophilic nature of chitosan. The antibiotic ciprofloxacin was trapped within the polymer matrix of chitosan, which supported the slow release of drugs through the diffusion process. Taken together, it was noted that burst CIP release at 8 hours, followed by a sustained release in next 24 hours. Shah and co-

workers have documented the continued release of moxifloxacin from nanocomposite of chitosan and their findings are in agreement with the current results (Shah et al., 2019).

The viability pattern using different concentration of synthesized nanoformulations exhibited in **Figure 7.11**.Similar results were reported, where chitosan considered as safe therapeutic agent due to nontoxic effect on cell lines (Campos et al., 2004). The current study deep-rooted the biocompatibility of synthesized nanoformulation for BMGE cells by displaying good viability pattern. Tomankova reported cytotoxic effect of Ag NPs in comparison with TiO_2 NPs (Tomankova et al., 2015) but in the current study chitosan nanoparticles encapsulation masks cytotoxic effects of these metals.

Green synthesized nanomaterial C, interact with RBCs of animals and findings were displayed in the **Figure 7.12**. Furthermore, study revealed that RBCs were viable and it was apparent that CIP-Ag/TiO_2/CS nanohybrid treated RBCs were more viable (98.23 %) caused no release of hemoglobin from RBCs when results compared with positive control Triton. Li et al 2008 had studies hemolysis of TiO_2 NPs (Li et al., 2018). Choi et al represented concentration and size dependent toxicity of Ag NPs and Ag NPs may cause hemolysis which were less than 20nm (Choi et al., 2011). According to the criterion in the ASTM E2524-08 standard, percent hemolysis >5% indicates that the test nanoparticle causes damage to RBCs. Hence, green synthesized CIP-Ag/TiO_2/CS nanohybrid showed excellent viabilities of RBCS and proposed hemocompatibility, biocompatibility and nontoxicity of CIP-Ag/TiO_2/CS nanohybrid for livestock animals.

In this study novel nanohybrid system, green synthesis nanomaterial D, CIP-Ag/TiO_2/ Fe_2O_3/ CS was designed by eco-friendly approach. *M. concanensis* leaves extract has been used to synthesize AgNPs, TiO_2 NPs, and Fe_2O_3. Wet chemical impregnation technique was used for incorporation of AgNPs onto the surface of TiO_2 and Fe_2O_3 nanomaterials and ionic gelation method was developed for CS encapsulation. These nanoparticles at low concentrations have the greatest antibacterial activity against drug resistant strains. The current study has synthesized new cheap, simple, and eco-friendly nanoparticles as a strong antimicrobial agent to treat mastitis causing infections and refining the worth of dairy yields.

Green synthesized nanomaterial D, was characterized by XRD for the analysis of purity and crystallinity. In the Figure**8.1** the XRD profile of synthesized nanomaterials, ciprofloxacin, and plant powder has been described. Ciprofloxacin exhibits the diffraction peaks at 2θ of 12^0, 20^0, 29^0,30^0,31^0,35^0,39^0 and plant powder exhibits irregular shaped peaks at 2θ ° = 19.5 and broader dominant peak at 29 expressed more prominently. Results show that Fe_2O_3 exhibit the characteristics peaks at 24°, 33°, 36° 41° 49°, 54° 58° 63° 64° corresponds to (012) (104) (110), (113), (024) (115), (112), (214), (300) were well matched with JCPDS Card No. (00-001-1053). The XRD patterns of silver nanoparticles exhibit peaks at 38.18°, 44.25°, 64.72°, and 77.40° corresponds to the crystallographic planes (111), (200), (220), and (311) and well matched with the previous findings (Georgekutty et al., 2008). The XRD of TiO_2 nanoparticles represents the (101), (004), (200), (105), (211), and (204) plane indices that corresponding to crystalline anatase phase as supported by JCPDSNo. 84-1285 (Lei et al., 2012). XRD profile of drug loaded chitosan encapsulated Ag/TiO2nano-hybrid system possesses the diffraction peaks of Ag, anatase TiO_2 (Lei et al., 2012) and chitosan. It is observed that the peak of Ag nanoparticles at 38.18° overlapped with the peak of TiO_2 nanoparticles at 38° and suppressed the signal of TiO_2. XRD patterns of CIP-Ag/TiO_2/ Fe_2O_3/ CS Ternary composite confirm the characteristic peaks of chitosan at 21.8^0, TiO_2 at 29^0, 44.2^0, Fe_2O_3 at 2θ ° = 33^0,36^0,49^0,54^0 and dominant signal of Ag NPs at 64^0 were observed in **Figure 8.1(h)**.

Surface morphology and size of nanomaterials have been analyzed by SEM and TEM. SEM analysis revealed the size of chitosan NPs as 23-30nm, Ag/TiO_2 NPs 25-40nm, Fe_2O_3 nanorods diameter of 2-6nm, and CIP-Ag/TiO_2/ Fe_2O_3/ CS Ternary composite ranging from 5-7nm. Spherical and agglomerated morphology was observed for both chitosan and Ag/TiO_2 hybrid. **Figure 8.2D** represents that in green synthesized CIP-Ag/TiO_2/ Fe_2O_3/ CS Ternary compositethat Ag NPs and $Fe_2O_3$are incorporated on the surface of TiO_2. Ag NPs are not integrated into the lattice of crystalline TiO_2 and chitosan anchored the whole surface of spherical Ag/TiO_2 / Fe_2O_3 nano-hybrid and selected drug. In the previous study Tomke, et aldescribed the SEM analysis of Fe_3O_4@ Chitosan –Ag nano-composite that shows the spherical morphology with an average diameter of 3–4 μm. Study explained the Ag nanoparticles uniform distribution with the size of 100nm on the surface of Fe_3O_4@ Chitosan

–Ag nanocomposite. EDX analysis shows the elemental distribution of synthesized materials which shows the signals of Ti, O, Ag, Fe and C that are supported by the findings of Tomke, et al., 2020 (Tomke & Rathod, 2020).

HR-TEM analysis was done to analyze the structure, size, and dispersion of materials. TEM image of $Ag/TiO_2/ Fe_2O_3$ showed mixed elongated nanorods which were consistent with FESEM findings. TEM image of Ciprofloxacin loaded $Ag/TiO_2/ Fe_2O_3/$ CS Ternary composite depicted nanorods shaped morphology with average diameter ranges ~6-10 nm as also confirmed by XRD analysis. The purity of CIP- $Ag/TiO_2/ Fe_2O_3/$ CS Ternary composite was presented by SAED. SEAD pattern shows the first ring that shows the combination of two different planes (111) and (200) and second ring shows the plane (220) and third ring that signifies plane of silver at (311) These diffraction peaks resemble the face-centered cubic structure of silver (JCPDS 04-0783). It is validated by TEM description that chitosan doping provides a supportive substrate that helps to avoid Ag nanoparticles aggregation. Results are well consistent with the results of Tomke, et al., 2020 (Tomke & Rathod, 2020).

FTIR spectra of synthesized nanomaterials were recorded in the range of 500–4000 cm−1 shows the peak patterns that appeared in the regions of 499 to 1074 cm−1 metallic oxide region and broad peaks appeared at 3450 cm−1 and 1650 cm−1 corresponds to –OH and NH_2 group stretching and bending vibrations mode. The FTIR spectrum of pure TiO_2 exhibits the emergence of absorption characteristic peaks at 3408cm^{-1} belongs to superposition of the hydroxyl groups (O–H) that is the evidence of coordination of water molecules to Ti^{4+}cations and signature at 1603 cm^{-1} can be attributed to and C=O stretching. The absorption band cantered at 2928 cm^{-1} is assigned to the C–H stretching vibrations. The absorption band in the range of 766-610 cm-1 is related to the Ti – O bonding that authenticates the formation of titanium dioxide. Literature studies revealed the FTIR peaks for TiO_2 nanoparticles at 800 and 450 cm^{-1} that is close to our data (Kumar et al., 2014). The band corresponding to the Fe-O stretching mode of Fe_2O_3 is observed at 560 cm−1.and 700cm-1. Absorption band at 571 cm−1 in a spectrum of Fe3O4 NPs observed in a previous study that closely matches with the current data (Nehra et al., 2018). The FTIR analysis of Ag nanoparticles interprets the characteristic peak at 3424 cm^{-1} corresponding to O–H stretching vibration of adsorbed water molecules. The peaks at 2919 cm^{-1} and 2841 cm^{-1} indicate alkanes (C=C) stretching

vibration. Signature appeared at 1625 cm^{-1} is attributed to bending vibration of alkene group (Li et al., 2018). In case of Ag/TiO_2 hetero system bands ranges in the region from 530 to 800cm^{-1} are attributed to Ti–O stretching mode and Ti–O–Ag/Ag–O–Ti linkage respectively corresponds with the previous findings. (Bokare et al., 2013). The FTIR spectrum of chitosan (Li et al., 2018) exhibits a high absorption peak of 3423 cm-1 and 1636 cm-1 due to the availability of a free –OH group and NH_2 moiety group of chitosan monomers molecules respectively. The characteristic amide I and II peaks at 1650 and 1600 cm^{-1} observed for chitosan in a recent study (Tomke & Rathod, 2020).The value at 1018 cm^{-1} corresponds to the vibration of the C–O–C bond of epoxy or alkoxy. The signature at 1269 cm^{-1} and 1419 cm^{-1} is due to C–O and CH–OH bonds. Peaks at around 1010 and 1600 cm^{-1} in nano-hybrid spectra have been correlated with benzene rings which indicates presence of Ciprofloxacin conjugation with metallic oxide ternary heterojunction. The absorption peak centered at 596 cm^{-1} is due to the metal oxygen metal (Ti–O–Ag) mode of vibration and Fe-O stretching mode was observed in the spectra. The peak at 1074 cm–1 is due to the stretching vibration Fe-Ti-Ag and the strong band below 700 cm–1 is assigned to Fe-O-Ti and Fe-O-Ag stretching mode. The peak at 1099 cm^{-1} represents asymmetric and symmetric C=O stretching vibration due to carbonyl group present in leaf extraction. Alkanes, alkenes and carbonyl groups of leaves extract encountered the reduction of Ag^{+}, Ti^{+} and Fe^{+3} to Ag, TiO_2 and Fe_2O_3 nanorods. The reduction in the intensity of all the peaks was observed in case of composites after the incorporation of Fe_2O_3 and Ti-O bond of TiO_2, which was found to be shifted to 525 cm^{-1} after the incorporation of chitosan and ciprofloxacin. The linkages further confirmed the blending of organic and inorganic materials which presents tight junctions of ternary composites.

In UV-Vis profile of TiO_2, the absorption edge relative to O^{2-}– Ti^{4+} responsible for charge transition at 300–390 nm in anatase TiO_2; according to well mentioned results in literature (Sajjad et al., 2009). It is observed in the absorption spectrum of chitosan NPs single band centered at 280nm. The band gap energies for plant 2.7, Fe_2O_3 2.4, drug 3.2 and CIP-Ag/TiO_2/ Fe_2O_3/ CS Ternary composite have displayed transition energies between 1.3 and 3.1 eVwhich are corresponding to the charge transition from O^{2-}– Fe^{4+} and O^{2-}– Fe^{3+} respectively .Having large band gap value (3.12 eV) of TiO_2; light absorption is restricted

only in UV region. Surface modifications of Ag/TiO_2 by incorporation of chitosan and ciprofloxacin could strongly enhance the absorption in whole UV-Vis region. The reduced band values in CIP- CIP-Ag/TiO_2/ Fe_2O_3/ CS Ternary compositeare noted. The clusters of Fe^{2+} and Fe^{3+} in different regions of host Ag/TiO_2 act as the electron trappers, firmly inhibited the recombination process and proliferate the absorption in visible region (Ho et al., 2014). These clusters are also responsible for generation of oxygen vacancies below the conduction bands of TiO_2 and reduced the band gap values of CIP-Ag/TiO_2/ Fe_2O_3/ CS Ternary compositesamples. In CIP-Ag/TiO_2/ Fe_2O_3/ CS Ternary composite integration of Fe_2O_3 is fruitful in absorption of light in visible region by existence of oxygen moieties, fast electronic transition properties and innovative connection between Ag–O-Ti-O–FeO is very supportive in the antimicrobial activity.

In this study, encapsulation efficiency of CIP-TiO_2/Ag/CS nanohybrid in the CS system was found as 94% ± 1.26. Hanna and Saad also reported good encapsulation efficiency of CIP inside hydrogel made up of chitosan(Abreu et al., 2012; Hanna & Saad, 2019). It was reported in the previous studies that antimicrobial activity can be increased by chitosan coated metal nanoparticles. Cationic charge of chitosan amino group combines with the anionic component of cell membrane of microbes like neuraminic acid, sialic acid and N-acetylmuramic acid. Chitosan inhibits the growth of microbes by chelating transition metal ions, enzyme inhibition and exchange with the medium. Antimicrobial activity increased due to the chitosan coated nanoparticles stability in aqueous media as compared to the pure metal nanoparticles as chitosan help to protect metal nanoparticles from aggregation (Nehra et al., 2018).

The synthesized CIP-Ag/TiO_2/ Fe_2O_3/ CS Ternary compositeshowed excellent antibacterial activity which predominantly depends on morphology, size, specific surface area, polar surface, and cross linking of doped materials. Moreover, electrostatic attraction between negatively charged bacterial cells and positively charged CIP-Ag/TiO_2/ Fe_2O_3/ CS Ternary compositeis a fundamental step for the antimicrobial reactions. This interaction is not only able to inhibit the growth of microbes but also induces the production of ROS, which ultimately leads to cell death(Burello& Worth, 2011; Xia et al., 2008).The growth of Gram-negative MDR *E.Coli* was prominently inhibited by the CIP-Ag/TiO_2/ Fe_2O_3/ CS Ternary

composite treatment as compared to Gram positive *S. aureus*as shown in the **Table 8.1**(Arumugam et al., 2015). Most importantly, the antibacterial activity of CIP-Ag/TiO_2/ Fe_2O_3/ CS Ternary compositewas improved significantly due to its unique morphological appearance as antibacterial activity principally depends on morphology (Irshad et al., 2017). Nano encapsulation of chitosan on the surface of Ag/TiO_2/Fe_2O_3 ternary heterojunction amplified antimicrobial potential by increasing concentrations against resistant strains of MRSA,MDR *E.coli* and *C.albicans*(Assali et al., 2017). The successful synthesis of CIP-Ag/TiO_2/ Fe_2O_3/ CS Ternary composite was confirmed by FTIR diffraction signals of ternary composite. The zeta potential value 85.26± 0.12 supported stability and super reactivity of ternary structure against the MDR pathogens. In the present study biogenic engineered CIP-Ag/TiO_2/ Fe_2O_3/ CS Ternary compositeshowed brilliant antibacterial activity against tested strains and launching an alternative therapeutic agent to cure mastitis which has been become challenge for both developed and under developing countries. (Batista et al., 2013; Kannan & Sundrarajan, 2014).

Experiments to evaluate the bactericidal effects of zero-valent iron and the theoretical mechanisms that lead to cell death have already been reportedas studied cell death of *E. coli*by cell membrane disruption after interaction with zero-valent iron NPs, implying the dissolved iron inactivation or amplified biocidal effects, as well as oxidative stress as pathways of cell death. Moreover study alsoreported that zerovalent iron nanoparticles, B.*subtilis*was found more tolerant to these nanoparticles than *E.coli* but it was communicated that bactericidal mechanism of these nanoparticles has not yet been expounded. Despite these findings, there is no consensus in the literature on the effect; another article published asserts that zero-valent iron had no negative impact on total bacterial abundance in microcosms (Nehra et al., 2018).

Nehra and co-worker reported that iron oxide NPs have antibacterial activity against *E. coli* that is dosage dependent and antifungal activity of Fe_3O_4 NPs was assessed which showed that iron (II, III) oxide NPs were synthesized with negative surface potential and chitosan coating to change the surface potential and functional group. Because the chitosan polymer contains a free hydroxyl group, it forms a strong hydrogen bond with the iron (II, III) oxide NPs (Nehra et al., 2018).

Kumar et al synthesized TiO_2 nanoparticles by *Hibiscus rosasinensis* flower extract exhibited potent antibacterial activity even at low concentrations as compared to chemically synthesized TiO_2 nanoparticles. These nanoparticles do not exhibit a mechanism of action (Kumar et al., 2014).

Yuan et al represented antibacterial studies of AgNPs synthesized by bio-molecule quercetin were evaluated against MDR pathogenic bacteria *P. acruginosa* and *S. aureus* that were isolated from milk of mastitis infected goats. The MICs values of AgNPs against *P. acruginosa* and *S. aureus* were evaluated as 1 and 2 μg/mL, respectively. Dose- and time-dependent manner antibacterial effects of AgNPs were studied. AgNPs possess the antibacterial activity due to the generation of reactive oxygen species, malondialdehyde, and proteins and sugars leakage in bacterial cells. Furthermore, bacteria treated with Ag NPs displayed decreased glutathione (GSH) expression, increased glutathione S-transferase (GST), and decreased superoxide dismutase (SOD) and catalase expression (CAT). These Ag NP-treated bacteria, show the physiological and biochemical measurements that suggest that Ag NPs can stimulate bacterial cell death (Yuan et al., 2017).

In this study antimicrobial study was explained with more intense detailed analysis by undergoing flow cytometry of MRSA strains, MDR *E.coli* and C.albicans after interacting CIP-Ag/TiO_2/ Fe_2O_3/ CS Ternary compositeat MIC value, allowing 6hrs of incubation time to assess the early apoptosis,late apoptosis death rate in the selected population density (Hussain et al., 2012). As shown in the **Figure 8.9A**, for 0hrs of incubation as control 98.76% cells were alive and sustainable while the survival rate of MRSA isolates after 6hrs of incubation was 14% and death of 75.34%. The antimicrobial potential revealed in the **Figure 8.9B** at the 6hrs of aging with CIP-Ag/TiO_2/ Fe_2O_3/ CS Ternary composite, causing cell death of MDR *E.Coli* strains 80.85% the. The **Figure 8.9C** showed excellent antifungal activity of combined effect of all constituent Nano antimicrobial agents after incubation with CIP-Ag/TiO_2/ Fe_2O_3/ CS Ternary composite induces changes in the morphology and cells cycle causing death of 89.01%, which was detected using special dyes(Maglica et al., 2015). The PI fluorescent dye, which is not cell wall permeating, is generally used to detect dead cells in the population. The CIP-Ag/TiO_2/ Fe_2O_3/ CS Ternary composite mode of action disrupt the integrity of the cell by damaging cell wall and membrane , which enhances the PI

permeability and uptake into the cell and leads to intercalation with the DNA that results in a shift in PI fluorescence. These findings are consistent with previous study regarding the toxicity of nanomedicines against bacteria as calvin et al reported polymeric coated drug loaded nanovesicle had showed 98.5 ± 1.49% death rate in the selected population against MRSA strains (Omolo et al., 2018).

Ashmore et al revealed dose dependent toxicity of nanoparticles to bacterial cellsas current study showed that CIP-Ag/TiO_2/ Fe_2O_3/ CS Ternary composite an increased rate of toxicity against*C.albicans*, MDR *E.coli*, and MRSA *(*Ashmore et al., 2018). The SEM study was applied to further investigate the morphological changes in the *C.albicans*, MDR *E.coli*, and MRSA after exposure to CIP-Ag/TiO_2/ Fe_2O_3/ CS Ternary composite. In this regard controlled group showed intact cells, cell wall and membrane presenting uniform morphology (**Figure 8.10A, C, and E**), which means the cellular proliferation of remained normal. Themicrobial cultures after exposure to CIP-Ag/TiO_2/ Fe_2O_3/ CS Ternary composite at the 6 hrs of incubation viewed under SEM analysis for observing destruction of *C.albicans* (**Figure 8.10B**),MDR *E.coli* (**Figure 8.10D**) and MRSA strains (**Figure8.10F**). MDR *E.coli* (**Figure 8.10D**) showed remarkable changes in the morphology as many were detached from outer membrane and cellular fragments were seen clearly. The prominent morphological changes could be seen for *C.albicans*(**Figure 8.10B**) almost all the cells have low density regions in their center, which clearly indicates that cytoplasm was damaged and outer membrane was disintegrated by CIP-Ag/TiO_2/ Fe_2O_3/ CS Ternary composite. The morphological changes incurred in the MRSA cells when encountered with CIP-Ag/TiO_2/ Fe_2O_3/ CS Ternary composite as shown in the **Figure 8.10F** the deformation in the spherical structure of MRSA. This proposes lysis of bacterial cells with release of cytosolic content and wrinkled cells upon their interaction with CIP-Ag/TiO_2/ Fe_2O_3/ CS Ternary composite. Results revealed that strong bonding between MRSA and CIP-Ag/TiO_2/ Fe_2O_3/ CS Ternary composite is responsible for the profound antibacterial activity (Huang *et al.*, 2017). The zeta potential value of CIP-Ag/TiO_2/ Fe_2O_3/ CS Ternary compositeis positive while bacterial cell wall is negatively charged, this established electrostatic attachment and prompt ROS production which ultimately cause inhibition of microbial growth and eventually caused cell death (Saravanakumar et al., 2018; Wang et al., 2014).

The relative percentage viability of BMGE cells were found more viable and safe after interaction with CIP-Ag/TiO_2/ Fe_2O_3/ CS Ternary composite at all tested concentrations due to chitosan encapsulations as shown in the **Figure 8.13**(Omolo et al., 2018). Previous studies reported nontoxic nature of metallic oxide NPs which is accountable feature for the use of NPs in the biological applications (Arumugam et al., 2015; Caputo et al., 2017; Prasad & Rattan, 2010). BMG cell lines after treating with CIP-Ag/TiO_2/ Fe_2O_3/ CS Ternary composite exhibited excellent viability of cells and posed ternary composite nontoxic for mammalian cells moreover results of cytotoxicity were in accordance with previous results(Campos et al., 2004). The CIP-Ag/TiO_2/ Fe_2O_3/ CS Ternary composite was found safe and biocompatible as compare to positive control (Celecoxib). The cells treated at lowest concentrations were more viable and stable as compare to higher concentrations of nano antibacterial agents included in the study(Shafai et al., 2019).

Hemocompatibility is one of the important aspects for the *in-vivo* application of nanomaterials as the injected nanomaterials interact firstly with RBCs before the immune cells (Choi et al., 2011). Therefore, potential hemolytic activity of CIP-Ag/TiO_2/ Fe_2O_3/ CS ternary composite tested on RBCs of cow **(Figure 8.14)** andresults have revealed negligible hemolytic activity of CIP-Ag/TiO_2/ Fe_2O_3/ CS ternary composite(Choi et al., 2011). Previous studies reported CS as nontoxic and hemocompatible making it highly useful for biomedical applications such as in antimicrobial delivery metallic-based nanocarriers thanks to its good interactions with metal oxide (Guibal, 2004).

Invivo antibacterial potential was studied by induced Infection in the rabbit model was completely controlled in the test group treated with CIP-Ag/TiO_2/ Fe_2O_3/ CS Ternary composite and showing no viable bacterial colony on blood and MH agar plates at 72 hrs using respective MIC, indicating that the cells were killed (Huang et al., 2017).After treatment with CIP-Ag/TiO_2/ Fe_2O_3/ CS Ternary composite in the Invivo investigation, many indicators of renal and hepatic function were assessed. Renal functions after treatment were not compromised in all the test groups of rabbits. Renal functions which were evaluated including urinary volume, protein concentrations, glucose levels, and creatinine levels werestudied amongtested groups as shown in the **Figure 8.16.** Hepatic functions were also evaluated in all the groups of rabbits and various parameters associated in blood plasma were

also taken into account. The levels of ALT and AST and albumin in the CIP-Ag/TiO_2/ Fe_2O_3/ CS Ternary composite treated groups were examined and no disturbance was found. Other studies reveal no mortality, no aberrant reactions, and little effect on kidney and liver indices in male and female Sprague Dawley rats given 2,000 mg/kg bw of Ag-NPs produced by Sargassumsiliquosum orally, demonstrating that these nanoparticles are safe (Vasquez et al., 2016).

The results of *Invivo* antibiotic release studies from CIP-Ag/TiO_2/ Fe_2O_3/ CS ternary composite were depicted in **Figure 8.19**. The CIP-Ag/TiO_2/ Fe_2O_3/ CS ternary composite exhibited highest active drug release (89% ± 0.57) at the 8^{th} hrs , which was remarkable in the 24hrs of release study when compared to control (CIP alone) showing 90% ± 0.78 release kinetics from the skin.

Data of the *Invivo* release was fit into different equations and kinetic models to explain the release kinetics of nanoformulations rabbit skin membrane. The kinetic models (Costa & Lobo, 2001)used were zero-order equation, first-order equation, Higuchi and Korsemeyer-Peppas models. The cumulative amount of the drug released from the CIP-Ag/TiO_2/ Fe_2O_3/ CS ternary composite, when plotted against square-root of time, the release profiles of drug seemed to follow Higuchi model the data was further treated as per the following equation

$$M_t/M_\infty = \mathrm{K}.t^n$$

where, M_t/M_8 is the fractional release of the drug, Mt is the amount released at time t, M_8 is the total amount of drug crossed skin barriers , t is the release time, K is a kinetic constant, and n is the diffusional release exponent indicative of the operating release mechanism (Costa & Lobo, 2001).

Future prospective

Nanotechnology is expected to grow fast in future, and it will provide new avenues for the improved treatment options. The efficiency of nanoparticle bioapplication targeting is a critical parameter. An effective treatment drug may build up in the target organism, killing MDR pathogens. It is consequently expected that nanoparticles will have a controlled dispersion and clearance for site-specific applications. More importantly, nanoparticles' various delivery capabilities and custom-made characteristics improve target accumulation

effects. In recent years, available bio-nanoparticle design methodologies and rules have been gathering and developing. Nanoparticle delivery will be gradually but dramatically improved during the next 5–10 years. Optimizing medication pharmacokinetic parameters to improve treatment effects and limit adverse effects is an important feature of nanoparticle design, which takes into account both physiological and nanoparticle-specific factors. Further in vivo experiments should be performed to investigate the biocompatibility and undesired adverse effects for their possible therapeutic use on various model and different rout of administration. The use of available antibiotics conjugated or attached to nanoparticles offers an alternate angle to antibiotic therapy. The interaction between organs and nanoparticles is responsible for all therapeutic side effects. More In vivo experiments should be performed to investigate the biocompatibility, histopathological, biochemical parameters and undesired adverse effects of nanomaterials that prove nanomaterials as alternative therapeutic agents to replace conventional antibiotics.

REFERENCES

AalbæK, B., Stenderup, , Jensen, H. E., Valbak, , Nylin, B., & Huda, A. (1994). Mycotic and algal bovine mastitis in Denmark. *Apmis*, *102*(1-6), 451-456.

Abd Elgadir, M., Uddin, M. S., Ferdosh, S., Adam, A., Chowdhury, A. K., & Sarker, M. Z. I. (2015). Impact of chitosan composites and chitosan nanoparticle composites on various drug delivery systems: A review. *Journal of food and drug analysis*, *23*(4), 619-629.

Abd Rani, N. Z., Husain, K., & Kumolosasi, E. (2018). Moringa Genus: A Review of Phytochemistry and Pharmacology [Review]. *Frontiers in Pharmacology*, *9*(108). https://doi.org/10.3389/fphar.2018.00108

Abebe, R., Hatiya, H., Abera, M., Megersa, B., & Asmare, K. (2016). Bovine mastitis: prevalence, risk factors and isolation of Staphylococcus aureus in dairy herds at Hawassa milk shed, South Ethiopia. *BMC Veterinary Research*, *12*(1), 270.

Abid, S., Uzair, B., Niazi, M. B. K., Fasim, F., Bano, S. A., Jamil, N., Batool, R., & Sajjad, S. (2021). Bursting the Virulence Traits of MDR Strain of Candida albicans Using Sodium Alginate-based Microspheres Containing Nystatin-loaded MgO/CuO Nanocomposites. *International journal of nanomedicine*, *16*, 1157.

Abreu, F. O., Oliveira, E. F., Paula, H. C., & de Paula, R. C. (2012). Chitosan/cashew gum nanogels for essential oil encapsulation. *Carbohydrate polymers*, *89*(4), 1277-1282.

Acar, , & Goldstein, F. (1997). Trends in bacterial resistance to fluoroquinolones. *Clinical Infectious Diseases*, *24*(Supplement_1), S67-S73.

Addis, Z., Kebede, N., Sisay, Z., Alemayehu, H., Wubetie, A., & Kassa, T. (2011). Prevalence and antimicrobial resistance of Salmonella isolated from lactating cows and in contact humans in dairy farms of Addis Ababa: a cross sectional study. *BMC infectious diseases*, *11*(1), 222.

Agga, G. E., Arthur, T. M., Durso, L. M., Harhay, D. M., & Schmidt, W. (2015). Antimicrobial-resistant bacterial populations and antimicrobial resistance genes obtained from environments impacted by livestock and municipal waste. *PLoS One*, *10*(7), e0132586.

Agnihotri, S., & Wakode, S. (2010). Antimicrobial activity of essential oil and various extracts of fruits of greater cardamom. *Indian journal of pharmaceutical sciences*, *72*(5), 657.

Ahmed, S., Ahmad, M., Swami, B. L., & Ikram, S. (2016). A review on plants extract mediated synthesis of silver nanoparticles for antimicrobial applications: a green expertise. *Journal of advanced research*, *7*(1), 17-28.

Akhavan, O., & Ghaderi, E. (2010). Cu and CuO nanoparticles immobilized by silica thin films as antibacterial materials and photocatalysts. *Surface and Coatings Technology*, *205*(1), 219-223.

Akhtar, A., Ameer, M., & Aeshad, M. (2012). Prevalence of sub clinical mastitis in buffaloes in district DI Khan. *Pakistan Journal of Science*, *64*(2).

Akintelu, S. A., Folorunso, A. S., Folorunso, F. A., & Oyebamiji, A. K. (2020). Green synthesis of copper oxide nanoparticles for biomedical application and environmental remediation. *Heliyon*, *6*(7), e04508.

Alagumuthu, G., & Kumar, T. A. (2013). Synthesis and characterization of Chitosan/TiO 2 nanocomposites using liquid phase deposition technique. *Int. Nanosci. Nanotechnol*, *4*, 105-111.

Álvarez, L. G., Holden, M., Lindsay, H., Webb, C., Brown, D., Curran, M., Walpole, E., Brooks, K., Pickard, D., & Teale, C. (2011). Methicillin-resistant Staphylococcus aureus with a novel mecA homologue in human and bovine populations in the UK and Denmark: A descriptive study. *Lancet*, *11*, 595-603.

Anbazhakan, S., Dhandapani, R., Anandhakumar, P., & Balu, S. (2007). Traditional medicinal knowledge on Moringa concanensis Nimmo of perambalur District, Tamilnadu. *Ancient science of life*, *26*(4), 42.

Anderson, V. E., Gootz, T. D., & Osheroff, N. (1998). Topoisomerase IV catalysis and the mechanism of quinolone action. *Journal of Biological Chemistry*, *273*(28), 17879-17885.

Arabi, H., Pakzad, I., Nasrollahi, A., Hosainzadegan, H., Jalilian, F. A., Taherikalani, M., Samadi, N., & Sefidan, A. M. (2015). Sulfonamide resistance genes (sul) M in extended Spectrum Beta lactamase (ESBL) and non-ESBL producing Escherichia Coli isolated from Iranian hospitals. *Jundishapur journal of microbiology*, *8*(7).

Archambault, M., Petrov, P., Hendriksen, R. S., Asseva, G., Bangtrakulnonth, A., Hasman, H., & Aarestrup, F. M. (2006). Molecular characterization and occurrence of extended-spectrum β-lactamase resistance genes among Salmonella enterica serovar Corvallis from Thailand, Bulgaria, and Denmark. *Microbial Drug Resistance*, *12*(3), 192-198.

Arora, N., Thangavelu, K., & Karanikolos, G. N. (2020). Bimetallic nanoparticles for antimicrobial applications. *Frontiers in Chemistry*, *8*, 412.

Arumugam, A., Karthikeyan, C., Hameed, A. S. H., Gopinath, K., Gowri, S., & Karthika, V. (2015). Synthesis of cerium oxide nanoparticles using Gloriosa superba L. leaf extract and their structural, optical and antibacterial properties. *Materials Science and Engineering: C*, *49*, 408-415.

Ashmore, D. A., Chaudhari, A., Barlow, B., Barlow, B., Harper, T., Vig, K., Miller, M., Singh, S., Nelson, E., & Pillai, S. (2018). Evaluation of E. coli inhibition by plain and polymer-coated silver nanoparticles. *Revista do Instituto de Medicina Tropical de São Paulo*, *60*.

Ashraf, A., & Imran, M. (2020). Causes, types, etiological agents, prevalence, diagnosis, treatment, prevention, effects on human health and future aspects of bovine mastitis. *Animal health research reviews*, *21*(1), 36-49.

Assali, M., Zaid, A. N., Abdallah, F., Almasri, M., & Khayyat, R. (2017). Single-walled carbon nanotubes-ciprofloxacin nanoantibiotic: strategy to improve ciprofloxacin antibacterial activity. *International journal of nanomedicine*, *12*, 6647.

ASTM, F. (2000). 756-00. Standard practice for assessment of hemolytic properties of materials. *Philadelphia: American Society for Testing and Materials*.

Atanasov, A. G., Waltenberger, B., Pferschy-Wenzig, E.-M., Linder, T., Wawrosch, C., Uhrin, P., Temml, V., Wang, L., Schwaiger, S., & Heiss, E. H. (2015). Discovery and resupply of pharmacologically active plant-derived natural products: A review. *Biotechnology advances*, *33*(8), 1582-1614.

Atif, M., Iqbal, S., Ismail, M., Mansoor, Q., Mughal, L., Aziz, M. H., Hanif, A., & Farooq, W. (2019). Manganese-doped cerium oxide nanocomposite induced photodynamic therapy in MCF-7 cancer cells and antibacterial activity. *BioMed research international*, *2019*.

Awad, A. (2017). Molecular and Phenotypic Characterization of Antimicrobial Resistance in Gram Negative Bacteria Recovered from Subclinical Mastitis. *Advances in Animal and Veterinary Sciences*, *5*. https://doi.org/10.17582/journal.aavs/2017/5.5.196.204

Awad, F., El-Molla, A., Fayed, A., Abd-El-Halim, M., & Refai, M. (1980). Studies on mycotic mastitis in Egypt. *Journal of the Egyptian Veterinary Medical Association*, *40*(3), 35-41.

Aydın, M. T. A., Hoşgün, H. L., Dede, A., & Güven, K. (2018). Synthesis, characterization and antibacterial activity of silver-doped TiO2 nanotubes. *Spectrochimica Acta Part A: Molecular and Biomolecular Spectroscopy*, *205*, 503-507.

Babic, M., Hujer, A. M., & Bonomo, R. A. (2006). What's new in antibiotic resistance? Focus on beta-lactamases. *Drug resistance updates*, *9*(3), 142-156.

Bailey, K., Pinyon, L., Anantham, S., & Hall, R. M. (2011). Distribution of the bla TEM gene and bla TEM-containing transposons in commensal Escherichia coli. *Journal of antimicrobial chemotherapy*, *66*(4), 745-751.

Balamurugan, V., Balakrishnan, V., & Sundaresan, A. (2015). GC-MS analysis of leaf and Bark Extract of Moringa concanensis Nimmo, a siddha medicinal plant of South India. *European J Biotechnol Biosci*, *3*(12), 57-61p.

Bald, D., & Koul, A. (2013). Advances and strategies in discovery of new antibacterials for combating metabolically resting bacteria. *Drug discovery today*, *18*(5-6), 250-255.

Bancroft, D., & Gamble, M. (2008). *Theory and practice of histological techniques*. Elsevier health sciences.

Banerjee, M., Mallick, S., Paul, A., Chattopadhyay, A., & Ghosh, S. S. (2010). Heightened reactive oxygen species generation in the antimicrobial activity of a three component iodinated chitosan− silver nanoparticle composite. *Langmuir*, *26*(8), 5901-5908.

Bankier, C., Cheong, Y., Mahalingam, S., Edirisinghe, M., Ren, G., Cloutman-Green, E., & Ciric, L. (2018). A comparison of methods to assess the antimicrobial activity of nanoparticle combinations on bacterial cells. *PLoS One*, *13*(2), e0192093.

Barkema, H. W., Von Keyserlingk, M., Kastelic, , Lam, T., Luby, C., Roy, -P., LeBlanc, S., Keefe, G., & Kelton, D. (2015). Invited review: Changes in the dairy industry affecting dairy cattle health and welfare. *Journal of dairy science*, *98*(11), 7426-7445.

Basavegowda, N., & Baek, K.-H. (2021). Multimetallic Nanoparticles as Alternative Antimicrobial Agents: Challenges and Perspectives. *Molecules*, *26*(4), 912.

Basiuk, V. A., & Basiuk, E. V. (2015). Green processes for nanotechnology. *Springer*, 446.

Batista, M. , Gómez-Cerezo, M. N., Kubacka, A., Tudela, D., & Fernández-García, M. (2013). Role of interface contact in CeO2–TiO2 photocatalytic composite materials. *ACS Catalysis*, *4*(1), 63-72.

Batool, A., Menaa, F., Uzair, B., Khan, B. A., & Menaa, B. (2020). Progress and prospects in translating nanobiotechnology in medical theranostics. *Current Nanoscience*, *16*(5), 685-707.

Benveniste, R., & Davies, (1973). Aminoglycoside antibiotic-inactivating enzymes in actinomycetes similar to those present in clinical isolates of antibiotic-resistant bacteria. *Proceedings of the National Academy of Sciences*, *70*(8), 2276-2280.

Bertrand, N., & Leroux, -C. (2012). The journey of a drug-carrier in the body: an anatomo-physiological perspective. *Journal of Controlled Release*, *161*(2), 152-163.

Bhuyan, L., Hassan, S., Dash, K., Panda, A., Behura, S., & Ramachandra, S. (2018). Candida species diversity in oral cavity of type 2 diabetic patients and their In vitro antifungal susceptibility [Original Article]. *Contemporary Clinical Dentistry*, *9*(5), 83-88. https://doi.org/10.4103/ccd.ccd_70_18

Bikiaris, D., Koutris, E., & Karavas, E. (2007). New aspects in sustained drug release formulations. *Recent patents on drug delivery & formulation*, *1*(3), 201-213.

Birla, S., Tiwari, V., Gade, A., Ingle, A., Yadav, A., & Rai, M. (2009). Fabrication of silver nanoparticles by Phoma glomerata and its combined effect against Escherichia coli, Pseudomonas aeruginosa and Staphylococcus aureus. *Letters in Applied Microbiology*, *48*(2), 173-179.

Blecher, K., Nasir, A., & Friedman, A. (2011). The growing role of nanotechnology in combating infectious disease. *Virulence*, *2*(5), 395-401.

Bokare, A., Sanap, A., Pai, M., Sabharwal, S., & Athawale, A. A. (2013). Antibacterial activities of Nd doped and Ag coated TiO2 nanoparticles under solar light irradiation. *Colloids and Surfaces B: Biointerfaces*, *102*, 273-280.

Bolla, -M., Alibert-Franco, S., Handzlik, , Chevalier, , Mahamoud, A., Boyer, G., Kieć-Kononowicz, K., & Pagès, -M. (2011). Strategies for bypassing the membrane barrier in multidrug resistant Gram-negative bacteria. *FEBS letters*, *585*(11), 1682-1690.

Bomila, R., Srinivasan, S., Venkatesan, A., Bharath, B., & Perinbam, K. (2018). Structural, optical and antibacterial activity studies of Ce-doped ZnO nanoparticles prepared by wet-chemical method. *Materials Research Innovations*, *22*(7), 379-386.

Bradley, A. (2002). Bovine mastitis: an evolving disease. *The veterinary journal*, *164*(2), 116-128.

Breser, M. L., Felipe, V., Bohl, L. P., Orellano, M. S., Isaac, P., Conesa, A., Rivero, V. E., Correa, S. G., Bianco, I. D., & Porporatto, C. (2018). Chitosan and cloxacillin combination improve antibiotic efficacy against different lifestyle of coagulase-negative Staphylococcus isolates from chronic bovine mastitis. *Scientific reports*, *8*(1), 1-13.

Briones, E., Colino, C. I., & Lanao, M. (2008). Delivery systems to increase the selectivity of antibiotics in phagocytic cells. *Journal of Controlled Release*, *125*(3), 210-227.

Brown, K., Uwiera, R. R., Kalmokoff, M. L., Brooks, S. P., & Inglis, G. D. (2017). Antimicrobial growth promoter use in livestock: a requirement to understand their modes of action to develop effective alternatives. *International journal of antimicrobial agents*, *49*(1), 12-24.

Burello, E., & Worth, A. P. (2011). A theoretical framework for predicting the oxidative stress potential of oxide nanoparticles. *Nanotoxicology*, *5*(2), 228-235.

Burton, M., Fileccia, T., Gulliver, A., Qamar, M., & Tayyab, A. (2012). Pakistan: priority areas for investment in the agricultural sector. *FAO Investment Centre. Country Highlights (FAO)*.

Bush, K., & Jacoby, G. A. (2010). Updated functional classification of β-lactamases. *Antimicrobial agents and Chemotherapy*, *54*(3), 969-976.

Butler, M. S., Blaskovich, M. A., & Cooper, M. A. (2013). Antibiotics in the clinical pipeline in 2013. *The Journal of antibiotics*, *66*(10), 571-591.

Cain, A. K., & Hall, R. M. (2012). Evolution of a multiple antibiotic resistance region in IncHI1 plasmids: reshaping resistance regions in situ. *Journal of Antimicrobial Chemotherapy*, *67*(12), 2848-2853.

Cain, A. K., Liu, X., Djordjevic, S. P., & Hall, R. M. (2010). Transposons related to Tn 1696 in IncHI2 plasmids in multiply antibiotic resistant Salmonella enterica serovar Typhimurium from Australian animals. *Microbial Drug Resistance*, *16*(3), 197-202.

Calap, P., & Martínez, (2018). Bacteriophages: protagonists of a post-antibiotic era. *Antibiotics*, *7*(3), 66.

Campolis, D. M., Monk, P., Price, A., Benfield, P., Todd, P. A., & Ward, A. (1988). Ciprofloxacin. *Drugs*, *35*(4), 373-447.

Campos, A. M., Diebold, Y., Carvalho, E. L., Sánchez, A., & Alonso, M. (2004). Chitosan nanoparticles as new ocular drug delivery systems: in vitro stability, in vivo fate, and cellular toxicity. *Pharmaceutical research*, *21*(5), 803-810.

Caputo, F., Mameli, M., Sienkiewicz, A., Licoccia, S., Stellacci, F., Ghibelli, L., & Traversa, E. (2017). A novel synthetic approach of cerium oxide nanoparticles with improved biomedical activity. *Scientific reports*, *7*(1), 1-13.

Carattoli, A. (2008). Animal reservoirs for extended spectrum β-lactamase producers. *Clinical Microbiology and Infection*, *14*, 117-123.

Cervinkova, D., Vlkova, H., Borodacova, I., Makovcova, , Babak, V., Lorencova, A., Vrtkova, I., Marosevic, D., & Jaglic, Z. (2013). Prevalence of mastitis pathogens in milk from clinically healthy cows. *Veterinarni medicina*, *58*(11), 567-575.

Chandrasekaran, D., Venkatesan, P., Tirumurugaan, K., Nambi, A., Thirunavukkarasu, P., Kumanan, K., Vairamuthu, S., & Ramesh, S. (2014). Pattern of antibiotic resistant mastitis in dairy cows. *Veterinary World*, *7*(6).

Chang, Q., Wang, W., Regev-Yochay, G., Lipsitch, M., & Hanage, W. P. (2015). Antibiotics in agriculture and the risk to human health: how worried should we be? *Evolutionary applications*, *8*(3), 240-247.

Charbgoo, F., Ahmad, M. B., & Darroudi, M. (2017). Cerium oxide nanoparticles: green synthesis and biological applications. *International journal of nanomedicine*, *12*, 1401.

Cheng, G., Hao, H., Xie, S., Wang, X., Dai, M., Huang, L., & Yuan, Z. (2014). Antibiotic alternatives: the substitution of antibiotics in animal husbandry? *Frontiers in microbiology*, *5*, 217.

Choi, , Reipa, V., Hitchins, V. M., Goering, P. L., & Malinauskas, R. A. (2011). Physicochemical characterization and in V itro hemolysis evaluation of silver nanoparticles. *Toxicological Sciences*, *123*(1), 133-143.

Choo, K., Ching, Y. C., Chuah, C. H., Julai, S., & Liou, N.-S. (2016). Preparation and characterization of polyvinyl alcohol-chitosan composite films reinforced with cellulose nanofiber. *Materials*, *9*(8), 644.

Ciro, Y., Rojas, , Oñate-Garzon, , & Salamanca, C. H. (2019). Synthesis, Characterisation and Biological Evaluation of Ampicillin–Chitosan–Polyanion Nanoparticles Produced by Ionic Gelation and Polyelectrolyte Complexation Assisted by High-Intensity Sonication. *Polymers*, *11*(11), 1758.

CLSI, (2016) "Performances Standards for Antimicrobial Susceptibility Testing; Twenty-Fourth Informational Supplement. M100-S26. Wayne, PA: Clinical Laboratory Standards Institute."

Coetzee, , Corcoran, C., Prentice, E., Moodley, M., Mendelson, M., Poirel, L., Nordmann, P., & Brink, A. (2016). Emergence of plasmid-mediated colistin resistance (MCR-1) among Escherichia coli isolated from South African patients. *SAMJ: South African Medical Journal*, *106*(5), 449-450.

Colom, K., Pérez, , Alonso, R., Fernández-Aranguiz, A., Lariño, E., & Cisterna, R. (2003). Simple and reliable multiplex PCR assay for detection of bla TEM, bla SHV and bla OXA–1 genes in Enterobacteriaceae. *FEMS microbiology letters*, *223*(2), 147-151.

Commission, C. A. (2011). Guidelines for risk analysis of foodborne antimicrobial resistance. *Geneva: Food and Agriculture Organization*.

Condas, L. A., De Buck, , Nobrega, D. B., Carson, D. A., Naushad, S., De Vliegher, S., Zadoks, R. N., Middleton, R., Dufour, S., & Kastelic, P. (2017). Prevalence of non-aureus staphylococci species causing intramammary infections in Canadian dairy herds. *Journal of dairy science*, *100*(7), 5592-5612.

Costa, E., Gandra, C., Pires, M., Coutinho, S., Castilho, W., & Teixeira, C. (1993). Survey of bovine mycotic mastitis in dairy herds in the State of São Paulo, Brazil. *Mycopathologia*, *124*(1), 13-17.

Costa, P., & Lobo, M. S. (2001). Modeling and comparison of dissolution profiles. *European journal of pharmaceutical sciences*, *13*(2), 123-133.

Cronin, G., Turner, M. L., Goetze, L., Bryant, C. E., & Sheldon, I. M. (2012). Toll-like receptor 4 and MYD88-dependent signaling mechanisms of the innate immune system are essential for the response to lipopolysaccharide by epithelial and stromal cells of the bovine endometrium. *Biology of reproduction*, *86*(2), 51, 51-59.

Cui, Z., Zheng, Z., Lin, L., Si, , Wang, Q., Peng, X., & Chen, W. (2018). Electrospinning and crosslinking of polyvinyl alcohol/chitosan composite nanofiber for transdermal drug delivery. *Advances in Polymer Technology*, *37*(6), 1917-1928.

D'Orazio, G., Di Gennaro, P., Boccarusso, M., Presti, I., Bizzaro, G., Giardina, S., Michelotti, A., Labra, M., & La Ferla, B. (2015). Microencapsulation of new probiotic formulations for gastrointestinal delivery: in vitro study to assess viability and biological properties. *Applied microbiology and biotechnology*, *99*(22), 9779-9789.

Daum, T., Schaberg, D., Terpenning, M., Sottile, W., & Kauffman, C. (1990). Increasing resistance of Staphylococcus aureus to ciprofloxacin. *Antimicrobial agents and Chemotherapy*, *34*(9), 1862-1863.

Devendra, C. (2001). Smallholder dairy production systems in developing countries: characteristics, potential and opportunities for improvement-review. *Asian-Australasian Journal of Animal Sciences*, *14*(1), 104-113.

Dhama, K., Tiwari, R., Chakraborty, S., Saminathan, M., Kumar, A., Karthik, K., Wani, M. Y., Amarpal, S. S., & Rahal, A. (2014). Evidence based antibacterial potentials of medicinal plants and herbs countering bacterial pathogens especially in the era of emerging drug resistance: An integrated update. *Int J pharmacol*, *10*(1), 1-43.

Diaz, F. (2013). Antimicrobial use in animals: analysis of the OIE survey on monitoring of the quantities of antimicrobial agents used in animals. Proceeding of the OIE Global Conference on the Responsible and Prudent Use of Antimicrobial Agents for Animals held in March,

Dickinson, E. (2017). Biopolymer-based particles as stabilizing agents for emulsions and foams. *Food Hydrocolloids*, *68*, 219-231.

Dilshad, S. R., Rehman, N., Ahmad, N., & Iqbal, A. (2010). Documentation of ethnoveterinary practices for mastitis in dairy animals in Pakistan. *Pakistan Veterinary Journal*, *30*(3), 167-171.

DiMasi, A., Grabowski, H. G., & Hansen, R. W. (2016). Innovation in the pharmaceutical industry: new estimates of R&D costs. *Journal of health economics*, *47*, 20-33.

DiMasi, A., Hansen, R. W., Grabowski, H. G., & Lasagna, L. (1991). Cost of innovation in the pharmaceutical industry. *Journal of health economics*, *10*(2), 107-142.

dos Santos, R. d. C., & Marin, M. (2005). Isolation of Candida spp. from mastitic bovine milk in Brazil. *Mycopathologia*, *159*(2), 251-253.

Dudley, M. N., Ambrose, P. G., Bhavnani, S. M., Craig, W. A., Ferraro, M. , Jones, R. N., Clinical, A. S. T. S. o. t., & Institute, L. S. (2013). Background and rationale for revised Clinical and Laboratory Standards Institute interpretive criteria (breakpoints) for Enterobacteriaceae and Pseudomonas aeruginosa: I. Cephalosporins and aztreonam. *Clinical infectious diseases*, *56*(9), 1301-1309.

Edmond, M. B., Wallace, S. E., McClish, D. K., Pfaller, M. A., Jones, R. N., & Wenzel, R. P. (1999). Nosocomial bloodstream infections in United States hospitals: a three-year analysis. *Clinical Infectious Diseases*, *29*(2), 239-244.

Ernst, C., Bartel, A., Elferink, W., Huhn, , Eschbach, E., Schönfeld, K., Feßler, A. T., Oberheitmann, B., & Schwarz, S. (2019). Improved DNA extraction and purification with magnetic nanoparticles for the detection of methicillin-resistant Staphylococcus aureus. *Veterinary microbiology*, *230*, 45-48.

Ewers, C., Bethe, A., Semmler, T., Guenther, S., & Wieler, L. (2012). Extended-spectrum β-lactamase-producing and AmpC-producing Escherichia coli from livestock and companion animals, and their putative impact on public health: a global perspective. *Clinical Microbiology and Infection*, *18*(7), 646-655.

Fan, W., Yan, W., Xu, Z., & Ni, H. (2012). Colloids and Surfaces B: Biointerfaces Formation Mechanism of Monodisperse, Low Molecular Weight Chitosan Nanoparticles by Ionic Gelation Technique. *Colloids Surfaces B Biointerfaces*, *90*, 21-27.

Fawaz, F., Bonini, F., Maugein, , & Lagueny, A. (1998). Ciprofloxacin-loaded polyisobutylcyanoacrylate nanoparticles: pharmacokinetics and in vitro antimicrobial activity. *International journal of pharmaceutics*, *168*(2), 255-259.

Finance, M. o. (2017). Pakistan economic survey.

Fodouop, S. P. C., Tala, S. D., Keilah, L. P., Kodjio, N., Yemele, M. D., kamdje Nwabo, A. H., Nji-Kah, B., Tchoumboue, , & Gatsing, D. (2017). Effects of Vitellaria paradoxa

(CF Gaertn.) aqueous leaf extract administration on Salmonella typhimurium-infected rats. *BMC complementary and alternative medicine*, *17*(1), 1-11.

Founou, L. L., Founou, R. C., & Essack, S. Y. (2016). Antibiotic resistance in the food chain: a developing country-perspective. *Frontiers in microbiology*, *7*, 1881.

Fridkin, S. K., Cleveland, A. A., See, I., & Lynfield, R. (2015). Emerging infections program as surveillance for antimicrobial drug resistance. *Emerging infectious diseases*, *21*(9), 1578.

Fujisawa, H., Watanabe, K., Suma, K., Origuchi, K., Matsufuji, H., Seki, T., & Ariga, T. (2009). Antibacterial potential of garlic-derived allicin and its cancellation by sulfhydryl compounds. *Bioscience, biotechnology, and biochemistry*, *73*(9), 1948-1955.

Gagnon, , Clift, M. , Vanhecke, D., Kuhn, D. A., Weber, P., Petri-Fink, A., Rothen-Rutishauser, B., & Fromm, K. M. (2015). Integrating silver compounds and nanoparticles into ceria nanocontainers for antimicrobial applications. *Journal of Materials Chemistry B*, *3*(9), 1760-1768.

Gao, P., Nie, X., Zou, M., Shi, Y., & Cheng, G. (2011). Recent advances in materials for extended-release antibiotic delivery system. *The Journal of antibiotics*, *64*(9), 625-634.

Gao, Y., Lin, X., Shi, K., Yan, Z., & Wang, Z. (2013). Bovine mammary gene expression profiling during the onset of lactation. *PloS one*, *8*(8), e70393.

García-Saucedo, C., Field, A., Otero-Gonzalez, L., & Sierra-Álvarez, R. (2011). Low toxicity of HfO2, SiO2, Al2O3 and CeO2 nanoparticles to the yeast, Saccharomyces cerevisiae. *Journal of hazardous materials*, *192*(3), 1572-1579.

Gatsing, D., Aliyu, R., Kuiate, R., Garba, I. H., Jaryum, K. H., Tedongmo, N., Tchouanguep, F. M., & Adoga, G. I. (2005). Toxicological evaluation of the aqueous extract of Allium sativum bulbs on laboratory mice and rats. *Cameroon Journal of Experimental Biology*, *1*(1), 39-45.

George, A., & Levy, S. (1983). Gene in the major cotransduction gap of the Escherichia coli K-12 linkage map required for the expression of chromosomal resistance to tetracycline and other antibiotics. *Journal of bacteriology*, *155*(2), 541-548.

Georgekutty, R., Seery, M. K., & Pillai, S. C. (2008). A highly efficient Ag-ZnO photocatalyst: synthesis, properties, and mechanism. *The Journal of Physical Chemistry C*, *112*(35), 13563-13570.

Geser, N., Stephan, R., & Hächler, H. (2012). Occurrence and characteristics of extended-spectrum β-lactamase (ESBL) producing Enterobacteriaceae in food producing animals, minced meat and raw milk. *BMC veterinary research*, *8*(1), 1-9.

Ghafar, A., McGill, D., Stevenson, M. A., Badar, M., Kumbher, A., Warriach, H. M., Gasser, R. B., & Jabbar, A. (2020). A participatory investigation of bovine health and production issues in Pakistan. *Frontiers in Veterinary Science*, *7*.

Gnanaprakasam, A., Sivakumar, V., Sivayogavalli, P., & Thirumarimurugan, M. (2015). Characterization of TiO2 and ZnO nanoparticles and their applications in photocatalytic degradation of azodyes. *Ecotoxicology and environmental safety*, *121*, 121-125.

Gonzalez, R., Giraudo, , & Busso, (1980). Studies on subclinical mastitis. II. Bacterial agents. *Revista de Medicina Veterinaria, Argentina*, *61*(3), 225-234.

Gross, R. A., & Kalra, B. (2002). Biodegradable polymers for the environment. *Science*, *297*(5582), 803-807.

Group, G. A. R. P.-I. W. (2011). Rationalizing antibiotic use to limit antibiotic resistance in India+. *The Indian journal of medical research*, *134*(3), 281.

Gualerzi, C. O., Brandi, L., Fabbretti, A., & Pon, C. L. (2013). *Antibiotics: targets, mechanisms and resistance*. John Wiley & Sons.

Guan, M., Chen, Y., Wei, Y., Song, H., Gao, C., Cheng, H., Li, Y., Huo, K., Fu, , & Xiong, W. (2019). Long-lasting bactericidal activity through selective physical puncture and controlled ions release of polydopamine and silver nanoparticles–loaded TiO2 nanorods in vitro and in vivo. *International journal of nanomedicine*, *14*, 2903.

Guibal, E. (2004). Interactions of metal ions with chitosan-based sorbents: a review. *Separation and purification technology*, *38*(1), 43-74.

Halasa, T., Huijps, K., Østerås, O., & Hogeveen, H. (2007). Economic effects of bovine mastitis and mastitis management: A review. *Veterinary quarterly*, *29*(1), 18-31.

Haldorai, Y., & Shim, (2014). Novel chitosan-TiO2 nanohybrid: Preparation, characterization, antibacterial, and photocatalytic properties. *Polymer Composites*, *35*(2), 327-333.

Hanna, D. H., & Saad, G. R. (2019). Encapsulation of ciprofloxacin within modified xanthan gum-chitosan based hydrogel for drug delivery. *Bioorganic chemistry*, *84*, 115-124.

Hao, H., Cheng, G., Iqbal, Z., Ai, X., Hussain, H. I., Huang, L., Dai, M., Wang, Y., Liu, Z., & Yuan, Z. (2014). Benefits and risks of antimicrobial use in food-producing animals. *Frontiers in microbiology*, *5*, 288.

Harakeh, S., Saleh, I., Zouhairi, O., Baydoun, E., Barbour, E., & Alwan, N. (2009). Antimicrobial resistance of Listeria monocytogenes isolated from dairy-based food products. *Science of The Total Environment*, *407*(13), 4022-4027.

Harmon, R. (1995). Mastitis and milk quality. In *Milk quality* (pp. 25-39). Springer.

Hart, C., & Kariuki, S. (1998). Antimicrobial resistance in developing countries. *Bmj*, *317*(7159), 647-650.

Hartmann, M., Berditsch, M., Hawecker, , Ardakani, M. F., Gerthsen, D., & Ulrich, A. S. (2010). Damage of the bacterial cell envelope by antimicrobial peptides gramicidin S and PGLa as revealed by transmission and scanning electron microscopy. *Antimicrobial agents and chemotherapy*, *54*(8), 3132-3142.

Hashemi, S. R., & Davoodi, H. (2011). Herbal plants and their derivatives as growth and health promoters in animal nutrition. *Veterinary research communications*, *35*(3), 169-180.

Hawkey, P. M., & Jones, A. M. (2009). The changing epidemiology of resistance. *Journal of Antimicrobial Chemotherapy*, *64*(suppl_1), i3-i10.

Hazlett, M., Little, P., Maxie, M., & Barnum, D. (1984). Fatal mastitis of dairy cows: a retrospective study. *Canadian Journal of Comparative Medicine*, *48*(2), 125.

Heinlaan, M., Ivask, A., Blinova, I., Dubourguier, H.-C., & Kahru, A. (2008). Toxicity of nanosized and bulk ZnO, CuO and TiO2 to bacteria Vibrio fischeri and crustaceans Daphnia magna and Thamnocephalus platyurus. *Chemosphere*, *71*(7), 1308-1316.

Hemeg, H. A. (2017). Nanomaterials for alternative antibacterial therapy. *International journal of nanomedicine*, *12*, 8211.

Hemme, T. (2007). IFCN dairy report 2007, international farm comparison network. *IFCN Dairy Research Center, Kiel, Germany*, 214.

Ho, C.-T., Weng, T.-H., Wang, C.-Y., Yen, S.-, & Yew, T.-R. (2014). Tunable band gaps of Co 3− x Cu x O 4 nanorods with various Cu doping concentrations. *RSC advances*, *4*(38), 20053-20057.

Hodaei, A., Ataie, A., & Mostafavi, E. (2015). Intermediate milling energy optimization to enhance the characteristics of barium hexaferrite magnetic nanoparticles. *Journal of Alloys and Compounds*, *640*, 162-168.

Hogeveen, H., Pyorala, S., Waller, K. P., Hogan, S., Lam, T. , Oliver, S. P., Schukken, Y. H., Barkema, H. W., & Hillerton, E. (2011). Current status and future challenges in mastitis research. Proceedings of the 50th Annual Meeting of the National Mastitis Council, 23-26 January, 2011, Arlington, USA,

Hogeveen, H., & Van Der Voort, M. (2017). Assessing the economic impact of an endemic disease: the case of mastitis. *Revue scientifique et technique/Office International des Epizooties*, *36*(1), 217-226.

Holt, G., Krieg, N., Sneath, P. H., Staley, , & Williams, S. (1994). Bergey's manual of determinative bacteriology. 9th. *Baltimor: William & Wilkins*.

Hoog, G. S., Guarro, , Gené, , & Figueras, M. (2000). *Atlas of clinical fungi*. Centraalbureau voor Schimmelcultures (CBS).

Hoseinzadeh, E., Makhdoumi, P., Taha, P., Hossini, H., Stelling, , & Amjad Kamal, M. (2017). A review on nano-antimicrobials: metal nanoparticles, methods and mechanisms. *Current drug metabolism*, *18*(2), 120-128.

Hossain, F., Perales-Perez, O. , Hwang, S., & Román, F. (2014). Antimicrobial nanomaterials as water disinfectant: applications, limitations and future perspectives. *Science of The Total Environment*, *466*, 1047-1059.

Huang, X., Bao, X., Liu, Y., Wang, Z., & Hu, Q. (2017). Catechol-functional chitosan/silver nanoparticle composite as a highly effective antibacterial agent with species-specific mechanisms. *Scientific reports*, *7*(1), 1-10.

Huang, X., Li, L.-D., Lyu, G.-M., Shen, B.-Y., Han, Y.-F., Shi, -L., Teng, -L., Feng, L., Si, S.-Y., & Wu, -H. (2018). Chitosan-coated cerium oxide nanocubes accelerate

cutaneous wound healing by curtailing persistent inflammation. *Inorganic Chemistry Frontiers*, *5*(2), 386-393.

Huh, A. , & Kwon, Y. (2011). "Nanoantibiotics": a new paradigm for treating infectious diseases using nanomaterials in the antibiotics resistant era. *Journal of Controlled Release*, *156*(2), 128-145.

Hussain, S., Al-Nsour, F., Rice, A. B., Marshburn, , Yingling, B., Ji, Z., Zink, I., Walker, N. , & Garantziotis, S. (2012). Cerium dioxide nanoparticles induce apoptosis and autophagy in human peripheral blood monocytes. *ACS nano*, *6*(7), 5820-5829.

Hussein, E. M., Desoky, W. M., Hanafy, M. F., & Guirguis, O. W. (2021). Effect of TiO2 nanoparticles on the structural configurations and thermal, mechanical, and optical properties of chitosan/TiO2 nanoparticle composites. *Journal of Physics and Chemistry of Solids*, *152*, 109983.

Huyghebaert, G., Ducatelle, R., & Van Immerseel, F. (2011). An update on alternatives to antimicrobial growth promoters for broilers. *The Veterinary Journal*, *187*(2), 182-188.

Ibeagha-Awemu, E. M., Lee, -W., Ibeagha, A. E., Bannerman, D. D., Paape, M. , & Zhao, X. (2008). Bacterial lipopolysaccharide induces increased expression of toll-like receptor (TLR) 4 and downstream TLR signaling molecules in bovine mammary epithelial cells. *Veterinary research*, *39*(2), 1-12.

Imperial, I. C., & Ibana, A. (2016). Addressing the antibiotic resistance problem with probiotics: reducing the risk of its double-edged sword effect. *Frontiers in microbiology*, *7*, 1983.

Iqbal, H., Khan, B. A., Khan, Z. U., Razzaq, A., Khan, N. U., Menaa, B., & Menaa, F. (2020a). Fabrication, physical characterizations and in vitro antibacterial activity of cefadroxil-loaded chitosan/poly (vinyl alcohol) nanofibers against Staphylococcus aureus clinical isolates. *International journal of biological macromolecules*, *144*, 921-931.

Iqbal, H., Khan, B. A., Khan, Z. U., Razzaq, A., Khan, N. U., Menaa, B., & Menaa, F. (2020b). Fabrication, physical characterizations and in vitro antibacterial activity of cefadroxil-loaded chitosan/poly(vinyl alcohol) nanofibers against Staphylococcus aureus clinical isolates. *International journal of biological macromolecules*, *144*, 921-931. https://doi.org/https://doi.org/10.1016/ijbiomac.2019.09.169

Iqbal, M., Ahmad, M., & Jehangir, W. A. (1999). An assessment of livestock production potential in Pakistan: implications for livestock sector policy [with comments]. *The Pakistan Development Review*, 615-628.

Iqbal, N., Liu, X., Yang, T., Huang, Z., Hanif, Q., Asif, M., Khan, Q. M., & Mansoor, S. (2019). Genomic variants identified from whole-genome resequencing of indicine cattle breeds from Pakistan. *PloS one*, *14*(4), e0215065.

Iqbal, Z., Jabbar, A., Akhtar, M. S., Muhammad, G., & Lateef, M. (2005). Possible role of ethnoveterinary medicine in poverty reduction in Pakistan: use of botanical anthelmintics as an example. *Journal of Agriculture and Social Sciences*, *1*(2), 187-195.

Irshad, R., Tahir, K., Li, B., Ahmad, A., R Siddiqui, A., & Nazir, S. (2017). Antibacterial activity of biochemically capped iron oxide nanoparticles: A view towards green chemistry. *Journal of photochemistry and photobiology. B, Biology*, *170*, 241-246. https://doi.org/10.1016/jphotobiol.2017.04.020

Ito, T., Hiramatsu, K., Tomasz, A., De Lencastre, H., Perreten, V., Holden, M. T., Coleman, D. C., Goering, R., Giffard, P. M., & Skov, R. L. (2012). Guidelines for reporting novel mecA gene homologues. *Antimicrobial agents and Chemotherapy*, *56*(10), 4997-4999.

Jamali, H., Paydar, M., Radmehr, B., Ismail, S., & Dadrasnia, A. (2015). Prevalence and antimicrobial resistance of Staphylococcus aureus isolated from raw milk and dairy products. *Food Control*, *54*, 383-388.

Jamil, B., Habib, H., Abbasi, S. A., Ihsan, A., Nasir, H., & Imran, M. (2016). Development of cefotaxime impregnated chitosan as nano-antibiotics: De novo strategy to combat biofilm forming multi-drug resistant pathogens. *Frontiers in microbiology*, *7*, 330.

Jamil, B., & Syed, M. A. (2017). Nano-antimicrobials: A Viable Approach to Tackle Multidrug-Resistant Pathogens. In *Nanotechnology Applied To Pharmaceutical Technology* (pp. 31-54). Springer.

Jamila, G. S., Sajjad, S., Leghari, S. A. K., & Long, M. (2020). Nitrogen doped carbon quantum dots and GO modified WO3 nanosheets combination as an effective visible photo catalyst. *Journal of hazardous materials*, *382*, 121087. https://doi.org/https://doi.org/10.1016/jhazmat.2019.121087

Jesline, A., John, N. P., Narayanan, P., Vani, C., & Murugan, S. (2015). Antimicrobial activity of zinc and titanium dioxide nanoparticles against biofilm-producing methicillin-resistant Staphylococcus aureus. *Applied Nanoscience*, *5*(2), 157-162.

Jeters, R. T., Wang, G.-R., Moon, K., Shoemaker, N. B., & Salyers, A. A. (2009). Tetracycline-associated transcriptional regulation of transfer genes of the Bacteroides conjugative transposon CTnDOT. *Journal of bacteriology*, *191*(20), 6374-6382.

Jiang, , Pi, , & Cai, (2018). The advancing of zinc oxide nanoparticles for biomedical applications. *Bioinorganic chemistry and applications*, *2018*.

Jiang, L., Wang, F., Han, F., Prinyawiwatkul, W., No, H., & Ge, B. (2013). Evaluation of diffusion and dilution methods to determine the antimicrobial activity of water-soluble chitosan derivatives. *Journal of applied microbiology*, *114*(4), 956-963.

Jiménez, A. L., Vázquez-Olmos, A. R., Acosta-Gío, E., & Álvarez-Pérez, M. A. (2019). In vitro antimicrobial activity evaluation of metal oxide nanoparticles. *Nanoemulsions Prop. Fabr. Appl*, 1-18.

Jin, T., & He, Y. (2011). Antibacterial activities of magnesium oxide (MgO) nanoparticles against foodborne pathogens. *Journal of Nanoparticle Research*, *13*(12), 6877-6885.

Kalayou, S., Haileselassie, M., Gebre-egziabher, G., Tiku'e, T., Sahle, S., Taddele, H., & Ghezu, M. (2012). In–vitro antimicrobial activity screening of some ethnoveterinary medicinal plants traditionally used against mastitis, wound and gastrointestinal tract complication in Tigray Region, Ethiopia. *Asian Pacific journal of tropical biomedicine*, *2*(7), 516-522.

Kandi, V., & Kandi, S. (2015). Antimicrobial properties of nanomolecules: potential candidates as antibiotics in the era of multi-drug resistance. *Epidemiology and health*, *37*.

Kannan, S., & Sundrarajan, M. (2014). A green approach for the synthesis of a cerium oxide nanoparticle: characterization and antibacterial activity. *International Journal of Nanoscience*, *13*(03), 1450018.

Kaszak, B., Krutkiewicz, A., Szopa, D., Kleczkowski, M., & Biegańska, M. (2012). High Prevalence of Candida Yeast in Milk Samples from Cows Suffering from Mastitis in Poland. *The Scientific World Journal*, *2012*, 196347. https://doi.org/10.1100/2012/196347

Kaszanyitzky, É., Jánosi, S., Somogyi, P., Dán, Á., vanderGraaf van Bloois, L., Van Duijkeren, E., & Wagenaar, A. (2007). MRSA transmission between cows and humans. *Emerging infectious diseases*, *13*(4), 630.

Kim, I. Y., Lee, T. G., Reipa, V., & Heo, M. B. (2021). Titanium dioxide induces apoptosis under UVA irradiation via the generation of lysosomal membrane permeabilization-dependent reactive oxygen species in HaCaT cells.

Kimera, Z. I., Mshana, S. E., Rweyemamu, M. M., Mboera, L. E., & Matee, M. I. (2020). Antimicrobial use and resistance in food-producing animals and the environment: an African perspective. *Antimicrobial Resistance & Infection Control*, *9*(1), 1-12.

Kipre, B., Guessennd, N., Koné, M., Gbonon, V., Coulibaly, , & Dosso, M. (2017). Antibacterial activity of the stem bark of Tieghemella Heckelii Pierre ex. A Chev against methicillin-resistant Staphylococcus aureus. *BMC complementary and alternative medicine*, *17*(1), 170.

Kochkodan, V., Tsarenko, S., Potapchenko, N., Kosinova, V., & Goncharuk, V. (2008). Adhesion of microorganisms to polymer membranes: a photobactericidal effect of surface treatment with TiO2. *Desalination*, *220*(1), 380-385. https://doi.org/https://doi.org/10.1016/desal.2007.01.042

Kourtesi, C., Ball, A. R., Huang, Y.-Y., Jachak, S. M., Vera, D. M. A., Khondkar, P., Gibbons, S., Hamblin, M. R., & Tegos, G. P. (2013). Suppl 1: Microbial efflux systems and inhibitors: approaches to drug discovery and the challenge of clinical implementation. *The open microbiology journal*, *7*, 34.

Kravanja, G., Primožič, M., Knez, Ž., & Leitgeb, M. (2019). Chitosan-based (Nano) materials for novel biomedical applications. *Molecules*, *24*(10), 1960.

[Record #192 is using a reference type undefined in this output style.]

Krishnamoorthy, K., Manivannan, G., Kim, S. , Jeyasubramanian, K., & Premanathan, M. (2012). Antibacterial activity of MgO nanoparticles based on lipid peroxidation by oxygen vacancy. *Journal of Nanoparticle Research*, *14*(9), 1-10.

Krukowski, H., Tietze, M., Majewski, T., & Różański, P. (2001). Survey of yeast mastitis in dairy herds of small-type farms in the Lublin region, Poland. *Mycopathologia*, *150*(1), 5-7.

Kuang, Y., Tani, K., Synnott, A. , Ohshima, K., Higuchi, H., Nagahata, H., & Tanji, Y. (2009). Characterization of bacterial population of raw milk from bovine mastitis by culture-independent PCR–DGGE method. *Biochemical engineering journal*, *45*(1), 76-81.

Kubacka, A., Fernández-García, M., Cerrada, M. L., & Fernández-García, M. (2012). Titanium Dioxide–Polymer Nanocomposites with Advanced Properties. In *Nano-Antimicrobials* (pp. 119-149). Springer.

Kumar, M., Curtis, A., & Hoskins, C. (2018). Application of nanoparticle technologies in the combat against anti-microbial resistance. *Pharmaceutics*, *10*(1), 11.

Kumar, P. S. M., Francis, A. P., & Devasena, T. (2014). Biosynthesized and chemically synthesized titania nanoparticles: comparative analysis of antibacterial activity. *Environ. Nanotechnol*, *3*(3), 73-81.

Lago, A., Godden, S., Bey, R., Ruegg, P., & Leslie, K. (2011). The selective treatment of clinical mastitis based on on-farm culture results: I. Effects on antibiotic use, milk withholding time, and short-term clinical and bacteriological outcomes. *Journal of dairy science*, *94*(9), 4441-4456.

Lam, S. , Wong, E. H., Boyer, C., & Qiao, G. G. (2018). Antimicrobial polymeric nanoparticles. *Progress in polymer science*, *76*, 40-64.

Laxminarayan, R., Duse, A., Wattal, C., Zaidi, A. K., Wertheim, H. F., Sumpradit, N., Vlieghe, E., Hara, G. L., Gould, I. M., & Goossens, H. (2013). Antibiotic resistance—the need for global solutions. *The Lancet infectious diseases*, *13*(12), 1057-1098.

Leavis, H. L., Willems, R. , Top, , Spalburg, E., Mascini, E. M., Fluit, A. C., Hoepelman, A., de Neeling, A. , & Bonten, M. (2003). Epidemic and nonepidemic multidrug-resistant Enterococcus faecium. *Emerging infectious diseases*, *9*(9), 1108.

Lee, H.-, Lee, G., Jang, N. R., Yun, H., Song, Y., & Kim, B. S. (2011). Biological synthesis of copper nanoparticles using plant extract. *Nanotechnology*, *1*(1), 371-374.

Lee, H. (2003). Methicillin (oxacillin)-resistant Staphylococcus aureus strains isolated from major food animals and their potential transmission to humans. *Applied and environmental microbiology*, *69*(11), 6489-6494.

Lee, H., Jung, K. Y., & Park, S. B. (1999). Modification of titania particles by ultrasonic spray pyrolysis of colloid. *Journal of materials science*, *34*(16), 4089-4093.

Lei, B.-X., Luo, Q.-P., Yu, X.-Y., Wu, W.-Q., Su, C.-Y., & Kuang, D.-B. (2012). Hierarchical TiO 2 flowers built from TiO 2 nanotubes for efficient Pt-free based flexible dye-sensitized solar cells. *Physical Chemistry Chemical Physics*, *14*(38), 13175-13179.

Leung, Y. H., Yung, M. M., Ng, A. M., Ma, A. P., Wong, S. W., Chan, C. M., Ng, Y. H., Djurišić, A. B., Guo, M., & Wong, M. T. (2015). Toxicity of CeO2 nanoparticles–The effect of nanoparticle properties. *Journal of Photochemistry and Photobiology B: Biology*, *145*, 48-59.

Lhermie, G., Gröhn, Y. T., & Raboisson, D. (2017). Addressing antimicrobial resistance: an overview of priority actions to prevent suboptimal antimicrobial use in food-animal production. *Frontiers in microbiology*, *7*, 2114.

Li, , Xie, B., Xia, K., Li, Y., Han, , & Zhao, C. (2018). Enhanced antibacterial activity of silver doped titanium dioxide-chitosan composites under visible light. *Materials*, *11*(8), 1403.

Li, S., Cai, , Wu, X., & Zheng, F. (2018). Sandwich-like TiO2@ ZnO-based noble metal (Ag, Au, Pt, or Pd) for better photo-oxidation performance: Synergistic effect between noble metal and metal oxide phases. *Applied Surface Science*, *443*, 603-612.

Lima, R., Del Fiol, F. S., & Balcão, V. M. (2019). Prospects for the use of new technologies in combating multidrug-resistant bacteria. *Frontiers in Pharmacology*, *10*, 692.

Lin, H.-F., Liao, S.-C., & Hung, S.-W. (2005). The dc thermal plasma synthesis of ZnO nanoparticles for visible-light photocatalyst. *Journal of photochemistry and photobiology A: Chemistry*, *174*(1), 82-87.

Lin, , Fan, L., Miao, R., Le, X., Chen, S., & Zhou, X. (2015). Enhancing catalytic performance of laccase via immobilization on chitosan/CeO2 microspheres. *International Journal of Biological Macromolecules*, *78*, 1-8.

Littmann, , & Viens, A. M. (2015). The ethical significance of antimicrobial resistance. *Public health ethics*, *8*(3), 209-224.

Liu, Y.-Y., Wang, Y., Walsh, T. R., Yi, L.-X., Zhang, R., Spencer, , Doi, Y., Tian, G., Dong, B., & Huang, X. (2016). Emergence of plasmid-mediated colistin resistance mechanism MCR-1 in animals and human beings in China: a microbiological and molecular biological study. *The Lancet infectious diseases*, *16*(2), 161-168.

Liu, Z., Wang, F., Ren, , & Qu, X. (2019). A series of MOF/Ce-based nanozymes with dual enzyme-like activity disrupting biofilms and hindering recolonization of bacteria. *Biomaterials*, *208*, 21-31.

Lu, H. D., Yang, S. S., Wilson, B. K., McManus, S. A., Chen, C. V.-H., & Prud'homme, R. K. (2017). Nanoparticle targeting of Gram-positive and Gram-negative bacteria for magnetic-based separations of bacterial pathogens. *Applied Nanoscience*, *7*(3-4), 83-93.

Luber, P., Bartelt, E., Genschow, E., Wagner, , & Hahn, H. (2003). Comparison of broth microdilution, E test, and agar dilution methods for antibiotic susceptibility testing of Campylobacter jejuni and Campylobacter coli. *Journal of clinical microbiology*, *41*(3), 1062.

Luseba, D., & Tshisikhawe, M. (2013). Medicinal plants used in the treatment of livestock diseases in Vhembe region, Limpopo province, South Africa. *Journal of Medicinal Plants Research*, *7*(10), 593-601.

Ma, Z., Garrido-Maestu, A., & Jeong, K. C. (2017). Application, mode of action, and in vivo activity of chitosan and its micro-and nanoparticles as antimicrobial agents: A review. *Carbohydrate Polymers*, *176*, 257-265.

Maglica, Ž., Özdemir, E., & McKinney, D. (2015). Single-cell tracking reveals antibiotic-induced changes in mycobacterial energy metabolism. *MBio*, *6*(1).

Makovec, , & Ruegg, P. (2003). Results of milk samples submitted for microbiological examination in Wisconsin from 1994 to 2001. *Journal of dairy science*, *86*(11), 3466-3472.

Malvindi, M. A., De Matteis, V., Galeone, A., Brunetti, V., Anyfantis, G. C., Athanassiou, A., Cingolani, R., & Pompa, P. P. (2014). Toxicity assessment of silica coated iron oxide nanoparticles and biocompatibility improvement by surface engineering. *PLoS One*, *9*(1), e85835.

Mamatha, T., Venkateswara Rao, , Mukkanti, K., & Ramesh, G. (2010). Development of matrix type transdermal patches of lercanidipine hydrochloride: physicochemical and in-vitro characterization. *Daru : journal of Faculty of Pharmacy, Tehran University of Medical Sciences*, *18*(1), 9-16. https://pubmed.ncbi.nlm.nih.gov/22615587

https://www.ncbi.nlm.nih.gov/pmc/articles/PMC3232088/

Mann, G. S., Singh, L. P., & Kumar, P. (2021). Potential applications of polymeric-nanomaterial as drug delivery carriers in the biomedical field. In *Additive Manufacturing with Functionalized Nanomaterials* (pp. 109-134). Elsevier.

Mapara, M., Thomas, B. S., & Bhat, K. (2012). Rabbit as an animal model for experimental research. *Dental research journal*, *9*(1), 111.

Maqbool, Q., Nazar, M., Naz, S., Hussain, T., Jabeen, N., Kausar, R., Anwaar, S., Abbas, F., & Jan, T. (2016). Antimicrobial potential of green synthesized CeO2 nanoparticles from Olea europaea leaf extract. *International journal of nanomedicine*, *11*, 5015.

Maqbool, S. (2015). A comparative ethno-botanical study of Cholistan (an arid area) and Pothwar (a semi-arid area) of Pakistan for traditional medicines. *Journal of Ethnobiology and Ethnomedicine*.

Maron, D. F., Smith, T. , & Nachman, K. E. (2013). Restrictions on antimicrobial use in food animal production: an international regulatory and economic survey. *Globalization and health*, *9*(1), 48.

Marshall, B. M., & Levy, S. B. (2011). Food animals and antimicrobials: impacts on human health. *Clinical microbiology reviews*, *24*(4), 718-733.

Marta, B., Potara, M., Iliut, M., Jakab, E., Radu, T., Imre-Lucaci, F., Katona, G., Popescu, O., & Astilean, S. (2015). Designing chitosan–silver nanoparticles–graphene oxide nanohybrids with enhanced antibacterial activity against Staphylococcus aureus. *Colloids and Surfaces A: Physicochemical and Engineering Aspects*, *487*, 113-120.

Martinez, , & Baquero, F. (2000). Mutation frequencies and antibiotic resistance. *Antimicrobial agents and chemotherapy*, *44*(7), 1771-1777.

Martins, M., Dastidar, S. G., Fanning, S., Kristiansen, E., Molnar, , Pages, -M., Schelz, Z., Spengler, G., Viveiros, M., & Amaral, L. (2008). Potential role of non-antibiotics (helper compounds) in the treatment of multidrug-resistant Gram-negative infections: mechanisms for their direct and indirect activities. *International journal of antimicrobial agents*, *31*(3), 198-208.

Mathias, E. (2004). Ethnoveterinary medicine: harnessing its potential. *Veterinary Bulletin*, *74*(8).

Matsunaga, T., Tomoda, R., Nakajima, T., Nakamura, N., & Komine, T. (1988). Continuous-sterilization system that uses photosemiconductor powders. *Applied and environmental microbiology*, *54*(6), 1330-1333.

Matsunaga, T., Tomoda, R., Nakajima, T., & Wake, H. (1985). Photoelectrochemical sterilization of microbial cells by semiconductor powders. *FEMS Microbiology letters*, *29*(1-2), 211-214.

May, K. L., & Grabowicz, M. (2018). The bacterial outer membrane is an evolving antibiotic barrier. *Proceedings of the National Academy of Sciences*, *115*(36), 8852-8854.

McEwen, S. A., & Collignon, P. (2018). Antimicrobial resistance: a one health perspective. *Microbiology spectrum*, *6*(2), 6.2. 10.

McLeod, A. (2011). *World livestock 2011-livestock in food security*. Food and Agriculture Organization of the United Nations (FAO).

McMurry, L., Petrucci, R. E., & Levy, S. B. (1980). Active efflux of tetracycline encoded by four genetically different tetracycline resistance determinants in Escherichia coli. *Proceedings of the National Academy of Sciences*, *77*(7), 3974-3977.

McVey, S., & Shi, (2010). Vaccines in veterinary medicine: a brief review of history and technology. *Veterinary Clinics: Small Animal Practice*, *40*(3), 381-392.

Medema, M. H., Breitling, R., Bovenberg, R., & Takano, E. (2011). Exploiting plug-and-play synthetic biology for drug discovery and production in microorganisms. *Nature Reviews Microbiology*, *9*(2), 131-137.

Melo, D. A. d., Coelho, I. d. S., Motta, C. C. d., Rojas, A. C. C. M., Dubenczuk, F. C., Coelho, S. d. M. d. O., & Souza, M. M. S. d. (2014). Impairments of mecA gene detection in bovine Staphylococcus spp. *Brazilian Journal of Microbiology*, *45*(3), 1075-1082.

Menaa, F. (2013). When pharma meets nano or the emerging era of nanopharmaceuticals. *Pharmaceut Anal Acta*, *4*(4), 223.

Mishra, R. P., Oviedo-Orta, E., Prachi, P., Rappuoli, R., & Bagnoli, F. (2012). Vaccines and antibiotic resistance. *Current opinion in microbiology*, *15*(5), 596-602.

Mohamed, H. H., Alomair, N. A., Akhtar, S., & Youssef, T. E. (2019). Eco-friendly synthesized α-Fe2O3/TiO2 heterojunction with enhanced visible light photocatalytic activity. *Journal of Photochemistry and Photobiology A: Chemistry*, *382*, 111951.

Mohamed, N. (2020). Synthesis of Hybrid Chitosan Silver Nanoparticles Loaded with Doxorubicin with Promising Anti-cancer Activity. *BioNanoScience*, *10*, 758-765.

Mohammadi, F., Golafshan, N., Kharaziha, M., & Ashrafi, A. (2019). Chitosan-heparin nanoparticle coating on anodized NiTi for improvement of blood compatibility and biocompatibility. *International journal of biological macromolecules*, *127*, 159-168.

Mohandas, A., Deepthi, S., Biswas, R., & Jayakumar, R. (2018). Chitosan based metallic nanocomposite scaffolds as antimicrobial wound dressings. *Bioactive materials*, *3*(3), 267-277.

Moo, C.-L., Yang, S.-K., Yusoff, K., Ajat, M., Thomas, W., Abushelaibi, A., Lim, S. H. E., & Lai, K.-S. (2019). Mechanisms of antimicrobial resistance (AMR) and alternative approaches to overcome AMR. *Current Drug Discovery Technologies*.

Moon, -S., Lee, A.-R., Kang, H.-M., Lee, E.-S., Kim, M.-N., Paik, Y., Park, Y. H., Joo, Y.-S., & Koo, H. (2007). Phenotypic and genetic antibiogram of methicillin-resistant staphylococci isolated from bovine mastitis in Korea. *Journal of dairy science*, *90*(3), 1176-1185.

Morrissey, I., Bouchillon, S. K., Hackel, M., Biedenbach, D. , Hawser, S., Hoban, D., & Badal, R. E. (2014). Evaluation of the Clinical and Laboratory Standards Institute phenotypic confirmatory test to detect the presence of extended-spectrum β-lactamases from 4005 Escherichia coli, Klebsiella oxytoca, Klebsiella pneumoniae and Proteus mirabilis isolates. *Journal of medical microbiology*, *63*(4), 556-561.

Moudgil, P., Bedi, , Moudgil, A. D., Gill, , & Aulakh, R. (2018). Emerging issue of antibiotic resistance from food producing animals in India: Perspective and legal framework. *Food reviews international*, *34*(5), 447-462.

Muñoz-Atienza, E., Gómez-Sala, B., Araújo, C., Campanero, C., Del Campo, R., Hernández, P. E., Herranz, C., & Cintas, L. M. (2013). Antimicrobial activity, antibiotic susceptibility and virulence factors of lactic acid bacteria of aquatic origin intended for use as probiotics in aquaculture. *BMC microbiology*, *13*(1), 15.

Naber, K. G., Bergman, B., Bishop, M. C., Bjerklund-Johansen, T. E., Botto, H., Lobel, B., Cruz, F. , & Selvaggi, F. P. (2001). EAU Guidelines for the Management of Urinary and Male Genital Tract Infectionstextsuperscript1. *European urology*, *40*(5), 576--588.

Nagarwal, R. C., Kant, S., Singh, P., Maiti, P., & Pandit, (2009). Polymeric nanoparticulate system: a potential approach for ocular drug delivery. *Journal of Controlled Release*, *136*(1), 2-13.

Naraginti, S., & Li, Y. (2017). Preliminary investigation of catalytic, antioxidant, anticancer and bactericidal activity of green synthesized silver and gold nanoparticles using Actinidia deliciosa. *Journal of Photochemistry and Photobiology B: Biology*, *170*, 225-234.

Neculai, A. S., Ariton, A. M., Mădescu, B. M., Rîmbu, C. M., & Creangă, Ş. (2021). Nanomaterials and Essential Oils as Candidates for Developing Novel Treatment Options for Bovine Mastitis. *Animals*, *11*(6), 1625.

Nehra, P., Chauhan, R., Garg, N., & Verma, K. (2018). Antibacterial and antifungal activity of chitosan coated iron oxide nanoparticles. *British journal of biomedical science*, *75*(1), 13-18.

Nielsen, C. (2009). *Economic impact of mastitis in dairy cows* (Vol. 2009).

Normanno, G., Corrente, M., La Salandra, G., Dambrosio, A., Quaglia, N., Parisi, A., Greco, G., Bellacicco, A., Virgilio, S., & Celano, G. (2007). Methicillin-resistant Staphylococcus aureus (MRSA) in foods of animal origin product in Italy. *International journal of food microbiology*, *117*(2), 219-222.

Normanno, G., La Salandra, G., Dambrosio, A., Quaglia, N., Corrente, M., Parisi, A., Santagada, G., Firinu, A., Crisetti, E., & Celano, G. (2007). Occurrence, characterization and antimicrobial resistance of enterotoxigenic Staphylococcus aureus isolated from meat and dairy products. *International journal of food microbiology*, *115*(3), 290-296.

Nouman, W., Basra, S. M. A., Siddiqui, M. T., Yasmeen, A., Gull, T., & Alcayde, M. A. C. (2014). Potential of Moringa oleifera L. as livestock fodder crop: a review. *Turkish Journal of Agriculture and Forestry*, *38*(1), 1-14.

O'Toole, G. A. (2011). Microtiter dish biofilm formation assay. *Journal of visualized experiments: JoVE*(47).

O'Brien-Simpson, N. M., Pantarat, N., Attard, T. , Walsh, K. A., & Reynolds, E. C. (2016). A rapid and quantitative flow cytometry method for the analysis of membrane disruptive antimicrobial activity. *PloS one*, *11*(3), e0151694.

[Record #225 is using a reference type undefined in this output style.]

OIE, W. (2010). Terrestrial animal health code. *Prevention, detection and control of Salmonella in poultry*.

Oliver, S. P., Murinda, S. E., & Jayarao, B. M. (2011). Impact of antibiotic use in adult dairy cows on antimicrobial resistance of veterinary and human pathogens: a comprehensive review. *Foodborne pathogens and disease*, *8*(3), 337-355.

Olson, , Casman, E., Baer, E., & Stone, E. (1970). Enterotoxigenicity of Staphylococcus aureus cultures isolated from acute cases of bovine mastitis. *Applied microbiology*, *20*(4), 605-607.

Omolo, C. A., Kalhapure, R. S., Agrawal, N., Jadhav, M., Rambharose, S., Mocktar, C., & Govender, T. (2018). A hybrid of mPEG-b-PCL and G1-PEA dendrimer for enhancing delivery of antibiotics. *Journal of Controlled Release*, *290*, 112-128.

Organization, W. H. (2014). WHO's first global report on antibiotic resistance reveals serious, worldwide threat to public health. *New WHO report provides the most comprehensive picture of antibiotic resistance to date, with data from*, *114*.

Padla, E. P., Solis, L. T., Levida, R. M., Shen, C.-C., & Ragasa, C. Y. (2012). Antimicrobial isothiocyanates from the seeds of Moringa oleifera Lam. *Zeitschrift für Naturforschung C*, *67*(11-12), 557-564.

Palmer, K. L., Kos, V. N., & Gilmore, M. S. (2010). Horizontal gene transfer and the genomics of enterococcal antibiotic resistance. *Current opinion in microbiology*, *13*(5), 632-639.

Parvathi, V. P., Umadevi, M., Sasikala, R., Parimaladevi, R., Ragavendran, V., Mayandi, , & Sathe, G. (2020). Novel silver nanoparticles/activated carbon co-doped titania nanoparticles for enhanced antibacterial activity. *Materials Letters*, *258*, 126775.

Patil, S., Sandberg, A., Heckert, E., Self, W., & Seal, S. (2007). Protein adsorption and cellular uptake of cerium oxide nanoparticles as a function of zeta potential. *Biomaterials*, *28*(31), 4600-4607.

Patra, K., Das, G., Fraceto, L. F., Campos, E. V. R., del Pilar Rodriguez-Torres, M., Acosta-Torres, L. S., Diaz-Torres, L. A., Grillo, R., Swamy, M. K., & Sharma, S. (2018). Nano based drug delivery systems: recent developments and future prospects. *Journal of nanobiotechnology*, *16*(1), 1-33.

Pelgrift, R. Y., & Friedman, A. (2013). Nanotechnology as a therapeutic tool to combat microbial resistance. *Advanced drug delivery reviews*, *65*(13-14), 1803-1815.

Perdikaki, A., Galeou, A., Pilatos, G., Prombona, A., & Karanikolos, G. N. (2018). Ion-based metal/graphene antibacterial agents comprising mono-ionic and bi-ionic silver and copper species. *Langmuir*, *34*(37), 11156-11166.

Pereira, R. V. V., Siler, D., Bicalho, R. C., & Warnick, L. D. (2014). In vivo selection of resistant E. coli after ingestion of milk with added drug residues. *PloS one*, *9*(12), e115223.

Poeloengan, M. (2011). The effect of red ginger (Zingiber officinale Roscoe) extract on the growth of mastitis causing bacterial isolates. *African Journal of Microbiology Research*, *5*(4), 382-388.

Poole, K. (2007). Efflux pumps as antimicrobial resistance mechanisms. *Annals of medicine*, *39*(3), 162-176.

Prasad, R., & Rattan, G. (2010). Preparation methods and applications of CuO-CeO2 catalysts: A short review. *Bulletin of Chemical Reaction Engineering & Catalysis*, *5*(1), 7.

Pura Naik, , Jagan Mohan Rao, L., Mohan Kumar, T., & Sampathu, S. (2004). Chemical composition of the volatile oil from the pericarp (husk) of large cardamom (Amomum subulatum Roxb.). *Flavour and Fragrance Journal*, *19*(5), 441-444.

Pyorala, S. *Efficacy of two therapy regimens for treatment of experimentally induced Escherichia coli mastitis in cows.--p. 453-461.*

Pyörälä, S., Kaartinen, L., Käck, H., & Rainio, V. (1994). Efficacy of two therapy regimens for treatment of experimentally induced Escherichia coli mastitis in cows. *Journal of dairy science*, *77*(2), 453-461.

Qi, M., Li, W., Zheng, X., Li, X., Sun, Y., Wang, Y., Li, C., & Wang, L. (2020). Cerium and Its Oxidant-Based Nanomaterials for Antibacterial Applications: A State-of-the-Art Review [Review]. *Frontiers in Materials*, *7*(213). https://doi.org/10.3389/fmats.2020.00213

Qian, T., Su, H., & Tan, T. (2011). The bactericidal and mildew-proof activity of a TiO2–chitosan composite. *Journal of Photochemistry and Photobiology A: Chemistry*, *218*(1), 130-136.

Qu, Y., Zhao, H., Nobrega, D. B., Cobo, E. R., Han, B., Zhao, Z., Li, S., Li, M., Barkema, H. W., & Gao, (2019). Molecular epidemiology and distribution of antimicrobial resistance genes of Staphylococcus species isolated from Chinese dairy cows with clinical mastitis. *Journal of dairy science*, *102*(2), 1571-1583.

Rabea, E. I., Badawy, M. E.-T., Stevens, C. V., Smagghe, G., & Steurbaut, W. (2003). Chitosan as antimicrobial agent: applications and mode of action. *Biomacromolecules*, *4*(6), 1457-1465.

Radostits, O. M., Gay, C. C., Hinchcliff, K. W., & Constable, P. D. (2006). *Veterinary Medicine E-Book: A textbook of the diseases of cattle, horses, sheep, pigs and goats*. Elsevier Health Sciences.

Raghunath, D. (2008). Emerging antibiotic resistance in bacteria with special reference to India. *Journal of biosciences*, *33*(4), 593-603.

Rahimi, E., Ameri, M., & Momtaz, H. (2010). Prevalence and antimicrobial resistance of Listeria species isolated from milk and dairy products in Iran. *Food Control*, *21*(11), 1448-1452.

Ramos, S., Igrejas, G., Rodrigues, , Capelo-Martinez, -L., & Poeta, P. (2012). Genetic characterisation of antibiotic resistance and virulence factors in vanA-containing enterococci from cattle, sheep and pigs subsequent to the discontinuation of the use of avoparcin. *The Veterinary Journal*, *193*(1), 301-303.

Raney, T. (2009). The state of food and agriculture: livestock in the balance. *Food and Agriculture Organization of the United Nations, Rome, Italy*.

Rao, P. R., & Diwan, P. V. (1998). Formulation and in vitro evaluation of polymeric films of diltiazem hydrochloride and indomethacin for transdermal administration. *Drug development and industrial pharmacy*, *24*(4), 327-336.

Raveendran, P., Fu, , & Wallen, S. L. (2003). Completely "green" synthesis and stabilization of metal nanoparticles. *Journal of the American Chemical Society*, *125*(46), 13940-13941.

Raza, Z. A., Khalil, S., Ayub, A., & Banat, I. M. (2020). Recent developments in chitosan encapsulation of various active ingredients for multifunctional applications. *Carbohydrate Research*, *492*, 108004. https://doi.org/https://doi.org/10.1016/carres.2020.108004

Razani, A., Abdullah, A. H., Fitrianto, A., Yusof, N. A., & Gaya, U. I. (2017). Sol-gel synthesis of Fe2o3-doped Tio2 photocatalyst for optimized photocatalytic degradation of 2, 4-dichlorophenoxyacetic acid. *Oriental Journal of Chemistry*, *33*(4), 1959.

Reddy, M. K., Gupta, S. K., Jacob, M. R., Khan, S. I., & Ferreira, D. (2007). Antioxidant, antimalarial and antimicrobial activities of tannin-rich fractions, ellagitannins and phenolic acids from Punica granatum L. *Planta medica*, *53*(05), 461-467.

Rehman, A., Jingdong, L., Chandio, A. A., & Hussain, I. (2017). Livestock production and population census in Pakistan: Determining their relationship with agricultural GDP using econometric analysis. *Information Processing in Agriculture*, *4*(2), 168-177.

Reygaert, W. C. (2018). An overview of the antimicrobial resistance mechanisms of bacteria. *AIMS microbiology*, *4*(3), 482-501. https://doi.org/10.3934/microbiol.2018.3.482

Righter, (1987). Ciprofloxacin treatment of Staphylococcus aureus infections. *Journal of Antimicrobial Chemotherapy*, *20*(4), 595-597. https://doi.org/10.1093/jac/20.4.595

Ruegg, P. L. (2014). Risks, realities and responsibilities associated with mastitis treatments. NMC Regional Meeting, Ghent, Proceedings,

Rufus, A., Sreeju, N., & Philip, D. (2016). Synthesis of biogenic hematite (α-Fe 2 O 3) nanoparticles for antibacterial and nanofluid applications. *RSC advances*, *6*(96), 94206-94217.

Saeed, K., Ahmad, N., Dryden, M., Cortes, N., Marsh, P., Sitjar, A., Wyllie, S., Bourne, S., Hemming, , & Jeppesen, C. (2014). Oxacillin-susceptible methicillin-resistant Staphylococcusaureus (OS-MRSA), a hidden resistant mechanism among clinically significant isolates in the Wessex region/UK. *Infection*, *42*(5), 843-847.

Saha, B., Bhattacharya, , Mukherjee, A., Ghosh, A., Santra, C., Dasgupta, A. K., & Karmakar, P. (2007). In vitro structural and functional evaluation of gold nanoparticles conjugated antibiotics. *Nanoscale Research Letters*, *2*(12), 614.

Sajjad, A. K. L., Shamaila, S., Tian, B., Chen, F., & Zhang, (2009). One step activation of WOx/TiO2 nanocomposites with enhanced photocatalytic activity. *Applied Catalysis B: Environmental*, *91*(1-2), 397-405.

Sakoulas, G., Gold, H. S., Venkataraman, L., DeGirolami, P. C., Eliopoulos, G. M., & Qian, Q. (2001). Methicillin-resistant Staphylococcus aureus: comparison of susceptibility

testing methods and analysis of mecA-positive susceptible strains. *Journal of clinical microbiology*, *39*(11), 3946-3951.

Salmon, G., MacLeod, M., Claxton, , Ciamarra, U. P., Robinson, T., Duncan, A., & Peters, A. (2020). Exploring the landscape of livestock 'Facts'. *Global food security*, *25*.

Sansoucy, R. (1995). Livestock-a driving force for food security and sustainable development. *World*, *3074*(5389), 1035.

Saranya, A., Thamer, A., Ramar, K., Priyadharsan, A., Raj, V., Murugan, K., Murad, A., & Maheshwaran, P. (2020). Facile one pot microwave-assisted green synthesis of Fe2O3/Ag nanocomposites by phytoreduction: potential application as sunlight-driven photocatalyst, antibacterial and anticancer agent. *Journal of Photochemistry and Photobiology B: Biology*, *207*, 111885.

Saravanakumar, K., Chelliah, R., Shanmugam, S., Varukattu, N. B., Oh, D.-H., Kathiresan, K., & Wang, M.-H. (2018). Green synthesis and characterization of biologically active nanosilver from seed extract of Gardenia jasminoides Ellis. *Journal of Photochemistry and Photobiology B: Biology*, *185*, 126-135.

Saravanan, R., Aviles, , Gracia, F., Mosquera, E., & Gupta, V. K. (2018). Crystallinity and lowering band gap induced visible light photocatalytic activity of TiO2/CS (Chitosan) nanocomposites. *International journal of biological macromolecules*, *109*, 1239-1245.

Sasidharan, S., Prema, B., & Latha, L. Y. (2011). Antimicrobial drug resistance of Staphylococcus aureus in dairy products. *Asian Pacific journal of tropical biomedicine*, *1*(2), 130-132.

Sasikumar, S. (2013). Effect of particle size of calcium phosphate based bioceramic drug delivery carrier on the release kinetics of ciprofloxacin hydrochloride: an in vitro study. *Frontiers of Materials Science*, *7*(3), 261-268.

Savoia, D. (2012). Plant-derived antimicrobial compounds: alternatives to antibiotics. *Future microbiology*, *7*(8), 979-990.

Sawant, A. A., Hegde, N. V., Straley, B. A., Donaldson, S. C., Love, B. C., Knabel, S. , & Jayarao, B. M. (2007). Antimicrobial-resistant enteric bacteria from dairy cattle. *Applied and environmental microbiology*, *73*(1), 156-163.

Schukken, Y., Bennett, G., Zurakowski, M., Sharkey, H., Rauch, B., Thomas, M., Ceglowski, B., Saltman, R., Belomestnykh, N., & Zadoks, R. (2011). Randomized clinical trial to evaluate the efficacy of a 5-day ceftiofur hydrochloride intramammary treatment on nonsevere gram-negative clinical mastitis. *Journal of dairy science*, *94*(12), 6203-6215.

Seegers, H., Fourichon, C., & Beaudeau, F. (2003). Production effects related to mastitis and mastitis economics in dairy cattle herds. *Veterinary research*, *34*(5), 475-491.

Sendra, M., Yeste, P., Moreno-Garrido, I., Gatica, M., & Blasco, (2017). CeO2 NPs, toxic or protective to phytoplankton? Charge of nanoparticles and cell wall as factors which cause changes in cell complexity. *Science of The Total Environment*, *590*, 304-315.

Senthilkumar, P., Yaswant, G., Kavitha, S., Chandramohan, E., Kowsalya, G., Vijay, R., Sudhagar, B., & Kumar, D. R. S. (2019). Preparation and characterization of hybrid chitosan-silver nanoparticles (Chi-Ag NPs); A potential antibacterial agent. *International journal of biological macromolecules*, *141*, 290-298.

Serwecińska, L. (2020). Antimicrobials and antibiotic-resistant bacteria: a risk to the environment and to public health. *Water*, *12*(12), 3313.

Shafai, N., El-Khouly, M. E., El-Kemary, M., Ramadan, M., Eldesoukey, I., & Masoud, M. (2019). Graphene oxide decorated with zinc oxide nanoflower, silver and titanium dioxide nanoparticles: fabrication, characterization, DNA interaction, and antibacterial activity. *RSC advances*, *9*(7), 3704-3714.

Shah, A., Buabeid, M. A., Arafa, E.-S. A., Hussain, I., Li, L., & Murtaza, G. (2019). The wound healing and antibacterial potential of triple-component nanocomposite (chitosan-silver-sericin) films loaded with moxifloxacin. *International journal of pharmaceutics*, *564*, 22-38.

Shahriar, S., Mondal, , Hasan, M. N., Revuri, V., Lee, D. Y., & Lee, Y.-K. (2019). Electrospinning nanofibers for therapeutics delivery. *Nanomaterials*, *9*(4), 532.

Shahverdi, A. R., Fakhimi, A., Shahverdi, H. R., & Minaian, S. (2007). Synthesis and effect of silver nanoparticles on the antibacterial activity of different antibiotics against Staphylococcus aureus and Escherichia coli. *Nanomedicine: Nanotechnology, Biology and Medicine*, *3*(2), 168-171.

Shahzad, S., Yar, M., Siddiqi, S. A., Mahmood, N., Rauf, A., Anwar, M. S., & Afzaal, S. (2015). Chitosan-based electrospun nanofibrous mats, hydrogels and cast films: novel anti-bacterial wound dressing matrices. *Journal of Materials Science: Materials in Medicine*, *26*(3), 136.

Shameli, K., Ahmad, M. B., Yunus, W. Z. W., Ibrahim, N. A., & Darroudi, M. (2010). Synthesis and characterization of silver/talc nanocomposites using the wet chemical reduction method. *International journal of nanomedicine*, *5*, 743.

Sharif, A., & Muhammad, G. (2008). Somatic cell count as an indicator of udder health status under modern dairy production: A review. *Pakistan Vet. J*, *28*(4), 194-200.

Sharma, C., Rokana, N., Chandra, M., Singh, B. P., Gulhane, R. D., Gill, P. S., Ray, P., Puniya, A. K., & Panwar, H. (2018). Antimicrobial Resistance: Its Surveillance, Impact, and Alternative Management Strategies in Dairy Animals [Review]. *Frontiers in Veterinary Science*, *4*(237). https://doi.org/10.3389/fvets.2017.00237

Shende, P., Oza, B., & Gaud, R. (2018). Silver-doped titanium dioxide nanoparticles encapsulated in chitosan–PVA film for synergistic antimicrobial activity. *International Journal of Polymeric Materials and Polymeric Biomaterials*, *67*(18), 1080-1086.

Shrivastava, S. R., Shrivastava, P. S., & Ramasamy, (2018). World health organization releases global priority list of antibiotic-resistant bacteria to guide research, discovery, and development of new antibiotics. *Journal of Medical Society*, *32*(1), 76.

Singh, , Dutta, T., Kim, K.-H., Rawat, M., Samddar, P., & Kumar, P. (2018). 'Green'synthesis of metals and their oxide nanoparticles: applications for environmental remediation. *Journal of nanobiotechnology*, *16*(1), 1-24.

Singh, V., Jaryal, M., Gupta, , & Kumar, P. (2012). Antibacterial activity of medicinal plants against extended spectrum beta lactamase producing bacteria causing urinary tract infection. *Int J Drug Res Tech*, *2*, 263-267.

Slavin, Y. N., Asnis, , Häfeli, U. O., & Bach, H. (2017). Metal nanoparticles: understanding the mechanisms behind antibacterial activity. *Journal of nanobiotechnology*, *15*(1), 1-20.

Smith, K. L., Todhunter, D., & Schoenberger, P. (1985). Environmental mastitis: cause, prevalence, prevention. *Journal of Dairy Science*, *68*(6), 1531-1553.

Smitha, S., Nissamudeen, K., Philip, D., & Gopchandran, K. (2008). Studies on surface plasmon resonance and photoluminescence of silver nanoparticles. *Spectrochimica Acta Part A: Molecular and Biomolecular Spectroscopy*, *71*(1), 186-190.

Sobhani, Z., Samani, S. M., Montaseri, H., & Khezri, E. (2017). Nanoparticles of chitosan loaded ciprofloxacin: fabrication and antimicrobial activity. *Advanced pharmaceutical bulletin*, *7*(3), 427.

Sosnik, A., Carcaboso, Á. M., Glisoni, R. , Moretton, M. A., & Chiappetta, D. A. (2010). New old challenges in tuberculosis: potentially effective nanotechnologies in drug delivery. *Advanced drug delivery reviews*, *62*(4-5), 547-559.

Staff, D. (2010). Top 200 generic drugs by total prescriptions. *Drug Topics*.

Stafuzza, N. B., Zerlotini, A., Lobo, F. P., Yamagishi, M. E. B., Chud, T. C. S., Caetano, A. R., Munari, D. P., Garrick, D. , Machado, M. A., & Martins, M. F. (2017). Single nucleotide variants and InDels identified from whole-genome re-sequencing of Guzerat, Gyr, Girolando and Holstein cattle breeds. *PloS one*, *12*(3), e0173954.

Stanić, V., & Tanasković, S. B. (2020). Antibacterial activity of metal oxide nanoparticles. In *Nanotoxicity* (pp. 241-274). Elsevier.

Stavrovskaya, A., & Stromskaya, T. (2008). Transport proteins of the ABC family and multidrug resistance of tumor cells. *Biochemistry (Moscow)*, *73*(5), 592-604.

Sung, H., Hwang, M.-R., Kim, O., Lee, H., Kim, Y. I., Kim, H., Chang, S. W., Jin, S. G., Kim, A., & Lyoo, W. S. (2010). Gel characterisation and in vivo evaluation of minocycline-loaded wound dressing with enhanced wound healing using polyvinyl alcohol and chitosan. *International journal of pharmaceutics*, *392*(1-2), 232-240.

Suojala, L., Kaartinen, L., & Pyörälä, S. (2013). Treatment for bovine E scherichia coli mastitis–an evidence-based approach. *Journal of veterinary pharmacology and therapeutics*, *36*(6), 521-531.

Susić, E. (2004). Mechanisms of resistance in Enterobacteriaceae towards beta-lactamase antibiotics. *Acta medica Croatica: casopis Hravatske akademije medicinskih znanosti*, *58*(4), 307-312.

Taga, I., Lan, C. Q., & Altosaar, I. (2012). Plant essential oils and mastitis disease: Their potential inhibitory effects on pro-inflammatory cytokine production in response to

bacteria related inflammation. *Natural Product Communications*, *7*(5), 1934578X1200700534.

Taponen, S., & Pyörälä, S. (2009). Coagulase-negative staphylococci as cause of bovine mastitis—Not so different from Staphylococcus aureus? *Veterinary microbiology*, *134*(1-2), 29-36.

Tasli, H., & Bahar, I. H. (2005). Molecular characterization of TEM-and SHV-derived extended-spectrum beta-lactamases in hospital-based Enterobacteriaceae in Turkey. *Japanese journal of infectious diseases*, *58*(3), 162.

Thomson, E., Kaufmann, R. v., Li Pun, H., Treacher, T., & Houten, H. v. (2000). Global agenda for livestock research: Proceedings of a consultation on setting livestock research priorities in West Asia and North Africa (WANA) region.

Thorley, A. , & Tetley, T. D. (2013). New perspectives in nanomedicine. *Pharmacology & therapeutics*, *140*(2), 176-185.

Thu, H. P., Nam, N. H., Quang, B. T., Son, H. A., Toan, N. L., & Quang, D. T. (2015). In vitro and in vivo targeting effect of folate decorated paclitaxel loaded PLA–TPGS nanoparticles. *Saudi Pharmaceutical Journal*, *23*(6), 683-688.

Thukkaram, M., Sitaram, S., & Subbiahdoss, G. (2014). Antibacterial efficacy of iron-oxide nanoparticles against biofilms on different biomaterial surfaces. *International Journal of biomaterials*, *2014*.

Tian, , Wong, K. K., Ho, C. M., Lok, C. N., Yu, W. Y., Che, C. M., Chiu, F., & Tam, P. K. (2007). Topical delivery of silver nanoparticles promotes wound healing. *ChemMedChem*, *2*(1), 129-136.

Tinelli, M., Cataldo, M. A., Mantengoli, E., Cadeddu, C., Cunietti, E., Luzzaro, F., Rossolini, G. M., & Tacconelli, E. (2012). Epidemiology and genetic characteristics of extended-spectrum β-lactamase-producing Gram-negative bacteria causing urinary tract infections in long-term care facilities. *Journal of antimicrobial chemotherapy*, *67*(12), 2982-2987.

Tomankova, K., Horakova, , Harvanova, M., Malina, L., Soukupova, , Hradilova, S., Kejlova, K., Malohlava, , Licman, L., Dvorakova, M., Jirova, D., & Kolarova, H. (2015). Cytotoxicity, cell uptake and microscopic analysis of titanium dioxide and

silver nanoparticles in vitro. *Food and Chemical Toxicology*, *82*, 106-115. https://doi.org/https://doi.org/10.1016/fct.2015.03.027

Tomke, P. D., & Rathod, V. K. (2020). Facile fabrication of silver on magnetic nanocomposite (Fe3O4@ Chitosan–AgNP nanocomposite) for catalytic reduction of anthropogenic pollutant and agricultural pathogens. *International journal of biological macromolecules*, *149*, 989-999.

Tripathi, R., Narayan, A., Bramhecha, I., & Sheikh, (2019). Development of multifunctional linen fabric using chitosan film as a template for immobilization of in-situ generated CeO2 nanoparticles. *International journal of biological macromolecules*, *121*, 1154-1159.

Tsubakishita, S., Kuwahara-Arai, K., Baba, T., & Hiramatsu, K. (2010). Staphylococcal cassette chromosome mec-like element in Macrococcus caseolyticus. *Antimicrobial agents and Chemotherapy*, *54*(4), 1469-1475.

Turutoglu, H., Hasoksuz, M., Ozturk, D., Yildirim, M., & Sagnak, S. (2009). Methicillin and aminoglycoside resistance in Staphylococcus aureus isolates from bovine mastitis and sequence analysis of their mecA genes. *Veterinary research communications*, *33*(8), 945-956.

Udaondo, Z., & Huertas, M. (2020). Fighting the enemy: one health approach against microbial resistance. *Microbial biotechnology*, *13*(4), 888.

ul Hassan, H., Murad, W., Tariq, A., & Ahmad, A. (2014). Ethnoveterinary study of medicinal plants in Malakand Valley, District Dir (Lower), Khyber Pakhtunkhwa, Pakistan. *Irish Veterinary Journal*, *67*(1), 6.

Unnerstad, H. E., Lindberg, A., Waller, K. P., Ekman, T., Artursson, K., Nilsson-Öst, M., & Bengtsson, B. (2009). Microbial aetiology of acute clinical mastitis and agent-specific risk factors. *Veterinary microbiology*, *137*(1-2), 90-97.

Uzair, B., Liaqat, A., Iqbal, H., Menaa, B., Razzaq, A., Thiripuranathar, G., Fatima Rana, N., & Menaa, F. (2020). Green and Cost-Effective Synthesis of Metallic Nanoparticles by Algae: Safe Methods for Translational Medicine. *Bioengineering*, *7*(4), 129.

van der Putten, B. C. L., Remondini, D., Pasquini, G., Janes, V. A., Matamoros, S., & Schultsz, C. (2018). Quantifying the contribution of four resistance mechanisms to

ciprofloxacin MIC in Escherichia coli: a systematic review. *Journal of Antimicrobial Chemotherapy*, *74*(2), 298-310. https://doi.org/10.1093/jac/dky417

Van Vleck Pereira, R., Lima, S., Siler, D., Foditsch, C., Warnick, L. D., & Bicalho, R. C. (2016). Ingestion of milk containing very low concentration of antimicrobials: longitudinal effect on fecal microbiota composition in preweaned calves. *PloS one*, *11*(1), e0147525.

Vanhauteghem, D., Audenaert, K., Demeyere, K., Hoogendoorn, F., Janssens, G. P., & Meyer, E. (2019). Flow cytometry, a powerful novel tool to rapidly assess bacterial viability in metal working fluids: Proof-of-principle. *PloS one*, *14*(2), e0211583.

Vasoo, S., Barreto, N., & Tosh, P. K. (2015). Emerging issues in gram-negative bacterial resistance: an update for the practicing clinician. Mayo Clinic Proceedings,

Vasquez, R. D., Apostol, G., de Leon, D., Mariano, D., Mirhan, C. M. C., Pangan, S. S., Reyes, A. G. M., & Zamora, E. T. (2016). Polysaccharide-mediated green synthesis of silver nanoparticles from Sargassum siliquosum JG Agardh: Assessment of toxicity and hepatoprotective activity. *OpenNano*, *1*, 16-24.

Veeraraghavan, B., Jesudason, M. R., Prakasah, A. , Anandan, S., Sahni, R. D., Pragasam, A. K., Bakthavatchalam, Y. D., Selvakumar, R. , Dhole, T., & Rodrigues, C. (2018). Antimicrobial susceptibility profiles of gram-negative bacteria causing infections collected across India during 2014–2016: Study for monitoring antimicrobial resistance trend report. *Indian journal of medical microbiology*, *36*(1), 32.

Venter, H., Henningsen, Michael L., & Neville, S. (2017). Antimicrobial resistance in healthcare, agriculture and the environment: The biochemistry behind the headlines. *Essays In Biochemistry*, *61*, 1-10. https://doi.org/10.1042/EBC20160053

Ventola, C. L. (2015). The antibiotic resistance crisis: part 1: causes and threats. *Pharmacy and therapeutics*, *40*(4), 277.

Vijayalakshmi, K., & Sivaraj, D. (2016). Synergistic antibacterial activity of barium doped TiO 2 nanoclusters synthesized by microwave processing. *RSC advances*, *6*(12), 9663-9671.

Vissio, C., Agüero, D., Raspanti, C., Odierno, L., & Larriestra, A. (2015). Productive and economic daily losses due to mastitis and its control expenditures in dairy farms in Córdoba, Argentina. *Archivos de Medicina Veterinaria*, *47*(1), 7-14.

Wady, A. F., Machado, A. L., Foggi, C. C., Zamperini, C. A., Zucolotto, V., Moffa, E. B., & Vergani, C. E. (2014). Effect of a Silver Nanoparticles Solution on Staphylococcus aureus and Candida spp. *Journal of Nanomaterials, 2014.*

Waller, K. P., Aspán, A., Nyman, A., Persson, Y., & Andersson, U. G. (2011). CNS species and antimicrobial resistance in clinical and subclinical bovine mastitis. *Veterinary microbiology, 152*(1-2), 112-116.

Wang, C., He, C., Tong, Z., Liu, X., Ren, B., & Zeng, F. (2006). Combination of adsorption by porous CaCO3 microparticles and encapsulation by polyelectrolyte multilayer films for sustained drug delivery. *International journal of pharmaceutics, 308*(1-2), 160-167.

Wang, L., He, H., Yu, Y., Sun, L., Liu, S., Zhang, C., & He, L. (2014). Morphology-dependent bactericidal activities of Ag/CeO2 catalysts against Escherichia coli. *Journal of Inorganic Biochemistry, 135*, 45-53.

Wang, L., Hu, C., & Shao, L. (2017). The antimicrobial activity of nanoparticles: present situation and prospects for the future. *International journal of nanomedicine, 12*, 1227.

Wang, S., Zeng, X., Yang, Q., & Qiao, S. (2016). Antimicrobial peptides as potential alternatives to antibiotics in food animal industry. *International journal of molecular sciences, 17*(5), 603.

Wang, X., & Li, Y. (2003). Synthesis and formation mechanism of manganese dioxide nanowires/nanorods. *Chemistry–A European Journal, 9*(1), 300-306.

Waterman, C., Rojas-Silva, P., Tumer, T. B., Kuhn, P., Richard, A. , Wicks, S., Stephens, M., Wang, Z., Mynatt, R., & Cefalu, W. (2015). Isothiocyanate-rich Moringa oleifera extract reduces weight gain, insulin resistance, and hepatic gluconeogenesis in mice. *Molecular nutrition & food research, 59*(6), 1013-1024.

Wellington, E. M., Boxall, A. B., Cross, P., Feil, E. , Gaze, W. H., Hawkey, P. M., Johnson-Rollings, A. S., Jones, D. L., Lee, N. M., & Otten, W. (2013). The role of the natural environment in the emergence of antibiotic resistance in Gram-negative bacteria. *The Lancet infectious diseases, 13*(2), 155-165.

Woolhouse, M., Ward, M., van Bunnik, B., & Farrar, (2015). Antimicrobial resistance in humans, livestock and the wider environment. *Philosophical Transactions of the Royal Society B: Biological Sciences*, *370*(1670), 20140083.

Xia, T., Kovochich, M., Liong, M., Madler, L., Gilbert, B., Shi, H., Yeh, I., Zink, I., & Nel, A. E. (2008). Comparison of the mechanism of toxicity of zinc oxide and cerium oxide nanoparticles based on dissolution and oxidative stress properties. *ACS nano*, *2*(10), 2121-2134.

Xiao, Q. (2021). Coating and Film-Forming Properties. In *Food Hydrocolloids* (pp. 267-306). Springer.

Xiong, K.-r., Liang, Y.-r., Ou-yang, Y., Wu, D.-c., & Fu, R.-w. (2019). Nanohybrids of silver nanoparticles grown in-situ on a graphene oxide silver ion salt: Simple synthesis and their enhanced antibacterial activity. *New Carbon Materials*, *34*(5), 426-433.

Xu, Z., Li, L., Shirtliff, M., Peters, B., Li, B., Peng, Y., Alam, M. , Yamasaki, S., & Shi, L. (2011). Resistance Class 1 integron in clinical methicillin-resistant Staphylococcus aureus strains in southern China, 2001–2006. *Clinical Microbiology and Infection*, *17*(5), 714-718.

Yadav, P., Gaur, P., Yadav, A. B., Huma, Z. I., & Sharma, N. (2020). Bioengineered ciprofloxacin loaded chitosan nanoparticles for the treatment of Bovine Mastitis. *bioRxiv*, 2020.2005.2009.085563. https://doi.org/10.1101/2020.05.09.085563

Yang, B., Li, X., Shi, S., Kong, X., Guo, G., Huang, M., Luo, F., Wei, Y., Zhao, X., & Qian, Z. (2010). Preparation and characterization of a novel chitosan scaffold. *Carbohydrate Polymers*, *80*(3), 860-865.

Yang, X. H., Fu, H. T., Wang, X. C., Yang, L., Jiang, X. C., & Yu, A. B. (2014). Synthesis of silver-titanium dioxide nanocomposites for antimicrobial applications. *Journal of Nanoparticle Research*, *16*(8), 2526. https://doi.org/10.1007/s11051-014-2526-8

Younis, G., Awad, A., & Ashraf, N. (2017). Molecular and phenotypic characterization of antimicrobial resistance in gram negative bacteria recovered from subclinical mastitis. *Adv. Anim. Vet. Sci*, *5*(5), 196-204.

Yuan, G., Chen, X., & Li, D. (2016). Chitosan films and coatings containing essential oils: The antioxidant and antimicrobial activity, and application in food systems. *Food Research International*, *89*, 117-128.

Yuan, Y.-G., Peng, Q.-L., & Gurunathan, S. (2017). Effects of silver nanoparticles on multiple drug-resistant strains of Staphylococcus aureus and Pseudomonas aeruginosa from mastitis-infected goats: an alternative approach for antimicrobial therapy. *International journal of molecular sciences*, *18*(3), 569.

Yusof, N. A. A., Zain, N. M., & Pauzi, N. (2019). Synthesis of ZnO nanoparticles with chitosan as stabilizing agent and their antibacterial properties against Gram-positive and Gram-negative bacteria. *International journal of biological macromolecules*, *124*, 1132-1136.

Zafar, N., Uzair, B., Niazi, M. B. K., Sajjad, S., Samin, G., Arshed, M. , & Rafiq, S. (2020). Fabrication & characterization of chitosan coated biologically synthesized TiO2 nanoparticles against PDR E. coli of veterinary origin. *Advances in Polymer Technology*, *2020*.

Zaman, M. B., Poolla, R., Singh, P., & Gudipati, T. (2020). Biogenic synthesis of CuO nanoparticles using Tamarindus indica L. and a study of their photocatalytic and antibacterial activity. *Environmental Nanotechnology, Monitoring & Management*, *14*, 100346.

Zhang, M., Zhang, C., Zhai, X., Luo, F., Du, Y., & Yan, C. (2019). Antibacterial mechanism and activity of cerium oxide nanoparticles. *Science China Materials*, *62*(11), 1727-1739.

Zhang, X.-F., Liu, Z.-G., Shen, W., & Gurunathan, S. (2016). Silver nanoparticles: synthesis, characterization, properties, applications, and therapeutic approaches. *International journal of molecular sciences*, *17*(9), 1534.

Zhao, K., & Singh, (1999). In vitro percutaneous absorption enhancement of propranolol hydrochloride through porcine epidermis by terpenes/ethanol. *Journal of Controlled Release*, *62*(3), 359-366.

Zhao, S. (2018). Chitosan-coated cerium oxide nanoparticles and sparfloxacin encapsulated polymersomes as a new drug system with antimicrobial properties.

Zia, U.-e., Mahmood, T., & Ali, M. (2011). Dairy development in Pakistan. *Rome: Food and agriculture organization of the united nations*.

Zielińska-Jurek, A., Wei, Z., Wysocka, I., Szweda, P., & Kowalska, E. (2015). The effect of nanoparticles size on photocatalytic and antimicrobial properties of Ag-Pt/TiO2 photocatalysts. *Applied Surface Science*, *353*, 317-325.

Zierdt, C. H., Peterson, D. L., Swan, C., & MAcLOWRY, D. (1982). Lysis-filtration blood culture versus conventional blood culture in a bacteremic rabbit model. *Journal of clinical microbiology*, *15*(1), 74-77.

Appendix A

Hindawi
Advances in Polymer Technology
Volume 2020, Article ID 8456024, 15 pages
https://doi.org/10.1155/2020/8456024

WILEY | Hindawi

Research Article

Fabrication & Characterization of Chitosan Coated Biologically Synthesized TiO_2 Nanoparticles against PDR *E. coli* of Veterinary Origin

Naheed Zafar,[1] Bushra Uzair ,[1] Muhammad Bilal Khan Niazi,[2] Shamaila Sajjad,[3] Ghufrana Samin,[4] Muhammad Javed Arshed,[5] and Sikander Rafiq [6]

[1]*Department of Biological Sciences, International Islamic University Islamabad, Islamabad, Pakistan*
[2]*Department of Chemical Engineering, SCME, National University of Science and Technology (NUST), Islamabad, Pakistan*
[3]*Department of Physics, International Islamic University Islamabad, Islamabad, Pakistan*
[4]*Department of Chemistry, University of Engineering and Technology Lahore, Faisalabad Campus, Pakistan*
[5]*National Veterinary Laboratory, Ministry of National Food Security and Research, Government of Pakistan, Park Road, Islamabad, Pakistan*
[6]*Department of Chemical Polymer & Composite Materials Engineering, University of Engineering and Technology, Lahore, New Campus, Pakistan*

Correspondence should be addressed to Bushra Uzair; bushra.uzair@stu.edu.pk

Received 10 July 2019; Accepted 21 November 2019; Published 20 January 2020

Academic Editor: Sébastien Déon

Treatment of pandrug resistant (PDR) *Escherichia coli* strain is the leading causative agent of bovine mastitis worldwide. Hence, becoming a potential threat to veterinary and public health. Therefore, to control the infection new nontoxic, biocompatible antimicrobial formulation with enhanced antibacterial activity is massively required. Current study was planned to synthesize chitosan coated titanium dioxide nanoparticles (CS-NPs coated TiO_2). Coating was being done by chitosan nanoparticles (CS-NPs) using ionic gelation method. Aqueous solution of *Moringa concanensis* leaf extract was used to synthesize titanium dioxide nanoparticles (TiO_2 NPs). The synthesized nanoformulations were characterized by using XRD, SEM, and FTIR. X-ray diffraction (XRD) analysis indicated the crystalline phase of TiO_2 NPs and CS-NPs coated TiO_2 NPs. Scanning Electron Microscopy (SEM) confirmed spherical shaped nanoparticles size of chitosan NPs ranging from 19–25 nm and TiO_2 NPs 35–50 nm. Thesize of CS-NPs coated TiO_2 NPs was in the range of 65–75 nm. The UV-Vis Spectra and band gap values illustrated the red shift in CS-NPs coated TiO_2 NPs. Fourier transform infrared (FTIR) spectroscopy confirmed the linkages between TiO_2 NPs and chitosan biopolymer. Zeta potential confirmed the stability of CS-NPs coated TiO_2 NPs by showing 95 mV peak value. *In-vitro* antibacterial activity of CS-NPs coated TiO_2 NPs and Uncoated TiO_2 NPs was evaluated by disc diffusion method against PDR strain of *E. coli* isolated from mastitic milk samples. The antibacterial activity of all the synthesized nanoformulations were noted and highest antibacterial activity was shown by CS-NPs coated TiO_2 NPs against pandrug resistant (PDR) *E. coli* strain with the prominent zone of inhibition of 23 mm. Morphological changes of *E. coli* cells after the treatment with MIC concentration (0.78 μg/ml) of CS-NPs coated TiO_2 NPs were studied by transmission electron microscopy. TEM showedrigorous morphological defectsand has disturbed the general appearance of the *E. coli* cells. Cytotoxicity (HepG2 cell line) and hemolytic (human blood) studies confirmed nontoxic/biocompatible nature of CS-NPs coated biologically synthesized TiO_2 NPs. The results suggested that biologically synthesized and surface modified TiO_2 NPs by mucoadhesive polysaccharides (e.g. chitosan) coating would be an effective and non-toxic alternative therapeutic agent to

Appendix B

crystals

MDPI

Article

Synthesis and Characterization of Potent and Safe Ciprofloxacin-Loaded Ag/TiO_2/CS Nanohybrid against Mastitis Causing *E. coli*

Naheed Zafar [1], Bushra Uzair [1,*], Muhammad Bilal Khan Niazi [2], Ghufrana Samin [3], Asma Bano [4], Nazia Jamil [5], Waqar-Un-Nisa [6], Shamaila Sajjad [7] and Farid Menaa [8]

1 Department of Biological Sciences, International Islamic University, Islamabad 44000, Pakistan; naheedzafar12@gmail.com
2 School of Chemical and Materials Engineering, National University of Sciences and Technology, Islamabad 44000, Pakistan; bilalniazi2@gmail.com
3 Department of Chemistry, Faisalabad Campus, University of Engineering and Technology Lahore, Faisalabad 38000, Pakistan; g.samin@uet.edu.pk
4 Department of Microbiology, University of Haripur, Haripur 22620, Pakistan; asma_baano@yahoo.com
5 Institute of Microbiology & Molecular Genetics, Punjab University, Lahore 54000, Pakistan; nazia.mmg@pu.edu.pk
6 Centre for Interdisciplinary Research in Basic and Applied Sciences, International Islamic University, Islamabad 44000, Pakistan; waqarunnisa@iiu.edu.pk
7 Department of Physics, International Islamic University, Islamabad 44000, Pakistan; shamaila.sajjad@iiu.edu.pk
8 Department of Nanomedicine and Advanced Technologies, California Innovations Corporation, San Diego, CA 92037, USA; dr.fmenaa@gmail.com
* Correspondence: bushra.uzair@iiu.edu.pk

check for updates

Citation: Zafar, N.; Uzair, B.; Niazi, M.B.K.; Samin, G.; Bano, A.; Jamil, N., Waqar-Un-Nisa; Sajjad, S.; Menaa, F. Synthesis and Characterization of Potent and Safe Ciprofloxacin-Loaded

Abstract: To improve the efficacy of existing classes of antibiotics (ciprofloxacin), allow dose reduction, and minimize related toxicity, this study was executed because new target-oriented livestock antimicrobials are greatly needed to battle infections caused by multidrug-resistant (MDR) strains.

Appendix C

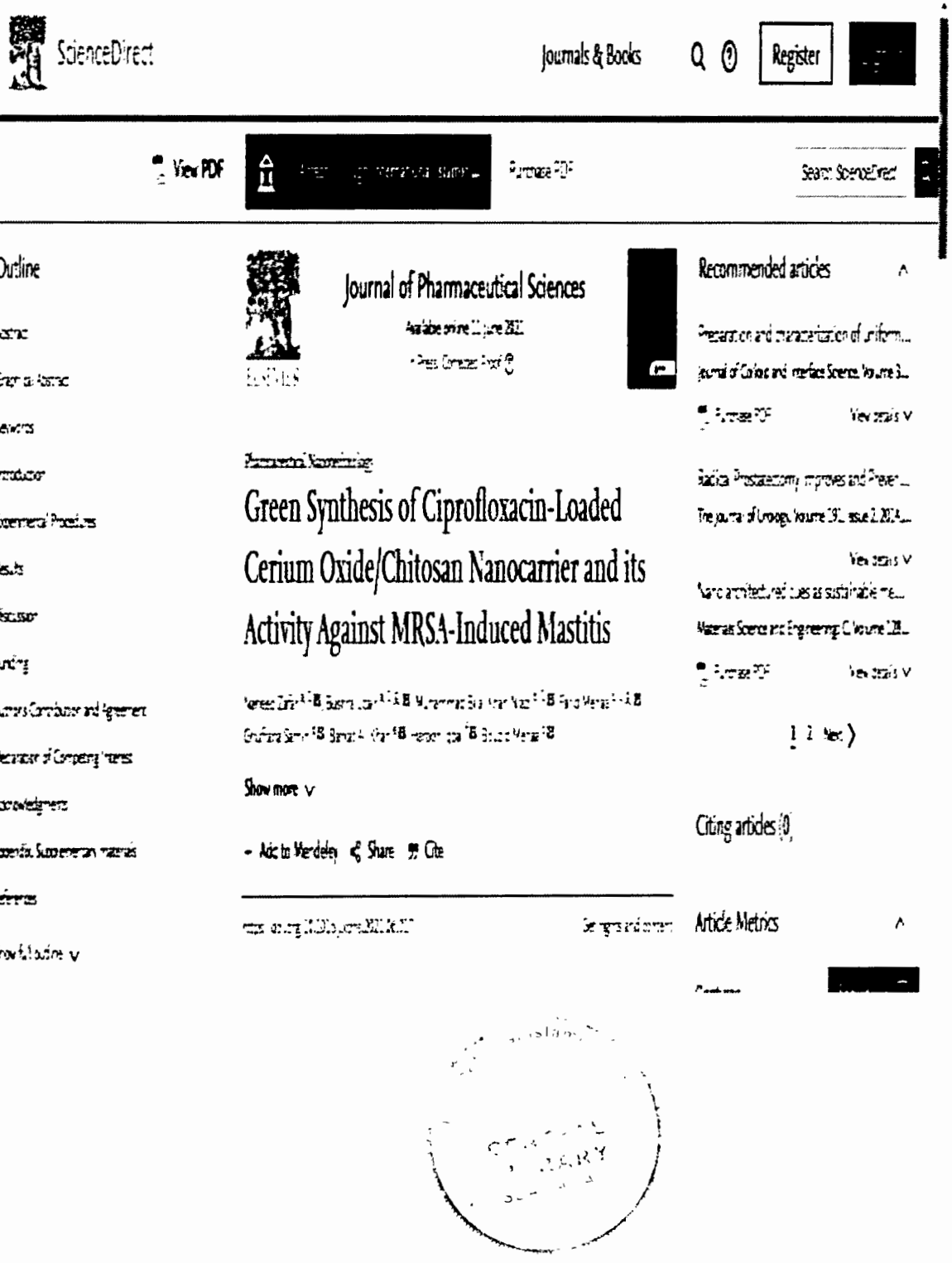
ScienceDirect
Journals & Books
Register
View PDF
Purchase PDF
Search ScienceDirect
Outline
Abstract
Graphical abstract
Keywords
Introduction
Experimental Procedures
Results
Discussion
Funding
Authors Contribution and Agreement
Declaration of Competing Interests
Acknowledgments
Appendix. Supplementary materials
References
Show full outline
Journal of Pharmaceutical Sciences
Available online 11 June 2021
In Press, Corrected Proof
Pharmaceutical Nanotechnology
Green Synthesis of Ciprofloxacin-Loaded Cerium Oxide/Chitosan Nanocarrier and its Activity Against MRSA-Induced Mastitis
Show more
Add to Mendeley
Share
Cite
Recommended articles
Preparation and characterization of uniform...
Journal of Colloid and Interface Science, Volume 3...
Purchase PDF
View details
Radical Prostatectomy improves and Preven...
The Journal of Urology, Volume 191, Issue 2, 2014...
View details
Nano-architectured cubes as sustainable ma...
Materials Science and Engineering: C, Volume 128...
Purchase PDF
View details
1 2 Next
Citing articles (0)
Article Metrics

DOCTOR OF PHILOSOPHY

CLASSIFIED THESIS EVALUATION FORM ENVISAGING FOREIGN (EXTERNAL) EVALUATOR'S RECOMMENDATIONS

Name of Student Naheed Zafar Reg. No. 22-FBAS/PHDBT/F14

Title of thesis Encapsulation of Metallic Oxide Nano-particles and Synthetic Antibiotics to Combat Mastitis Causing Multidrug Resistant Pathogens

Faculty/Deptt. Department of Biological Sciences Faculty of Basic and Applied Sciences

Name of Foreign Evaluator Chunyi Tong

Reasons quoted in my annexed report, I recommend that:

a) Thesis is being marked as PASSED and the candidate is recommended for award of degree of Doctor of Philosophy without further amendment and examination ***This section should be selected if, examiner thinks appropriate that no changes need to be undertaken in the thesis and viable to meet out the requirements of the degree. The examiner may have pin-pointed minor points that could be addressed but made it clear that is not necessary to do so.***	☐
b) Thesis is being marked as PASSED and the student is recommended for award of degree of Doctor of Philosophy subject to the minor amendments as mentioned in my report and correction of typographical errors being made to the satisfaction of the concerned supervisor. ***This section should be selected if, the amendments including typographical errors are minor in nature and the student can easily clear it. Such amendments are not to be expected in any cost to change the substance of the thesis but may include minor inaccuracies in referencing, minor errors in the statistical test, in using footnotes etc.***	☑
c) Thesis is being marked as PASSED and the student may be awarded the degree of Doctor of Philosophy subject to the substantial amendments recommended in my report and all typographical errors corrected as per entire satisfaction of the supervisor. ***This section should be opted if the amendments are more substantial in nature and its rectification will bring larger changes to the thesis than those in (b) above, but should be able to carry out under the guidance of the supervisor.***	☐

d) Thesis is being placed as <u>DEFERRED</u> and the candidate is being given period upto _____ months to review and resubmit the thesis for evaluation. ***This Section should be selected if the examiner thinks appropriate that the thesis currently does not meet any one or more of the degree requirements but has the potential to do so upon carrying out the recommended changes. The thesis clearly does not meet out the satiety of the requirements at present AND it can be supposed with confidence that the recommended changes can be addressed by the student, or if they are addressed will definitely lead to the thesis meeting the requirements. For example re-analysis data may be required and it is not clear whether the data are in a form that will allow the analysis to be conducted, or if they are, whether the re-analysis will lead to outcomes that reflect sufficiently original and/or substantial findings.***	☐
e) Thesis is classified as <u>FAILED</u> and the student should not be recommended for award of degree of Doctors of Philosophy on the basis of this thesis. ***The options is to be selected when the examiner is of clear perception that thesis does not meet at least any of the following requirements of the degree;*** ***1. A substantial and original contribution to knowledge;*** ***2. The candidate's ability to provide a analytical appraisal of relevant literature and available research to appreciate and understand the relationship of the investigations carried out by the students to the wider field of knowledge in which these investigations are located, and to draw out the contribution to knowledge made by these investigations;*** ***3. The candidate's knowledge and understanding of the methodological techniques used in the research and any shortcomings associated with these techniques;*** ***4. A satisfactory level of literary presentation reflecting an ability to communicate in a clear, concise and authoritative manner appropriate to the discipline and to the professional arena to which it is addressed.***	☐

Signature of Examiner Chunyi Tang Date Nov.8, 2021

It would be appreciated if you would fax/email this page and accompanying detailed report to the facsimile number to reduce delays mail deliveries may cause to the thesis examination process.

INTERNATIONAL ISLAMIC UNIVERSITY, ISLAMABAD
New Campus, Academic Block, H-10, Islamabad.
Contact No.051-9257997 Fax: 051-9257915
Email: ali.raafie@iiu.edu.pk

Qualitative Comments/Observations

Multidrug resistance (MDR) bacteria is becoming a monster threat to the dairy industry due to treatment failure by available expensive antibiotics. Nanobiotechnology is an emerging field to apply the new trends of nanotechnology find more reliable and eco-friendly methods for developing alternative nano-antibiotics with improved antimicrobial potentials. In this thesis, the author synthesized several metallic oxide nanoparticles (Ag NPs, CeO_2 NPs, TiO_2 NPs, and Fe_2O_3 NPs) using medicinally important plants. And the nanoparticles have efficient antibacterial. The green synthesis methods are economical method and suitable for developing country such as PA. The products will solve public health problems in PA. The conception of these works is very good and the data are rich and colorful. From the whole works of thesis, the author performances having basic

DOCTOR OF PHILOSOPHY

CLASSIFIED THESIS EVALUATION FORM ENVISAGING FOREIGN(EXTERNAL) EVALUATOR'S RECOMMENDATIONS

Name of Student: Naheed Zafar Reg.:22-FBAS/PHDBT/F14

Title of thesis Encapsulation of Metallic Oxide Nano-particles and Synthetic Antibiotics to Combat Mastitis Causing Multidrug Resistant Pathogens

Faculty/Dept.:Department of Biological Sciences

Name of Foreign Evaluator:

Mark Coyne, PhD

Reasons quoted in my annexed report, I recommend that:

a) **Thesis is being marked as PASSED and the candidate is recommended for award of degree of Doctor of Philosophy without further amendment and examination** *This section should be selected if, examiner thinks appropriate that no changes need to be undertaken in the thesis and viable to meet out the requirements of the degree. The examiner may have pin-pointed minor points that could be addressed but made it clear that is not necessary to do so.*	☐
b) **Thesis is being marked as PASSED and the student is recommended for award of degree of Doctor of Philosophy subject to the minor amendments as mentioned in my report and correction of typographical errors being made to the satisfaction of the concerned supervisor.** *This section should be selected if, the amendments including typographical errors are minor in nature and the student can easily clear it. Such amendments are not to be expected in any cost to change the substance of the thesis but may include minor inaccuracies in referencing, minor errors in the statistical test, in using footnotes etc.*	☐
c) **Thesis is being marked as PASSED and the student may be awarded the degree of Doctor of Philosophy subject to the substantial amendments recommended in my report and all typographical errors corrected as per entire satisfaction of the supervisor.** *This section should be opted if the amendments are more substantial in nature and its rectification will bring larger changes to the thesis than those in (b) above, but should be able to carry out under the guidance of the supervisor.*	X

Cont.....P/2

d) Thesis is being placed as <u>DEFERRED</u> and the candidate is being given period upto _____ months to review and resubmit the thesis for evaluation. *This Section should be selected if the examiner thinks appropriate that the thesis currently does not meet any one or more of the degree requirements but has the potential to do so upon carrying out the recommended changes. The thesis clearly does not meet out the satiety of the requirements at present AND it can be supposed with confidence that the recommended changes can be addressed by the student, or if they are addressed will definitely lead to the thesis meeting the requirements. For example re-analysis data may be required and it is not clear whether the data are in a form that will allow the analysis to be conducted, or if they are, whether the re-analysis will lead to outcomes that reflect sufficiently original and/or substantial findings.*	☐
e) Thesis is classified as <u>FAILED</u> and the student should not be recommended for award of degree of Doctors of Philosophy on the basis of this thesis. *The options is to be selected when the examiner is of clear perception that thesis does not meet at least any of the following requirements of the degree;* *1. A substantial and original contribution to knowledge;* *2. The candidate's ability to provide a analytical appraisal of relevant literature and available research to appreciate and understand the relationship of the investigations carried out by the students to the wider field of knowledge in which these investigations are located, and to draw out the contribution to knowledge made by these investigations;* *3. The candidate's knowledge and understanding of the methodological techniquesused in the research and any shortcomings associated with these techniques;* *4. A satisfactory level of literary presentation reflecting an ability to communicate in a clear, concise and authoritative manner appropriate to the discipline and to the professional arena to which it is addressed.*	☐

Signature of Examiner Mark Coyne Date:22 September 2021

It would be appreciated if you would fax/email this page and accompanying detailed report to the facsimile number to reduce delays mail deliveries may cause to the thesis examination process.

INTERNATIONAL ISLAMIC UNIVERSITY, ISLAMABAD
New Campus, Academic Block, H-10, Islamabad.
Contact No.051-9257997 Fax: 051-9257915
E.Mail: ethesis-fbas@iiu.edu.pk

<u>Qualitative Comments/Observations</u>

Review Naheed Zafar

This was a commendable amount of work for a PhD dissertation. The objectives stated in the conclusion were largely met. The critical new elements of synthesizing the novel nanoparticles, characterizing them, and showing their efficacy were listed in detail.

الجامعة الإسلامية العالمية إسلام آباد
International Islamic University, Islamabad
(Institutional Bioethics and Biosafety Committee)
Tel: 051- 9019401 Fax: 051-9019721 E-mail: abdul.hameed@iiu.edu.pk

April 17, 2019

Subject: **Certificate of Review/Ethics for PhD Research Topic "Nano-Encapsulation of Metallic Oxide Nano-Particles and Synthetic Antibiotics to Combat Mastitis Causing Multidrug Resistant pathogens"**

This is to certify that the subject PhD research topic of Ms. Naheed Zafar, Registration No. 22-FBAS/PHDBT/F14, is hereby ethically approved. She shall abide by the rules and regulations established by the Institutional Bioethical and Biosafety Committee.

(Prof. Dr. Abdul Hameed)
Director (ORIC)/Chairman Institutional Bioethics and Biosafety Committee (IBBS) for IIUI

Prof. Dr. Abdul Hameed
Director (ORIC)
International Islamic University
H-10, Islamabad